

This item was submitted to [Loughborough's Research Repository](#) by the author.  
Items in Figshare are protected by copyright, with all rights reserved, unless otherwise indicated.

## **Silica attached polymers and ligands for the selective removal of metal ions and radionuclides from aqueous solutions**

PLEASE CITE THE PUBLISHED VERSION

PUBLISHER

© James Donald Holt

PUBLISHER STATEMENT

This work is made available according to the conditions of the Creative Commons Attribution-NonCommercial-NoDerivatives 4.0 International (CC BY-NC-ND 4.0) licence. Full details of this licence are available at: <https://creativecommons.org/licenses/by-nc-nd/4.0/>

LICENCE

CC BY-NC-ND 4.0

REPOSITORY RECORD

Holt, James D.. 2019. "Silica Attached Polymers and Ligands for the Selective Removal of Metal Ions and Radionuclides from Aqueous Solutions". figshare. <https://hdl.handle.net/2134/16253>.



Silica Attached Polymers and Ligands for the Selective Removal  
of Metal Ions and Radionuclides from Aqueous Solutions

By

James Donald Holt

Doctoral Thesis

Submitted in partial fulfilment of the requirements for the award of

Doctor of Philosophy of Loughborough University

Supervisors: Dr Steve Christie, Dr Nick Evans and Dr Steve Edmondson

© James Donald Holt 2014

## Acknowledgments

There are so many people I would like to thank for the part they have played over the duration of my studies. Firstly I would like to thank my three supervisors Steve Christie, Nick Evans and Steve Edmondson for having faith in me and giving me the opportunity to do this PhD. Their enthusiasm, support and guidance has been extremely appreciated over the years and I have learnt so much from the experience. Thanks also go to Sandie Dann for her help and ideas along the way, as well as David Read who has had a keen interest in my work, provided me with some great advice and helped source samples I would otherwise have struggled to!

Thank you to the Nuclear Decommissioning Authority, without their support of research and funding of projects, this opportunity may never have arisen.

Thanks also go to Mark Edgar for his help and knowledge on my solid state NMR samples, to Pauline King for all those CHN samples you have run for me and to Mónica Felipe-Sotelo for all the help and support over the years, especially where ICP is concerned! Al Daley and Stuart Pinkney, your assistance has been massively appreciated when I have come to you for help and you have always gone out of your way to help. In the materials department, thanks go to Pat Cropper and Zhaoxia Zhou for their assistance with XPS and STEM respectively.

Over this period, the organic group and the largest stakeholders of the famous Acrylate Stanley have played a massive role in my PhD life: big thanks go to Ben, Marc, Rossi, TC, Andrew, Capel, Nat, Tash, Matt, Daz, Carlos, Emma, Bullous, Alex, Sam, Anish, Joel, Phil and Noble (ish!). Thanks to some great management from TC Capel, we have some success to be proud of! The atmosphere in the lab was always a good one and our socials have provided a great source of enjoyment so I thank you all for the memories! A special thank you goes to TC for taking me under his wing and getting me set up in a lab that was completely new to me.

To the Radiochemistry group, old and new, you been a fantastic group to work with, the friendship, knowledge and support of each other have helped me and many others get this far! In particular I'd like to thank Dr Stephen Pendleton, Dr Amy Young, Dr Ricky Hallam, Dr Sneh Jain, Dr Mónica Felipe-Sotelo, Dr Larry Anjolaiya, Mr Oliver Preedy and the soon to be Dr John Hinchliff. Thanks also go to Ms Joan Sutherland and Ms Julie Turner for all their help.

The inorganic group could always be relied upon for organising a good curry but a special thanks goes to Dr Rob King who has become a great friend and is solely to blame for initiating the number of stupid sporting events we have participated in over the last three years!

After over 8 years in Loughborough including my undergraduate years, many people have contributed to my experience and Michael Kyle deserves a special mention for the role you played during that time! Others from that time who I'm still in touch with, you know who you are and thank you – including Dr Andrew Wood who has been a top notch housemate for all these years.

My friends from Suffolk are an incredible bunch and meeting up for long weekends and holidays has provided a great opportunity to get out of Loughborough: Paul, Binx, Chris, Ali, Henly and Eggy, a big thank you to all of you.

An endless amount of thanks go to my parents and family for their support. Mum and Dad, I will never be able to thank you enough for the opportunities you have given me and the copious amount of love and support (emotionally and financially!) you have provided me with along the way. Michael, you deserve a special mention and I wish you all the best with your career. Thank you all so much for everything.

Finally to Meg, who has had to put up with the ups and downs that the PhD has thrown at me and taking such an interest in the project! Having spent all the working weeks apart, your company has been appreciated a lot at the weekends and holidays. Thank you for your support and for always being there!

## Abstract

Surface functionalised silica materials have been prepared, followed by the extensive testing of their ability to remove metal ions from aqueous solutions. Modifications include ligand attachment and polymer grafting from the silica surface whilst the metals tested range from first row transition metals right through to the lanthanides and actinides. Characterisation of the materials produced has been of paramount importance for the understanding of the modification process and this is also extensively discussed.

Atom transfer radical polymerisation (ATRP) has been used as the primary polymerisation method. Following polymerisation of 2-hydroxyethyl methacrylate (HEMA), post functionalisation was attempted. However, this was found to cause severe cross-linking and all attempts to attach ligands to this failed. Nonetheless, this process was transferred to grafting from silica surfaces and a novel approach to the characterisation of this material was implemented. (3-aminopropyl)triethoxysilane (APTES) was reacted with multiple forms of silica, primarily ZEOprep silica (average particle size 71.48  $\mu\text{m}$ ) and fumed silica (0.007  $\mu\text{m}$ ). This produced an amine coated surface to which 2-bromoisobutyryl bromide (BIBB) was attached, providing the required surface for radical polymerisation to proceed with a selected monomer. Solid State Nuclear Magnetic Resonance (SSNMR) has been utilised as the major characterisation technique for each step, leading to significant understanding of how this occurs. Thermogravimetric Analysis (TGA) and elemental analysis has supported this method at each stage whilst also enabling one to calculate the moles of APTES present, per gram of APTES-functionalised silica. For the ZEOprep silica this was calculated to be at up to  $1.51 \times 10^{-3} \text{ mol g}^{-1}$  and for the fumed silica  $1.63 \times 10^{-3} \text{ mol g}^{-1}$ .

As well as testing the selective nature of these materials, solutions of individual ions and radionuclides were used to measure the effectiveness of the materials for a specific ion.  $R_d$  values for these metals ions including solutions of Co(II), Ni(II), Cu(II),  $\text{Cd}^{2+}$ , Eu(III) and  $[\text{UO}_2]^{2+}$  have reached values ranging from  $7.49 \times 10^4 \text{ mL g}^{-1}$  to as high as  $2.17 \times 10^9 \text{ mL g}^{-1}$ . These values are regarded as outstanding by other groups that have reported similar results and these are discussed in the report. This range includes values that were observed when competing  $\text{Na}^+$  and  $\text{Ca}^{2+}$  ions were present at 0.5 % and 1 % (w/w). pH testing was also investigated with the materials using a solution of europium ions to determine the most effective range and this was found to fall between pH 4 and 5. X-ray Photoelectron Spectroscopy (XPS) has been utilised to help gain an understanding of the binding between

Cu(II) ions and APTES, suggesting that copper ions bind with oxygen atoms closer to the silica surface as well as the nitrogen atoms at the end of the ligand. Meanwhile STEM (Scanning Transmission Electron Microscope) has been used to show how effectively the surface area of the material is used by imaging the europium ions over a sample of APTES-functionalised fumed silica.

Ligands and polymers have been focussed on to build a catalogue of functional materials and this has been achieved in collaboration with PhosphonicS Ltd. The most significant finding from these selective investigations was that uranyl ions were found to be the most readily removed. Cu(II) and Eu(III) ions were also removed relatively effectively whilst Co(II), Ni(II),  $\text{Zn}^{2+}$  and  $\text{Cd}^{2+}$  proved the most challenging but certainly not impossible.  $[\text{UO}_2]^{2+}$  concentrations were reduced from 17.1 ppm to 1.6 ppm after 4 weeks with use of the ligand 'SEA' (2-aminoethyl sulfide ethyl silica) even with six other metal ions present at similar initial concentrations and a starting pH of 4.67 by adding just 50 mg of the material to a 45 mL solution.

## Table of Contents

Acknowledgments.....	iii
Abstract.....	v
Table of Contents.....	vii
List of Abbreviations .....	xii
1 Introduction .....	1
1.1 Literature Review .....	4
1.1.1 Surface attached ligands for metal removal.....	4
1.1.2 Polymers and surface attached polymers for metal removal .....	11
1.2 Summary .....	18
2 Experimental.....	20
2.1 Instrumentation.....	20
2.1.1 Infrared Spectroscopy .....	20
2.1.2 CHN Elemental Analysis.....	20
2.1.3 Solution State NMR.....	20
2.1.4 Solid State NMR.....	20
2.1.5 Mass Spectrometry.....	21
2.1.6 ICP-OES .....	21
2.1.7 ICP-MS .....	22
2.1.8 Liquid Scintillation Counting .....	23
2.1.9 Gamma Counting .....	23
2.1.10 Malvern Mastersizer 2000 .....	24
2.1.11 Freeze Drier .....	24
2.1.12 Chemicals.....	24
2.2 Synthesis of PHEMA <i>via</i> ATRP.....	25
2.3 Synthesis of PHEMA <i>via</i> ARGET ATRP.....	26
2.4 Synthesis of 3-ethoxy-3-oxopropanoic acid.....	27

2.5	Synthesis of ethyl malonyl chloride .....	27
2.6	Synthesis of free PGMA <i>via</i> ATRP .....	28
2.7	Synthesis of free PGMA <i>via</i> ARGET ATRP .....	29
2.8	Synthesis of tosylated HEMA .....	30
2.9	Synthesis of tosylated PHEMA <i>via</i> free radical polymerisation.....	31
2.10	Synthesis of 4-cyanobenzoyl chloride.....	31
2.11	Synthesis of 4-cyanobenzoyl chloride attachment to PHEMA.....	32
2.12	Synthesis of free PDMAEMA <i>via</i> ARGET ATRP .....	33
2.13	Deposition of APTES onto ZEOprep silica .....	34
2.14	Deposition of BIBB onto APTES-functionalised ZEOprep silica.....	35
2.15	Polymerisation of HEMA from BIBB-functionalised ZEOprep silica .....	36
2.16	Polymerisation of DMAEMA from BIBB-functionalised ZEOprep silica.....	37
2.17	Polymerisation of PEGMA from BIBB-functionalised ZEOprep silica.....	38
2.18	Deposition of APTES onto fumed silica .....	39
2.19	Deposition of BIBB onto APTES-functionalised fumed silica.....	40
2.20	Polymerisation of HEMA from BIBB-functionalised fumed silica.....	41
2.21	Polymerisation of PEGMA from BIBB-functionalised fumed silica .....	42
2.22	Synthesis of 3-(2-bromoisobutyramido)propyl(triethoxy)silane (BIBAPTES).....	43
2.23	Deposition of BIBAPTES onto porous silica microparticles (PSM) .....	43
2.24	Polymerisation of HEMA from BIBAPTES attached PSM .....	44
2.25	Deposition of TMSPDETA onto ZEOprep silica .....	45
2.26	Deposition of APTES onto silica coated magnetite .....	45
2.27	Attempted sequestration of nickel, copper and zinc from aqueous solutions using PHEMA and PHEMA-Malonate.....	46
2.28	Attempted sequestration of <sup>63</sup> Ni from aqueous solution using free PHEMA .....	46
2.29	General method for the sequestration of various transition metals and radioactive isotopes using silica attached APTES and TMSPDETA .....	47



2.30	General method for the selective removal of metals from a seven metal solution using functionalised silicas.....	47
2.31	Method for attempting metal removal from Talvivaara PLS pond sample.....	48
3	Polymerisation of monomers and post-polymerisation modification.....	49
3.1	Introduction .....	49
3.1.1	Atom Transfer Radical Polymerisation (ATRP).....	50
3.1.2	Activators ReGenerated by Electron Transfer (ARGET) ATRP.....	51
3.1.3	Uncontrolled radical polymerisation.....	52
3.1.4	Why ATRP methods were chosen .....	53
3.2	Results and Discussion.....	54
3.2.1	HEMA/PHEMA.....	54
3.2.2	GMA/PGMA.....	63
3.2.3	Tosylation of HEMA for further modification .....	67
3.3	Conclusion.....	68
3.4	Future Work .....	69
4	Surface attachment of ligands and polymers to silica surfaces .....	70
4.1	Introduction .....	70
4.1.1	Previous literature reporting the modification of silica surfaces .....	70
4.2	Results and Discussion.....	73
4.2.1	ZEOPrep silica .....	73
4.2.2	Fumed silica .....	74
4.2.3	Porous silica microparticles .....	75
4.2.4	Silica coated ferrous oxide microparticles .....	76
4.2.5	Deposition of APTES to ZEOPrep and fumed silica .....	77
4.2.6	Deposition of BIBB to ZEOPrep and fumed silica.....	79
4.2.7	Grafting of PHEMA from surface of ZEOPrep and fumed silica.....	79
4.2.8	Grafting of PDMAEMA from surface of ZEOPrep silica .....	80

4.2.9	Grafting of PEGMA from surface of ZEOprep and fumed silica.....	82
4.2.10	Modification of porous silica microparticles (PSM) .....	83
4.2.11	APTES attachment to SMP's.....	84
4.3	Conclusion.....	84
4.4	Future Work .....	85
5	Detailed and mechanistic characterisation of silica materials .....	86
5.1	Introduction .....	86
5.1.1	Solid State Nuclear Magnetic Resonance .....	86
5.1.2	Thermogravimetric Analysis .....	88
5.1.3	CHN Elemental Analysis .....	89
5.2	Results and Discussion.....	91
5.2.1	SSNMR of functionalised silicas .....	91
5.2.2	TGA analysis of ZEOprep silica.....	99
5.2.3	TGA analysis of fumed silica .....	102
5.2.4	TGA analysis of porous silica microparticles .....	104
5.2.5	TGA analysis of silica coated iron oxide microparticles .....	107
5.2.6	CHN Elemental analysis on functionalised silicas .....	107
5.3	Conclusion.....	109
5.4	Future Work .....	111
6	Sequestration of metals, kinetics and $R_d$ .....	112
6.1	Introduction .....	112
6.1.1	Radioisotopes used in this work .....	112
6.1.2	Analytical techniques.....	114
6.2	Results and Discussion.....	119
6.2.1	Metal ion sequestration with free PHEMA and PHEMA-Malonate .....	119
6.2.2	Initial metal ion sequestration with functionalised silica materials .....	121
6.2.3	Sequestration of metal ions with silica attached APTES.....	122

6.3	Cu(II) removal with SMP attached APTES .....	162
6.4	Langmuir isotherm model .....	163
6.5	Conclusion.....	166
6.6	Future Work .....	168
7	Selective removal of metal ions and use of materials produced by PhosphonicS Ltd ...	170
7.1	Introduction .....	170
7.1.1	PhosphonicS Ltd .....	170
7.1.2	Talvivaara mine water sample .....	172
7.2	Results and Discussion.....	172
7.2.1	Selective metal sequestration.....	172
7.2.2	Talvivaara mine water sample .....	188
7.3	Conclusion.....	190
7.4	Future Work .....	191
8	Summary and concluding remarks .....	193
9	References .....	196
10	Appendix 1 – Linear Langmuir plots.....	213
11	Appendix 2 – Reversibility and dissolution of metal ions following sequestration ...	219
12	Appendix 3 – Particle size of PhosphonicS Ltd samples.....	220

## List of Abbreviations

### Analytical Terms

Abbreviation	Full Name
$^{13}\text{C}$ NMR	Carbon-13 Nuclear Magnetic Resonance
$^1\text{H}$ NMR	Proton Nuclear Magnetic Resonance
$^{29}\text{Si}$ NMR	Silicon-29 Nuclear Magnetic Resonance
CHN	Carbon, Hydrogen and Nitrogen Microanalysis
EDS	Energy Dispersive X-ray Spectroscopy
FTIR/IR	Fourier Transform Infrared Spectroscopy
ICP-MS	Inductively Coupled Plasma Mass Spectrometry
ICP-OES	Inductively Coupled Plasma Optical Emission Spectrometry
LSC	Liquid Scintillation Counting
MAS	Magic Angle Spinning
MS	Mass Spectrometry
SSNMR	Solid State Nuclear Magnetic Resonance
STEM	Scanning Transmission Electron Microscope
TGA	Thermogravimetric Analysis
TLC	Thin Layer Chromatography
UATR	Universal Attenuated Total Reflectance
XPS	X-ray Photoelectron Spectroscopy

### Solvents

Abbreviation	Full Name
D <sub>2</sub> O	Deuterium Oxide

DCM	Dichloromethane
DMF	Dimethylformamide
DMSO	Dimethyl Sulfoxide
EtOAc	Ethyl Acetate
EtOH	Ethanol
MeOD	Deuterated Methanol
MeOH	Methanol
THF	Tetrahydrofuran

## Reagents

Abbreviation	Full Name
ABCN	1,1'-Azobis(Cyclohexanecarbonitrile)
AEMA	2-Aminoethyl methacrylate
APTES	(3-Aminopropyl)Triethoxysilane
BIBAPTES	3-(2-Bromoisobutyramido)Propyl(Triethoxy)Silane
BIBB	2-Bromoisobutyryl Bromide
Bpy	2,2'-Dipyridyl
DMAEMA	2-(Dimethylamino)Ethyl Methacrylate
DMAP	4-Dimethylaminopyridine
EBIB	Ethyl $\alpha$ -Bromoiso Butyrate
Et <sub>3</sub> N	Triethylamine
GMA	Glycidyl Methacrylate
HEMA	2-Hydroxyethyl Methacrylate
HMTETA	1,1,4,7,10,10-Hexamethyltriethylenetetramine

PDMAEMA	Poly(Dimethylamino)Ethyl Methacrylate
HEMA	Poly(2-Hydroxyethyl Methacrylate)
PEGMA	Poly(Ethylene Glycol) Monomethyl Ether Methacrylate
PSM	Porous Silica Microparticles
SMP	Superparamagnetic Microparticles
TEABr	Triethylammonium Bromide
TMSPDETA	N <sup>1</sup> -(3-Trimethoxysilylpropyl)Diethylenetriamine
TsO	p-Toluenesulfonic Acid

## **General Terms**

<b>Abbreviation</b>	<b>Full Name</b>
Bq	Becquerel
ca.	Circa
cpm	Counts per Minute
cps	Counts per Second
d	Day(s)
e.q.	Equivalents
h	Hour(s)
m	Minute(s)
pm	Pico meters
ppb	Parts per billion
ppm	Parts per million
ppt	Parts per trillion
ppt.	Precipitate

r.t.	Room Temperature
s	Second(s)
sat.	Saturated
soln.	Solution
t	Tonnes
u	Atomic Mass Unit
$\nu$	Wavenumber

# 1 Introduction

As part of the Nuclear Decommissioning Authority's (NDA) bursary call in 2010, the NDA sought after a novel method for the extraction of metal ions from aqueous environments. Due to the area of the work the NDA are involved with, the nature of the metal ions would include radionuclides, differ in oxidation states under the same environmental conditions and also include non-radioactive heavy metals (e.g. lead). The pH of the solution will often differ depending on the species in the solution and where the water is found: whether it be waste streams, surface water or groundwater.

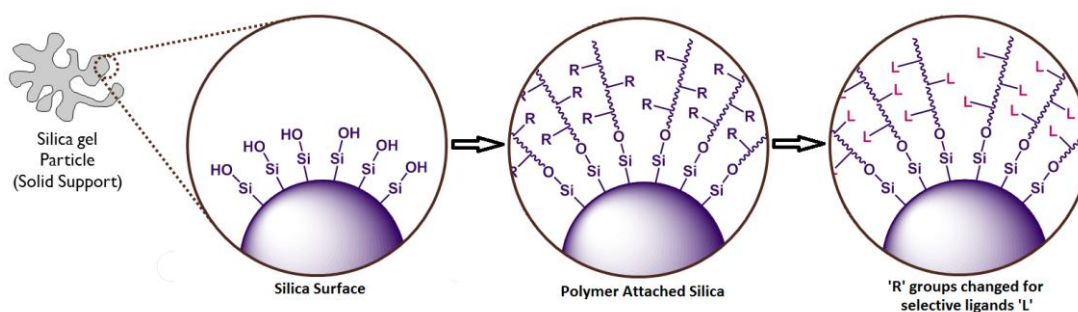
This introduction firstly presents the methodology that was put forward, followed by an account of the materials used with its application before familiarising the reader to the format of this report and the work undertaken.

The method uses a modular design of 1) a solid-support, 2) polymers to graft to the surface to produce a much larger surface area and 3) ligands to attach to the polymer, thus making the polymers as functional as possible. This would create a 'tool-box' where a range of materials would be developed and tested, each of which could be replaced for a more appropriate alternative depending on the conditions and the target ions.

By producing a material that was chemically bonded to a solid surface, the material would not dissolve (providing an appropriate solid was selected) and hence could be removed from the aqueous environment with the target species bound to the functionalised material.

Figure 1 explains this modular process using silica gel as the solid support. Silica was chosen as the solid support due to its properties that allow it to undergo vitrification: allowing radionuclides bound to the surface to be suitably stored as a solid waste form.<sup>1</sup> The hydroxyl groups at the surface of silica gel provide a functional group that is known to react well with other molecules and hence makes an ideal material for polymer attachment. The last step of Figure 1 shows the final product of the aim of this work. A ligand (L) would be attached to the polymer side chains to make the material more specific to its target and the known environment, replacing the natural 'R' groups that are part of the side chains of the polymer.





**Figure 1 – Demonstrative view of the object of this work where the final step shows the product to be used for selective metal sequestration with specific ligands replacing the natural ‘R’ groups that exist as part of the original polymer.**

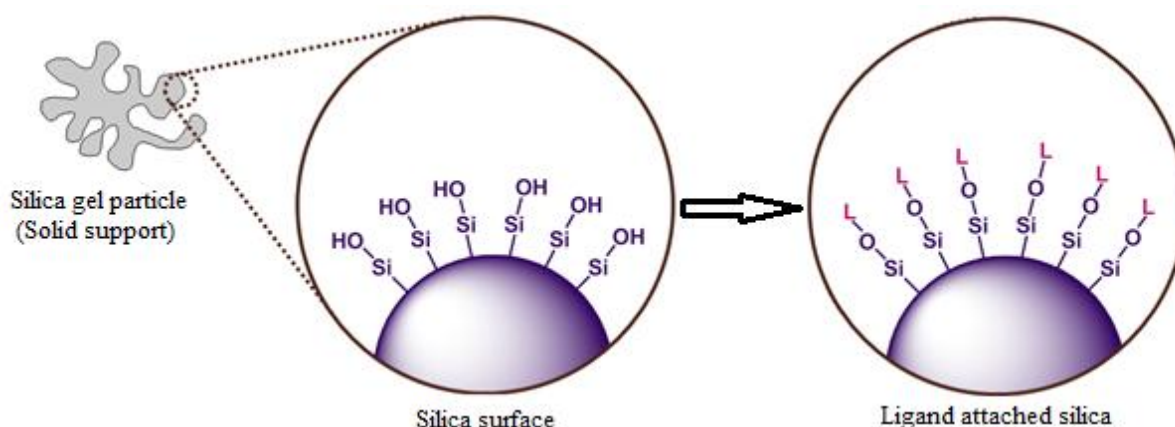
A short literature review follows this introduction, designed to make clear the origins of this idea. The literature reported provides an insight to what has been done before specifically with heavy metals and radionuclides as the target and why this modular ‘tool-box’ approach can be considered novel. Four variations of silica gel are reported as part of this work, but none have been specifically reported in this manner before. Instead, the literature focuses on other silica types such as MCM-41 and SAMMS (which are explained on pages 4-6) to make clear the differences but at the same time, why these approaches and literature are relevant. An introduction to chapters 3-7 is designed to provide the reader with a background to previous work or understanding more specific characterisation techniques at a more appropriate point.

Following the experimental section that discusses the range of methods used across many disciplines of chemistry, chapter 3 reports the initial work that was carried out to start this project. This focuses on free polymer synthesis (polymer that was not attached to a solid surface) to understand which polymers would be the best to work with and which polymerisation technique would be the most appropriate. Modification of these polymers is then introduced and how it became apparent that this was not as straight forward as one expected.

Chapter 4 introduces the four silica materials that are investigated in this work. The preparation techniques for surface initiated polymerisation are made familiar before explaining how the polymers used in chapter 3 are attached to the silica surface. Fourier Transform Infrared (FTIR) spectroscopy results are reported to illustrate how this characterisation technique provides qualitative information quickly to ascertain whether attachment has taken place or not based on the expected functional group change.

Next, three characterisation techniques are introduced that on their own provide a detailed understanding of the materials produced. These techniques include Solid State Nuclear Magnetic Resonance (SSNMR), Thermogravimetric Analysis (TGA) and elemental analysis and by using the three techniques to support one another, an even stronger case can be prepared to explain the structure of the materials produced. Each stage of the modification is analysed by all three methods and it is this detailed step-wise characterisation procedure that provides extremely detailed analysis.

Chapter 6 illustrates and discusses the results achieved with (3-aminopropyl)triethoxysilane (APTES) functionalised silica to bind to metal ions in aqueous solutions. Some metal ions such as Cu(II) and Eu(III) are tested in great detail where techniques such as X-ray photoelectron spectroscopy (XPS) and Scanning Transmission Electron Microscopy (STEM) are used to develop an understanding of how the ions are bound to the surface and to analyse how much of the surface appears to be involved with metal binding. Figure 2 illustrates how the APTES ligand (and other ligands trialled in chapter 6) was attached to the silica without the inclusion of polymers as shown in Figure 1.



**Figure 2 – Demonstrative view of how ligands have also been attached to the silica surfaces in this work.**

Due to the results achieved with APTES-functionalised silica, the ‘tool-box’ approach was prevented from being carried out to the extent that was originally planned. Instead, this material was thoroughly investigated for its behaviour and metal binding, whilst other ligands were tested and polymer synthesis was effectively halted.

Finally, chapter 7 investigates the selective properties of the materials developed but also tests many other ligand functionalised silicas that were donated by PhosphonicS Ltd. This illustrates the dissimilarities of ligand behaviour when used in aqueous solutions of very

similar conditions. Also discussed are the results found when materials were used in a ‘real-world’ mine water sample and the difficulties that this provided.

## **1.1 Literature Review**

Selective removal of metal ions from solutions with the use of ligands is not a novel idea – even with radionuclides. One of the most well-known separation methods is the PUREX (Plutonium URanium EXtraction) process and this was patented in 1960 following its application in 1947.<sup>2</sup> This process involves the ligand tributyl phosphate to separate Pu(IV) from some wastes in the nuclear fuel cycle.<sup>3</sup>

Surface attached ligands for metal removal have also been reported by various groups.<sup>4,5,6,7</sup> Synthetic organic reactions requiring high purity have reported the use of these to remove low concentrations of metal catalysts.<sup>8</sup> Similarly, polymers and surface-attached polymers have been reported for metal sequestration by various workers<sup>9,10,11,12</sup> but post-modification of polymers is recognised to be a difficult process – supported by results in this thesis.

Radioactive isotopes are quite often found in very low concentrations in millions of gallons of tank wastes (frequently  $10^{-8}$  to  $10^{-9}$  M).<sup>13</sup> This means that if only the radioactive components of the waste can be immobilized, the volume of wastes to be converted for long-term storage can be significantly reduced. The complexing agents used to remove tank wastes must be highly selective for the target species whilst also having the ability to ignore competing ligands and cations. By using silica based materials, following sequestration the material could be easily vitrified for long term disposal.<sup>13</sup>

### **1.1.1 Surface attached ligands for metal removal**

Work reported by Fryxell *et al.*<sup>14</sup> provided a significant source of information regarding previous work with surface attached ligands. Methodology was used from this work when designing the approach of the project due to the successful results reported.

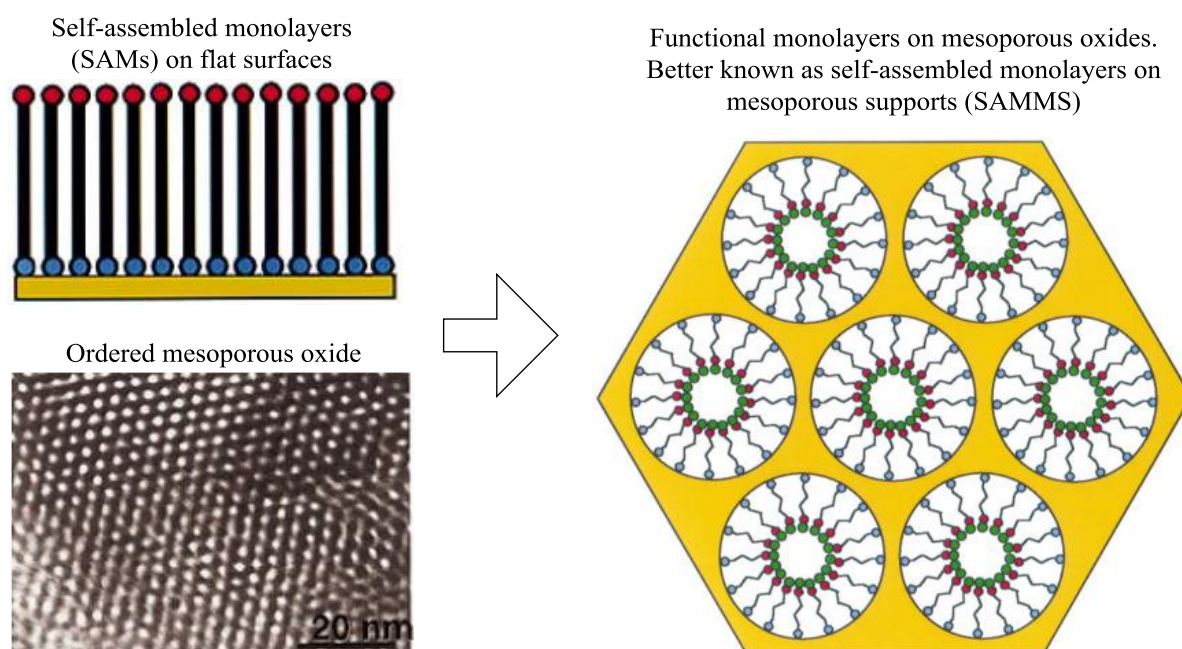
The group prepared their own solid support, MCM-41<sup>15,16</sup> (Mobil Composition of Matter no. 41) and this material is explained in more detail below. Synthesis was avoided in this work to concentrate on the functional end. However, due to the lack of literature specifically on the silica surfaces reported and used in this thesis, their work was studied for its behaviour and the route by which surface modifications took place.

Inorganic microporous solids (materials with pore diameters of  $\leq 2$  nm) and mesoporous solids (materials with pore diameters of 2-50 nm) have found great utility as catalysts and sorption media because of their large internal surface area.<sup>17</sup> In 1992, Mobil Oil Research successfully synthesised ordered mesoporous materials with a very high surface area ( $> 1000 \text{ m}^2 \text{ g}^{-1}$ ) and ordered pore structure (mostly hexagonal packed, with cylindrical pore channels). The materials also held extremely narrow pore size distribution where the pore diameter could be altered from 2 to 15 nm. The preparation method involved mixing a ceramic precursor (an inorganic, non-metallic material prepared by the action of heating followed by cooling – such as sodium aluminate, tetramethyl ammonium silicate or silica) in a surfactant (a compound that lowers surface tension between two liquids or between a liquid and a solid, for example cetyltrimethylammonium bromide, CTAB) and reacting at temperatures of sub 150 °C. The most common phase consists of rod-like micelles packed in hexagonal arrangements. The ceramic precursors bind to the head groups of the surfactant molecules before condensing together to form a continuous ceramic phase. Subsequently, the surfactant molecules can be removed by thermal or chemical treatment.<sup>16</sup> Members of this hexagonal family of materials are labelled MCM-41<sup>17,18</sup> whilst the cubic phase are known as MCM-48<sup>18</sup> (this type is not discussed here).

Since this research was published, mesoporous materials research has become a very active area because of the great potential for applications in the environment and industrial processes. However progress on the practical use of these materials has been slow because many of the applications such as adsorption, ion exchange and catalysis require the materials to have specific binding sites, stereochemical configuration or charge density and acidity.<sup>16,18,19</sup> Most mesoporous materials do not themselves have the appropriate surface properties for this and so require further modification.

Using materials known as self-assembled monolayers (SAMs),<sup>20</sup> Fryxell *et al.*<sup>14</sup> functionalised the surface of mesoporous supports to target specific metals. SAMs were developed long before their potential was recognised when Zisman *et al.*<sup>21</sup> published the preparation of a monomolecular layer by adsorption (self-assembly) of a surfactant onto a clean metal surface in 1946.<sup>21</sup> It is an ordered molecular assembly formed by the adsorption of a surfactant on a solid surface. This simple process makes SAMs fundamentally manufacturable and thus, technologically attractive for surface engineering.<sup>20</sup>

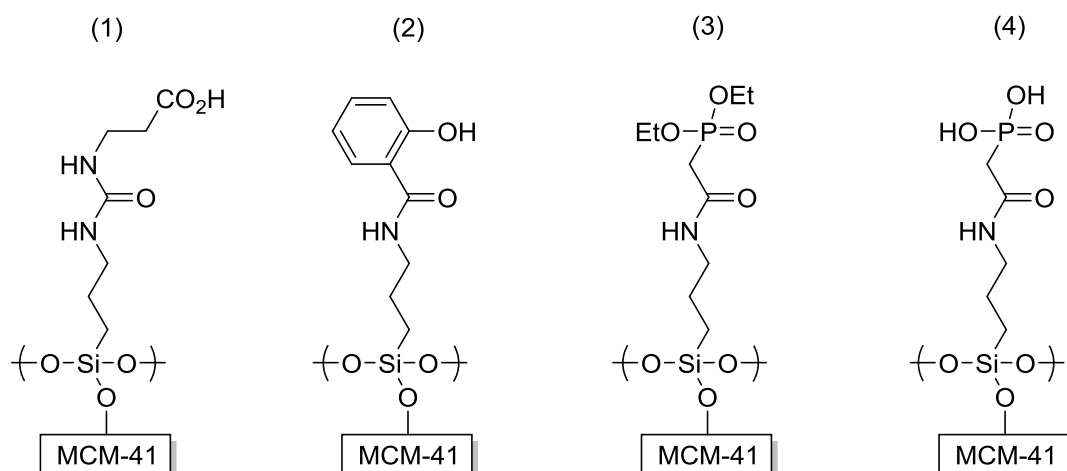
A powerful class of environmental sorbent materials called ‘self-assembled monolayers on mesoporous supports’ (SAMMS) are then created when the marriage of self-assembled monolayers (SAMs) and mesoporous ceramic supports takes place.<sup>22</sup> These materials have been described as highly effective sorbents and their chemistry can be tuned to selectively sequester a specific target species including but not limited to metals, tetrahedral oxometalate anions and radionuclides.<sup>14</sup> Figure 3 is effectively a cross-section of the SAMMS which shows the bulk of the silica or other ceramic material used in its hexagonal channels with its pores and how this concept was taken from the SAMs on flat surfaces. The blue dots illustrate the covalently attached molecules, the red are the functional end groups and the green are metal ions.



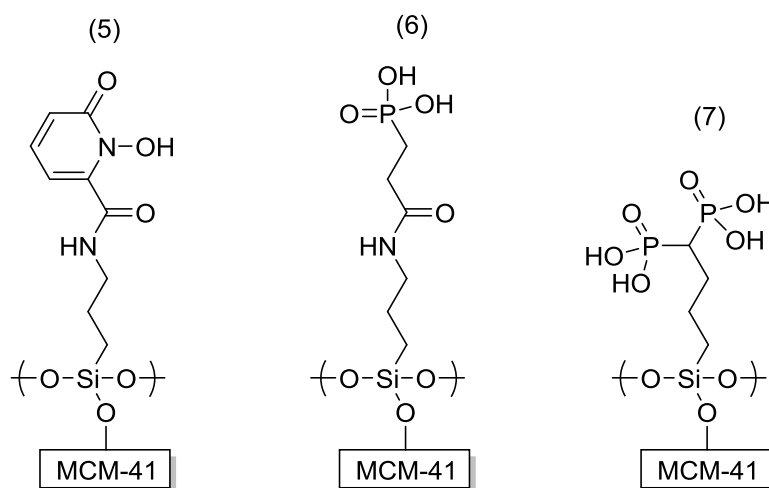
**Figure 3 – Preparation and schematic illustration of hybrid mesoporous materials. The functional molecules are attached to the mesoporous support similarly to the preparation of self-assembled monolayers (SAMs) on flat substrates. One end group of the functional monolayer is covalently bonded to the silica surface, and the other end group can be used to bind metals or other functional molecules forming the material known as SAMMS. Image adapted from Liu *et al.*<sup>16</sup>**

The structures attached to the SAMMS material are illustrated in Figure 4 and Figure 5 showing the ligands that Fryxell *et al.*<sup>14,23</sup> used for this work. A selection of the metal sequestration results follows these figures. The ligands illustrated on page 7 and their behaviours are important for this research to demonstrate the prior knowledge before new approaches are explored. Nitrogen and oxygen containing ligands are extremely common

and the results from the materials tested as part of the work in this thesis will show the extensive range of ligands that were used that included these atoms in their structures.



**Figure 4 – Chemical structures of SAMMS with various organic groups synthesised by Fryxell *et al.*<sup>14</sup> for metal sequestration. (1) Glycyl-urea SAMMS (Gly-UR-SAMMS), (2) Salicylamide SAMMS, (3) Acetamide-Phosphonate ('Ac-Phos') Ester SAMMS and (4) AC-Phos Acid SAMMS.**



**Figure 5 – Chemical structures of SAMMS with various organic groups synthesised by Fryxell *et al.*<sup>23</sup> for metal sequestration. (5) 1,2-HOPO SAMMS, (6) Prop-Phos SAMMS and (7) DiPhos SAMMS.**

The affinity of a sorbent for a target species is often represented with the distribution coefficient ( $K_d$ , more commonly in the unit of  $\text{mL g}^{-1}$ ). This is simply a mass-weighted partition coefficient between the solid phase and the liquid supernatant phase as follows:

$$K_d = \frac{C_o - C_f}{C_f} \cdot \frac{V}{M}$$

**Equation 1 – Equation to show the calculation of the distribution coefficient ( $K_d$ ).**

Where  $C_o$  and  $C_f$  are the initial and final concentrations in the solution of the target species,  $V$  is the solution volume in mL and  $M$  is the mass in grams of the sorbent. Previous literature has described  $K_d$  values of ca.  $10^3$  mL g<sup>-1</sup> as ‘good’ and those above  $5 \times 10^4$  mL g<sup>-1</sup> as ‘outstanding’,<sup>14,23</sup> thus providing a target value for future results.

A detailed method of distribution coefficient ( $K_d$ ) measurements is reported and were studied over a pH range of 1.0-6.5.<sup>14</sup> The solution/solids ratio employed in these experiments were typically 200 but was also studied in a range from 50-1000 to ensure cation binding was not influenced by the stoichiometric ratio of binding sites to solution cation content. Contact times were several hours (typically 1-4) to ensure all distribution coefficients reflected true equilibrium conditions.<sup>14</sup>

Actinide	pH	$K_d$ (mL g <sup>-1</sup> ) Gly-UR SAMMS <sup>(a)</sup>	$K_d$ (mL g <sup>-1</sup> ) Ac-Phos ester SAMMS <sup>(b)</sup>	$K_d$ (mL g <sup>-1</sup> ) Prop-Phos ester SAMMS <sup>(b)</sup>
Am(III)	0.78	0	600	0
	1.9	1	3900	0
	4.26	92000	210000	33
	5.24	240000	460000	48
Pu(IV)	0.66	160	94000	61000
	1.05	5100	72000	66000
	2.08	45000	52000	36000
Np(V)	0.72	0	60	0
	1.55	0	55	0
	3.68	86	43	0
	4.73	200	150	0
U(VI)	0.7	160	26000	170
	2.36	12000	31000	1400
	4.55	160000	24000	12000
Th(IV)	0.76	900	23000	21000
	2.43	91000	13000	31000

**Table 1 – Actinide distribution coefficients ( $K_d$ ) for the carboxylic acid phosphonate ester SAMMS as reported by Fryxell *et al.*<sup>14</sup> The structures of these are given in Figure 4 and Figure 5. <sup>(a)</sup>[Ac] = 2000 dpm/mL. 0.1 M NaNO<sub>3</sub>. 0.10 g SAMMS in 10 mL. <sup>(b)</sup>[Ac] = 2000 dpm/mL. 0.1 M NaNO<sub>3</sub>. 0.20 g SAMMS in 10 mL.**

The data in Table 1 provide an idea of the values already being reported and allow comparisons to be made where relevant. The U(VI) results are the only ones that are directly relevant based on the metal ions that were eventually investigated as part of this work, but tables such as the above are rarely reported with this area of work. It was considered important to report this table to use as a reference for the results reported in this thesis.

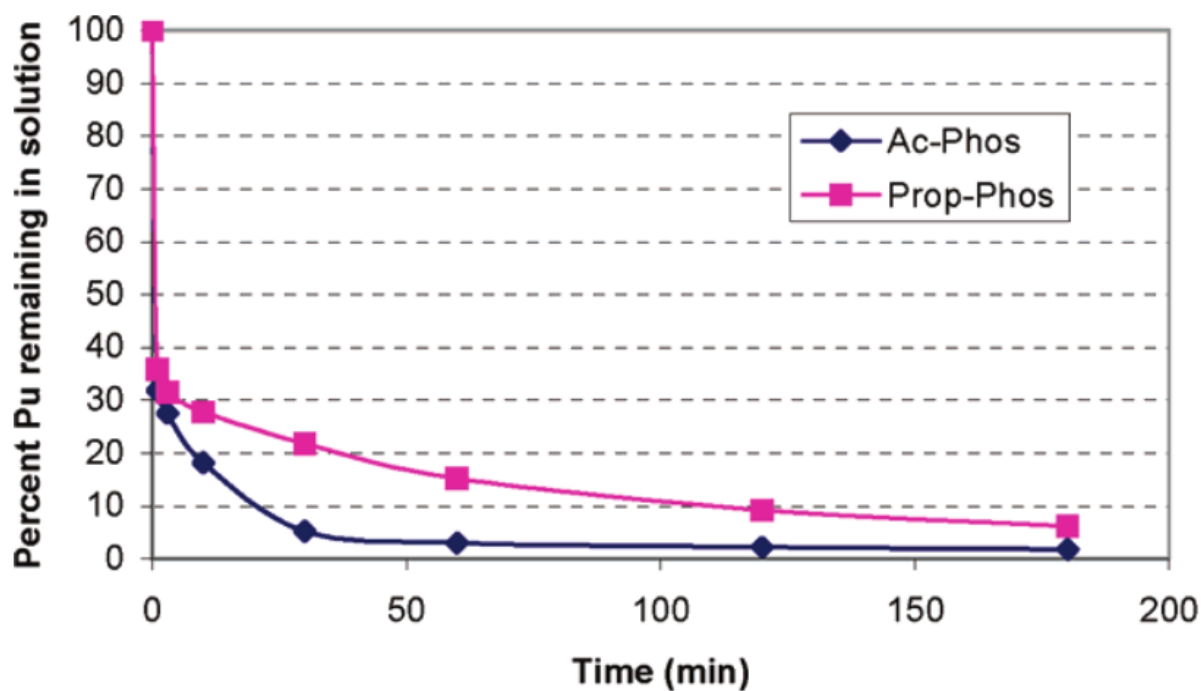


Figure 6 – Kinetics of Pu(IV) sorption using the phosphonate ester SAMMS.<sup>14</sup> The structures of these are given in Figure 4 and Figure 5.

Figure 6 shows a kinetics study for the sorption of Pu(IV) for the Ac-Phos and Prop-Phos SAMMS materials in both their acid and ester forms. It indicates that equilibrium is reached in 1-2 hours.<sup>14</sup> Similar investigations will be carried out on the materials produced in this thesis. These behaviours are important to be aware of so that novel materials are given optimum time in the solution. Comparisons with the literature also provide an invaluable reference when considering whether novel materials have shown significant gains in contribution to advancing this area.

Figure 7 illustrates further ligands that have been reported based on hydroxypyridinone and these have also been bound to the surface of SAMMS, again for actinide sequestration. Originally, it was agreed that the impending research would concentrate only on mono- or bidentate ligands. The result of this would be that ligands similar to those illustrated in Figure 7 would not be investigated. However, after collaboration with PhosphonicS Ltd, this



changed as samples were donated to the group for testing and a focus could be made on the ligand testing as opposed to synthesising functionalised materials.

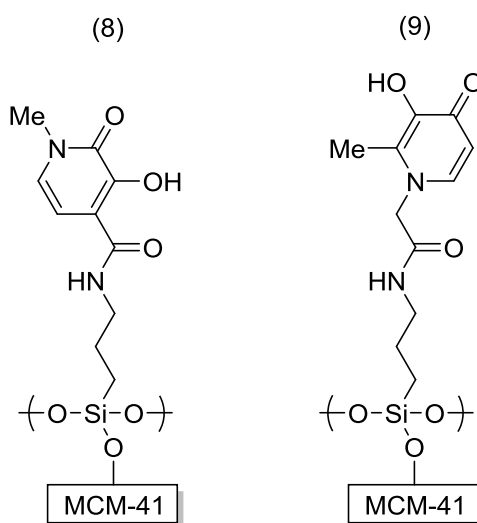


Figure 7 – Chemical structures of SAMMS with various organic groups synthesised by Fryxell *et al.*<sup>13</sup> for metal sequestration. (8) 3,2-HOPO SAMMS and (9) 3,4-HOPO SAMMS.

SAMMS are reported to have very good adsorbent properties which include: no suffering from solvent swelling, favourable kinetics for rapid sorption with their rigid, open pore structure, high functional density easily installed due to their enormously high surface area, and finally, being silica based, obviously makes them compatible with vitrification techniques for dealing with wastes. Rapid sequestration of U(VI), Np(V) and Pu(IV) was reportedly observed with very little competition from transition metal cations and common species.<sup>13</sup>

The class of tetrahydroxamate ligands that were developed by Gopalan *et al.*<sup>11</sup> and displayed good ability to bind to actinide ions in solution are illustrated in Figure 8. Encouraging results were reported when the ligands were evaluated for their binding ability to Pu(IV). They showed that both the *meta* and *para* tetrahydroxamate chelators bound to plutonium very strongly as well as showing selectivity for Pu(IV) over Fe(III).

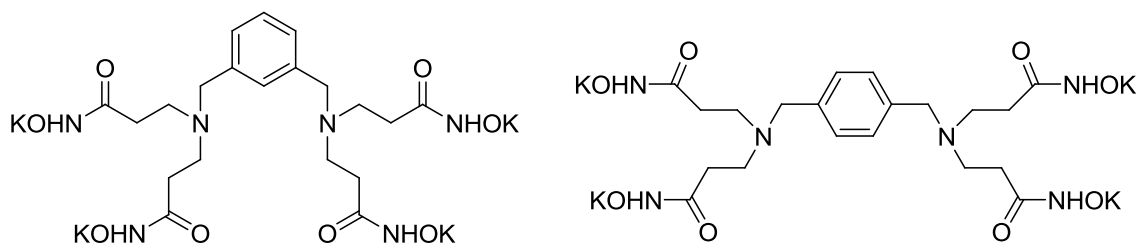


Figure 8 – Tetrahydroxamate ligands reported by Gopalan *et al.*<sup>11</sup>

As well as ligands, the literature on polymers is just as important, especially when considering the potential surface area increase. Some polymers may be produced from monomers that are naturally suited for metal binding and others may need modification/functionalisation with ligands such as those discussed to increase their efficiency. Polymers that have been reported for metal binding purposes are introduced below and help to explain the reasoning for the structures chosen as part of the forthcoming research in the following chapters.

### **1.1.2 Polymers and surface attached polymers for metal removal**

Polymers that chelate to metals are the basis of a number of successful industrial separations including the removal of calcium to very low levels from brine and the removal of radioactive caesium from alkaline waste waters.<sup>11,24,25</sup> Whilst both cyclic and acyclic backbones for anchoring ligand moieties should be considered, in some cases the greater stereochemical freedom of linear backbones can lead to more effective chelation.<sup>26</sup>

Geckeler *et al.*<sup>25</sup> described three general requirements which polymers as chelating agents should comply with. These are:

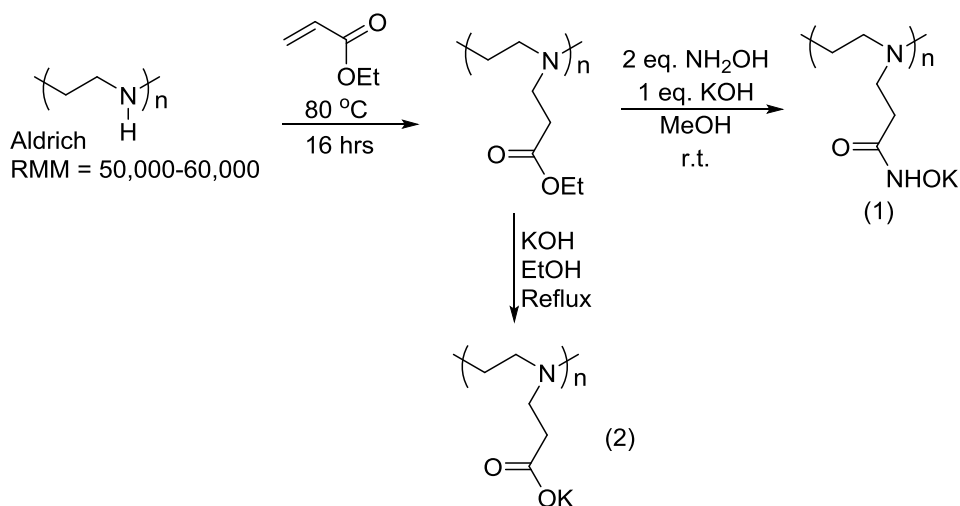
- 1) Sufficient solubilising power of the constitutional repeating unit which provides water-solubility of the polymer complexes.
- 2) A large number of functional groups of the complexing agent for a high capacity.
- 3) A high molecular weight which allows an easy separation by common methods from the metal not bound to the polymer.

As well as the ligands reported prior to this section, Gopalan *et al.*<sup>11</sup> reported the design, synthesis and evaluation of polyhydroxamate chelators for selective complexation of actinides. One of the main goals for their research was to develop ‘polymer supported ion specific extraction systems’ for the removal of actinides along with other hazardous metal ions from waste waters. They reported that water soluble and water insoluble polymers had been synthesised by attaching ligands to polymeric backbones and the abilities to selectively remove target metal ions was reported.

Gopalan *et al.*<sup>11</sup> describe how cost effective and efficient methods are required to selectively remove contaminating metals from groundwaters and waste streams to reduce the amount of non-radioactive and non-toxic material that is collected with those that are, but also to reduce the levels in order to meet stringent regulatory limits along with decreasing waste disposal

costs – supporting the research reported in this thesis. The authors of the paper also raise the important point on how technology needs to be developed to remove insoluble actinides from soils and contaminated equipment to reduce the amount of material being stored in the nuclear waste repositories.

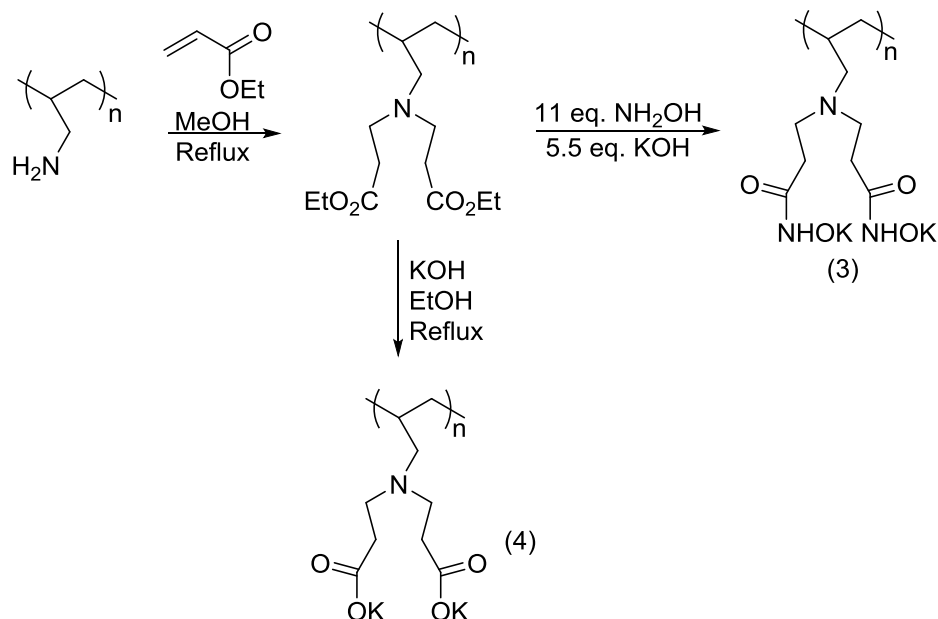
The synthesis of the polymers that were created as part of Gopalan's work are illustrated and discussed below with the first being in Scheme 1.



**Scheme 1 – Synthesis of water soluble polymeric chelators (1) and (2) reported by Gopalan *et al.*<sup>11</sup>**

Scheme 1 demonstrates the simple preparative route for the formation of the water soluble hydroxamates polymer (1) and the carboxylate analogue polymer (2) from polyethyleneimine. The hydrophilic backbone provides this water soluble property and is available in a wide range of molecular weights from commercial sources.<sup>11</sup>

The synthesis of water soluble hydroxamate polymer (3) and the carboxylate analogue (4) from commercially available polyallylamine has also been reported by the same group and the synthetic route for these new chelating polymers are described in Scheme 2.



**Scheme 2 – Synthesis of water soluble polymeric chelators (3) and (4) reported by Gopalan *et. al.*<sup>11</sup>**

Water insoluble polymers that contain preorganised ligand groups for selective actinide ion binding have also been synthesised by Gopalan *et al.*<sup>11</sup> The polymers illustrated in Figure 9 were being evaluated for their ability to remove target metal ions. Initial analysis of polymer (1) in Figure 9 was achieved in 1995<sup>11,27</sup> and its binding properties with plutonium show very promising results. It has been reported that approximately 98 % of  $\text{Pu(IV)}$  was removed from a solution of 0.1 M nitric acid and dilute sample of  $\text{Pu(IV)}$  solution when a sample (of undisclosed quantity) of this polymer was in contact with the solution for just 30 min. These limited experimental conditions were all that were reported, resulting in any comparable work impossible.

Both nitrogen and oxygen atoms are known to be good for metal ion binding due to the lone pairs of electrons. In this respect, these structures resemble the monomers, polymers and ligands that will be designed and tested as part of the results and findings within this thesis.

Figure 9 illustrates three further water insoluble polymeric chelators reported as part of the research. Polymer (3), polyallylamine amidoxime has shown to be quite effective when binding with uranyl ions across the acidic pH range and this is illustrated in Figure 10.

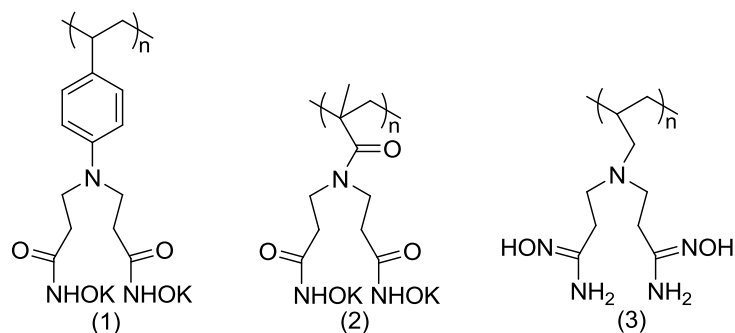


Figure 9 – Water insoluble polymeric chelators reported by Gopalan *et al.*<sup>11</sup>

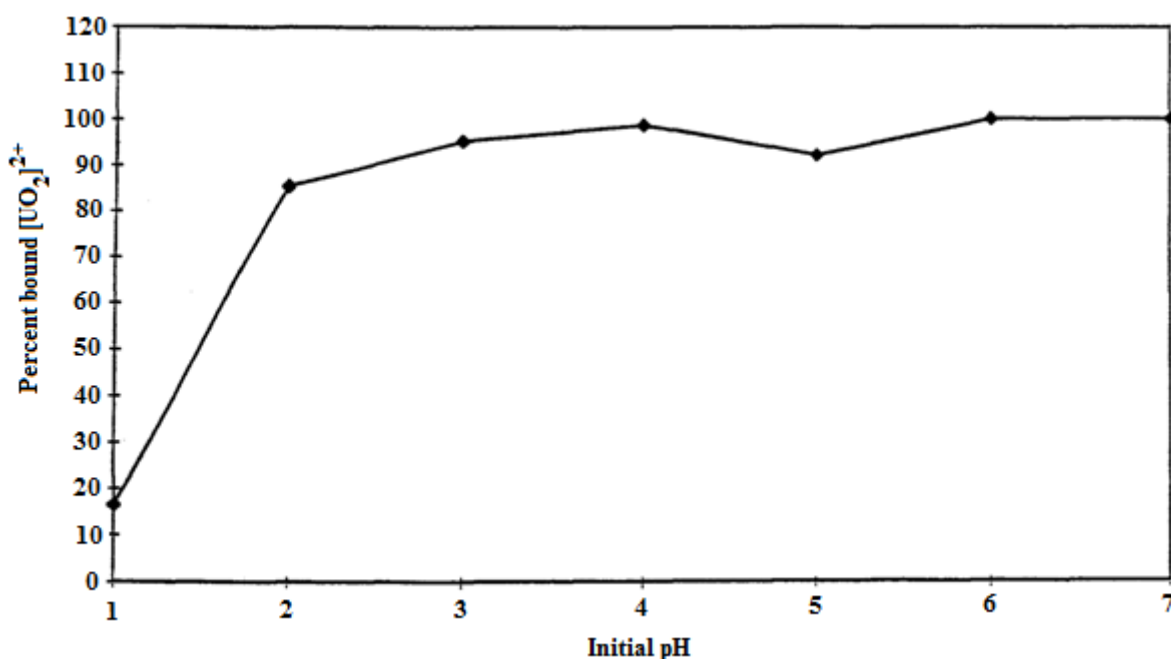
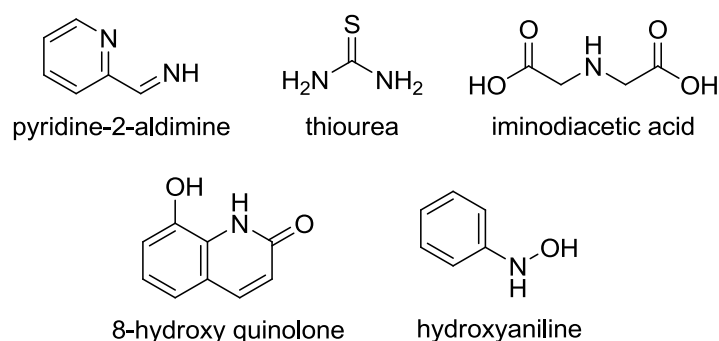


Figure 10 – Percentage of  $[UO_2]^{2+}$  bound to polymer (3) in Figure 9 as a function of pH.<sup>11</sup> Above pH 2, greater than 85 % of the uranyl ion was removed from solution whilst at pH 4, almost 100 % removal is observed. No errors for data points are presented.

Figure 10 demonstrates a range of pHs that show the amine group to be effective within. Although optimum pH is observed to be approximately pH 4, 85 % removal is observed from pH 2-7 – an encouraging result as this shows quite a large range of conditions where results can be targeted with other ligands and polymers. The proposed work would aim to improve materials like this by surface attachment to silica, enabling them to be vitrified for long term storage of radionuclide waste storage.

Geckeler *et al.*<sup>25</sup> have reported the preparation and application of water soluble polymer-metal complexes. A series of water soluble polymers with a range of chelating groups for the complex formation with various metals was investigated. It was reported that the

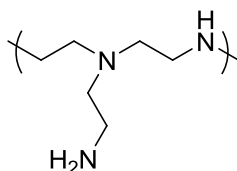
introduction of chelating groups such as pyridine-2-aldimine, thiourea, iminodiacetic acid, 8-hydroxy quinolone, and hydroxyaniline (illustrated in Figure 11) demonstrated good selectivity for metal ions including, cobalt, nickel, copper, cadmium, palladium, mercury, silver, gold and platinum. Cobalt, nickel, copper and cadmium ions are investigated thoroughly in chapter 6 whilst selectivity of ligands over these ions and others are considered in chapter 7. These ligands provided good background knowledge for structures to consider, increasing the probability of positive results and metal ion sequestration when investigations were carried out.



**Figure 11 – Structures discussed above for improvement of selectivity for metal ions.**

Water solubility is achieved by a high content of hydrophilic groups existing in the compound, e.g. amino, hydroxyl, carboxyl, amide and sulfonic acid groups. Alternatively, hydrophilic groups could be used in the backbone of the polymer such as ether or imino groups.<sup>25</sup>

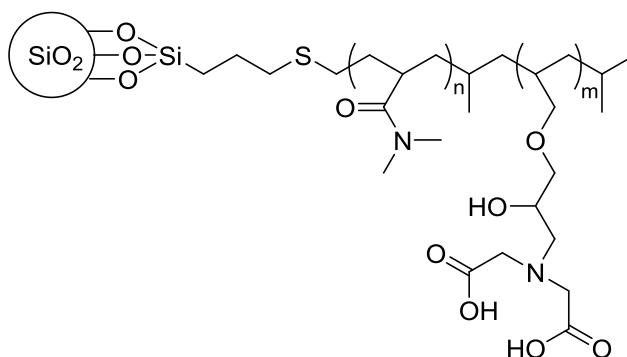
Poly(ethyleneimine) possesses a range of advantages as a polymer chelating agent including, good water solubility, high content of functional groups, good stability (chemically and physically) and suitable molecular weights. Commercially available poly(ethyleneimine) (polymin P, BASF) was used where ratios of primary, secondary and tertiary nitrogen atoms were equivalent (1:1:1) illustrated in Figure 12.



**Figure 12 – Poly(ethyleneimine), (Polymin P, BASF) with equivalent ratios of primary, secondary and tertiary nitrogen atoms.**

The complexes prepared from poly(ethyleneimine) could easily be isolated as dry powders which were not considered hygroscopic. One of the main results reported by Geckeler *et al.*<sup>25</sup> for 1 g of poly(ethyleneimine) was the binding of 0.37 g of copper, which was in agreement with Irving *et al.*<sup>28</sup> where ions of higher valence were found to be less strongly bound. The NH<sub>2</sub> group at the end of the side chain would make this polymer an ideal candidate for grafting from a surface as little or no modification would be required based on the literature reported with amino groups and metal binding.

An iminodiacetic acid-containing polymer, grafted onto silica gel was reported by Panahi *et al.*<sup>29</sup> This material was produced *via* a free radical co-polymerisation (a process explained in chapter 4 where more relevant) of N,N-dimethylacrylamide (DMAA) and a functional monomer containing the metal chelating group, 1-(N,N-bis-carboxymethyl)amino-3-allylglycerol, onto a silica surface that had previously been functionalised with (3-mercaptopropyl)trimethoxysilane (MPTMS). The material (known as poly(AGE/IDA-co-DMAA)-grafted silica gel) was studied for the preconcentration and determination of trace amounts of Cu(II) ions in environmental water samples. The sorption capacity was reported to be 32.3 mg g<sup>-1</sup> and its structure is illustrated in Figure 13.



**Figure 13 – Chemical structure of poly(AGE/IDA-co-DMAA)-grafted silica gel produced by Panahi *et al.*<sup>29</sup>**

Although the approach to this material is very closely related to that carried out in this thesis, post-polymerisation modification is not considered and neither were radionuclides nor heavier metals as a target species. The group successfully carried out fifteen sorption-desorption cycles without any significant change in sorption capacity using 0.5 mol L<sup>-1</sup> nitric acid to wash the material following metal uptake. This shows how stable the functionalised silica materials can be and helps justify this work for heavier metals.

Metal sorption by the grafted silica at different pH values were determined using a batch equilibrium technique – the optimum pH was reported to be 5.5 (Figure 14) where a maximum recovery of 95.4 % Cu(II) was achieved from a 10 ppm solution.

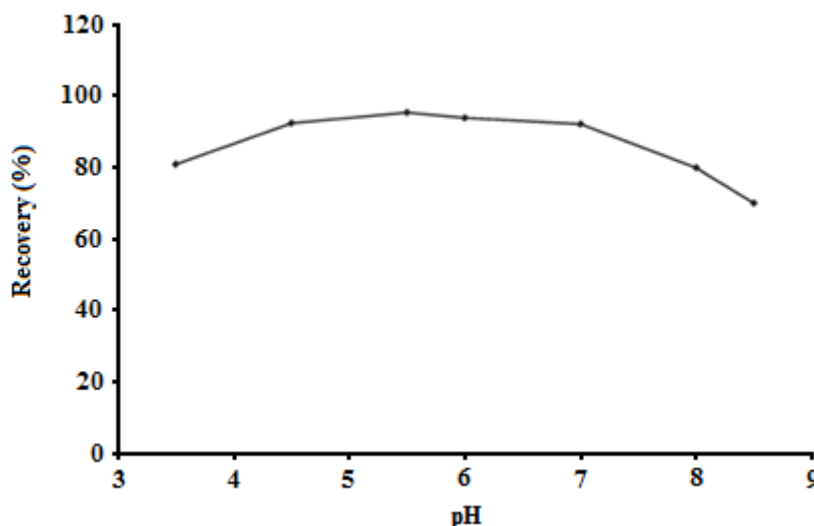


Figure 14 – Effect of pH on the sorption of Cu(II) on poly(AGE/IDA-co-DMAA)-grafted silica gel.<sup>29</sup>

The very high Cu(II) uptake on this sorbent reflects good accessibility of the chelating sites in the poly(AGE/IDA-co-DMAA)-grafted silica gel. Once more, a good recovery is observed across a wide pH range similar to that reported by Gopalan *et al.*<sup>11</sup>, restating that recovery should be achievable in a wide ranging set of conditions. This material would have benefitted greatly from selectivity testing and an environment where radionuclides are present to indicate how capable this and similar materials would be – something this thesis studies with its materials.

In 2006, Liu *et al.*<sup>30</sup> reported the successful grafting of polyacrylamide from the surfaces of the organo-modified fibrillar clay, attapulgite. This was carried out *via* the copper-mediated surface-initiated atom transfer radical polymerisation (SI-ATRP) technique in water. This process enables the grafting of polymer from a surface by generating a radical at the surface to react with an unsaturated monomer and is discussed in much more detail in chapter 4 where directly relevant to the work that was carried out in this project. The product, known as ‘polyacrylamide grafted attapulgite’ was characterised using elemental analysis, FTIR, TGA and TEM before preliminary tests were made to use the material as an adsorbent for removal of the metal ion Hg(II). It was anticipated that the problem of complete removal of water soluble polymers would be overcome by the polymer chain being chemically bonded to the clay’s surface. The authors reported a better dispersibility in water and it was found that



the material also had a higher adsorption capacity towards the Hg(II) ion although exactly how much better is unclear from the literature.

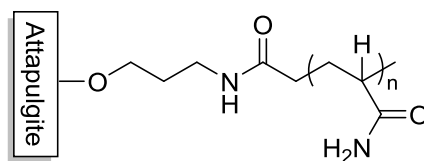


Figure 15 – Chemical structure of polyacrylamide grafted attapulgite synthesised by Liu *et al.*<sup>30</sup>

Although Hg(II) was not investigated in this thesis, the methodology of using SI-ATRP has shown to be an appropriate technique for modifying surfaces for metal ion removal and is a technique that was utilised to graft polymers to the surface of silica materials. Clays were not investigated either, but the initial idea to have a versatile modular system in which pieces of the ‘tool box’ could be swapped and changed, shows that a silica surface could be replaced for a material such as attapulgite.

## 1.2 Summary

The literature reported in this review has been narrowed to that closely related to the project idea as a whole. Further literature is used to introduce specific areas of the project in more depth in the relevant chapters whilst previous workers results are used throughout the thesis to compare findings and results where appropriate.

The use of ligands and polymers can create very effective materials for removing metal ions from aqueous solutions. If a metal ion is known to have a good affinity for a particular ligand, the selectivity will remain when attached to polymer chains but the large number of repeat units will allow a higher quantity of ions or radioactive isotopes to be removed.

The literature available has proven to be extremely valuable, provided a good understanding of previous work and how this can be built upon. It is clear that although research has already been reported, room still remains for rewarding and novel results to be collected along with significant contributions to be made to this area.

‘SAMMS’ have good attributes that allow them to be highly effective sorbents along with enabling their chemistry to be tuned to selectively sequester a specific target species including but not limited to heavy metals, tetrahedral oxometalate anions and radionuclides.<sup>7,13,14,23</sup> As previously stated, these materials are not specifically investigated in this thesis, however the surface chemistry that will be carried out is very similar. It is

anticipated that a range of ligands will be tested and found to be as successful as the research on 'SAMMS' has been found to be.

The many reports published with SAMMS and other silica materials suggest that silica is a practical solid support for the modular process intended for this work. Although perhaps not suitable for alkaline conditions above pH 9<sup>31</sup>, its surface allows straight forward chemistry to be carried out to synthesise a material much more functional than its natural form.

The work reported on polymers also provides good literature on methodology and more is provided where relevant in chapter 4. The range in which data is reported will make it difficult to make direct comparisons of material behaviours with some opting for percentages, others  $K_d$  values whilst others still have reported a direct reduction in concentration. The high percentages of metal removal may sound outstanding with figures of over 98 % removal but with an unknown amount of sample reported and  $K_d$  values not presented it is impossible to know how effective these materials really are.

## 2 Experimental

### 2.1 Instrumentation

#### 2.1.1 Infrared Spectroscopy

Infrared spectra were recorded using the UATR appliance for the majority, but where stated pressed KBr disks were used. They were measured in the range of 4000-380  $\text{cm}^{-1}$  on the UATR using a Perkin Elmer Spectrum 100 FT-IR Spectrometer.

#### 2.1.2 CHN Elemental Analysis

These were carried out at Loughborough University on a CHN CE-440 Elemental Analyser. All results are an average of three repeats carried out on the same batch. More information on this technique can be found at the start of chapter 5 where this technique is most relevant.

#### 2.1.3 Solution State NMR

$^1\text{H}$  and  $^{13}\text{C}$ -NMR spectra were recorded on a Bruker Avance spectrometer at 400 and 100 MHz, respectively. Samples were dissolved in  $\text{CDCl}_3$  (unless otherwise stated) using TMS (tetramethylsilane) as the internal reference at 0.0 ppm. Chemical shifts are quoted in ppm and coupling constants are measured in hertz which are quoted to the nearest 0.1 Hz.

#### 2.1.4 Solid State NMR

Solid state  $^1\text{H}$ ,  $^{13}\text{C}$  and  $^{29}\text{Si}$  NMR spectra were recorded using a Bruker Avance NMR spectrometer at 500, 125.7 and 99.3 MHz, respectively, equipped with a 4 mm MAS HX probe, a 100 W proton amplifier and a 500 W  $^{13}\text{C}$  amplifier. Cross Polarisation used a  $^1\text{H}$  pulse of 2 s (at -5.5 dB), a ramped-proton CP pulse of 2 ms (at -4.0 dB) and a carbon CP pulse of 2 ms (at -3.1 dB). TPPM15 ('two pulse phase modulation' – designed to greatly reduce the residual line widths arising from insufficient proton decoupling power in double resonance magic angle spinning (MAS) experiments<sup>32</sup>) proton decoupling was applied during the 30 ms acquisition time. Free induction decay (FIDs) contain 3000 data points which were Fourier transformed into 16000 data points. An exponential function of 20 Hz was applied to the FID using Bruker TOPSPIN(1.3) software. Spectra were referenced to external TMS ( $^1\text{H}$ ,  $^{13}\text{C}$ ,  $^{29}\text{Si}$ ) and the magic angle was set up using KBr. Magic angle spinning of 10 kHz was used and for CP-MAS  $^{29}\text{Si}$ , a relaxation delay of 10 s was used between each scan and DP-MAS  $^{29}\text{Si}$ , a relaxation of 300 s was used.

### 2.1.5 Mass Spectrometry

Where applicable, mass spectrometry was used to confirm product identity and these were run at Loughborough University using a Thermo Fischer Exactive with an ion max source and ESI probe fitted with Advion traversa nanomate.

### 2.1.6 ICP-OES

Samples were prepared by diluting down to ppm levels of concentration or in most cases, the work was carried out at 'ppm' levels so that dilutions were not required, and run on a Thermo Scientific iCAP 6000 series ICP Spectrometer in conjunction with a CETAC ASX-520 AutoSampler. 0.5 % HNO<sub>3</sub> acid was added to all the samples and a calibration graph was always made with solutions of known concentration run prior to the samples in question with the same plasma. This ensured the plasma was calibrated as accurately as possible. iTEVA ICP software was used to collect the data before being processed with a spread sheet package.

Statistical methods for assessing and comparing limits of detection are important and in general terms, the limit of detection (LOD) of an analyte may be described as the concentration which gives an instrument signal (y) significantly different from the 'blank' or 'background' signal. There is no full agreement between researchers, publishers and professional and statutory bodies on this point but there is an increasing trend to define the limit of detection as the analyte concentration giving a signal equal to the blank signal,  $y_B$ , plus three standard deviations of the blank,  $s_B$ .<sup>33</sup>

$$LOD = y_B + 3s_B$$

**Equation 2 – Limit of detection**

It is important to state that this definition is quite arbitrary and there may be occasions when an analyst is anxious to avoid the possibility of reporting the absence of the analyte when it is in fact present, but relatively unworried about the opposite error. Evidently, whenever a LOD is cited, the definition used to calculate it must also be provided (in this case, see Equation 2). Some attempts have been made to define a further limit – the limit of quantification (LOQ, sometimes referred to as limit of determination), which is regarded as the lower limit for precise quantitative measurements, as opposed to qualitative detection. A value of  $y_B$  plus ten standard deviations of the blank has been suggested for this limit, see Equation 3.<sup>33</sup>

$$LOQ = y_B + 10s_B$$

**Equation 3 – Limit of quantification**

Limits of detection and quantification for ICP-OES are reported in Table 2.

Element	Wavelength	Limit of Detection (ppm)	Limit of Quantification (ppm)
Mg	279.5	0.008	0.026
Al	167.0	0.009	0.031
Cr	283.5	0.011	0.036
Mn	257.6	0.013	0.043
Fe	259.9	0.089	0.298
Co	228.6	0.004	0.012
Ni	221.6	0.029	0.095
Cu	324.7	0.204	0.679
Zn	213.8	0.002	0.007
Cd	228.8	0.002	0.008
Se	196.0	0.019	0.062
Sb	206.8	0.010	0.035
Pb	220.3	0.011	0.037
Eu	381.9	0.063	0.210
Th	283.7	0.173	0.576
U	367.0	1.387	4.624

**Table 2 – Limits of detection and Limits of quantification for ICP-OES for elements reported in this work.**

More in-depth information on this technique can be found at the start of chapter 6.

### 2.1.7 ICP-MS

Samples were prepared by diluting down to ppb levels of concentration and run on an Agilent Technologies 7700 Series ICP-MS. Samples were prepared as described in section 2.1.6. This ensured the plasma was calibrated as accurately as possible. Limits of detection and quantification for ICP-MS are reported in Table 3.

Element	Isotope	Limit of Detection (ppb)	Limit of Quantification (ppb)
Co	59	0.062	0.207
Ni	60	0.049	0.162
Cu	63	0.425	1.418
Zn	66	0.321	1.068
Cd	111	0.031	0.103
Eu	153	0.437	1.458
U	238	0.092	0.307

**Table 3 - Limits of detection and Limits of quantification for ICP-MS for elements reported in this work.**

More in-depth information on this technique can also be found at the start of chapter 6.

### **2.1.8 Liquid Scintillation Counting**

Samples were prepared as described in the experimental and placed on a Packard 2100 TR Liquid Scintillation Analyser. All samples were given at least one hour in the machine before running them so that no natural light could interfere with the results and produce more accurate results. Gold Star, multipurpose liquid scintillation cocktail (meridian) was used for the measurement of beta emitters (only  $^{63}\text{Ni}$  in this work).

Quenching was checked for by the sample channels ratio method.<sup>34</sup> The detected counts are divided into channels based on their relative energies: the number of high energy counts (recorded in the 'B' channel) is compared to the number of low energy counts (recorded in the 'A' channel). The ratio (calculated as  $B/A$  or  $B/(B+A)$ ) will change if the sample is quenched. Quenching reduces the intensity of each light pulse, so counts will appear to be of lower energy. This will shift counts from high to low energy channels, and decrease the channels ratio.<sup>35</sup> No quenching was observed in these checks and therefore quench correction of the measurements was not required. More information on this technique can be found at the start of chapter 6.

### **2.1.9 Gamma Counting**

Samples were prepared as described in the experimental and placed in racks onto a Packard COBRA II AUTO-GAMMA. A counting channel with a range between the associated keV for the isotopes used was prepared. These isotopes and ranges are discussed within the work

but include  $^{57}\text{Co}$ ,  $^{109}\text{Cd}$  and  $^{152}\text{Eu}$ . Again, more information on this technique can be found at the start of chapter 6.

#### **2.1.10 Malvern Mastersizer 2000**

The Malvern Mastersizer 2000 was used to measure the particle size of the samples donated to the group by PhosphonicS Ltd. This enabled comparisons to be made between these samples and the silica materials synthesised in this work. The Mastersizer 2000 uses the technique of laser diffraction to measure the size of particles. It does this by measuring the intensity of light scattered as a laser beam passes through a dispersed particulate sample. This data is then analysed to calculate the size of the particles that created the scattering pattern.<sup>36</sup> Results can be found in Appendix 3 – Particle size of PhosphonicS Ltd samples.

#### **2.1.11 Freeze Drier**

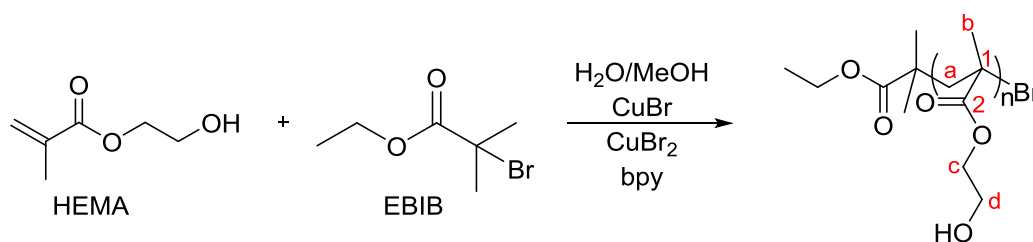
Polymers that were dried using the freeze drier were done so on a VirTis Benchtop ‘K’ Series SLC freeze drier, capable of condenser temperatures from  $-55^{\circ}\text{C}$  to  $-105^{\circ}\text{C}$ .

This process extracts moisture from the products *via* sublimation. The freeze drier creates a low-pressure zone to allow moisture to flow easily from the product. Since vapour naturally travels toward cooler surfaces, the condensing chamber is cooled to at least  $15^{\circ}\text{C}$  below that of the product to attract product moisture.<sup>37</sup> This process is preferred to rotary evaporators where warming or heating is involved to reduce the risk of cross-linking the polymer.

#### **2.1.12 Chemicals**

All chemicals were used as received and purchased from Sigma Aldrich unless otherwise indicated.  $\text{Cu(I)Br}$  and  $\text{Cu(II)Br}$  were stored in a vacuum desiccator.

## 2.2 Synthesis of PHEMA *via* ATRP



Scheme 3 – Synthesis of free PHEMA *via* ATRP

This synthesis was carried out using a similar method to Armes *et al.*<sup>38</sup> To a deoxygenated solution (achieved by bubbling nitrogen gas through the solution for 10 mins) of 2-hydroxyethyl methacrylate (HEMA, 97 %, 20 mL, 0.16 mol) in water (10 mL) and methanol (10 mL), CuBr (216 mg, 1.51 mmol), CuBr<sub>2</sub> (34 mg, 0.15 mmol) and bpy (576 mg, 3.69 mmol) were dissolved under a flow of nitrogen gas. Ethyl  $\alpha$ -bromoisobutyrate (EBIB, 0.22 mL, 1.52 mmol) was injected into the solution and polymerisation was left to commence overnight in a nitrogen atmosphere. As polymerisation commenced, an exothermic reaction occurred.

To purify, a large sintered glass column was prepared by packing down a thin layer of celite followed by a slurry of silica in methanol. To this, the viscous polymer solution, dissolved in methanol (500 mL) was pulled through under vacuum and repeated three times.

The eluent was poured into diethyl ether (400 mL) under vigorous stirring, causing the polymer to precipitate instantly and agglomerate. The solvent was decanted off and the polymer was dried on a freeze drier. This was ground down using a mortar and pestle which broke up the dry polymer very easily to leave a white solid (8.48 g, 39 % conversion).

**NMR:**  $\delta_H$ (400MHz, MeOD) 4.04(2H, bs,  $\underline{CH_2}OCO$ , **c**), 3.78(2H, bs,  $\underline{CH_2}OH$ , **d**), 2.02-1.61(2H, bd,  $\underline{CH_2}C$ , **a**), 1.01-0.94(3H, bd,  $\underline{CH_3}C$ , **b**)

$^{13}C$  (100MHz, MeOD) 17.8-19.9( $CH_3$ , **b**) 46.3-46.7(C, **1**) 53.6-55.8( $CH_2$ , **a**) 60.9-61.0( $CH_2$ , **d**) 68.04( $CH_2$ , **c**) 178.9-180.0(CO, **2**)

**FTIR:** 1727  $cm^{-1}$

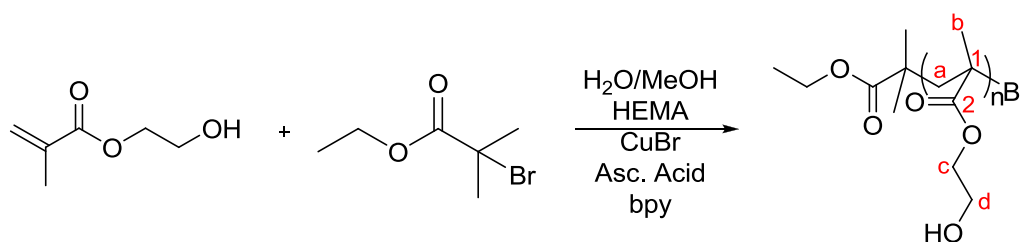
**Elemental Analysis (CHN): (Based on DP = 43, Mw = 5596 as calculated in 3.2.1.2)**

Calculated: %C = 54.8, %H = 7.7, %N = 0, %O = 36.2, %Br = 1.4

Actual: %C = 54.1, %H = 7.6, %N = 0.1, %R = 38.2



## 2.3 Synthesis of PHEMA via ARGET ATRP



**Scheme 4 – Synthesis of free PHEMA via ARGET ATRP**

To a deoxygenated solution of HEMA (97 %, 20 mL, 0.16 mol) in water (10 mL) and methanol (10 mL), CuBr (8 mg, 0.036 mmol), ascorbic acid (100 mg, 0.56 mmol) and bpy (12.2 mg, 0.078 mmol) were dissolved under a flow of nitrogen gas. EBIB (0.22 mL, 1.52 mmol) was injected into the solution and polymerisation was left to commence overnight in a nitrogen atmosphere. As polymerisation commenced, an exothermic reaction occurred.

To purify, a large sintered glass column was prepared by packing down a thin layer of celite followed by a slurry of silica in methanol. To this, the viscous polymer, dissolved in methanol (500 mL) was pulled through under vacuum and repeated three times.

The crude product was purified as described in section 2.2, leaving a white solid (14.07 g, 65 % conversion).

**NMR:**  $\delta_H$ (400MHz, MeOD) 4.04(2H, bs,  $\underline{CH_2}OCO$ , **c**), 3.78(2H, bs,  $\underline{CH_2}OH$ , **d**), 2.02-1.61(2H, bm,  $\underline{CH_2}C$ , **a**), 1.01-0.94(3H, bd,  $\underline{CH_3}C$ , **b**)

$^{13}C$  (100MHz, MeOD) 17.8-19.9( $CH_3$ , **b**) 46.3-46.7(C, **1**) 53.6-55.8( $CH_2$ , **a**) 60.9-61.0( $CH_2$ , **d**) 68.04( $CH_2$ , **c**) 178.9-180.0(CO, **2**)

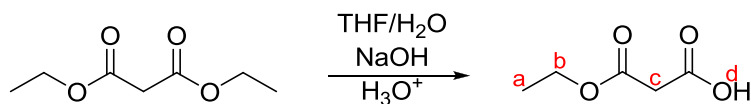
**FTIR:** 1728  $cm^{-1}$

**Elemental Analysis (CHN): (Based on DP = 72, Mw = 9370 as calculated in 3.2.1.2)**

Calculated: %C = 55.0, %H = 7.7, %N = 0, %O = 36.5, %Br = 0.8

Actual: %C = 53.4, %H = 7.5, %N = 0.2, %R = 38.9

## 2.4 Synthesis of 3-ethoxy-3-oxopropanoic acid



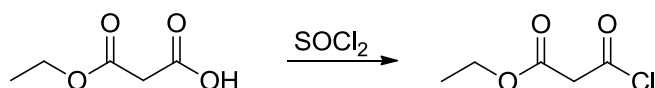
Scheme 5 – Synthesis of 3-ethoxy-3-oxopropanoic acid

This synthesis was carried out using a similar method to Niwayama *et al.*<sup>39</sup> To a solution of water (200 mL) and tetrahydrofuran (THF, 50 mL), diethyl malonate (5 g, 0.0312 mol) was added and cooled to 0 °C. NaOH solution (0.25 M, 125 mL) was added dropwise and stirred for 45 m before the solution was acidified to ca. pH 2 with HCl (1 M) whilst maintaining 0 °C. The reaction was immediately saturated with NaCl and extracted with ethyl acetate (3 × 200 mL). The solution was dried with Na<sub>2</sub>SO<sub>4</sub> and solvent removed *in vacuo*. Purification by silica gel column chromatography eluting with petrol:ethyl acetate (3:1 vol) gave the colourless/yellow liquid product (2.76 g, 67 %).

**MS (m/z):** Found: *m/z* 155 (100%), Calculated for *m/z* C<sub>5</sub>H<sub>8</sub>O<sub>4</sub>Na<sup>+</sup>

**NMR:** δ<sub>H</sub>(400MHz, CDCl<sub>3</sub>) 10.15(1H, bs, COH, **d**), 4.27-4.22(2H, J=6.8Hz, t, CH<sub>3</sub>CH<sub>2</sub>, **b**), 3.45-3.44(2H, J=3.2Hz, s, COCH<sub>2</sub>CO, **c**), 1.32-1.25(3H, J=7.2Hz, t, CH<sub>2</sub>CH<sub>3</sub>, **a**)

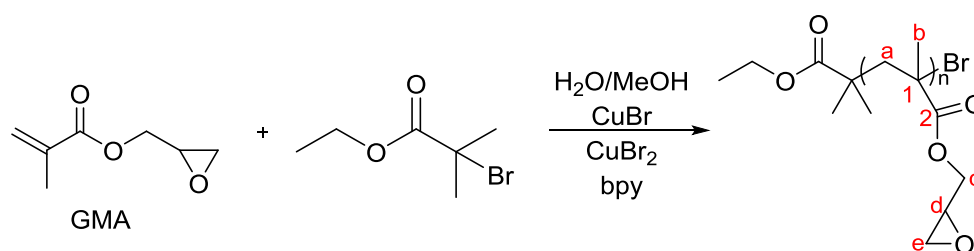
## 2.5 Synthesis of ethyl malonyl chloride



Scheme 6 – Synthesis of ethyl malonyl chloride

To a solution of mono-ethyl malonate (1.25 g, 9.44 mmol) excess thionyl chloride (3 mL) was added. The reaction refluxed overnight with continuous stirring. The thionyl chloride was removed by rotary evaporation. Following this, the product was immediately used for the attachment to the polymer. This synthesis is described in ‘2.6 Synthesis of free PHEMA with ethyl malonyl chloride’.

## 2.6 Synthesis of free PGMA *via* ATRP



Scheme 7 – Synthesis of free PGMA *via* ATRP

This synthesis was carried out using a similar method to Edmondson.<sup>40</sup> To a deoxygenated solution of glycidyl methacrylate (GMA, 10.0 g, 70.4 mmol) in water (10 mL) and methanol (10 mL), CuBr (61 mg, 0.43 mmol), CuBr<sub>2</sub> (8.2 mg, 0.04 mmol) and bpy (196 mg, 1.26 mmol) were dissolved under a flow of nitrogen gas. EBIB (6.2  $\mu$ L, 0.42 mmol) was injected into the solution and polymerisation was left to commence overnight in a nitrogen atmosphere. As polymerisation commenced, an exothermic reaction occurred.

To purify, the product was dissolved in dichloromethane (DCM, 200 mL) and poured into a separating funnel containing distilled water (200 mL). The water changed to a blue/green colour whilst the DCM was white.

The DCM extract was poured into cold methanol (200 mL) where the polymer precipitated as a white rubbery solid. The solvent was decanted off and the polymer was dried on a freeze drier to leave a white solid. This was ground down using a mortar and pestle which broke up the dry polymer very easily to leave a white solid (6.98 g, 69 %).

**NMR:**  $\delta_H$ (400MHz, CDCl<sub>3</sub>) 4.30(1H, bs, CH<sub>2</sub>O, c), 3.84-3.80(1H, bs, CH<sub>2</sub>O, c), 3.23(1H, bs, CHCH<sub>2</sub>CO, d), 2.84(1H, bs, CH<sub>2</sub>O, e), 2.64(1H, bs, CH<sub>2</sub>O, e), 2.03-1.90(2H, bm, CH<sub>2</sub>C, a), 1.14-0.86(3H, bd, CH<sub>3</sub>C, b).

$^{13}C$  (100MHz, CDCl<sub>3</sub>) 16.8(CH<sub>3</sub>, b), 29.7(CH<sub>2</sub>, e), 44.7(CH<sub>2</sub>, a), 48.8-48.9(CH, d), 65.7-65.9(CH<sub>2</sub>, c), 128.0(C, 1), 177.2-178.2(CO, 2).

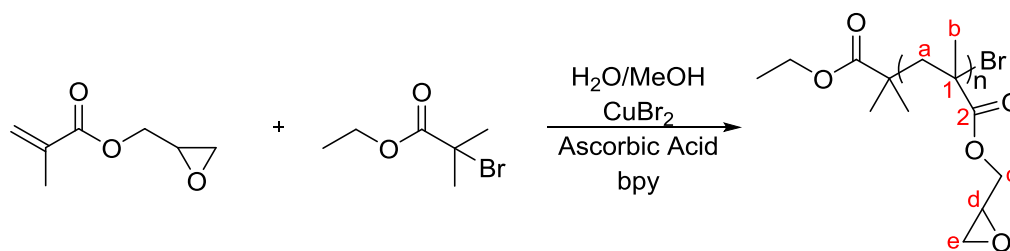
**FTIR:** 1723 cm<sup>-1</sup>, 1253 cm<sup>-1</sup>, 905 cm<sup>-1</sup>, 843 cm<sup>-1</sup>

**Elemental Analysis (CHN):** (Based on DP = 81, Mw = 11565 as calculated in 3.2.2.2)

Calculated: %C = 58.8, %H = 7.1, %N = 0, %O = 33.5, %Br = 0.5

Actual: %C = 58.4, %H = 6.9, %N = 0.1, %R = 34.6

## 2.7 Synthesis of free PGMA *via* ARGET ATRP



Scheme 8 – Synthesis of free PGMA *via* ARGET ATRP

To a deoxygenated solution of GMA (10.0 g, 70.4 mmol) in water (10 mL) and methanol (10 mL), CuBr<sub>2</sub> (4.7 mg, 0.021 mmol), ascorbic acid (67.1 mg, 0.38 mmol) and bpy (8.7 mg, 0.056 mmol) were dissolved under a flow of nitrogen gas. EBIB (5.4  $\mu$ L, 0.37 mmol) was injected into the solution and polymerisation was left to commence overnight in a nitrogen atmosphere. As polymerisation commenced, an exothermic reaction occurred.

To purify, the product was dissolved in DCM (200 mL) and poured into a separating funnel containing distilled water (200 mL). The water changed to a blue/green colour whilst the DCM was a white milky colour.

The crude product was purified as described in section 2.6, leaving a white solid (7.87 g, 78 %).

**NMR:**  $\delta_{\text{H}}$ (400MHz, CDCl<sub>3</sub>) 4.30(1H, bs, CH<sub>2</sub>O, c), 3.85-3.81(1H, bs, CH<sub>2</sub>O, c), 3.50-3.49(1H, bs, CHCH<sub>2</sub>CO, d), 2.84(1H, bs, CH<sub>2</sub>O, e), 2.64(1H, bs, CH<sub>2</sub>O, e), 1.97-1.90(2H, bm, CH<sub>2</sub>C, a), 1.10-0.94(3H, bd, CH<sub>3</sub>C, b).

$^{13}\text{C}$  (100MHz, CDCl<sub>3</sub>) 16.8(CH<sub>3</sub>, b), 29.7(CH<sub>2</sub>, e), 44.7(CH<sub>2</sub>, a), 48.8-48.9(CH, d), 65.7-65.9(CH<sub>2</sub>, c), 128.0(C, 1), 177.2-178.2(CO, 2).

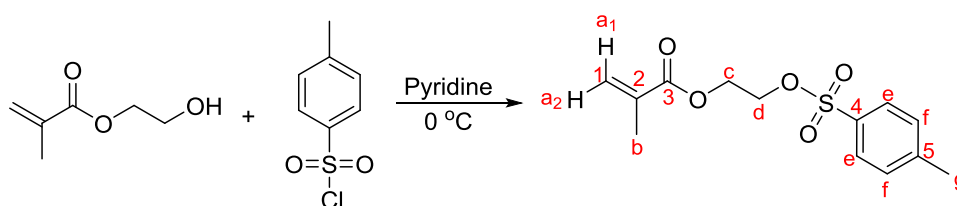
**FTIR:** 1723 cm<sup>-1</sup>, 1253 cm<sup>-1</sup>, 905 cm<sup>-1</sup>, 843 cm<sup>-1</sup>

**Elemental Analysis (CHN):** (Based on DP = 104, Mw = 14841 as calculated in 3.2.2.2)

Calculated: %C = 58.9, %H = 7.1, %N = 0, %O = 33.5, %Br = 0.5

Actual: %C = 58.4, %H = 6.9, %N = 0.1, %O = 34.6

## 2.8 Synthesis of tosylated HEMA



Scheme 9 – Synthesis of tosylated HEMA

This synthesis was carried out using a similar method to Stolle *et al.*<sup>41</sup> To a solution of pyridine (100 mL) at 0 °C, HEMA (10.01 g, 0.08 mol) and p-toluenesulfonyl chloride (22.12 g, 0.12 mol) were dissolved and stirred for 4 h.

The mixture was extracted by addition of DCM, followed by HCl (2M, 2 x 100 mL washes) and brine solution (2 x 100 mL). The DCM layer was dried over MgSO<sub>4</sub> and concentrated *in vacuo* to give the desired product as a colourless oil (13.30 g, 61 %).

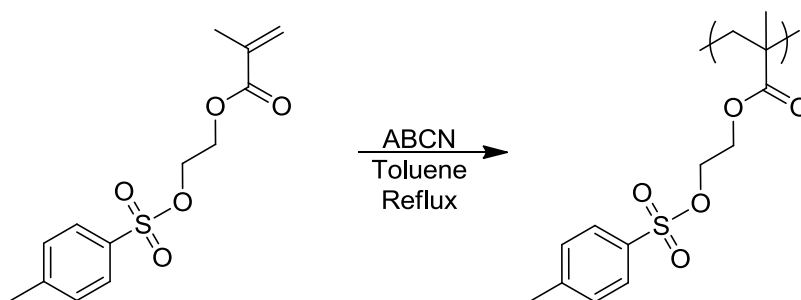
**MS (m/z):** Found: *m/z* 307 (100 %), Calculated C<sub>13</sub>H<sub>16</sub>O<sub>5</sub>SNa<sup>+</sup>

**FTIR:** 1720 cm<sup>-1</sup>, 1401 cm<sup>-1</sup>, 1177 cm<sup>-1</sup>

**NMR:** δ<sub>H</sub>(400MHz, CDCl<sub>3</sub>) 7.808-7.787(2H, d, ArH, e), 7.358-7.270(2H, d, ArH, f), 6.060(1H, s, CCH<sub>2</sub>, a<sub>1</sub>), 5.579(1H, s, CCH<sub>2</sub>, a<sub>2</sub>), 4.329-4.306(2H, t, CH<sub>2</sub>CH<sub>2</sub>, c), 4.267-4.251(2H, t, CH<sub>2</sub>CH<sub>2</sub>, d), 2.452(3H, s, ArCH<sub>3</sub>, g), 1.893(3H, s, CCH<sub>3</sub>, b).

<sup>13</sup>C (100MHz, CDCl<sub>3</sub>) 18.25(CH<sub>3</sub>, b), 21.65(CH<sub>3</sub>, g), 61.83(CH<sub>2</sub>, d), 67.69(CH<sub>2</sub>, c), 126.48(CH<sub>2</sub>, 1), 127.92(CH, e), 129.96(CH, f), 132.71(CH<sub>3</sub>CPh, 5), 135.53(CH<sub>3</sub>CCO, 2), 145.09(SO<sub>3</sub>CPh, 4), 166.82(CO, 2).

## 2.9 Synthesis of tosylated PHEMA *via* free radical polymerisation



Scheme 10 – Synthesis of tosylated PHEMA

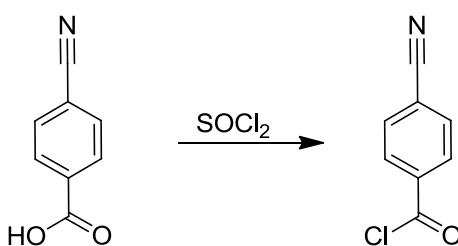
To a solution of toluene (25 mL), tosylated HEMA (HEMA-OTs, 5 g, 0.018 mol) and 1,1'-Azobis(Cyclohexanecarbonitrile, ABCN, ~50 mg) were added and dissolved before being stirred under reflux for 5 h.

Once the solution was heated (150 °C) a polymer gel was observed to precipitate out of solution. When the reaction was stopped, the toluene was decanted off and the polymer was left to dry overnight in a vacuum oven. The polymer was ground down using a mortar and pestle which broke up the dry polymer very easily resulting in a white product (3.56 g, 71 %).

The polymer was insoluble for NMR analysis but FTIR clearly showed no hydroxyl group and indicated the tosylate group was still attached.

**FTIR:** 1729  $\text{cm}^{-1}$ , 1356  $\text{cm}^{-1}$ , 1173  $\text{cm}^{-1}$

## 2.10 Synthesis of 4-cyanobenzoyl chloride

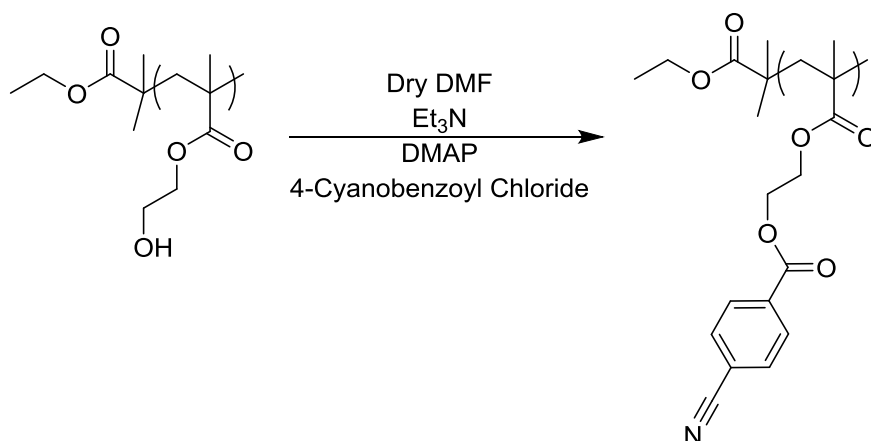


Scheme 11 – Synthesis of 4-cyanobenzoyl chloride

To a solution of thionyl chloride (30 mL), 4-cyanobenzoic acid (2.11 g, 0.014 mol) was added and stirred under reflux for 4 h.

This product was concentrated *in vacuo* and used immediately for the attachment to PHEMA.

## 2.11 Synthesis of 4-cyanobenzoyl chloride attachment to PHEMA



Scheme 12 – Synthesis of 4-cyanobenzoyl chloride attachment to PHEMA

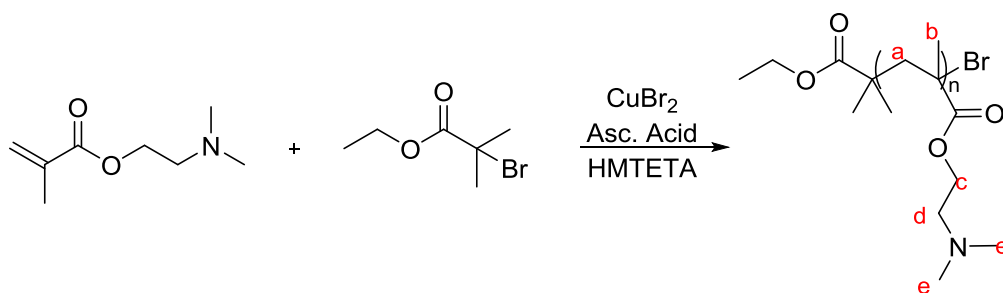
To a solution of dry DMF (20 mL) and Et<sub>3</sub>N (2 mL, 0.014 mol), 4-Dimethylaminopyridine (DMAP, 50 mg, 0.41 mmol) and PHEMA (0.5 g, 3.84 mmol) were dissolved and sealed under a nitrogen atmosphere. 4-cyanobenzoyl chloride (2.38 g, 0.014 mol) was then added to the solution and stirred for 1 h.

The product precipitated out in diethyl ether which was decanted off and the product was washed exhaustively with water, followed by diethyl ether. The product was transferred onto filter paper and dried *in vacuo*. The polymer was ground down using a mortar and pestle which broke up the dry polymer very easily to leave a light yellow coloured solid (0.52 g).

The polymer was insoluble for NMR analysis but FTIR analysis did show cyano- peaks to be visible.

**FTIR:** 2232 cm<sup>-1</sup>, 1699 cm<sup>-1</sup>

## 2.12 Synthesis of free PDMAEMA via ARGET ATRP



Scheme 13 – Synthesis of PDAEMA via ARGET ATRP

To a deoxygenated solution of 2-(dimethylamino)ethyl methacrylate (DMAEMA, 14 mL, 0.05 mol) in 2-propanol (14 mL) and water (0.7 mL),  $\text{CuBr}_2$  (7.4 mg, 0.033 mmol), ascorbic acid (58.1 mg, 0.330 mmol) and 1,1,4,7,10,10-hexamethyltriethylenetetramine (HMTETA, 44.7  $\mu\text{L}$ , 0.164 mmol) were dissolved under a flow of nitrogen gas. EBIB (55.6  $\mu\text{L}$ , 0.379 mmol) was injected into the solution and polymerisation was left to commence overnight in a nitrogen atmosphere. As polymerisation commenced, an exothermic reaction occurred.

To purify, a large sintered glass column was prepared by packing down a thin layer of celite followed by a slurry of silica in 2-propanol. To this, the viscous polymer, dissolved in 2-propanol (100 mL) was pulled through under vacuum and repeated three times.

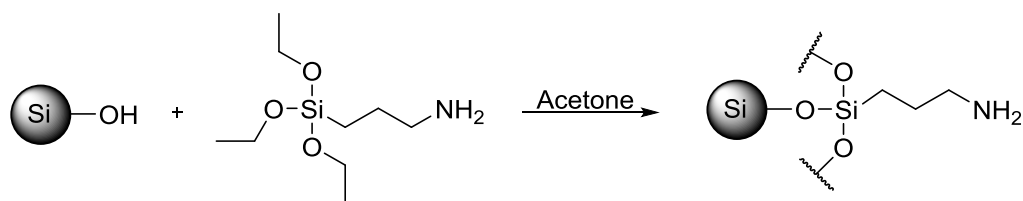
After failing to precipitate the product in a range of solvents, the product was obtained by removing the solvent *in vacuo*. The polymer was ground down using a mortar and pestle which broke up the dry polymer very easily to leave a light green coloured product (9.01g, 76 %).

**NMR:**  $\delta_{\text{H}}$ (400MHz, MeOD) 4.06(2H, bs,  $\text{CH}_2\text{O}$ , c), 3.29-3.26(3H, s,  $\text{CH}_3\text{C}$ , b), 2.62-2.59(2H, bs,  $\text{CH}_2\text{N}(\text{CH}_3)_2$ , d), 2.33-2.29(6H, s,  $\text{N}(\text{CH}_3)_2$ , e), 0.90(1H, bs,  $\text{CH}_2\text{C}$ , a).

**FTIR:**  $\nu$  2945  $\text{cm}^{-1}$ , 2821  $\text{cm}^{-1}$ , 2769  $\text{cm}^{-1}$ , 1722  $\text{cm}^{-1}$ , 1454  $\text{cm}^{-1}$ , 1392  $\text{cm}^{-1}$  agreeing with that reported by Gillies *et al.*<sup>42</sup> in their supporting information.



### 2.13 Deposition of APTES onto ZEOprep silica



Scheme 14 – Synthesis of APTES onto silica

To acetone (150 mL), ZEOprep 60 ECO silica gel; 40-63 micron (12.0 g) was added. The solution was heated to 60 °C before (3-aminopropyl)triethoxysilane (APTES, 30 mL, 0.13 mol) was added and stirred for 2 h. After this, the solution was poured into a sintered glass filter under vacuum and thoroughly washed with excess acetone. The product was then dried in vacuo to leave a cream coloured product (12.83 g).

**FTIR:**  $\nu$  1099  $\text{cm}^{-1}$ , 1643  $\text{cm}^{-1}$

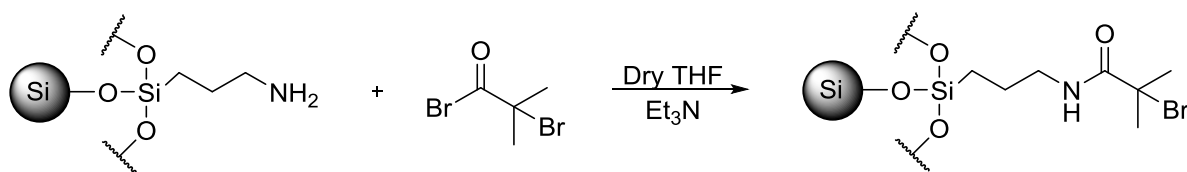
#### Elemental Analysis (CHN):

Calculated values unable to be determined, results given are actual results to illustrate the difference between the materials. All ZEOprep and fumed silica products are reported as seen below.

ZEOprep silica: %C = 0.04, %H = 0.3, %N = 0.04, %R = 99.6

APTES-functionalised ZEOprep silica: %C = 5.2, %H = 1.0, %N = 1.6, %R = 92.2

## 2.14 Deposition of BIBB onto APTES-functionalised ZEOprep silica



Scheme 15 – Deposition of BIBB onto APTES-functionalised ZEOprep silica.

To a suspension of APTES-functionalised ZEOprep silica (4.8 g) and dry THF (40 mL),  $\text{Et}_3\text{N}$  (13.2 mL, 9.49 mmol) was added under a nitrogen atmosphere and stirred at 0 °C. 2-bromoisobutyryl bromide (BIBB, 10 mL, 0.081 mol) was added dropwise with caution. A white vapour evolved instantly and the solution was left to stir for 30 m.

After this, the solution was poured into a sintered glass filter under vacuum, leaving the silica product. This was thoroughly washed with excess THF, methanol and water and repeated three times to purify the product. The product was transferred to a watch glass and dried in a vacuum oven for 30 min to ensure dryness, leaving the yellow coloured product (4.19 g).

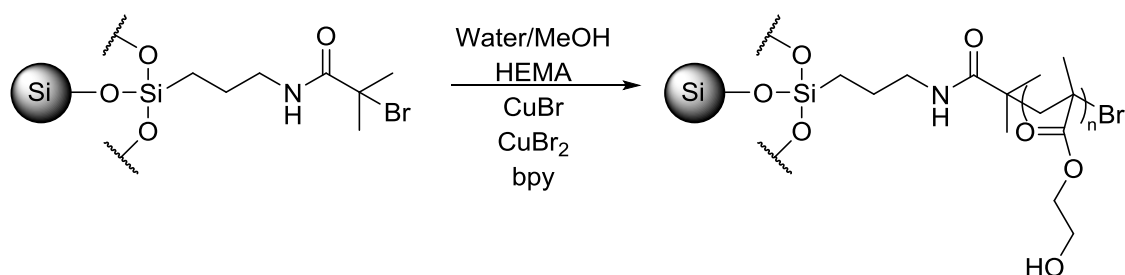
**IR:**  $\nu$  1057  $\text{cm}^{-1}$ , 1537  $\text{cm}^{-1}$ , 1648  $\text{cm}^{-1}$

### Elemental Analysis (CHN):

APTES-functionalised ZEOprep silica: %C = 5.2, %H = 1.0, %N = 1.6, %R = 92.2

BIBB-functionalised ZEOprep silica: %C = 9.4, %H = 1.6, %N = 1.5, %R = 87.6

## 2.15 Polymerisation of HEMA from BIBB-functionalised ZEOprep silica



**Scheme 16 – Polymerisation of HEMA from BIBB-functionalised ZEOprep silica.**

To a deoxygenated solution of HEMA (97 %, 5.0 g, 0.038 mol), water (2.5 mL) and methanol (2.5 mL), CuBr (54.9 mg, 0.38 mmol), CuBr<sub>2</sub> (9.1 mg, 0.041 mmol) and bpy (145.9 mg, 0.93 mmol) were dissolved under a flow of nitrogen gas.

BIBB-functionalised ZEOprep silica (0.52 g) was prepared in a second deoxygenated flask before the HEMA solution was injected in. Following this, the solution was agitated on a shaker for 3 d.

The solution was then poured into a sintered glass column under vacuum and thoroughly washed with water and methanol (1:1 v/v) to leave a cream coloured powder (0.53 g).

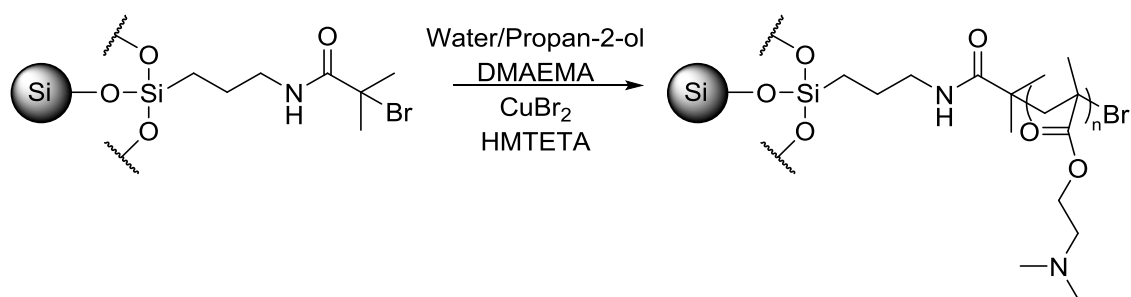
**FTIR:**  $\nu$  1079 cm<sup>-1</sup>, 1547 cm<sup>-1</sup>, 1647 cm<sup>-1</sup>, 1736 cm<sup>-1</sup>

### **Elemental Analysis (CHN):**

BIBB-functionalised ZEOprep silica: %C = 9.4, %H = 1.6, %N = 1.5, %R = 87.6

PHEMA functionalised ZEOprep silica: %C = 30.2, %H = 4.3, %N = 0.8, %R = 64.8

## 2.16 Polymerisation of DMAEMA from BIBB-functionalised ZEOprep silica



Scheme 17 – Polymerisation of DMAEMA from BIBB-functionalised ZEOprep silica.

To a deoxygenated solution of DMAEMA (98 %, 5 mL, 0.030 mol), water (0.5 mL) and propan-2-ol (9.5 mL),  $\text{CuBr}_2$  (8.0 mg, 0.035 mmol) and HMTETA (50  $\mu\text{L}$ , 0.184 mmol) were dissolved under a flow of nitrogen gas.

BIBB-functionalised ZEOprep silica (0.51 g) was prepared in a second degassed flask before the DMAEMA solution was injected in. Following this, the solution was agitated on a shaker for 3 d.

The solution was then poured into a sintered glass column under vacuum and thoroughly washed with water followed by propan-2-ol to leave a cream coloured powder (0.53 g).

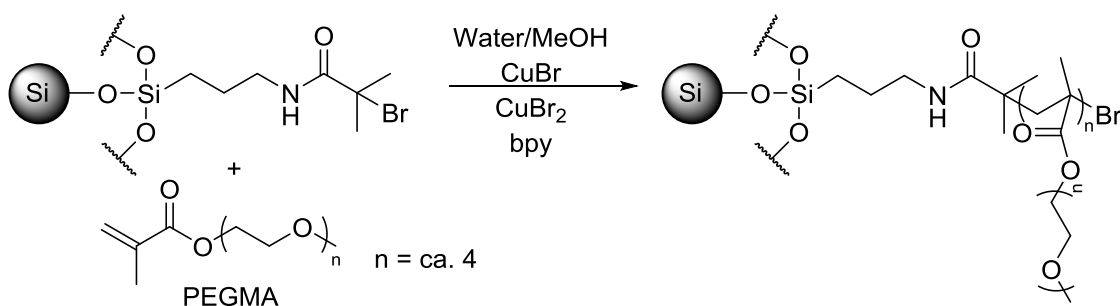
**FTIR:**  $\nu$  1040  $\text{cm}^{-1}$ , 1457  $\text{cm}^{-1}$ , 1534  $\text{cm}^{-1}$ , 1647  $\text{cm}^{-1}$ , 1727  $\text{cm}^{-1}$

### Elemental Analysis (CHN):

BIBB-functionalised ZEOprep silica: %C = 9.4, %H = 1.6, %N = 1.5, %R = 87.6

PDMAEMA functionalised ZEOprep silica: %C = 20.2, %H = 3.3, %N = 3.0, %R = 73.5

## 2.17 Polymerisation of PEGMA from BIBB-functionalised ZEOprep silica



**Scheme 18 – Polymerisation of PEGMA from BIBB-functionalised ZEOprep silica.**

To a deoxygenated solution of poly(ethylene glycol) monomethyl ether methacrylate (PEGMA, MW 300, 5.0 g, 0.017 mol), water (2.5 mL) and methanol (2.5 mL), CuBr (55.3 mg, 0.39 mmol), CuBr<sub>2</sub> (9.5 mg, 0.043 mmol) and bpy (150.6 mg, 0.96 mmol) were dissolved under a flow of nitrogen gas.

BIBB-functionalised ZEOprep silica (0.55 g) was prepared and added to the reaction. Following this, the solution was stirred for 2 h.

The solution was then poured into a sintered glass column under vacuum and thoroughly washed with water and methanol (1:1 v/v) to leave a dark yellow coloured powder (0.62 g).

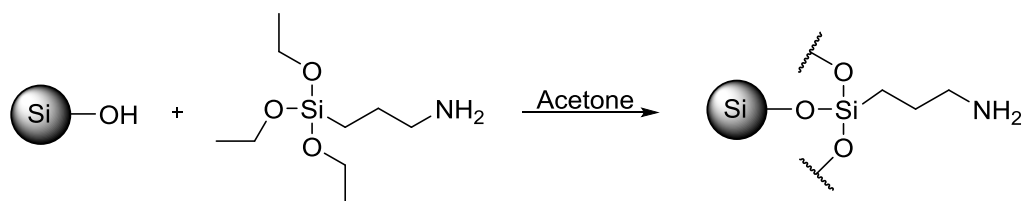
**FTIR:**  $\nu$  1043 cm<sup>-1</sup>, 1535 cm<sup>-1</sup>, 1649 cm<sup>-1</sup>, 1727 cm<sup>-1</sup>

### Elemental Analysis (CHN):

BIBB-functionalised ZEOprep silica: %C = 9.4, %H = 1.6, %N = 1.5, %R = 87.6

PEGMA functionalised ZEOprep silica: %C = 20.2, %H = 3.2, %N = 1.2, %R = 75.4

## 2.18 Deposition of APTES onto fumed silica



Scheme 19 – Deposition of APTES onto fumed silica.

To acetone (60 mL), fumed silica, 0.007 $\mu$ m (2.4 g) was added. The solution was heated to 60 °C before APTES (7 mL, 0.04 mol) was added and stirred for 2 h. After this, the solution was poured into a sintered glass column under vacuum and thoroughly washed with excess acetone. The product was then dried in vacuo to leave a cream coloured product (2.85 g).

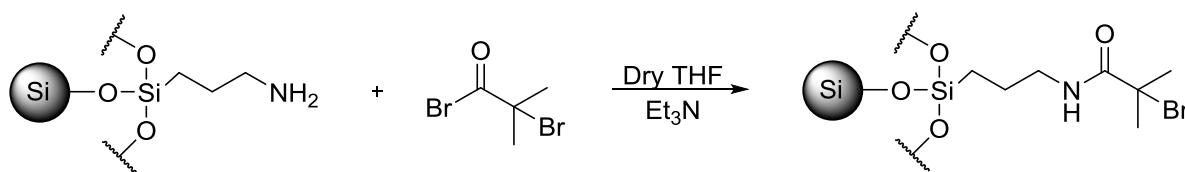
**FTIR:**  $\nu$  1044  $\text{cm}^{-1}$ , 1666  $\text{cm}^{-1}$

### Elemental Analysis (CHN):

Fumed silica: %C = 0.3, %H = 0.2, %N = 0.07, %R = 99.4

APTES-functionalised fumed silica: %C = 6.9, %H = 1.4, %N = 2.3, %R = 89.4

## 2.19 Deposition of BIBB onto APTES-functionalised fumed silica



Scheme 20 – Deposition of BIBB onto APTES-functionalised fumed silica.

To a suspension of APTES-functionalised fumed silica (1.1 g) and dry THF (10 mL),  $\text{Et}_3\text{N}$  (3.3 mL, 0.024 mmol) was added under a nitrogen atmosphere and stirred at 0 °C. BIBB (2.5 mL, 0.02 mol) was added dropwise with caution. A white vapour evolved instantly and the solution was left to stir for 30 m.

After this, the solution was poured into a sintered glass column under vacuum and thoroughly washed with excess THF, methanol and water. This was repeated three times to purify the product. The product was transferred to a watch glass and dried in a vacuum oven for 30 m to ensure dryness, leaving the yellow coloured product (1.08 g).

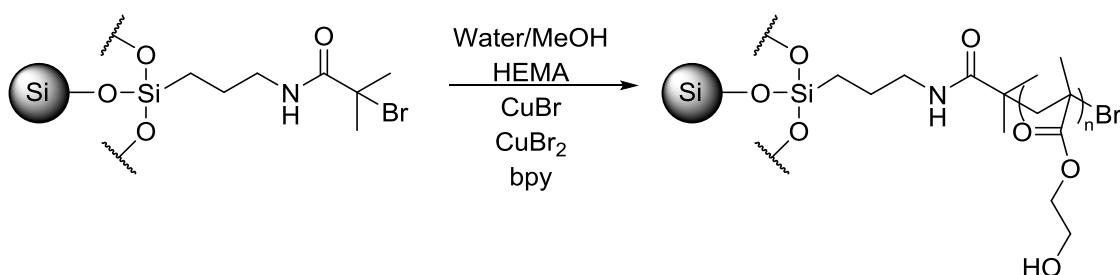
**FTIR:**  $\nu$  1041  $\text{cm}^{-1}$ , 1642  $\text{cm}^{-1}$ , 1537  $\text{cm}^{-1}$

### Elemental Analysis (CHN):

APTES-functionalised fumed silica: %C = 6.9, %H = 1.4, %N = 2.3, %R = 89.4

BIBB-functionalised fumed silica: %C = 10.9, %H = 1.6, %N = 1.7, %R = 85.8

## 2.20 Polymerisation of HEMA from BIBB-functionalised fumed silica



Scheme 21 – Polymerisation of HEMA from BIBB-functionalised fumed silica.

To a deoxygenated solution of HEMA (97 %, 5.0 g, 0.038 mol), water (2.5 mL) and methanol (2.5 mL), CuBr (56.8 mg, 0.40 mmol), CuBr<sub>2</sub> (8.2 mg, 0.037 mmol) and bpy (148.3 mg, 0.95 mmol) were dissolved under a flow of nitrogen gas.

BIBB-functionalised fumed silica (0.54 g) was prepared in a second degassed flask before the HEMA solution was injected in. Following this, the solution was agitated for 3 d.

The solution was then poured into a sintered glass column under vacuum and thoroughly washed with water and methanol (1:1 v/v) to leave a cream coloured powder (1.51 g).

**FTIR:**  $\nu$  1065 cm<sup>-1</sup>, 1719 cm<sup>-1</sup>

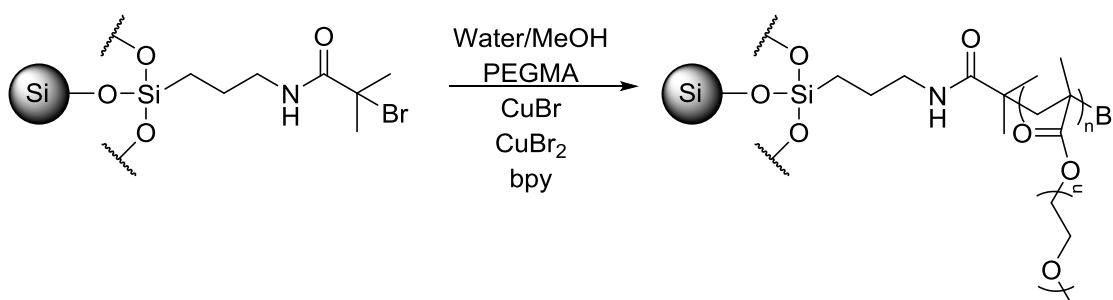
**Elemental Analysis (CHN):**

BIBB-functionalised fumed silica: %C = 10.9, %H = 1.6, %N = 1.7, %R = 85.8

PHEMA functionalised fumed silica: %C = 43.9, %H = 6.3, %N = 0.5, %R = 49.3



## 2.21 Polymerisation of PEGMA from BIBB-functionalised fumed silica



Scheme 22 – Polymerisation of PEGMA from BIBB-functionalised fumed silica.

To a deoxygenated solution of PEGMA (MW 300, 5.0 g, 0.017 mol), water (5 mL) and methanol (5 mL), CuBr (55.0 mg, 0.38 mmol), CuBr<sub>2</sub> (9.8 mg, 0.044 mmol) and bpy (154.4 mg, 0.99 mmol) were dissolved under a flow of nitrogen gas.

BIBB-functionalised fumed silica (0.33 g) was prepared and added to the reaction. Following this, the solution was stirred for 1 h.

The solution was then poured into a sintered glass column under vacuum and thoroughly washed with water and methanol (1:1 v/v) to leave a dark yellow coloured powder (0.35 g).

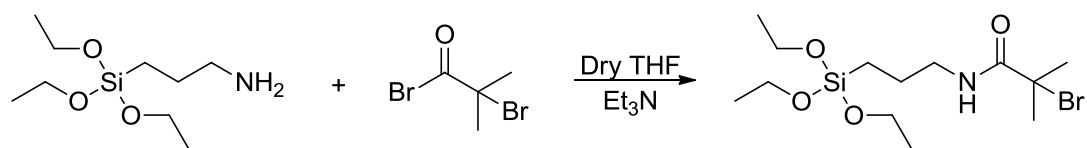
**FTIR:**  $\nu$  1042 cm<sup>-1</sup>, 1537 cm<sup>-1</sup>, 1646 cm<sup>-1</sup>, 1726 cm<sup>-1</sup>

### Elemental Analysis (CHN):

BIBB-functionalised fumed silica: %C = 10.9, %H = 1.6, %N = 1.7, %R = 85.8

PEGMA functionalised fumed silica: %C = 30.2, %H = 4.7, %N = 1.1, %R = 64.0

## 2.22 Synthesis of 3-(2-bromoisobutyramido)propyl(triethoxy)silane (BIBAPTES)



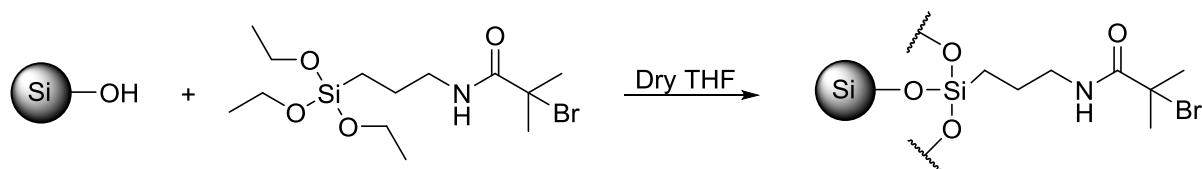
Scheme 23 – Synthesis of BIBAPTES.

This synthesis was carried out using a similar method to Chen *et al.*<sup>43</sup> To a solution of dry THF (30 mL), APTES (4.7 mL, 20 mmol) and Et<sub>3</sub>N (3.5 mL, 25 mmol) were dissolved. BIBB (3.2 mL, 25 mmol) was added slowly under ice-cooling. The solution was warmed to r.t. whilst stirring for 4 h under nitrogen.

Triethylammonium bromide (TEABr) was removed by filtration, and the filtrate was reduced to ca. ¼ of its volume. Residual TEABr precipitated by evaporation and was removed by centrifugation. The solvent from the decanted solution was removed *in vacuo* to dryness.

The product was immediately used for attachment to silica microparticles.

## 2.23 Deposition of BIBAPTES onto porous silica microparticles (PSM)



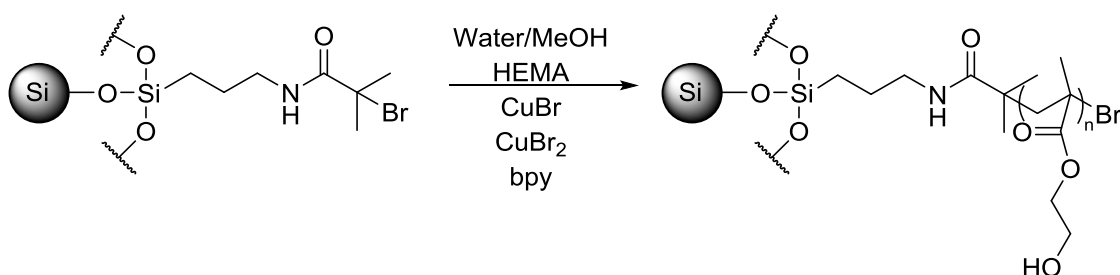
Scheme 24 – Deposition of BIBAPTES onto porous silica microparticles.

To a solution of dry THF (10 mL) deoxygenated for 10 minutes, silica microparticles (0.1011 g) and BIBAPTES (2 g, 5.4 mmol) were added. The reaction was left to stir under nitrogen overnight.

The solution was poured through a sintered glass column under vacuum and washed with excess water, methanol and THF to leave a cream/yellow coloured product (0.0872 g).

**FTIR:**  $\nu$  1053 cm<sup>-1</sup>, 1542 cm<sup>-1</sup>, 1632 cm<sup>-1</sup>

## 2.24 Polymerisation of HEMA from BIBAPTES attached PSM



Scheme 25 – Polymerisation of HEMA from BIBAPTES attached PSM.

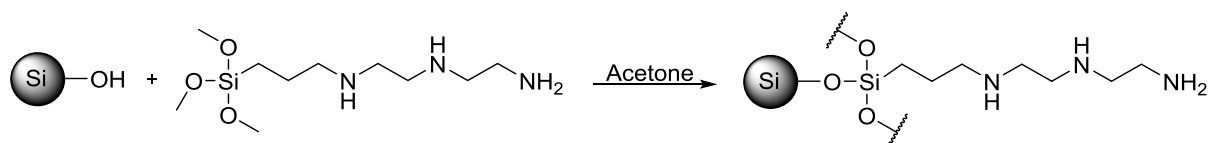
To a deoxygenated solution of HEMA (97 %, 5.0 g, 0.038 mol), water (2.5 mL) and methanol (2.5 mL), CuBr (54.8 mg, 0.38 mmol), CuBr<sub>2</sub> (8.5 mg, 0.038 mmol) and bpy (149.8 mg, 0.96 mmol) were dissolved under a flow of nitrogen gas.

BIBAPTES-functionalised silica microparticles (0.039 g) were weighed into a second degassed flask before the HEMA solution was injected in. Following this, the solution was agitated on a shaker for 3 d.

The solution was then poured into a sintered glass column under vacuum and thoroughly washed with water and methanol (1:1 v/v) before being given time to dry and leave a cream coloured powder (0.0415 g).

**FTIR:**  $\nu$  1053 cm<sup>-1</sup>, 1732 cm<sup>-1</sup>

## 2.25 Deposition of TMSPDETA onto ZEOprep silica



Scheme 26 – Deposition of TMSPDETA onto silica.

To acetone (15 mL), ZEOprep silica (1.2 g) was added. The solution was heated to 60 °C before  $\text{N}^1$ -(3-trimethoxysilylpropyl)diethylenetriamine (TMSPDETA, 4 mL, 0.02 mol) was added and stirred for 2 h. After this, the solution was poured into a sintered glass column under vacuum and thoroughly washed with excess acetone. The product was then dried in vacuo to leave a cream coloured product (1.19 g).

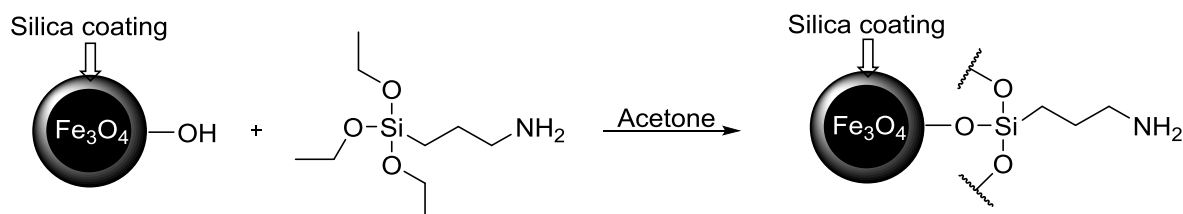
**FTIR:**  $\nu$  1043  $\text{cm}^{-1}$ , 1458  $\text{cm}^{-1}$ , 1665  $\text{cm}^{-1}$

### Elemental Analysis (CHN):

ZEOprep silica: %C = 0.04, %H = 0.3, %N = 0.04, %R = 99.6

TMSPDETA functionalised ZEOprep silica: %C = 10.8, %H = 2.2, %N = 4.8, %R = 82.3

## 2.26 Deposition of APTES onto silica coated magnetite



Scheme 27 – Deposition of APTES onto silica coated magnetite.

A typical preparative route to the nanoparticles is described by Platt *et al.*<sup>44</sup> To acetone (3 mL), magnetite coated silica (3.7 mg) was added. The solution was heated to 60 °C before APTES (200  $\mu\text{L}$ , 0.85  $\mu\text{mol}$ ) was added and stirred for 2 h. Due to the magnetic properties of the silica, the reaction was carried out on a rotary evaporator and water bath without the vacuum to heat and agitate the solution as much as possible. Following this, the solution was decanted off by holding a magnet to the solution to keep the product in place. This was thoroughly washed with excess acetone before it was then dried in vacuo to leave a cream coloured product (2.5 mg).

**FTIR:**  $\nu$  1645  $\text{cm}^{-1}$

### **2.27 Attempted sequestration of nickel, copper and zinc from aqueous solutions using PHEMA and PHEMA-Malonate**

To water (100 mL), either  $\text{NiCl}_2$  (0.008 g, 40 ppm),  $\text{CuSO}_4$  (0.01 g, 40 ppm) or  $\text{ZnCl}_2$  (0.008 g, 40 ppm) aqueous solutions were prepared. To 90 mL of the solution, PHEMA or PHEMA-Malonate (1.0 g, 7.7 mmol) was added, whilst the remaining 10 mL was kept as an accurate starting concentration reference. The solutions were stirred for 1 week.

The solution was filtered to remove the PHEMA (or PHEMA-Malonate) and analysed using ICP-OES. The difference in concentration between the two solutions was then analysed.

### **2.28 Attempted sequestration of $^{63}\text{Ni}$ from aqueous solution using free PHEMA**

To a solution of water (10 mL), a  $^{63}\text{Ni}$  solution (20  $\mu\text{L}$ , 1.48 MBq) in HCl was added. To eight LSC bottles, deionised water (15 mL) was added followed by the diluted  $^{63}\text{Ni}$  solution (100  $\mu\text{L}$ ). To five of these solutions, PHEMA (1.0 g, 7.7 mmol) was added. The remaining three were left as they were so they could be used as reference solutions. All solutions were shaken for one week.

Into eight new liquid scintillation cocktail (LSC) bottles, the  $^{63}\text{Ni}$  test solutions (1 mL) were syringe filtered. This was repeated for all eight samples and liquid scintillation cocktail (10 mL) was added to these vials. Following this, two additional LSC bottles were prepared with liquid scintillation cocktail (10 mL) and the original  $^{63}\text{Ni}$  stock (100  $\mu\text{L}$ ) to ensure the metal had not adsorbed to the surface of the original test bottles.

## **2.29 General method for the sequestration of various transition metals and radioactive isotopes using silica attached APTES and TMSPDETA**

A range of concentrations of single metal solutions in deionised water (160 ppm, 80 ppm, 40 ppm, 20 ppm, 10 ppm, 5 ppm and 2.5 ppm) were prepared including Co(II), Ni(II), Cu(II), Zn<sup>2+</sup>, Cd<sup>2+</sup>, Eu(III) and [UO<sub>2</sub>]<sup>2+</sup> using CoCl<sub>2</sub>·6H<sub>2</sub>O, NiCl<sub>2</sub>, CuCl<sub>2</sub>·2H<sub>2</sub>O, ZnCl<sub>2</sub>, Cd(NO<sub>3</sub>)<sub>2</sub>·4H<sub>2</sub>O, EuCl<sub>3</sub>·6H<sub>2</sub>O and UO<sub>2</sub>(NO<sub>3</sub>)<sub>2</sub>. To these solutions (45 mL), APTES-functionalised silica (50 mg) was added (much like the work by Johnson *et al.*<sup>45</sup>) and the concentration change was measured using ICP-OES (or ICP-MS if concentration fell below the relevant LOD for ICP-OES). Preliminary investigations were carried out on solutions with a concentration in the range of 20-40 ppm. Tracers of <sup>57</sup>Co, <sup>63</sup>Ni, <sup>109</sup>Cd and <sup>152</sup>Eu were added at ca. 3 KBq per sample and weighed into each batch.

A colour change of the silica was seen with some metals, especially when sequestering cobalt and copper where the silica material changed to a pink and blue colour respectively.

Where discussed, solutions of 1 % sodium (w/w using NaCl) and 1 % calcium (w/w using CaCl<sub>2</sub>) were also used to make these metal concentrations to create a solution where a large excess of competitive ions existed and to investigate the effect of ionic strength.

## **2.30 General method for the selective removal of metals from a seven metal solution using functionalised silicas**

A 5 L stock solution of Co(II), Ni(II), Cu(II), Zn<sup>2+</sup>, Cd<sup>2+</sup>, Eu(III) and [UO<sub>2</sub>]<sup>2+</sup> at ca. 20 ppm per metal was prepared in deionised water. The salts used to make these solutions were CoCl<sub>2</sub>·6H<sub>2</sub>O, NiCl<sub>2</sub>, CuCl<sub>2</sub>·2H<sub>2</sub>O, ZnCl<sub>2</sub>, Cd(NO<sub>3</sub>)<sub>2</sub>·4H<sub>2</sub>O, EuCl<sub>3</sub>·6H<sub>2</sub>O and UO<sub>2</sub>(NO<sub>3</sub>)<sub>2</sub>. Each 45 mL aliquots were prepared from this solution and 50 mg of functionalised silica was added. The functionalised silica investigations were repeated five times and the standard deviation was used to display the error on the appropriate graphs. The silicas were left in the solution for 24 h before being measured *via* ICP-OES to measure the change in concentration when compared to the stock solution. The investigations were carried out in plastic centrifuge tubes (50 mL). This preparation process was repeated for the same investigations but for a 4 w experiment also. No radioisotopes were added as tracers for these investigations.

### **2.31 Method for attempting metal removal from Talvivaara PLS pond sample**

A 1 L sample from the pregnant leach solution (PLS) pond was acquired from the Talvivaara Nickel mine in Finland. This sample was kept in a nitrogen filled glove box to prevent precipitation of ions in extremely high concentrations that would otherwise precipitate once in contact with air due to oxidation of sample. Twelve samples of 22.5 mL of this solution were made. Four were used to investigate the original concentration of the major ions in the sample using ICP-OES. Four had 25 mg of ZEOprep silica-APTES added to them and the remaining four had 25 mg of fumed silica-APTES added to them, keeping the ratio constant between other investigations where a limited sample had not been a factor.

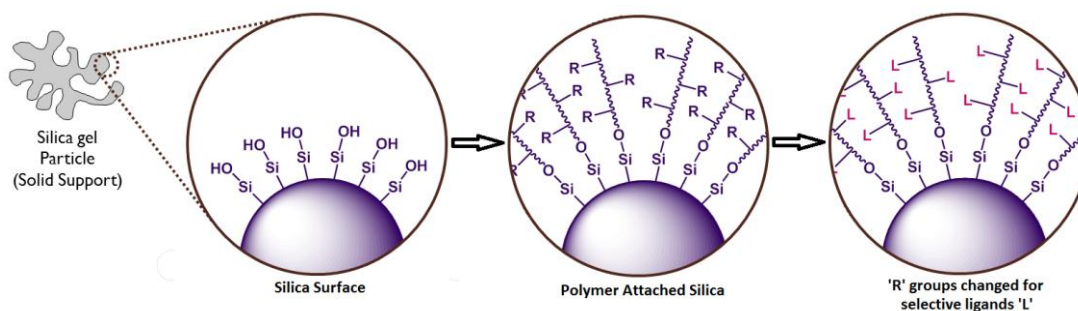
After 24 h and four weeks, an aliquot of ca. 1 g (calculated by pre-weighing ICP tube and lid, acid and water for dilution before deducting this from the total weight once aliquot was added) was added to an ICP centrifuge tube that contained ca. 9 g of a 2 %  $\text{HNO}_3$  solution made in deionised water – all carried out in a glove box.

ICP-OES showed the concentration of the sample to still be too high and that the detector was saturated, so 1.25 mL of the solution was added to 8.75 mL of a 2 % acid solution to further dilute the sample.

### 3 Polymerisation of monomers and post-polymerisation modification

#### 3.1 Introduction

As a reminder to the reader, Figure 16 demonstrates the overall aim of the project.



**Figure 16 - Demonstrative view of the object of this work where the final step shows the product to be used for selective metal sequestration with specific ligands replacing the natural 'R' groups that exist as part of the original polymer.**

The desirable outcome is that high ligand supporting density will be attained i.e. a large functionalised surface area to remove metal ions from solutions. This will be achieved by the use of polymers, leading to a large number of functional side chains that can be modified for ligand attachment. The class of polymerisation discussed in this work is referred to as a 'living radical polymerisation' (LRP).<sup>46</sup> The LRP process produces polymers without termination reactions, so in theory the polymer length can always be increased – hence 'living polymerisation'.<sup>47</sup> These are highly desirable because they allow the molecular weight of the polymer to be controlled easily<sup>48</sup> and for the case of this work it allows the opportunity to explore different chain lengths once an efficient method has been established.

LRP is a term that includes atom-transfer radical polymerisations (ATRP) which proceeds with reversible chain capping. It was not until the mid-1990s that extensive exploration of living polymerisations started because until then, it was thought radical polymerisation was a mature process with relatively little left to discover.<sup>47</sup>

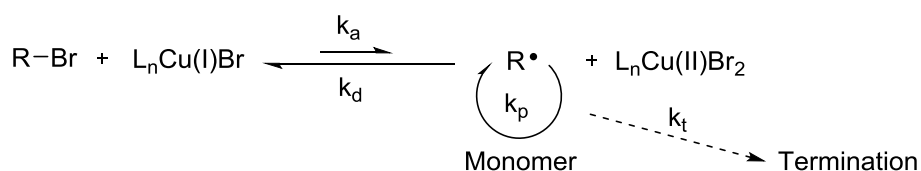
This chapter focuses on the polymer synthesis and functionalisation without being attached to the solid support, i.e. the 'free polymer'. Surface attached methods and results are presented and discussed in chapter 4. By carrying out free polymer synthesis, it was anticipated that synthesis and modifications could take place as per everyday organic synthesis and would also make initial characterisation easier and faster. Once the materials were produced and characterisation was understood, the methods could be transferred to the solid support.



### 3.1.1 Atom Transfer Radical Polymerisation (ATRP)

ATRP<sup>49</sup> is a versatile technique that is compatible with a wide variety of functional unsaturated monomers, most notably acrylates and methacrylates<sup>40</sup> and is one of the most widely used controlled radical polymerisation (CRP) methods.<sup>46</sup> This process also removes the rigorous conditions required for anionic or cationic polymerisation. Instead, the polymer growth is catalysed by a transition metal complex in its lower oxidation state where examples with copper(I)<sup>38,50</sup>, nickel(II)<sup>51,52</sup>, iron(II)<sup>53,54</sup>, ruthenium(II)<sup>55</sup>, rhodium(I)<sup>56</sup>, palladium(0)<sup>57</sup> and many others<sup>58</sup> have been shown. The metal centre removes the halogen atom in a reversible process from an initiator molecule or growing polymer chain, thus forming an organic radical. Free radical polymerisation follows with the radical, accumulating several monomers before transferring back the halogen atom and ‘capping’ the growing chain (Scheme 28).<sup>40</sup>

Scheme 28 shows clearly that the equilibrium for this redox process lies strongly to the side of the halogen-capped chain end. Therefore at any time, the overall radical concentration is very low and hence greatly reduces termination reactions since the main termination method is radical-radical coupling. This ‘pseudo-living’ character allows good control of molecular weight, low polydispersity (keeping each chain length to similar sizes) and if required, the reliable synthesis of block copolymers. The main drawback of this methodology is the resulting low polymerisation rates compared to relatively uncontrolled radical techniques.<sup>40</sup>



**Scheme 28 – General scheme for ATRP where R–Br is the halogen-capped initiator or growing polymer chain,  $\text{L}_n\text{Cu}^{1+}$  is the ligated catalyst (copper) and  $k_a$ ,  $k_d$ ,  $k_p$  and  $k_t$  are the rate constants for activation, deactivation, propagation and termination respectively.**

The ligand that complexes with the transition metal is used to help solubilise the metal in the organic reactions system whilst activation of the initiator involves the metal centre undergoing an electron transfer with simultaneous halogen atom abstraction and expansion of its coordination sphere.<sup>47</sup> The free radical nature of ATRP is well established through a number of studies by Matyjaszewski *et al.*<sup>59</sup>

As with any radical process however, ATRP has to be carried out in rigorously deoxygenated systems to prevent trapping of propagating radicals by oxygen.<sup>60</sup>

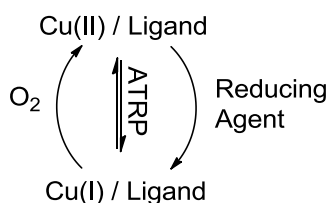
### 3.1.2 Activators ReGenerated by Electron Transfer (ARGET) ATRP

In recent times, considerable time and attention has been devoted to decreasing the amount of catalyst in the ATRP systems. Green routes to well-defined high-molecular weight polymers overcome a significant drawback of traditional ATRP techniques requiring systems of plentiful amounts of metal – in most scenarios, copper. Lowering the amount of catalyst would be beneficial both towards the environment and commercially.<sup>61</sup>

ARGET ATRP provides a greener route that is very often sought for in modern day chemistry by greatly reducing the quantity of metal required. In the example shown in Scheme 30, an excess of reducing agent, relative to the catalyst, is used to continuously regenerate the activators by reduction of copper(II) products that accumulate because of the inevitable and unavoidable radical termination. ARGET ATRP therefore, allows the concentration of copper(I) to be used at ‘ppm’ levels using various reducing agents including: tin(II) octoate<sup>62</sup>, ascorbic acid (vitamin C)<sup>63</sup>, or copper(0).<sup>61,64</sup>

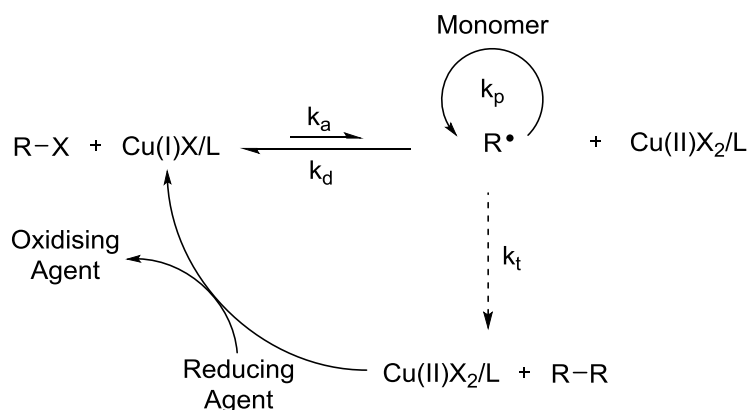
One of the drawbacks of ARGET ATRP is the ligand use - this must be added to metal at 3 to 10 times molar excess in order to achieve a controlled polymerisation. This excess ligand helps maintain the catalyst complex and protect it from destabilising side reactions – generally involving monomer complexation to catalyst.<sup>65</sup> As these ligands are expensive, often quite specific and not widely available, scaling these reactions up can be difficult.<sup>66</sup>

Scheme 29 demonstrates simply but effectively how the reducing agent returns the copper metal back to Cu(I) from Cu(II) and hence, enabling polymerisation. With an excess of reducing agent used, another advantage of this process is the ability to carry out this reactive radical synthesis without the need to deoxygenate the systems. This system may be particularly well-suited for grafting from large substrates because they simply would not fit inside a Schlenk flask.<sup>60</sup>



Scheme 29 – Simple reaction scheme for ARGET ATRP in limited amounts of air.<sup>60</sup>

To achieve polymers with high purity and avoid possible toxicity issues (important when considering drinking water), the metal catalyst must be removed. With a much lower starting amount in ARGET ATRP, there is much less to remove, unlike ATRP where much more metal is wasted after the synthesis.



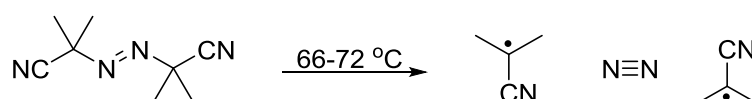
**Scheme 30 – General scheme for ARGET ATRP where R–X is the halogen-capped initiator or growing polymer chain, Cu(I)X/L is the ligated catalyst (copper) and  $k_a$ ,  $k_d$ ,  $k_p$  and  $k_t$  are the rate constants for activation, deactivation, propagation and termination respectively.<sup>67</sup>**

### 3.1.3 Uncontrolled radical polymerisation

Some examples of uncontrolled radical polymerisations were carried out so comparisons could be made to ATRP and ARGET ATRP methods. Uncontrolled radical polymerisations require no metal catalyst, therefore certain not to affect the purity of the polymer.

Bond homolysis is one of the most important ways of forming radicals.<sup>68</sup> Temperatures of over 200 °C will homolyse most bonds but some will undergo homolysis at temperatures little over room temperature. Light is a possible energy source too where red light has 167 kJ mol<sup>-1</sup> associated with it, blue light ca. 293 kJ mol<sup>-1</sup> and ultraviolet (200 nm) 586 kJ mol<sup>-1</sup> which will decompose many organic compounds including DNA.<sup>69</sup>

Azoisobutyronitrile (AIBN) is a compound often used in synthetic reactions because it can act as an initiator of radical reactions simply on heating.<sup>69</sup>



**Scheme 31 – Radical formation by heating of AIBN.<sup>69</sup>**

When reacted with the functional monomers discussed in this work, it provides a simple method of forming the polymer.

### 3.1.4 Why ATRP methods were chosen

ATRP and ARGET ATRP were preferred for this work because of their reasonably quick propagation but the molecular weight can still be controlled.<sup>70</sup> Polymerisation can also take place at room temperature and the reagents involved are easy to obtain.<sup>71</sup> The systems versatility including its ‘functional group tolerance’, the vast quantity of literature available and the experience within our research group of this technique<sup>40</sup> was also a key factor. As will be evident in more than one area of this work, ATRP and ARGET ATRP have been utilised for free polymerisations and surface attached polymerisations. These are discussed in their relevant chapters.

The post-polymerisation modification of polymer brushes is well documented<sup>72,73</sup> and examples of modification of copolymers<sup>74</sup> have also been reported. It was anticipated this methodology from the literature could be transferred to both the free polymer and moreover, to the surface grafted polymers later in the project.

Boyer *et al.*<sup>75</sup> have specifically reported the post-functionalisation of ATRP produced polymers by exploiting the halide end group however, this method does not utilise the side chains of the polymer and therefore is not a beneficial method for the work proposed in this thesis. A review by Goldmann *et al.*<sup>76</sup> on post-functionalisation of polymers *via* orthogonal ligation chemistry does however provide evidence of feasible methods although none of these appear to be for metal binding purposes. Transition metal ions including Cu(II), Ni(II) and Cd<sup>2+</sup> have reportedly been separated *via* a process similar to that proposed but have not targeted heavier metals such as the lanthanide and actinides which this work does.

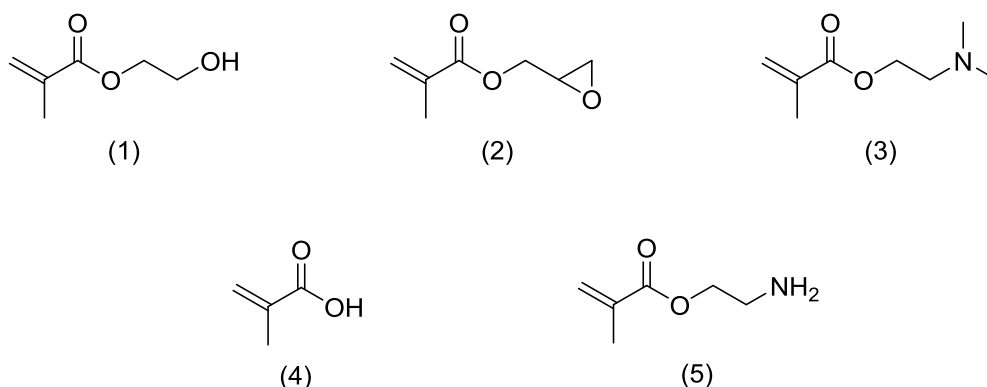


Figure 17 – Possible monomers discussed to use as a basis for this work. (1) 2-hydroxyethyl methacrylate (HEMA), (2) glycidyl methacrylate (GMA), (3) 2-(dimethylamino)ethyl methacrylate (DMAEMA), (4) Methacrylic acid (5) 2-aminomethyl methacrylate.

Figure 17 illustrates the monomers considered as a starting point for this work. (1), (2) and (3) are used and discussed in this thesis but (4) and (5) are not. Methacrylic acid (4) was avoided simply because previous workers within the research group had difficulty with it and other options were preferred. Meanwhile, the nature of 2-aminomethyl methacrylate (5) means it is simply unable to undergo polymerisation without crosslinking<sup>77</sup> or self-reacting<sup>78</sup>, hence when purchased the reagent is stabilised with ca. 500 ppm phenothiazine.

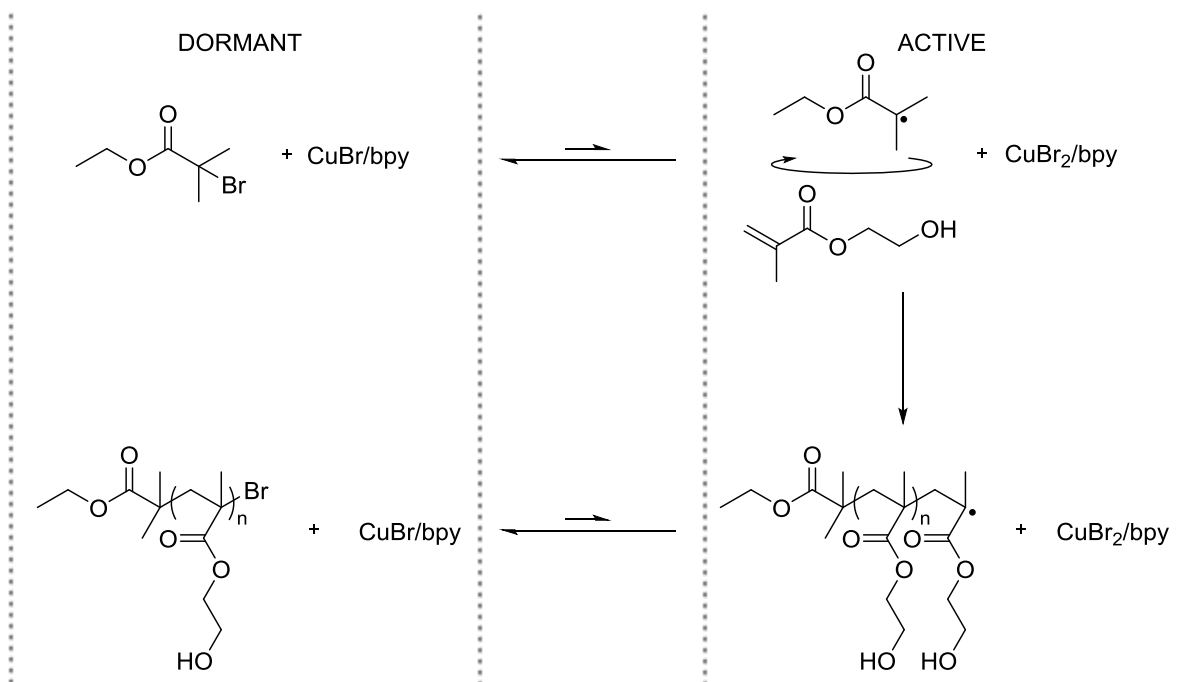
## 3.2 Results and Discussion

### 3.2.1 HEMA/PHEMA

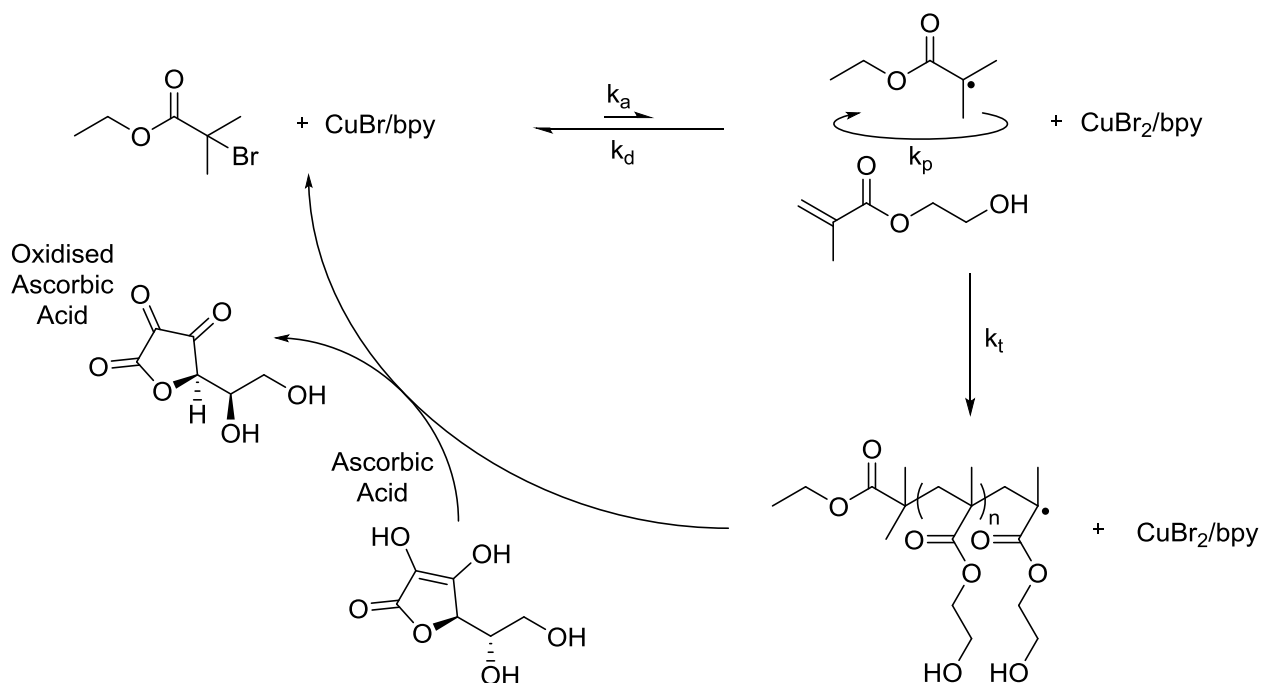
HEMA is an important functional monomer with many uses, including the manufacturing of soft contact lenses<sup>38,79</sup>, dentistry<sup>80</sup> and drug delivery.<sup>81</sup> Being a methacrylate makes it very appropriate for ATRP due to its unsaturated double bond. However, the available functional hydroxyl group makes it even more ideal as this is a potential candidate for sequestration of metal.

PHEMA is hydrophilic and has a high degree of hydration, however it is not water-soluble. This property makes it a good candidate for a starting point when looking at sequestering metals from water supplies. PHEMA itself was investigated to discover its potential at carrying out this task but its functional hydroxyl group allows for further functionalisation by the addition of other useful ligands to help improve its ability to sequester metal ions. These syntheses are discussed below.

The first reaction was to polymerise HEMA *via* ATRP in a methanol/water (1:1) solvent in order to test that this was going to be an appropriate method and product to use. After initial polymerisations were successfully carried out on a 5 g scale, it was soon scaled up to 20 g. At this scale it was more appropriate to carry out ARGET ATRP to reduce the amount of copper required. **Error! Reference source not found.** shows the product of this PHEMA ample. Polymerisation of HEMA *via* ATRP<sup>38</sup> (Scheme 32) and ARGET ATRP<sup>67</sup> (Scheme 33) is thoroughly reported in literature.



**Scheme 32 – Reaction scheme for synthesis of PHEMA *via* ATRP. The majority of the reaction time is spent in the ‘dormant’ state to achieve the greatest control. For a small proportion of time, the reaction sits in the ‘active’ state where polymerisation and chain growth commences.**



**Scheme 33 – Reaction scheme for synthesis of PHEMA *via* ARGET ATRP. Ascorbic acid is used as the reducing agent to regenerate the catalyst to help continuously promote polymerisation and chain growth.**

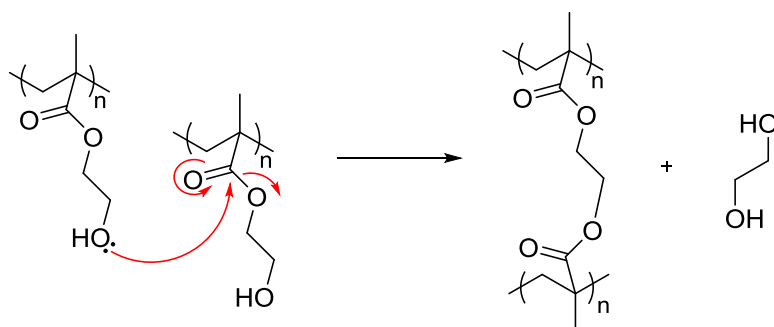
It was found that precipitating the polymer in diethyl ether worked faster than in the reported THF.<sup>38</sup> Increasing the scale of the reaction also (from 5 mL to 20 mL) did not appear to have a detrimental effect on the conversion of the polymer and also made it easier to retrieve the majority of the polymer when precipitating it out. Conversion describes the percentage of monomer converted into polymer whereas yield describes how much was recovered at the end. In practice, yield is always less than conversion (mainly due to loss in workup) and so for the purpose of this report, it will be assumed that 100 % recovery of polymer is achieved: resulting in yield being equal to conversion.

Elemental analysis was carried out to show the purity of the polymer. Theoretically, nitrogen content should be observed as 0 %, with carbon at 55.0 %, hydrogen at 7.7 % and oxygen at 36.5 %. Oxygen is not directly recorded on an elemental analyser but can be estimated as bromine is the only other element known to be present in the polymer (est. to be ca. 1 % depending on the size of the polymer) and the value is given as 'R'. Results show nitrogen levels were minimal at 0.16 %, carbon was 53.40 %, hydrogen 7.46 % and R at 38.88 %. The 2,2'-bipyridyl ligand present in low quantities is the most likely explanation for the nitrogen content and it is also possible that a small amount of CuBr<sub>2</sub> could still be present which is interfering with the measurements.

An important note when synthesising the polymer is that crosslinking does not occur. This will quickly reduce the amount of functional groups available and therefore will prevent surface area efficiency from being achieved when attempting sequestration of metals. A simple test to investigate whether the polymer has undergone crosslinking is to examine whether the polymer dissolves or swells in a solvent that would be expected to dissolve a non-crosslinked example of the polymer. If the polymer swells, it suggests that crosslinking has occurred, this happens as solvent molecules get trapped between the long chains. A non-cross-linked polymer would be expected to dissolve in an appropriate solvent.

To dry PHEMA, freeze drying was utilised. This considerably speeds up the drying process as firstly, the solvent system is MeOH and water (i.e. not particularly volatile) and secondly, for all the solvent to remove itself naturally would take a long time through the polymer, especially when the outside of the polymer begins to dry up first and increase the difficulty for the solvent to diffuse through.

Vacuum oven drying was avoided because it was thought cross-linking would be encouraged by the trans-esterification of ethylene glycol as illustrated in Scheme 34.



Scheme 34 - Transesterification of ethylene glycol.

To freeze dry, the MeOH is removed by swelling the polymer in water and replacing the water a couple of times over a period of time. This replaces any MeOH that might find itself trapped in the polymer and reduces damage that the solvent may do to the freeze drier. The polymer is removed from the water and transferred to a flask that attaches to the drier and the water is removed *via* sublimation over a period of 24 hours.

### 3.2.1.1 <sup>1</sup>H NMR of PHEMA

<sup>1</sup>H NMR spectroscopy of PHEMA were run in MeOD. Good quality <sup>1</sup>H and <sup>13</sup>C NMR spectra were produced, matching previously reported spectra by Paterson *et al.*<sup>82</sup>

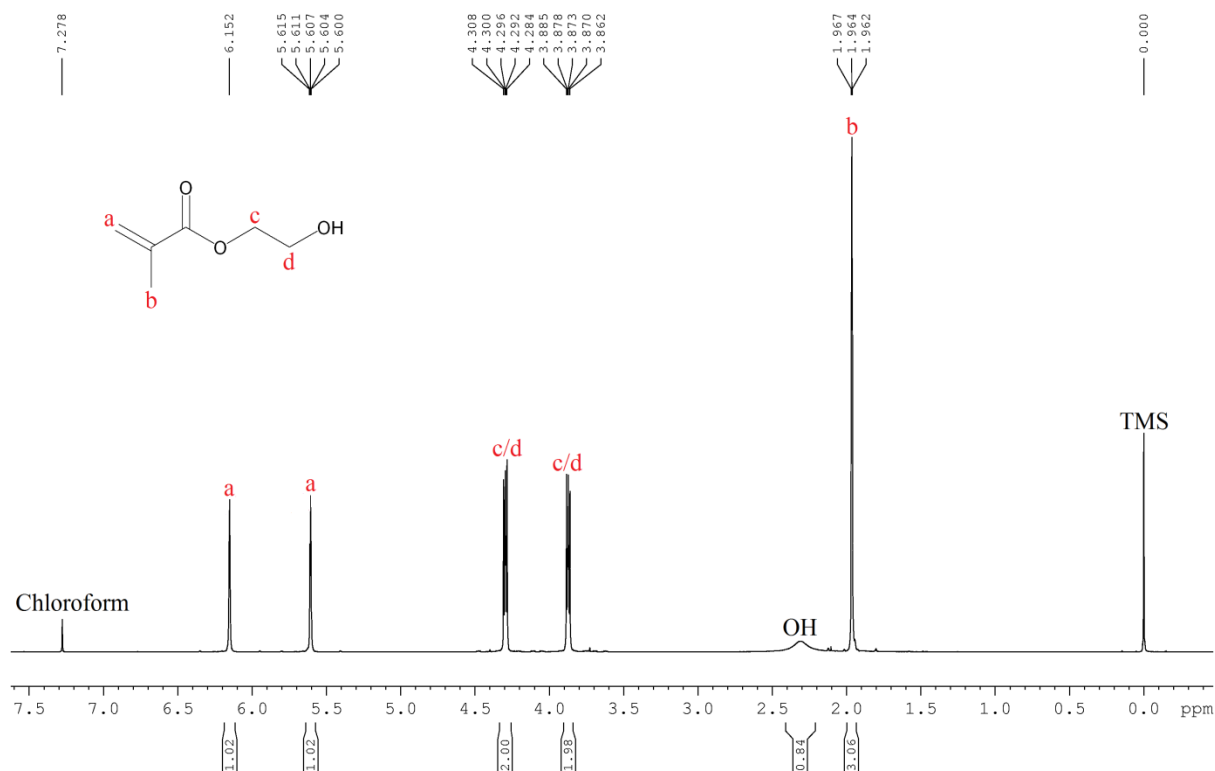
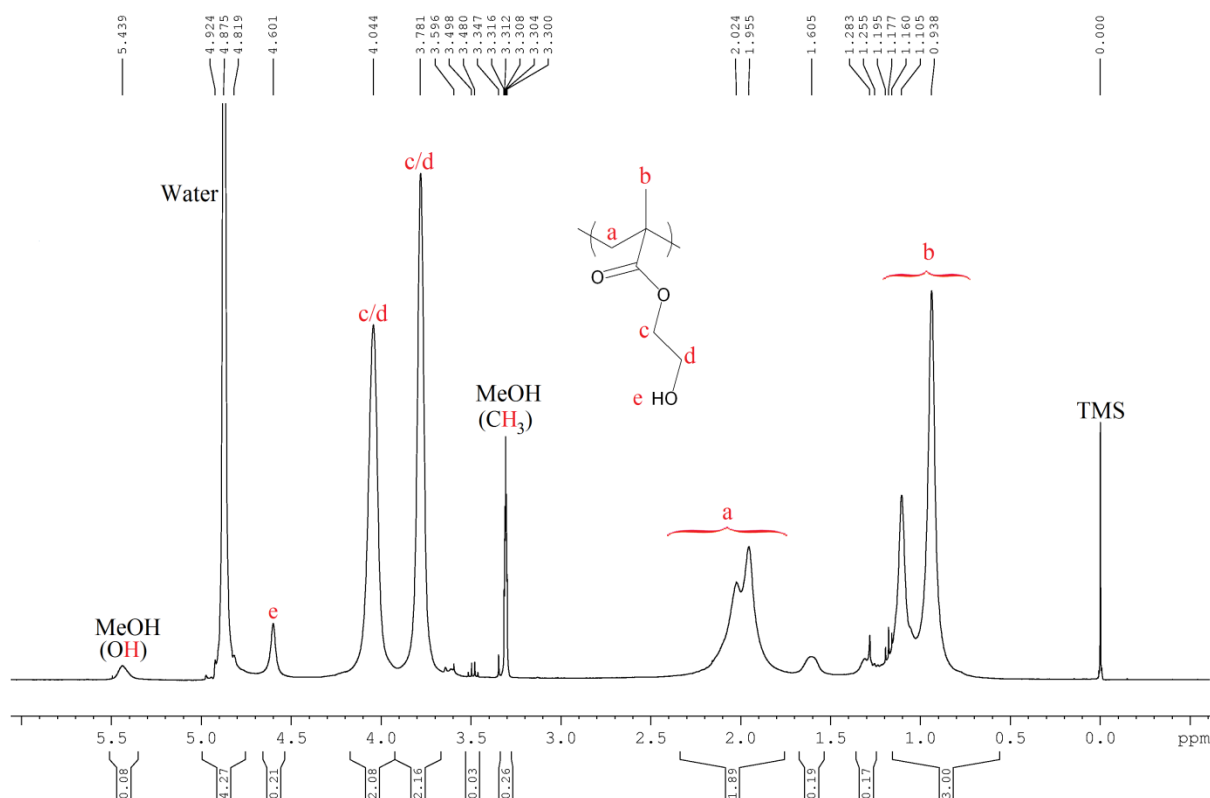


Figure 18 – <sup>1</sup>H NMR of HEMA, included to illustrate the difference in characteristics between the monomer of HEMA and the polymer, PHEMA.



Figure 18 and Figure 19 are included to demonstrate the difference in spectra between the monomer, HEMA and its polymer, PHEMA. The  $^1\text{H}$  NMR spectrum of HEMA shows protons **a**, **c** and **d** can be differentiated but is irrelevant for this work.



**Figure 19 –  $^1\text{H}$  NMR of PHEMA. PHEMA was formed from HEMA via ARGET ATRP. The difference in the nature of the spectra is very apparent when compared to its monomer in Figure 18. Similar spectra were reported by Paterson *et al.*<sup>82</sup>**

Figure 19 shows the spectrum of PHEMA with peak assignments, produced *via* the ARGET ATRP process. Paterson *et al.*<sup>82</sup> and Weaver *et al.*<sup>83</sup> have both reported similar spectra and assignment of peaks is based on this.  $^1\text{H}$  NMR peaks from the initiator used (EBIB) are likely to be hidden under the broad polymer peaks which would explain why they cannot be seen. The sharp peaks observed at 1.18 ppm (on the shoulder of what has been assigned as proton **b**) and 3.49 ppm is diethyl ether<sup>84</sup> which was used to precipitate the polymer as explained in chapter 2. The broad peak at 1.6 ppm is likely to exist due to hydrogen bonded hydroxyl groups.

### 3.2.1.2 Molecular Weight of PHEMA

The molecular weight (MW) can be determined theoretically using the formula shown in Equation 6. Although not a large focus point for this research, it was calculated to allow

future work to benefit from and enable research into the effect of different molecular weight PHEMA if thought to be necessary. The degree of polymerisation (DP, simply described as the number of monomeric or ‘repeat units’ in a polymer) can also be calculated theoretically (see Equation 4) whilst the actual value is for the ATRP method is calculated in Equation 5. This is required for the theoretical molecular weight calculation shown in Equation 6 with actual values used in Equation 7. Equation 8 and Equation 9 show the theoretical DP and MW of PHEMA produced *via* ARGET ATRP.

$$DP = \frac{[M]}{[I]} \times \text{conversion (as a fraction)}$$

**Equation 4 – Theoretical DP where ‘[M]’ is the monomer concentration or number of moles and [I] is the initiator concentration or number of moles**

Theoretical DP for PHEMA formed *via* ATRP:

$$\frac{165 \text{ mmol}}{1.50 \text{ mmol}} \times 0.39 = 43$$

**Equation 5 – Theoretical DP of PHEMA formed *via* the ATRP method**

Theoretical PHEMA MW formed *via* ATRP:

$$DP \times \text{monomer MW}$$

**Equation 6 – Theoretical MW of PHEMA formed *via* the ATRP method**

Which in this case is:

$$43 \times 130.14 = 5596$$

**Equation 7 – Theoretical MW of PHEMA formed *via* ATRP**

Theoretical DP for PHEMA formed *via* ARGET ATRP:

$$\frac{165 \text{ mmol}}{1.50 \text{ mmol}} \times 0.65 = 72$$

**Equation 8 – Theoretical DP of PHEMA formed *via* ARGET ATRP method**

Theoretical PHEMA MW formed *via* ARGET ATRP:

$$72 \times 130.14 = 9370$$

**Equation 9 – Theoretical MW of PHEMA formed *via* ARGET ATRP**

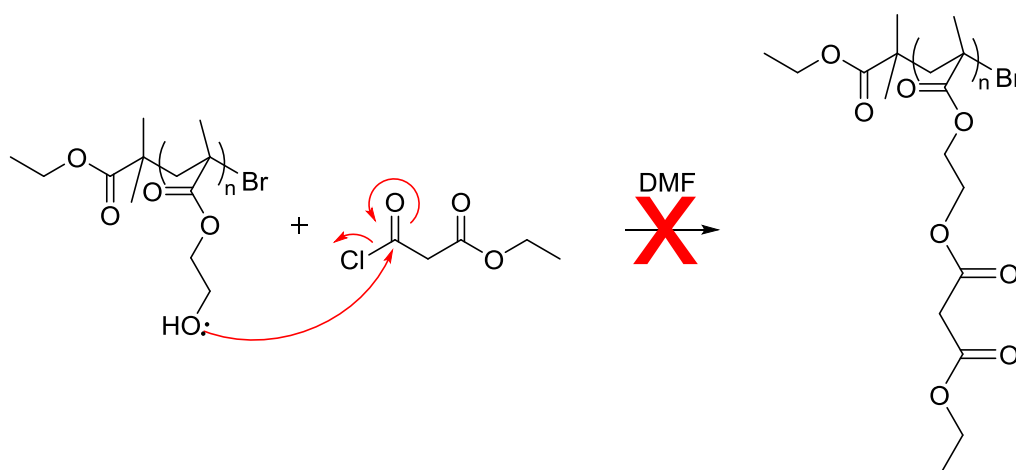
### 3.2.1.3 Post-Polymerisation Modification of PHEMA

As discovered when preparing PHEMA for  $^1\text{H}$  NMR spectroscopy, solvents for further reactions with PHEMA were limited due to the poor solubility of PHEMA in many common solvents. Nevertheless, DMF proved to dissolve PHEMA well and was used as the solvent for post-polymerisation modification reactions.

Ethyl malonyl chloride was used as the ligand to functionalise PHEMA. This was based on the success reported with a similar ligand, acetamidophosphonate, by Fryxell *et al.*<sup>14</sup> with removal of actinides such as Pu(IV). The work reported by his group focuses on attaching ligands directly to high surface area supports (SAMMS) whereas the work discussed here attempts to post modify PHEMA and other polymers with the intention of also creating highly functionalised material that may prove to be more suitable. It is known that the hydroxyl groups can serve as reactive sites for functional group attachment, Huang *et al.*<sup>85</sup> have reported the attachment of acetyl chloride and cinnamoyl chloride with PHEMA films *via* the acid chloride route. It was also reported that complete disappearance of the hydroxyl peak was observed, suggesting quantitative conversion to the corresponding ester. Ethyl malonyl chloride functionalisation was attempted *via* the acid chloride route in this thesis although the difference here was that free PHEMA was used and not a thin film attached to a gold surface.

The attempted reaction method is described here but a successful product was never obtained. To a solution of poly(2-hydroxyethyl methacrylate (PHEMA, 1.00 g, 7.68 mmol) dissolved in dimethylformamide (DMF, 21 mL), ethyl malonyl chloride (ca. 1.71 mL, 13.28 mmol) was added very slowly dropwise *via* a pipette. A white gas evolved as the ethyl malonyl chloride was added and the colour of the solution became a darker yellow. The reaction was stirred for 1 h at r.t.

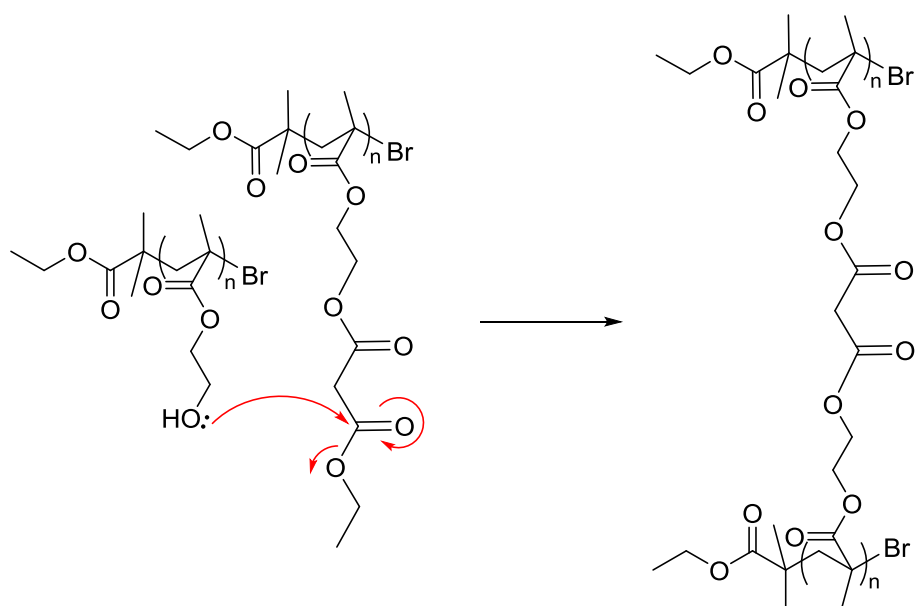
The solution was poured into diethyl ether (100 mL) under vigorous stirring that had been cooled to 0 °C, causing the polymer to precipitate instantly and agglomerate. The solvent was decanted off and the polymer was dried on a freeze drier. The polymer was ground down using a mortar and pestle which broke up the dry polymer very easily to leave a yellow/orange coloured solid (0.79 g, 42 % yield). A mechanism for what was anticipated to occur is presented in Scheme 35.



**Scheme 35 – Attempted functionalisation of PHEMA with ethyl malonyl chloride, however no indication was found that the reaction had worked.**

Once the product was recovered and dried *via* the method described in chapter 2, a strong indication was given that the product heavily cross-linked and that the reaction had been unsuccessful. Limited characterisation could only be carried out on the product due to its insolubility in many solvents and FTIR was only able to indicate esters and ketones present which already existed before functionalisation was attempted. Following more literature research, it was evident that groups had reported successful post-polymerisation reactions with PHEMA *via* the hydroxyl group but all were functionalised when attached to surfaces such as silicon substrates<sup>86,87</sup>, titanium<sup>88</sup>, carbon nanotubes<sup>89</sup> or gold.<sup>90</sup>

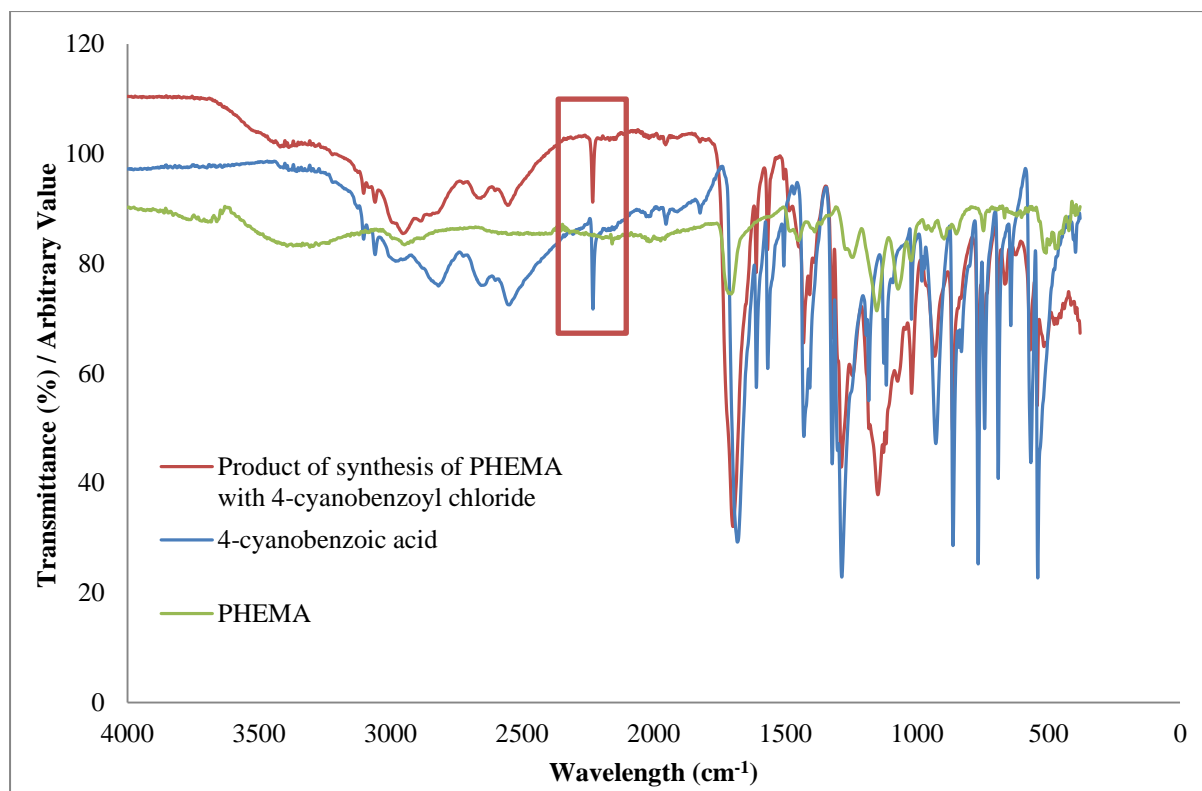
Longer reaction times were introduced and slower addition of the ligand to the reaction too. However, none of the methods had a significant change on the resulting product as all produced an acidic smelling, orange/brown coloured insoluble product. A proposed mechanism for what might be taking place is given in Scheme 36.



**Scheme 36 – Proposed mechanism for cross-linking taking place during the post-polymerisation functionalisation of PHEMA with ethyl malonyl chloride.**

Work by other researchers on brushes is quite different to the work on free polymers in terms of mobility of the chains. Due to the polymers being surface grafted, they are much more restricted in terms of their movement which could be an important factor when considering the kinetics of the reaction and the probability of initiating cross-linking reactions.

It has certainly proven very difficult to find literature on the modification and functionalisation of free polymers in the way this project has set out to do. The free polymer has demonstrated to be very different in behaviour to that reported on surface attached examples and it is for this reason that the post-polymerisation functionalisation approach was reconsidered. Instead, rather than focussing on the polymer to be designed for metal removal, attachment of a group that would be easily characterised and lead towards proving the successful modification of a free polymer was targeted. The compound used for this was 4-cyanobenzoyl chloride due to the diagnostic cyano peak at  $2260\text{--}2000\text{ cm}^{-1}$  *via* FTIR. The peak at  $2231\text{ cm}^{-1}$  was present as it was on the starting material of 4-cyanobenzoic acid (synthesised in a neat solution of thionyl chloride under reflux for 4 h to produce 4-cyanobenzoyl chloride). The product was washed thoroughly (with water, followed by diethyl ether) to ensure that the peak was not present due to residue. However, this does not guarantee the attachment was successful.



**Figure 20 – FTIR spectra of 4-cyanobenzoic acid, PHEMA and the product from the synthesis of PHEMA with 4-cyanobenzoic acid. The spectra are inconclusive as to whether post-polymerisation modification has been successful due to a lack of shifts in the product. The spectra have been offset for clarity.**

PHEMA and the attempted PHEMA functionalised with ethyl malonyl chloride were kept for testing in aqueous solutions to measure their ability at removal of metal ions and these results are discussed in chapter 6. Meanwhile, GMA was also explored as a possible candidate to form a basis for this work and the findings from this work are reported below.

### 3.2.2 GMA/PGMA

GMA is very similar to HEMA in terms of its structure and again, having an unsaturated double bond makes it very suitable for ATRP. However, its end group is an epoxide as opposed to a hydroxyl group resulting in a different approach to the chemistry that can be carried out.

Its polymerisations have also been extensively studied *via* ATRP and ARGET ATRP.<sup>91, 92, 73, 93</sup> It has most commonly been used to grow PGMA brushes from surfaces that can be post-functionalised by ring-opening of the epoxide group.<sup>94,95</sup> Little has been reported on post-polymerisation of free polymer but Liu et al.<sup>96</sup> have reported work on micro granules. The epoxide group would not be expected to remove metal but it does provide an alternative route for modification where the epoxide ring can be opened and a ligand be attached. When

polymerising the GMA however, it is important that the epoxide ring is not broken else post-polymerisation modification will not be possible.

### 3.2.2.1 $^1\text{H}$ NMR spectroscopy of PGMA

$^1\text{H}$  NMR spectroscopy of the PGMA polymer showed the epoxide ring still to be intact with broad peaks observed at 2.64 ppm, 2.84 ppm, 3.23 ppm (Figure 22). Hayek et al.<sup>93</sup> have also reported the polymerisation of GMA and produced similar spectra (Figure 21) to prove the epoxide ring to still be intact.

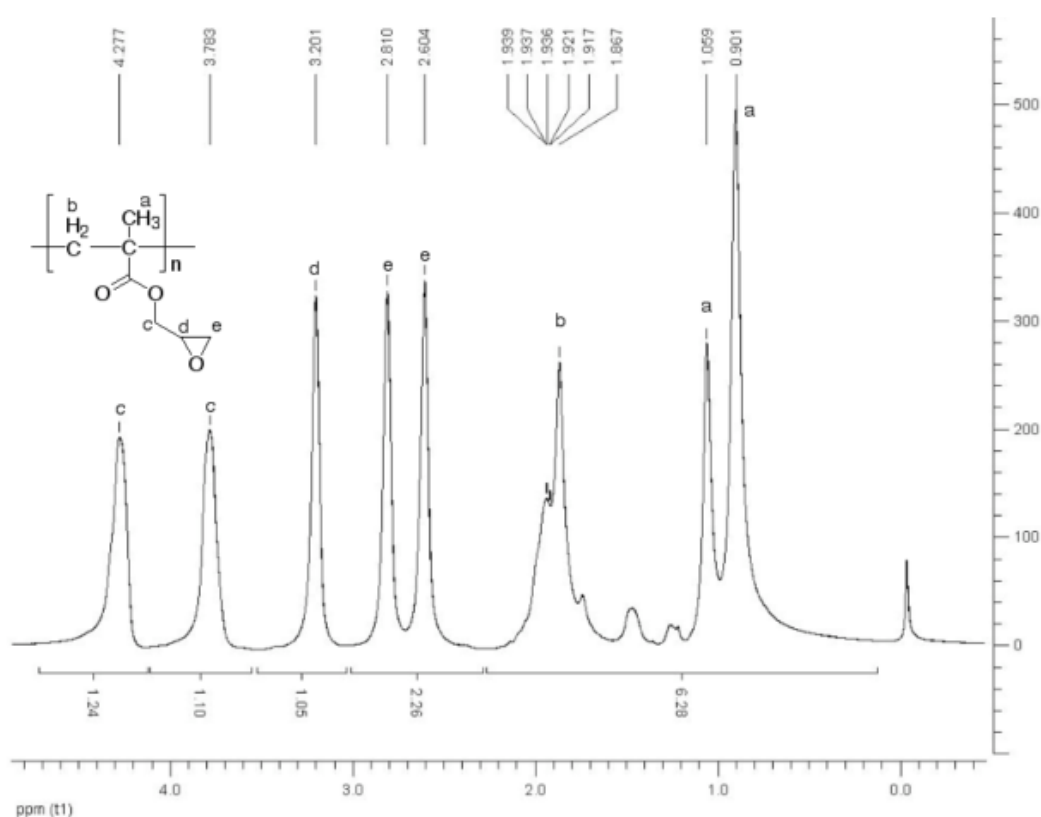
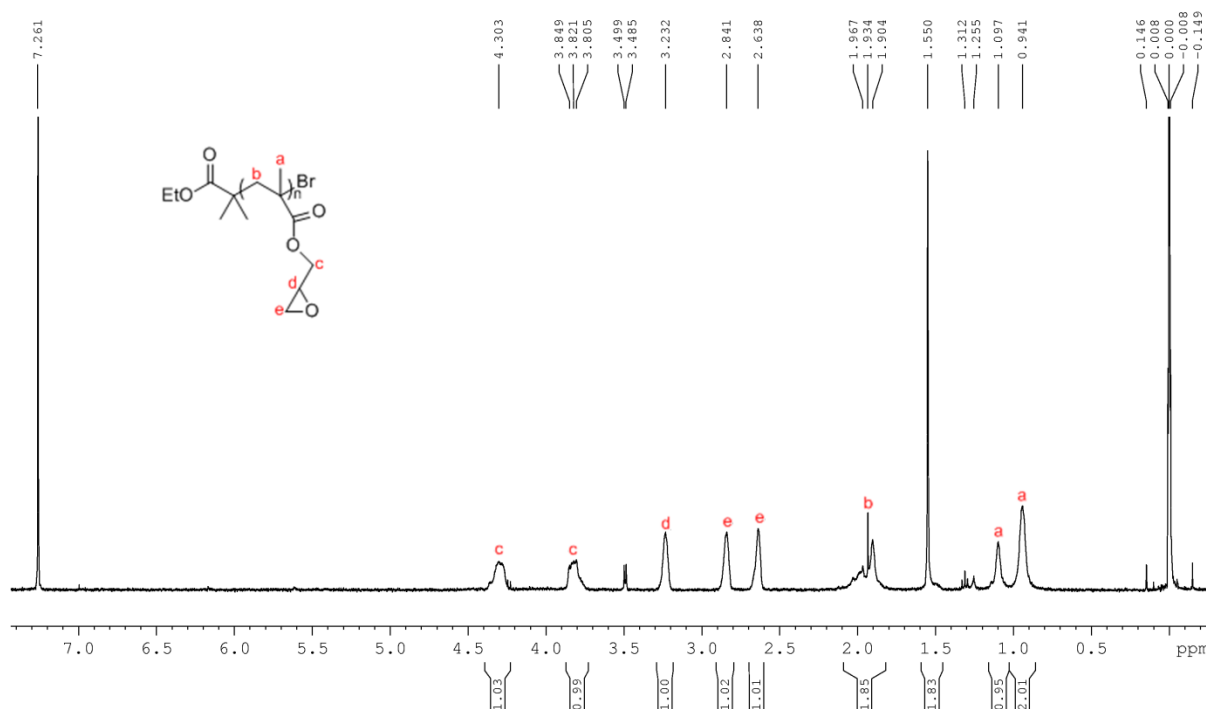


Figure 21 – NMR spectrum of PGMA reported by Hayek et al.<sup>93</sup> indicates the epoxy groups in PGMA remain intact during the polymerisation of GMA as the observed ratio of the peak areas of (a), (d) and (e) is about 3:1.



**Figure 22 – NMR spectrum of PGMA produced as part of this work, again indicating the epoxy groups remain intact during the polymerisation of GMA as the observed ratio of the peak areas of (a), (d) and (e) is about 3:1.**

This was also confirmed by FTIR where expected bands for epoxides<sup>96,97</sup> at ca. 1250 cm<sup>-1</sup>, ca. 900 cm<sup>-1</sup> and ca. 800 cm<sup>-1</sup>, were observed at 1253 cm<sup>-1</sup>, 905 cm<sup>-1</sup> and 843 cm<sup>-1</sup>.

### 3.2.2.2 Molecular Weight and DP of PGMA

Polymerisation was carried out under the same conditions as HEMA, by using both ATRP and ARGET ATRP but the purification process of the product was quite different as discussed in chapter 2. Nevertheless, the theoretical molecular weight and DP are reported below.

	Molecular Weight	Degree of Polymerisation
PGMA (ATRP)	11565	81
PGMA (ARGET ATRP)	14841	104

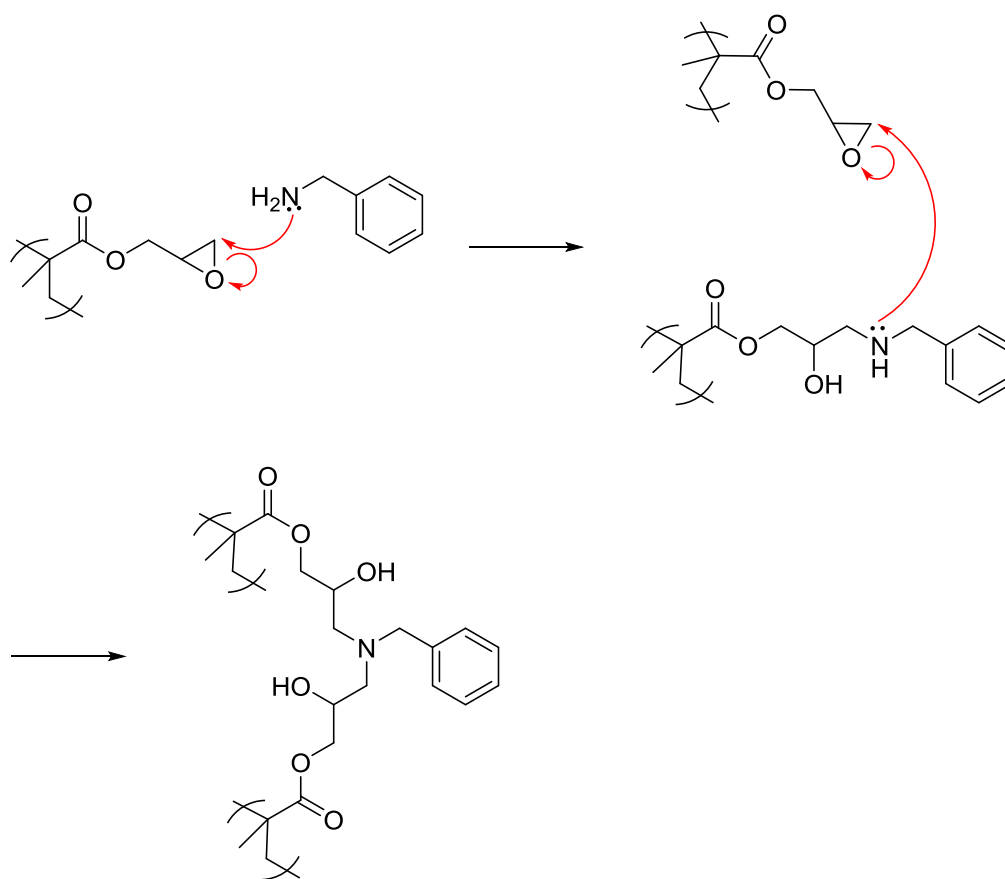
**Table 4 – Theoretical Mw and DP of PGMA products *via* ATRP and ARGET ATRP, calculated as shown for PHEMA.**

### 3.2.2.3 Post-Polymerisation Modification of PGMA

The polymer dissolved immediately in DCM and benzylamine was used to attempt post-polymerisation modification. Benzylamine was chosen purely to use the benzene group to prove quickly whether the reaction was successful *via* NMR. However, the resulting product



suggested that cross-linking had occurred. The product was jelly-like in appearance and after drying on a freeze drier, was insoluble after a variety of solvents tested. It is proposed that undesirably, further polymerisation occurred *via* the opening of epoxide rings. Barbey *et al.*<sup>98</sup> reports that cross-linking reactions with primary amines are possible, since the secondary amine group that is formed after the first ring-opening step can open a second epoxide ring. The example below in Scheme 37 is based on a proposed mechanism by Edmondson *et al.*<sup>73</sup> for a primary amine. This work uses benzylamine and hence the mechanism uses this as the primary amine.



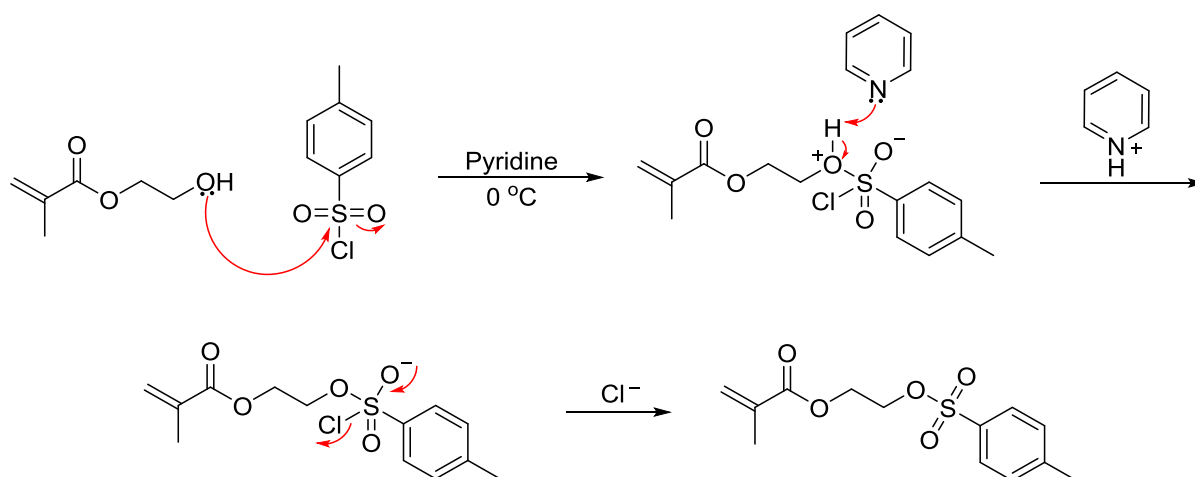
**Scheme 37 – Proposed mechanism by which PGMA crosslinks *via* the opening of epoxide rings, initiated by benzylamine based on Edmondson *et al.*<sup>73</sup>**

PGMA, much like PHEMA, demonstrated a much higher preference for cross-linking rather than the preferred functionalisation of the side chains from the backbone of the polymer. In hindsight the crosslinking was unavoidable when it came to post-polymerisation functionalisation of free polymer, but by carrying out both routes, it has been demonstrated that it does not matter which reagent holds the nucleophile, crosslinking will occur either way. The fact that these products were so difficult to dissolve was ideal for their end use,

making it easier to remove the product once metal sequestration was complete. However, characterisation was virtually impossible and what was truly formed remains unknown.

### 3.2.3 Tosylation of HEMA for further modification

As previous functionalisation attempts had failed and had produced cross-linked products, an alternative method was trialled with HEMA by attaching a well-known leaving group to promote further reactions. Alcohol groups are considered very poor leaving groups, unlike tosylate groups.<sup>69</sup> The tosylation of alcohols is a common transformation which is often used to facilitate subsequent nucleophilic reactions<sup>99</sup> and has been reported on HEMA by Reymond *et al.*<sup>100</sup> to produce tosyl-activated microspheres. Similar conditions were used to those by Stolle *et al.*<sup>41</sup> although only 4 hours were required, unlike the 14 reported. The reaction was carried out at 0 °C in pyridine and Scheme 38 illustrates this process that was shown to be a successful reaction *via* <sup>1</sup>H NMR and <sup>13</sup>C NMR.



Scheme 38 – Tosylation of HEMA in pyridine.

The tosylated HEMA did not polymerise under ATRP conditions used for HEMA. To find successful conditions (including the solvent system) would have been extremely time consuming<sup>101</sup> so instead an uncontrolled polymerisation was carried out using the radical initiator 1,1'-Azobis(Cyclohexanecarbonitrile, ABCN) in toluene. Once heated to 150 °C and refluxed for 5 hours as described in chapter 2, the polymer precipitated as a spongy gel. The product's insolubility once again proved a hindrance for further modifications although pyridine was found as a potential solvent. 4-hydroxybenzonitrile was used for post-polymerisation attachment, again for characterisation purposes rather than metal binding. It

was anticipated the cyano containing compound would act as a clear indicator *via* FTIR analysis and quickly confirm whether a reaction had taken place.

FTIR did indicate a cyano group but again was inconclusive as no shift was observed from the starting material (as might be expected as no chemistry had changed around this area of the molecule). It had been expected that a more intense peak would be observed with many repeat units available for attachment, however this was not the case.

Overall, this proved to be unsuccessful when it came to functionalising the polymer. Evidence of successful tosylation of HEMA monomer was determined by NMR but once polymerisation was carried out, the polymer was no longer miscible in common deuterated solvents for NMR and became very difficult to characterise. The fact that the PHEMA-Ts precipitated out suggests cross-linking<sup>102,103</sup> has taken place once again and if this was the case, further functionalisation would be very difficult.

### 3.3 Conclusion

PHEMA and PGMA have been successfully prepared *via* the polymerisation process known as ATRP and ARGET ATRP. <sup>1</sup>H and <sup>13</sup>C NMR have been used to prove the polymerisation was successful, allowing the work to be taken to the next stage whereby the processes can be adapted to grow the polymer from a solid surface.

Post-polymerisation modification processes have demonstrated to be extremely challenging in terms of the synthetic process, purification and characterisation. Cross-linking was one of the major complications with this process as evidence strongly suggested that PHEMA and PGMA both cross-linked when functionalisation was carried out. It was shown that it made no difference whether the nucleophile was on the side chain of the polymer or the ligand attaching to the side chain. Although this process was attempted with many reactants and many products recovered, a product that was conclusively functionalised without cross-linking and fully characterised could not be produced.

Modification was focussed on polymers and not their monomers because when this work was taken forward to surface attached materials, the monomer needed to be grafted from the surface using ATRP. If the monomer was modified from HEMA or similar monomers to a much larger monomer, the ATRP conditions would change too much that it would not work as ATRP is difficult to optimise.<sup>101</sup> The uncontrolled polymerisation would not be an option

with surface attached materials because ABCN would generate free polymer and not graft it from the surface.

FTIR provided the primary characterisation method for these materials due to their insolubility which provided limited knowledge on the product. Molecules with the easily characterisable cyano group were used to help but conclusive results could not be made from these spectra.

Tosylation of HEMA proved to be successful but could not be taken forward to the polymer stage in a way that took this work forward. This result did prove however that HEMA could be polymerised following modification. If time was spent on this area, new ATRP conditions could perhaps be developed to polymerise these functionalised HEMA products.

The reactions on free polymer have shown the ease at which cross-linking can occur. Due to the little success that had been achieved, it was decided that a focus should be prioritised to surface attachment and modification for the development of materials, chapter 4 presents these findings.

### **3.4 Future Work**

If ATRP for functionalised HEMA and other monomers was developed, this process could help produce many functionalised structures for metal sequestration in significantly less time. The functionalisation of monomers *via* organic chemistry as opposed to polymers would be much simpler and once a functionalised material was synthesised, it could be polymerised and used without the concern of cross-linking.

## 4 Surface attachment of ligands and polymers to silica surfaces

### 4.1 Introduction

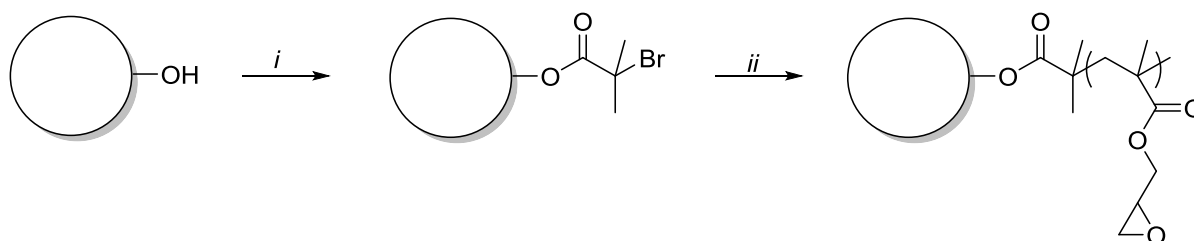
Following successful synthesis of PHEMA (see sections 2.2 and 2.3), surface attachment of PHEMA to silica was carried out. To graft the polymer from the silica, the surface has to be prepared so that a radical can be generated at the surface of the silica and initiate polymerisation. In total, four varieties of silica were investigated for polymer growth and/or ligand attachment and the results are deliberated in the discussion following.

Prior to introducing the silica materials used for this work, a review of the literature surrounding this area will be discussed, resulting in the reasoning for the approach taken in this project. Surface-initiated atom transfer radical polymerisation (SI-ATRP) is also a very well reported area and an extensive review including the synthesis, characterisation, properties and applications has been carried out by Barbey *et al.*<sup>98</sup> This acted as an extremely useful source to review previous work on the modification of surfaces, including silicon, metal oxides, clay minerals, gold and carbon as well as silica.

Work such as that published by Zhao *et al.*<sup>104</sup> on the use of surface attached polymers containing acrylic and crotonic acid to remove metal ions and Chen *et al.*<sup>105</sup> reporting ATRP methods for boron removal from aqueous solutions again demonstrate that by combining surface attachment of polymers with ligands targeted for specific metals could produce worthwhile results. This chapter will make clear how the chemistry from the free material is transferred to enable surface attachment and hence produce surface grafted polymers with the aim of producing highly functional materials.

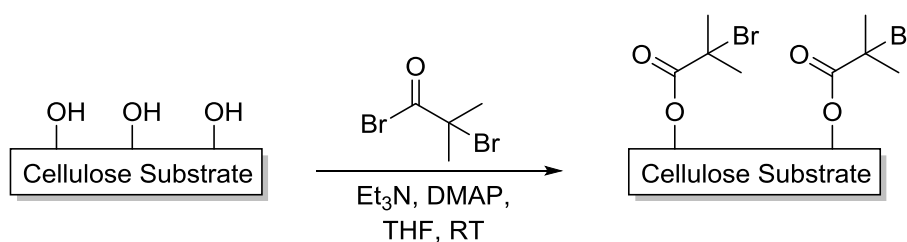
#### 4.1.1 Previous literature reporting the modification of silica surfaces

The first literature method reported is that by Jonsson *et al.*<sup>106</sup> and Perruchot *et al.*<sup>107</sup> Here, a one-step processes is used where the hydroxyl groups on the surface are directly used to form  $\alpha$ -bromo esters. Scheme 39 and Scheme 40 illustrates these methods and the conditions reported.



**Scheme 39** – Illustration of the synthetic strategy used in the surface modification of microspheres. (i) Conversion of hydroxyl groups to  $\alpha$ -bromo esters, (ii) ARGET ATRP using the  $\alpha$ -bromo ester as the initiating site. Conditions: (i) BIBB,  $\text{Et}_3\text{N}$ , DMAP,  $\text{CH}_2\text{Cl}_2$  or THF, RT, 2 h; (ii) GMA,  $\text{CuBr}_2$ , PMDETA, EBIB, ascorbic acid, toluene (50 % v/v),  $30\text{ }^\circ\text{C}$ .<sup>106</sup>

A similar concept was reported by Hansson *et al.*<sup>108</sup> (illustrated in Scheme 40) whereby cellulose substrates were prepared for ARGET ATRP, again by utilising the hydroxyl groups to form  $\alpha$ -bromo esters.

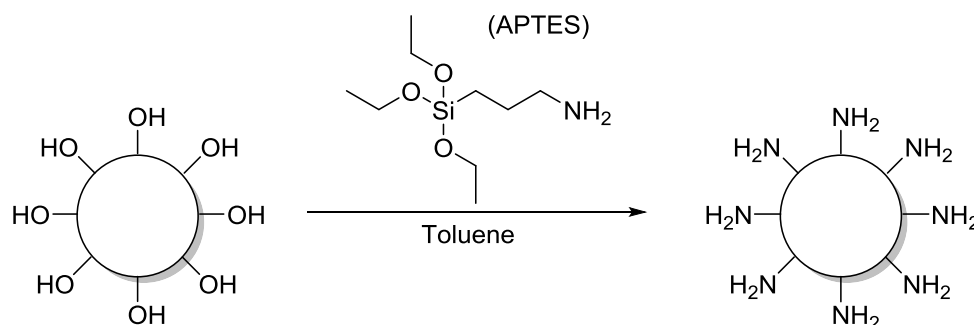


**Scheme 40** – Preparation of cellulose substrates for ARGET ATRP as proposed by Hansson *et al.*<sup>108</sup> before polymers were grafted *via* ARGET ATRP.

This method was not one the group felt was appropriate for silica surfaces based on the different reactivity of C–OH to Si–OH. It is highly unlikely this method would work directly on silica because of this but also the Si–O–C bond is readily hydrolysed<sup>109</sup> – putting severe limitations on its use in aqueous solutions and making it impractical for its purpose. The reactive carbonyl that would be located very close to the silica surface would also limit the monomers to be used for polymerisation. For these reasons, alternative methods were researched.

Zhang *et al.*<sup>110</sup> published work in 2006 on SI-ATRP of MMA and HEMA that was carried out on spherical silica gel following surface modification. This modification used a two-step synthesis where APTES was attached to provide an aminopropyl-silanation of silica gel as reported by Haller<sup>111</sup> (Scheme 41) before immobilisation of the surface initiator (2-bromopropionyl bromide) was carried out as illustrated in Scheme 42. Monomers of methyl

methacrylate (MMA) and HEMA were then polymerised by grafting from the surface, using the functionalised silica gel as the initiator.

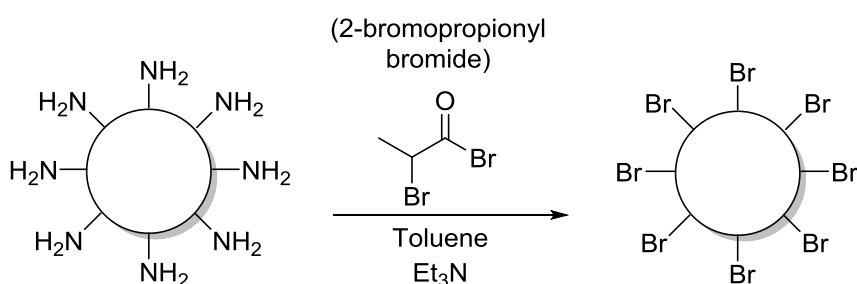


**Scheme 41 – The deposition of APTES to a surface.**<sup>110</sup>

The use of APTES is very common for the functionalisation of silica as well as other surfaces<sup>112,113,114</sup> and similar methods to that illustrated in Scheme 41 are reported by Liu *et al.*<sup>115</sup> and Wu *et al.*<sup>116,117</sup>

The main advantage of using APTES is because a strong surface bond is formed to support further modifications. Si–O bonds are much stronger ( $452 \text{ kJ mol}^{-1}$ ) than C–O bonds ( $358 \text{ kJ mol}^{-1}$ )<sup>118</sup> which are produced *via* this method and hence is a more practical approach when considering the end use. The amine group of the APTES provides a reactive end group that allows further modification to take place.

To carry out SI-ATRP, a halogen (often bromine or chlorine) end group is required meaning that at least one further step will be required before polymer grafting from the surface can be considered.



**Scheme 42 – The deposition of 2-bromopropionyl bromide to a surface.**<sup>110</sup>

2-Bromopropionyl bromide is often replaced with 2-bromoisobutyryl bromide (BIBB)<sup>115,117</sup> but both are reported to work efficiently and appears to make little to no difference on the polymerisation process.

The two-step modification process using APTES followed by 2-bromopropionyl bromide or BIBB is an extremely common method and one that appears to be very robust based on the number of groups that have reported successful results.<sup>115,117</sup> Not only has this two-step process worked well, but grafting polymers from these synthesised surfaces has also been part of the same literature and again positive results have been reported. Monomers including HEMA<sup>115</sup> and GMA<sup>119</sup> which were the two original target monomers to work with as well as DMAEMA<sup>85,120</sup> have all been thoroughly reported in literature to be successfully grafted from surfaces.

A further method that has been reported by Chen *et al.*<sup>43</sup> is the synthesis of 3-(2-bromoisobutyramido)propyl(triethoxy)silane (BIBAPTES) from APTES and BIBB *via* a typical organic reaction and reported in chapter 2.22. This method achieved the same as the two step reaction discussed above. Although this method only requires the one surface attachment reaction, a laborious synthetic reaction is required beforehand which inevitably requires a work up. This work up is avoided by doing the two step modification and hence was not anticipated to be used.

In this chapter, two materials are studied extensively for their full potential in carrying out the aims of this work. As stated in section 1.1, literature specifically reporting the modification of these materials, especially for the purpose of metal sequestration has not been found. The first silica to be used is referred to as ‘ZEOprep’ silica as this is the name given by the manufacturer whilst the second to be studied was fumed silica. The properties of these follow shortly. The capability of porous silica microparticles<sup>121</sup> was also investigated before a short period of time was given to explore the modification of the surface of silica that was bound around a ferrous oxide centre, thus making it retrievable from solution *via* magnetisation.

## **4.2 Results and Discussion**

### **4.2.1 ZEOprep silica**

The ZEOprep silica was the first to be used with this work and proved to be a practical substrate for surface modification. Used by many organic chemists for preparative and liquid chromatography, this silica was readily available and at an affordable price when scaling up of the reactions would be required. Due to chromatography being its main purpose, it is designed to have a wide particle size range to allow easy separation scale-up from laboratory



to production scales whilst also possessing exceptionally narrow pore size distribution - although no figures are provided.<sup>122</sup>

Figure 23 illustrates the ZEOprep particles observed under an optical microscope and Figure 24, the distribution graph, reveals the range of the particle size. The mean particle size is calculated to be 71.5  $\mu\text{m}$  despite the manufacturer claiming an average size of 40-63  $\mu\text{m}$ .<sup>122</sup> Both these figures were collected on behalf of the group by the Materials Department at Loughborough University.

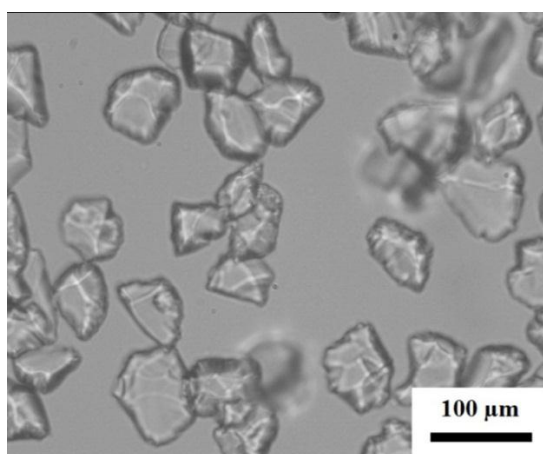


Figure 23 – A microphotograph of the ZEOprep silica particles using a Leitz Ergolux optical microscope.

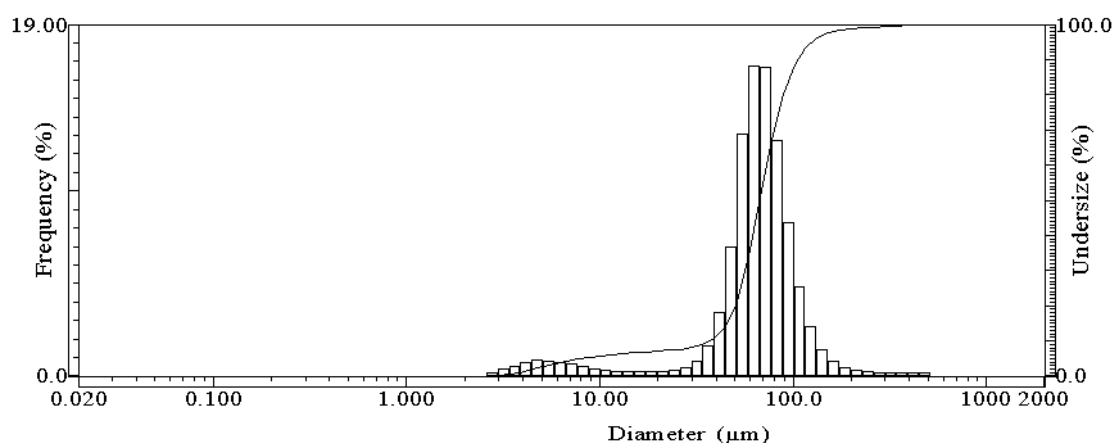


Figure 24 – A graph to show the size distribution of the ZEOprep silica particles using a particle size distribution analyser LA-920.

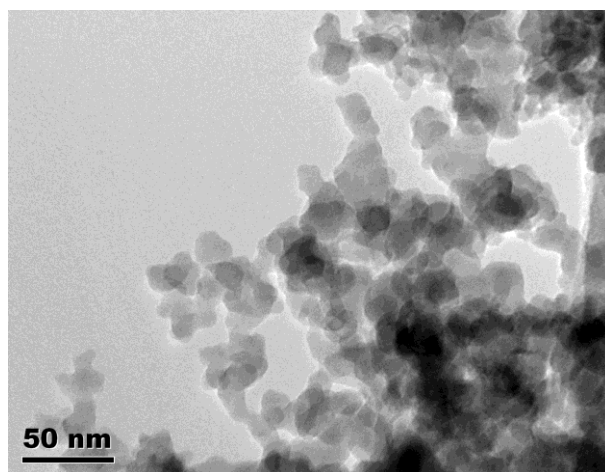
#### 4.2.2 Fumed silica

Fumed silica is used in commercial industries such as enhancing the viscosity of many liquids and paints. The most common application in biochemistry is for clarifying sera by removing lipids and one trade name reported is Aerosil 380.<sup>123</sup>

Fumed silica has a significantly smaller particle size of 0.007  $\mu\text{m}$  (7 nm) and a very large surface area of  $395 \pm 25 \text{ m}^2/\text{g}$ .<sup>124</sup> To acquire an accurate measurement of the particle sizes of this silica, a TEM (Transmission Electron Microscopy) image was produced (Figure 25) as the particle size distribution analyser LA-920 would have been unable to accurately measure these much smaller particles. More information on TEM is available in chapter 6 where it was used to carry out a range of studies, but here it is used to simply illustrate the particle size.

Fumed silica is produced by burning silicon tetrachloride in a flame of hydrogen and oxygen (ca. 1800 °C) to produce molten spheres of silicon dioxide. The sizes of the silica spheres (measured by an electron micrograph) can be varied by varying the process parameters and within a given batch still show uniformity. The molten spheres collide and fuse together to form branched, three dimensional chain-like aggregates.<sup>125</sup>

Many of these aggregates contain chains of 10-30 spheres in length which is equal to 0.1-0.2  $\mu\text{m}$ . As these aggregates cool down below the melting point of silica (1600 °C), reversible mechanical entanglement or agglomeration results from further collisions. The manufacturer estimates 3.5-4.5 hydroxyl groups per square nanometre of silica surface.<sup>125</sup>



**Figure 25 – TEM image of fumed silica. Although the manufacturer claims a 7 nm particle size, it was found that most range between 10 and 20 nm.**

### **4.2.3 Porous silica microparticles**

Porous silica microparticles (PSM) by membrane emulsification have been produced and reported by Dragosavac *et al.*<sup>121</sup> The process reported allows for the production of near-monodispersed spherical silica particles with controllable porosity.

A sample with an average pore size of 2.6 nm was obtained from the group at Loughborough University<sup>121</sup> and by utilising the surface of the pores along with the outer surface also, it was expected that a larger number of ligands and polymers could be attached and grafted from this surface.

#### 4.2.4 Silica coated ferrous oxide microparticles

Magnetite coated with silica provided a material that is magnetic, resulting in an alternative method of removal once functionalised. When using the silica powders in a real environment such as a waste pond, it was thought this material may be able to offer a more practical method of retrieving it from the waters.

Commonly known as superparamagnetic microparticles (SMPs), they are defined as microparticles over 100 nm in diameter, typically spherical and composed of an assembly of iron oxide ( $\text{Fe}_3\text{O}_4$  or  $\text{Fe}_2\text{O}_3$ ) superparamagnetic nanoparticles with diameters of 3 to 50 nm.<sup>44</sup> They are used in biological affinity separations which requires a high surface area and high magnetic mobility, making them appropriate to trial for this project. The following SEM images (Figure 26 and Figure 27) were supplied with the material donated from Platt and coworkers<sup>44</sup> at Loughborough University prior to functionalisation carried out in section 2.26. The images give a good insight into their surface shape and particle size.

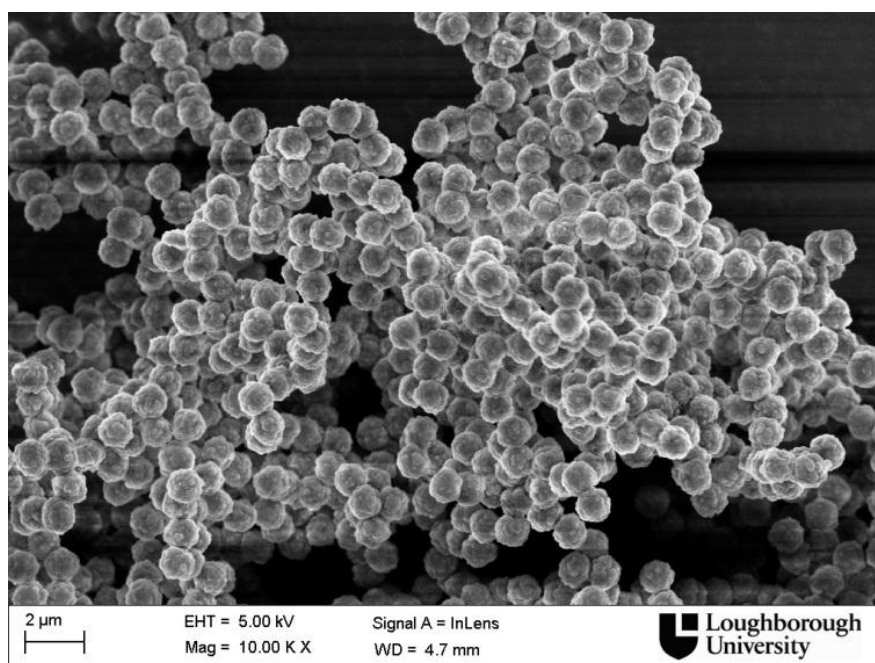


Figure 26 – SEM image of the superparamagnetic microparticles which were later functionalised by attaching the APTES ligand for metal removal trials.

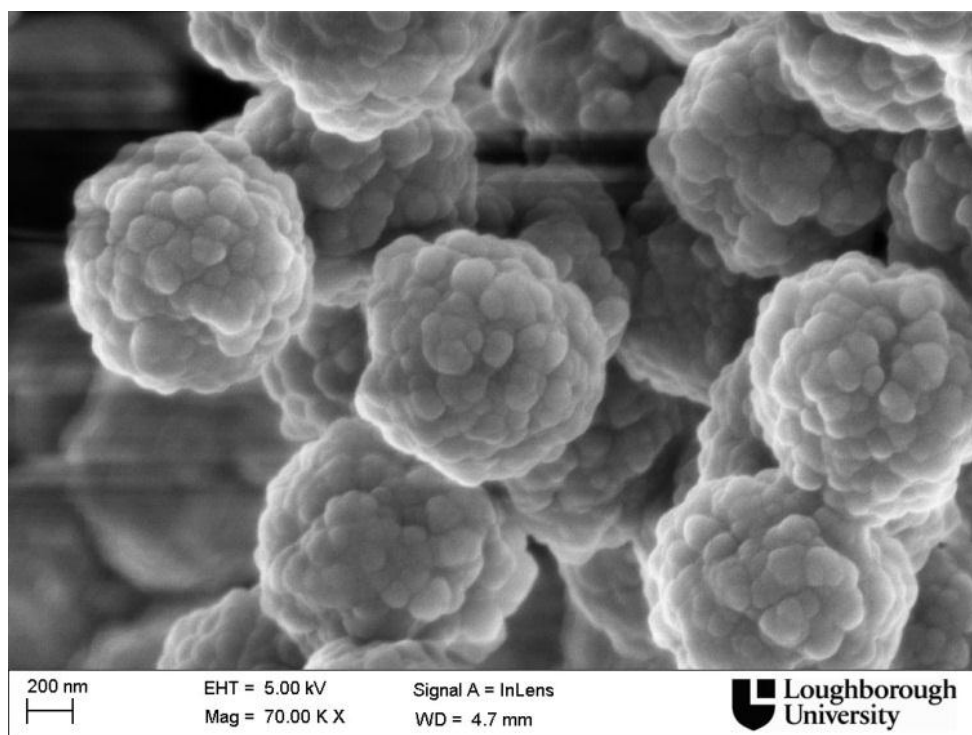
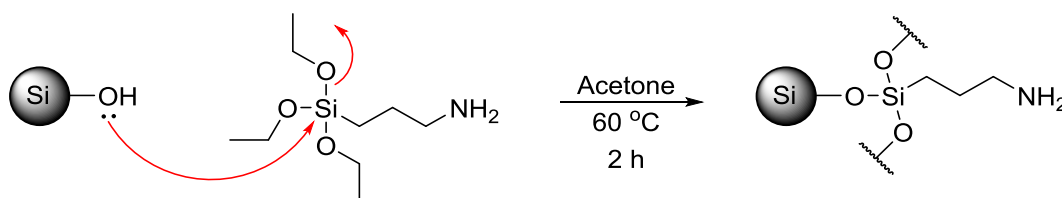


Figure 27 – SEM image clearly showing the silica coated nanoparticles fused together to produce SMPs.

Similar materials (SMPs also based on  $\text{Fe}_3\text{O}_4$ ) have been functionalised with dimercaptosuccinic acid for heavy metal removal from aqueous systems by Fryxell *et al.*<sup>126</sup> giving good reason to investigate this support.

#### 4.2.5 Deposition of APTES to ZEOprep and fumed silica

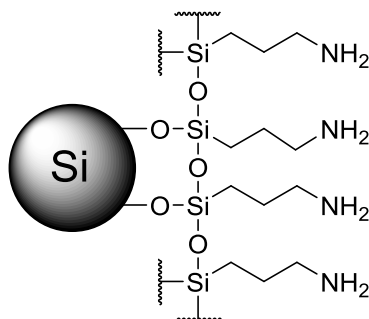
To graft the PHEMA from the silica, a multistep process was undertaken (as identified in the introduction and previous literature) in which the first step was to functionalise the silica with an amine-containing silane ((3-aminopropyl)triethoxysilane) known as APTES. The following mechanism in Scheme 43 shows how this is accomplished.



Scheme 43 – Mechanism and conditions required for deposition of APTES on silica.

Although toluene was identified as a common solvent for the deposition of APTES on silica and other surfaces, acetone had been identified by previous group members as a solvent system that is just as effective: hence this was the solvent system used. Figure 28 shows the accepted structure of APTES-functionalised silica<sup>127</sup> as a result of this synthesis. Steric

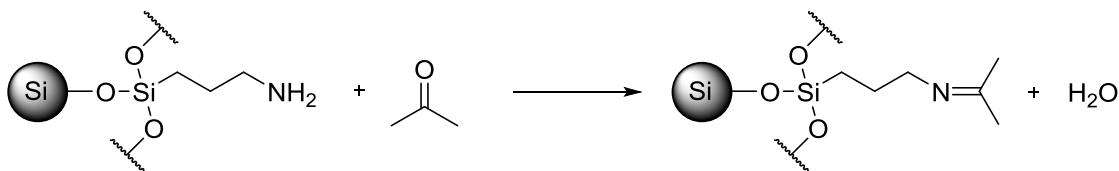
hindrance is understood to prevent the silicon atom in APTES being attached by three silica oxygen atoms. Instead, once attached to the silica, the APTES molecules bond with one another and essentially form a polymer around the surface.



**Figure 28 – Generally accepted structure of APTES-functionalised silica.<sup>127</sup> In reality, it is unlikely that the silane groups will remain as functionalised and amine groups so obtrusive.**

FTIR results were consistent with the expected stretches. A primary amine stretch is expected at between 1650-1560  $\text{cm}^{-1}$  and one is observed at ca. 1635  $\text{cm}^{-1}$ .<sup>128,129</sup> Another observed band includes the broad peak at ca. 1052  $\text{cm}^{-1}$  representing  $-\text{Si}-\text{O}-\text{Si}-$  expected at 1110-1000  $\text{cm}^{-1}$  which is also observed in the starting material.<sup>97</sup> Due to such a large peak, other expected peaks appear comparatively small due to a relatively small modification that is only taking place on the surface. Additional Si–O bonds are attached as a result of this first step in the silane group, which only helps to increase the bands prominence in the spectra.

Interestingly, work reported by Borak *et al.*<sup>130</sup> demonstrated that when APTES is already attached to silica particles and simply impregnated with acetone the amino groups converted into Schiff bases (also known as imino groups). Scheme 44 illustrates the reaction proposed by the group.



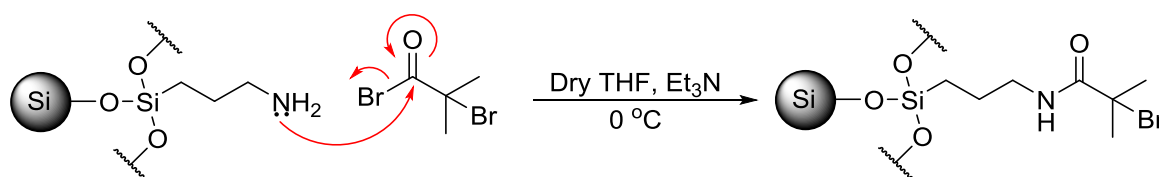
**Scheme 44 – The procedure of the coupling reaction of silica particles with amine groups and acetone as reported by Borak *et al.*<sup>130</sup> – specific reaction conditions including temperature were not reported.**

The group reported a new sharp band in FTIR at 1733  $\text{cm}^{-1}$  corresponding to the C=N groups of the Schiff bases. However, the peak at 1610  $\text{cm}^{-1}$  that was reported from the amine group still existed after this reaction with acetone suggesting not all the amine groups are converted.

The C=N peak was never observed in the work carried out for this project but why this is the case is not clear. If there was a preference for the amine group to go on to react with the acetone once it was attached to the silica, there was nothing to prevent this taking place in the system set out in this thesis. The only difference in the work by Borak *et al.*<sup>130</sup> was that the silica was already functionalised with APTES and added to pure acetone although conditions, including temperature were not reported.

#### 4.2.6 Deposition of BIBB to ZEOprep and fumed silica

Following the deposition of APTES, the next synthetic step involved the addition of the bromine initiating group known as alpha-bromoisobutyryl bromide (BIBB). After reflecting on literature discussed at the start of chapter 4, BIBB was chosen over 2-bromopropionyl bromide simply because the group had more experience with this compound based on work reported by Edmondson.<sup>40</sup> Scheme 45 illustrates the mechanism for the attachment of the BIBB group to the APTES group now grafted to the silica.

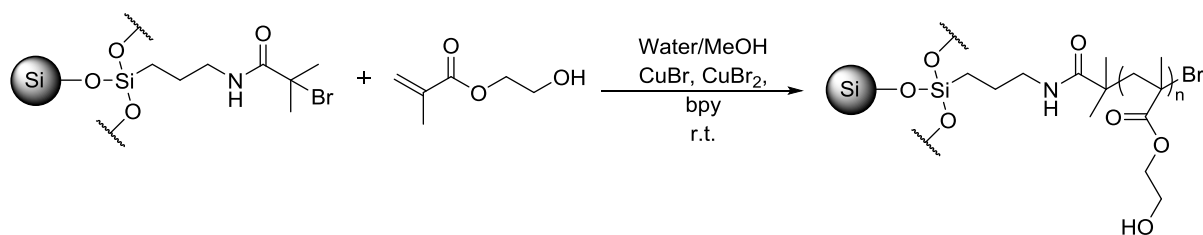


Scheme 45 – Mechanism and conditions required, illustrating the deposition of BIBB to the silica surface.

A shift in the IR would be expected for this change and is observed with the two amide peaks visible at ca. 1648  $\text{cm}^{-1}$  and ca. 1537  $\text{cm}^{-1}$ . For solid state IR, these peaks are expected at 1680-1630  $\text{cm}^{-1}$  and 1570-1515  $\text{cm}^{-1}$  which fits the spectra (see Figure 29) and the peak at 1680-1630  $\text{cm}^{-1}$  is also expected to be more intense<sup>97</sup> which is also observed.

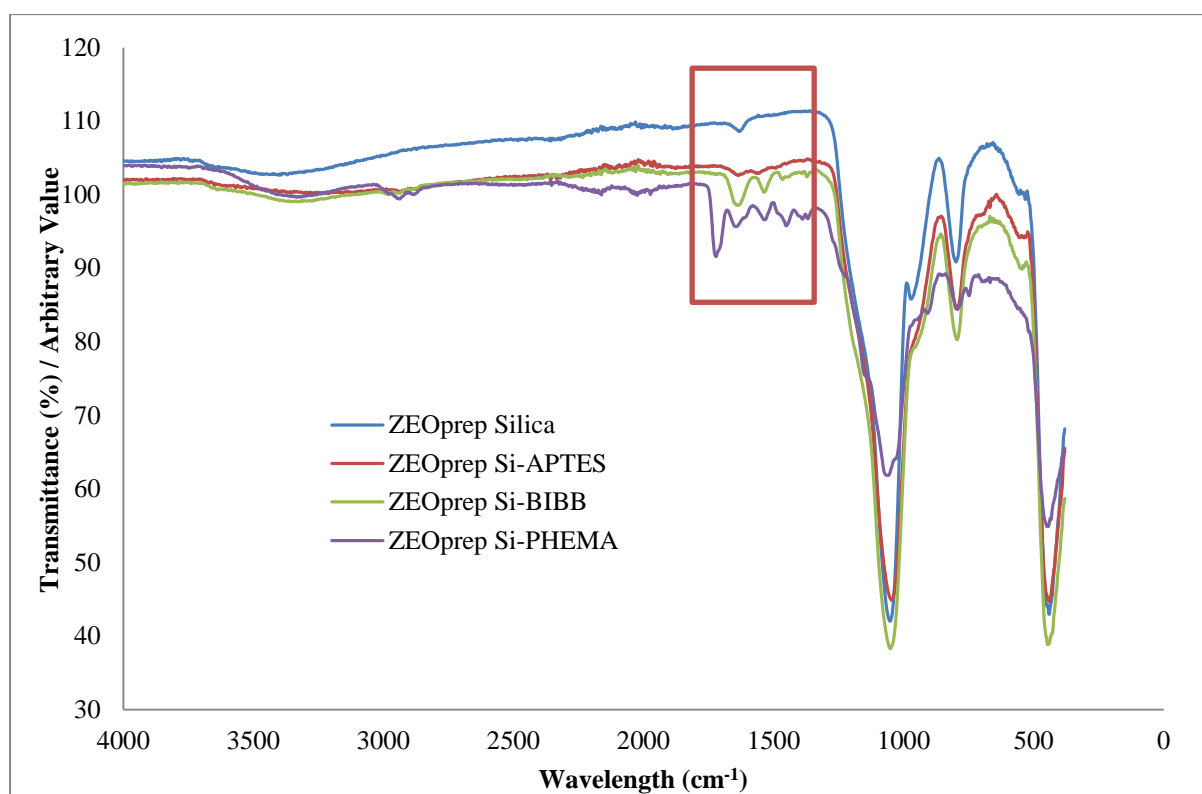
#### 4.2.7 Grafting of PHEMA from surface of ZEOprep and fumed silica

With the bromine atom attached to the surface of the silica *via* the organic chain now formed, the same principle for the grafting of the polymer can be utilised, but instead of using EBIB (used in the polymerisation of the free polymer), the functionalised silica is added to the solution.



**Scheme 46** – The grafting of PHEMA from the silica surface based on the mechanism shown in Scheme 32.

A more detailed characterisation has been carried out on this material and its precursors with more details of this described in the following chapter. However IR again enabled fast characterisation and a peak for the new ester group was observed at ca.  $1735\text{ cm}^{-1}$  which is shown in Figure 29. The two amide peaks were still present as would be expected and shown structurally in Scheme 32.

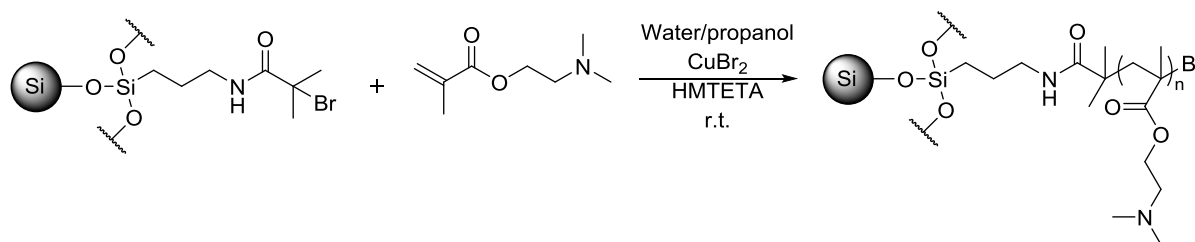


**Figure 29** – An example of the shifts observed *via* FTIR for each step of the silica modification. ZEOprep silica is the material used in the case of these spectra. The area highlighted shows where the differences in peaks are observed as the material undergoes functionalisation.

#### 4.2.8 Grafting of PDMAEMA from surface of ZEOprep silica

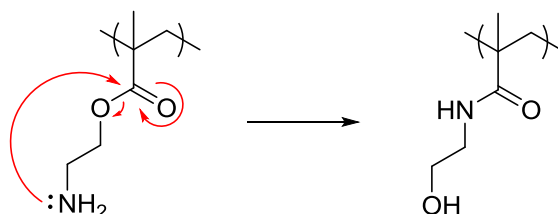
Surface attached PDMAEMA was synthesised as an alternative to PHEMA following the post-polymerisation modification work because work by Zhao *et al.*<sup>131</sup> has reported efficient Hg(II) removal (74.5 % recovery) as well as notable selectivity when present with other

divalent metals. The method used was very similar to that used by Zhou *et al.*<sup>120</sup> shown in Scheme 47. The metal sequestration results of the material can be found in chapter 6.



**Scheme 47 – Mechanism to show the grafting of PDAEMA from the silica surface.**

Incorporation of amines into synthetic polymers has been reported to be difficult<sup>77</sup> due to addition of the amine to activated vinylic double bonds<sup>132</sup> and oxygen-nitrogen acyl migration resulting in hydroxylated acrylamides when starting with amino acrylates.<sup>133</sup> 2-aminoethyl methacrylate (AEMA) would have been tested had it not been for its known tendency to react with itself and cross-link.<sup>77,78</sup> The primary amine group at the end of AEMA could have provided an ideal material for metal sequestration but because of its reported reactivity, this was avoided to concentrate on what the group thought would be a more productive use of time.



**Scheme 48 – Mechanism to demonstrate intramolecular amidation of PAEMA.**

Scheme 48 illustrates the mechanism by which intramolecular amidation could occur. Other forms of this could also take place such as two side chains reacting to form a 9 membered ring or intermolecular amidation could take place with two polymer chains and hence resulting in cross-linking.

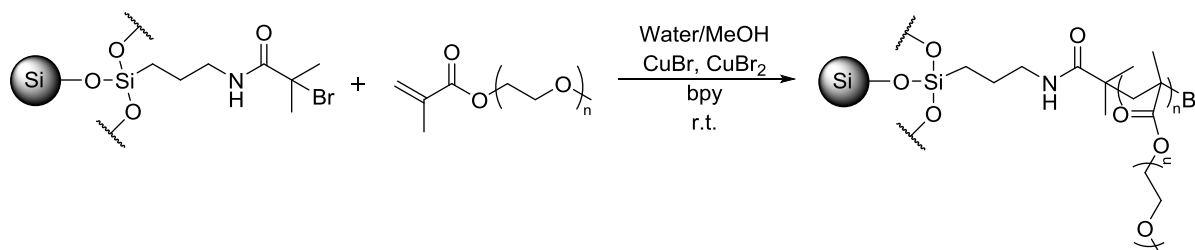
PDMAEMA was also considered to attempt quarternisation<sup>134</sup> and thus producing a positively charged nitrogen end group. The result of this would enable anions to be targeted and reverse the initial idea of the project. This never materialised due to a change in focus once metal sequestration had been trialled, however this could be a viable option if future work was ever considered.



The PDAEMA functionalised silica product was characterised by FTIR, showing strong peaks at ca.  $1040\text{ cm}^{-1}$ ,  $1460\text{ cm}^{-1}$ ,  $1535\text{ cm}^{-1}$ ,  $1643\text{ cm}^{-1}$ ,  $1727\text{ cm}^{-1}$ . The ester in the polymer is responsible for the peak at  $1727\text{ cm}^{-1}$  which is reported by Zhao *et al.*<sup>131</sup> whilst the peaks at  $1643\text{ cm}^{-1}$  and  $1535\text{ cm}^{-1}$  are due to the amide as discussed in the BIBB attachment process. Aliphatic  $\text{CH}_3$  bending is known to produce peaks at ca.  $1460\text{--}1380\text{ cm}^{-1}$  which could explain the peak at  $1460\text{ cm}^{-1}$  due to the  $\text{CH}_3$  groups at the end of each repeat unit attached to the nitrogen atom.<sup>135</sup> This peak is also reported by Zhao *et al.*<sup>131</sup>

#### 4.2.9 Grafting of PEGMA from surface of ZEOprep and fumed silica

PEGMA (molecular weight 300) was grafted from the surface of ZEOprep and the fumed material by replacing it for HEMA and carrying out the attachment in an almost identical process. PEGMA is already a short polymer itself and by attaching a small number of units to the silica, a large number of oxygen atoms could be attached for metal removal. In chapter 7 a range of materials are introduced and more specifically, so is a material named Polyol 2 alkyl silica (PhosphonicS Ltd). It is the results from this material and the similarity of this with PEGMA that prompted this polymer to be grafted from the two surfaces of ZEOprep and fumed silica.



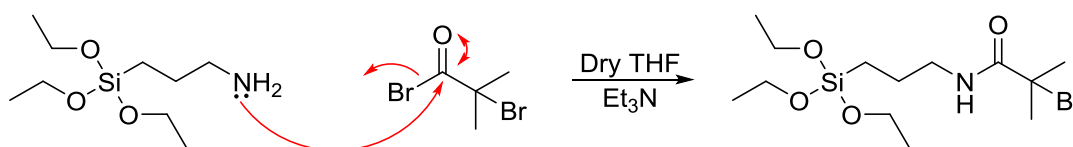
Scheme 49 – Mechanism to show the grafting of PEGMA from the silica surface

The conditions for this reaction were used from similar conditions given by Perruchot *et al.*<sup>107,136</sup> and Hu *et al.*<sup>137</sup> – full details of which can be found in chapter 2.17 and 2.21 for ZEOprep and fumed silica respectively. FTIR showed a new peak at ca.  $1727\text{ cm}^{-1}$  on both the ZEOprep and fumed silica materials from the ester group. Ether peaks (observed at  $1150\text{--}1070\text{ cm}^{-1}$ )<sup>97</sup> fall too close to the  $-\text{Si}-\text{O}-\text{Si}-$  (expected at  $1110\text{--}1000\text{ cm}^{-1}$ )<sup>97</sup> to take anything conclusively from this area of the spectrum. The initial SI-ATRP reaction was carried out on the ZEOprep silica but when the fumed silica was functionalised it was found that a larger amount of solvent was required as well as having to reduce the reaction time due to a large production of free polymer. The free polymer formed a gel which contained all the silica, making the retrieval of the surface attached material essentially impossible.

#### 4.2.10 Modification of porous silica microparticles (PSM)

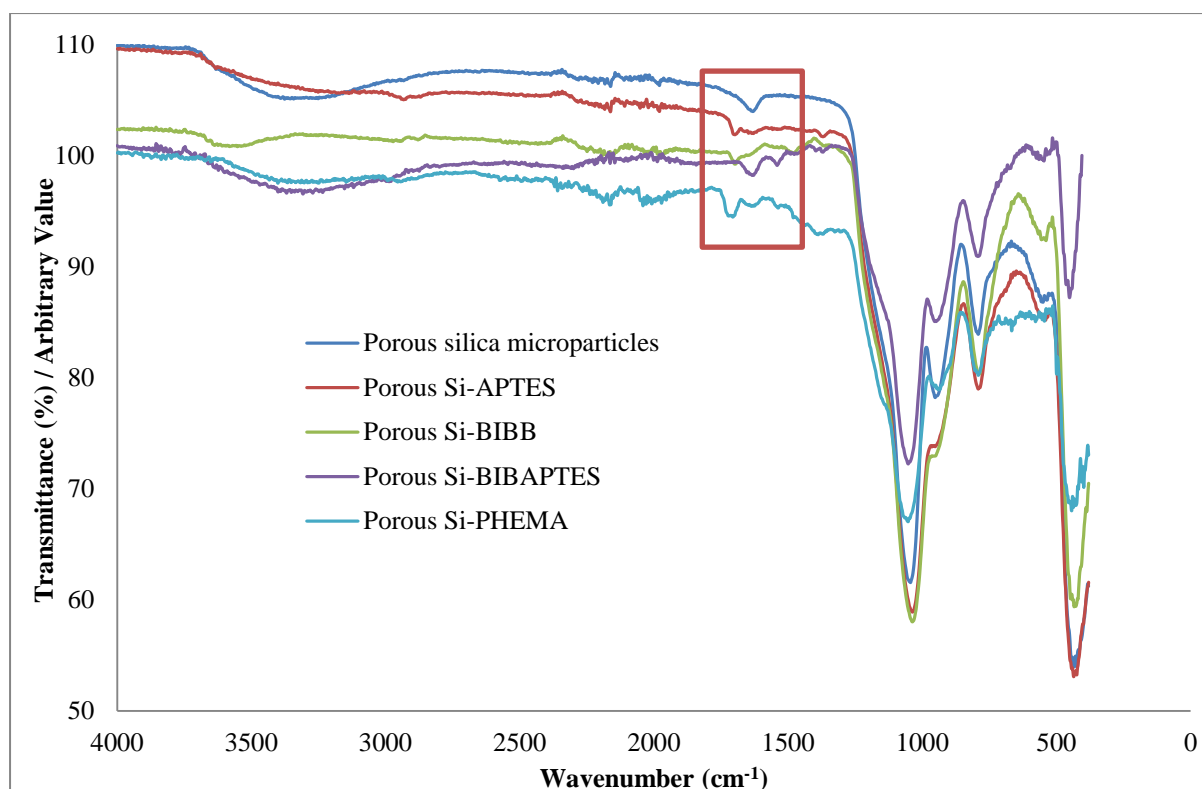
APTES was attached to this material in exactly the same way as reported for the ZEOprep and fumed silica. However, when analysed by FTIR, the amine peak was very weak. This contradicted the expectation that a larger quantity of APTES would be functionalised from the surface than had been observed with the previous surfaces of ZEOprep and fumed silica. O–H bending vibrations are observed at ca.  $1400\text{ cm}^{-1}$  and therefore suggested that available O–H sites still existed after the first APTES attachment. The material underwent APTES attachment for a second time which appeared to slightly increase the strength of the amine peak but certainly not to the extent observed on the previous silica materials. BIBB attachment was carried out but FTIR quickly ruled out any amide peaks following this and it was soon realised this process was not applicable for this material. It was thought that if the APTES molecules were binding to the hydroxyl groups of the silica in the pores, then this could be blocking the pores for further modification and hence, the amine end groups would not be available for the BIBB reaction. However, as explained in the TGA studies in chapter 5, it appears the pores were never available due to surfactant or carbon framework being present, resulting in a limited quantity of surface being accessible for functionalisation.

To overcome the lack of APTES deposition, a method was used by Chen *et al.*<sup>43</sup> whereby APTES and BIBB were reacted to form ‘BIBAPTES’ before being attached to the silica surface. This meant that if it was the case that APTES molecules were blocking the pores and the amine groups inaccessible, this larger molecule would graft from more suitable areas of the surface and prepare the surface for SI-ATRP.



**Scheme 50 – Synthesis of BIBAPTES before using for deposition from PSM surface. Full conditions of the reaction can be found in chapter 2.22.**

Once polymerisation of HEMA was carried out following the attachment of BIBAPTES, the ester peak was clearly observed at ca.  $1732\text{ cm}^{-1}$  although again, the peak was not as intense as expected. Further reasoning for this is explained in the following chapter. The FTIR spectra are shown in Figure 30 for the PSM and its modification.



**Figure 30 – FTIR spectra of the porous silica microparticles and its functionalised derivatives. Amide groups are only observed once BIBAPTES has been attached and not via the two step process of APTES followed by BIBB attachment. The ester peak is observed from the PHEMA following polymerisation of HEMA from the BIBAPTES. The red box highlights the main area where the bands that represent these functional groups are found.**

#### 4.2.11 APTES attachment to SMP's

Very little (ca. 3.7 mg) of this material was available as opposed to the vast quantities of the ZEOprep and fumed silica. As such, APTES deposition was carried out on a much smaller scale (see chapter 2.26 for full conditions) and metal removal studies had to be adjusted accordingly. This reaction was carried out on a rotary evaporator where the water bath was heated to 60 °C. FTIR was the only method used to prove the APTES had attached and an amine peak was observed at ca. 1632 cm<sup>-1</sup>.

### 4.3 Conclusion

This chapter has demonstrated the techniques used for modifying four different variants of silica surfaces. APTES was successfully attached to ZEOprep and fumed silica as well as the superparamagnetic microparticles (SMP) and porous silica microparticles (PSM). To ZEOprep and fumed silica, BIBB was successfully attached to the APTES-functionalised silica, preparing the material for ATRP of a monomer by the use of the bromine end group on the surface.

The problems that arose from work with the PSM were overcome by the synthesis of BIBAPTES. Although this was more time consuming, it provided a material that could undergo ATRP that otherwise could not have using the step-wise method of APTES attachment followed by BIBB. BIBB attachment and polymerisation of monomers were not attempted on the SMP material due to only a very small amount being provided to the group to study. Instead, this material was functionalised with APTES and kept for testing once this part of the project had commenced.

FTIR proved to be a very useful characterisation technique to provide a quick indication on whether the surface modification had been successful, although it was acknowledged this provided no guarantee that the molecule was bound to the surface. The easily identifiable peaks of amines and amides provided a very good indication as to whether the APTES and BIBB attachments had been successful before the attachment and growth of the polymers provided another easily characterisable group in the form of the ester group. Full characterisation of these materials using a wide range of techniques is rarely reported in publications and hence the following chapter looks at the characterisation of these materials in much more detail to ascertain a further understanding of their make-up.

Due to the difficulties encountered with ligand attachment to the free polymers in chapter 3, none of the surface attached polymers were post-functionalised for metal sequestration. Instead it was decided that PHEMA, PDMAEMA and PEGMA would be surface grafted and investigated in their natural form.

Prior to the metal sequestration testing, time was spent on thoroughly characterising the preparation steps and the PHEMA chain growth. A range of techniques were utilised which are discussed in the following chapter, enabling determination of distinct differences between the functionalisation of ZEOprep and fumed silica materials. This resulted in quantifiable differences between the two materials.

#### **4.4 Future Work**

Ligand modification to the grafted polymers was not investigated partly due to the difficulties encountered on the free polymer in the previous chapter but also due to time. It was felt the materials already produced should be tested before further materials were designed. As will be discovered in chapter 7, the strong focus on ligands resulted in a change of direction from the polymer work. However, with the results of those ligands now known, a focus on attaching them to polymers could enable more efficient removal of metal ions.

## 5 Detailed and mechanistic characterisation of silica materials

### 5.1 Introduction

To demonstrate the silica materials had been successfully functionalised and to further the knowledge regarding these materials, thermogravimetric analysis (TGA) and solid state NMR (SSNMR) was utilised, along with elemental analysis.

The lack of literature suggests full characterisation of materials produced and reported *via* those methods discussed in the previous chapters is very uncommon, especially the use of SSNMR.<sup>138,139</sup> However, this particular characterisation method has proven to be one of the most valuable in improving the understanding of the material's structure and the results are discussed in detail in this chapter.

It must be pointed out that SSNMR has been used and reported by some research groups in the past.<sup>139,140,141</sup> Nonetheless, to the author's knowledge it has not been used to the extent of characterising each step of this modification process or with the silica materials discussed (i.e. deposition of APTES, followed by BIBB then PHEMA).

#### 5.1.1 Solid State Nuclear Magnetic Resonance

SSNMR spectroscopy is a technique that can provide detailed structural information at a molecular level,<sup>142</sup> helping to fully characterise materials that would otherwise be extremely difficult to do so.

SSNMR allows the silica materials described in this work to be characterised in detail that other techniques cannot provide. It has helped demonstrate that surface attachment was successful along with the use of other experiments and techniques that would not have otherwise been as conclusive. The improvements made to this technique over the years along with a combination of high magnetic field, fast spinning speeds and efficient proton decoupling have allowed high quality  $^{13}\text{C}$  SSNMR to be obtained.<sup>142</sup> The surface modifications discussed see the attachment of many carbon atoms over a number of steps, making SSNMR one of the most valuable techniques available.  $^{29}\text{Si}$  SSNMR has also been recorded, providing qualitative and quantitative information.

Most SSNMR methods use Cross Polarisation Magic Angle Spinning (CPMAS) to obtain a high resolution spectrum. Whilst this method leads to an improved signal-to-noise ratio, it is

not quantitative, and the peak intensities cannot be directly related to the quantities.<sup>143</sup> A short introduction to these terms is given below.

#### 5.1.1.1 Magic Angle Spinning (MAS)

Typical solution-state NMR spectra appear as very sharp lines due to the fast motion and random tumbling of the molecules averaging the anisotropic interactions to zero and narrowing the resonance lines.<sup>144</sup> This means that for complex compounds, signals rarely overlap and hence, detailed information can be extracted.<sup>142, 145</sup>

This random tumbling is not possible in solid-state samples, resulting in dipole-dipole couplings dominating the NMR spectrum and by contrast, the peaks are very broad. High resolution spectra are produced by reproducing the tumbling of solution-state molecules. This is achieved by spinning the sample around an axis inclined at an angle of  $54^{\circ} 74''$  – also referred to as a magic angle.<sup>144</sup>

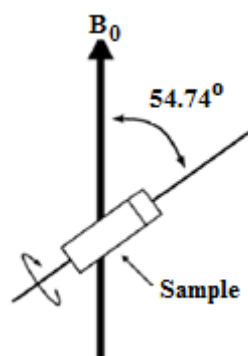


Figure 31 – Magic Angle Spinning where a sample is rotated at  $54^{\circ} 74''$  to the magnetic field ( $B_0$ ).

#### 5.1.1.2 Cross Polarisation (CP)

Cross polarisation is used to obtain adequate signal-to-noise in an SSNMR experiment which is important in obtaining coherent spectra: this technique is utilised for the experiments discussed. It is usually used to assist in observing dilute spins, such as  $^{13}\text{C}$ .<sup>145</sup> Acceptable signal-to-noise ratios are obtained after many scans and hence after a considerable amount of time. Time delays between each scan are also important, too short and the magnetisation becomes saturated and no signal can be recorded, too long and the experiment becomes an inefficient use of instrument time. To help overcome this problem the NMR pulse program has a relaxation delay that allows a state of equilibrium to be established. Typically this can be 10-300 s for  $^1\text{H}$  and 60-3000 s for  $^{13}\text{C}$  for solid organic crystalline material but reduced to

1-30 s for  $^1\text{H}$  and 2-60 s for  $^{13}\text{C}$  for poorly crystalline material very quickly amounting to exceptionally long experiment times – often weeks.<sup>142</sup>

The low abundance of  $^{13}\text{C}$  (relative abundance 1.1%) also makes signal to noise ratios inevitably poor. Cross polarisation overcomes this problem by observing  $^{13}\text{C}$  *via* the  $^1\text{H}$  (relative abundance ca. 100%) resulting in improved spectral resolution and allowing much shorter relaxation delays.

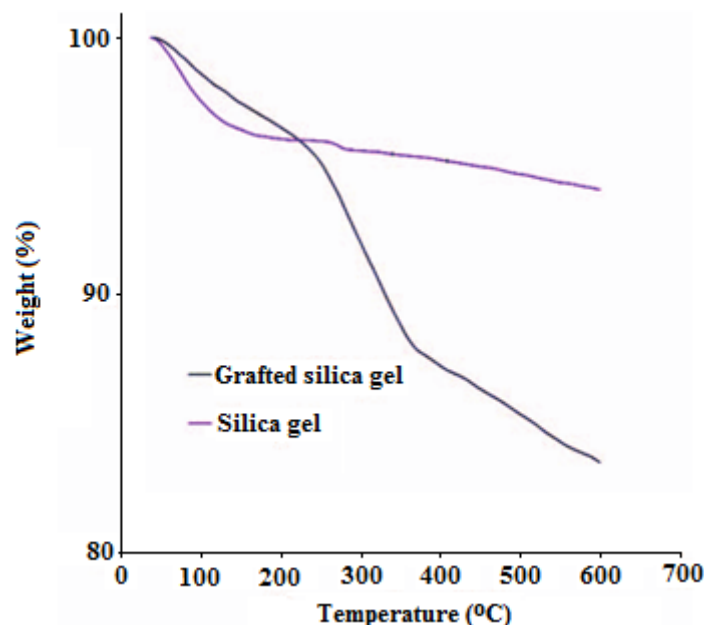
### 5.1.2 Thermogravimetric Analysis

Thermogravimetric analysis (TGA) is an analytical technique that accurately monitors the change in weight of a sample as a function of temperature. Providing the final products are known, the difference between the final and the starting compositions can be determined, where the additional atoms have been evolved as a gas.<sup>146</sup>

TGA is used across many areas of chemistry including polymers where it can be used to determine characteristics of products as described in the review by Coats *et al.*<sup>147</sup> and references therein. It can also be used to ascertain degradation temperatures, absorbed moisture content and the level of inorganic and organic components in a material.

By carefully increasing the temperature, often to temperatures greater than 1000 °C, the weight percentage can be plotted against temperature. Once the data has been obtained, the characteristics of the material can begin to be processed.

TGA analysis of poly(AGE/IDA-co-DMAA)-grafted silica gel (which was introduced in the literature review in chapter 1) was reported by Panahi *et al.*<sup>29</sup> This technique will be valuable to quantifying the amount of organics attached to the surface of the silica when a known mass of sample is analysed as shown in Figure 32.



**Figure 32 – TGA of silica gel and poly(AGE/IDA-co-DMAA)-grafted silica gel.<sup>29</sup>** The silica gel shows the majority of its weight lost at ca. 100 °C due to water before essentially levelling off. The grafted silica gel shows a much more significant weight loss due to the additional organic material now attached.

In the case of this work, TGA was used to determine just how much material was successfully attached to the silica surfaces being investigated. Assumptions do have to be made in what is accepted to be the final RMM of the silica but this is explained where necessary. All samples were heated to 800-1000 °C. The samples included all forms of silica that were introduced in chapter 4, with the exception of SMPs. These were followed by their corresponding functionalisation steps which included the APTES and BIBB attachment products, followed by the PHEMA growth. Each of these samples follow one another in the synthetic process and therefore each sample is expected to lose a larger percentage weight than the previous when run in that order. This is because more organic molecules are progressively being detached and cannot survive these high temperatures, hence are burnt off and the material loses mass.

### 5.1.3 CHN Elemental Analysis

Carbon, hydrogen and nitrogen content in organic and inorganic compounds are determined in this process. Combustion of weighed samples (typically 1-3 mg) occurs in a pure oxygen environment under static conditions.

Figure 33 illustrates the combustion train and analytical system, this being specific to the CE-440 elemental analyser that was used for the work in this project. Solenoid valves A–G



control the gas flow through the system whereas H and I are used for automatic leak testing and other maintenance purposes.

In the reduction tube, following combustion, oxides of nitrogen are converted to molecular nitrogen and residual oxygen is removed. The gases are homogenised in the mixing volume, before being released through the sample volume and into thermal conductivity detector.<sup>148</sup>

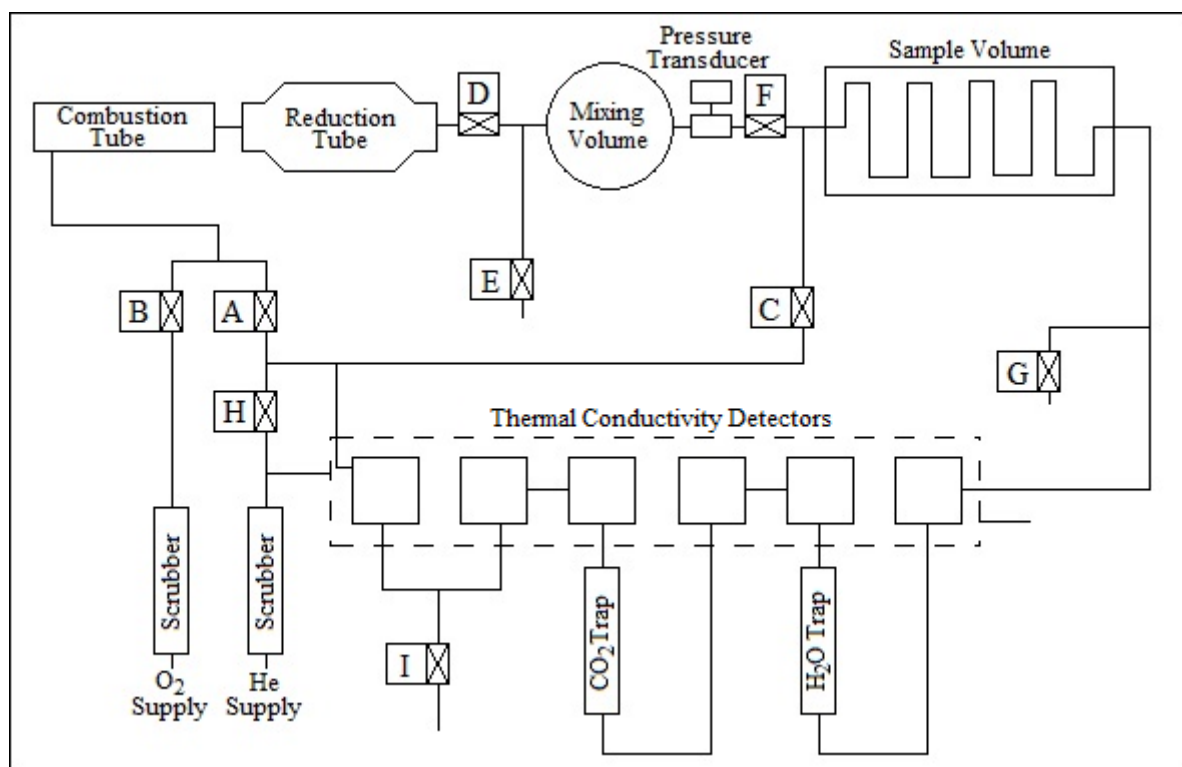


Figure 33 – Flow schematic of CHN elemental analyser CE-440.<sup>148</sup>

Water is removed from the sample gas between the first of the three pairs of thermal conductivity cells using an absorption trap. The difference in signal reading before and after the trap reflects the concentration of water and hence, hydrogen content is measured. Between the second pair of thermal conductivity cells, a similar measurement is made where carbon dioxide is removed by the trap and hence, carbon content is measured. The remaining gas (now containing only nitrogen and helium) passes through the final detector and the signal output is compared to a reference cell of which only helium flows, leaving nitrogen content to be calculated.<sup>148</sup>

## 5.2 Results and Discussion

### 5.2.1 SSNMR of functionalised silicas

The spectra obtained are able to show the progression of the newly attached components of each stage, including the polymer unit.  $^1\text{H}$ ,  $^{13}\text{C}$  and  $^{29}\text{Si}$  have all been run on the samples, signifying attachments of groups and successful polymerisation to the surface. The direct interpretation of peaks however is very much different to solution state NMR and can be very tentative.

#### 5.2.1.1 $^1\text{H}$ SSNMR of ZEOprep silica materials

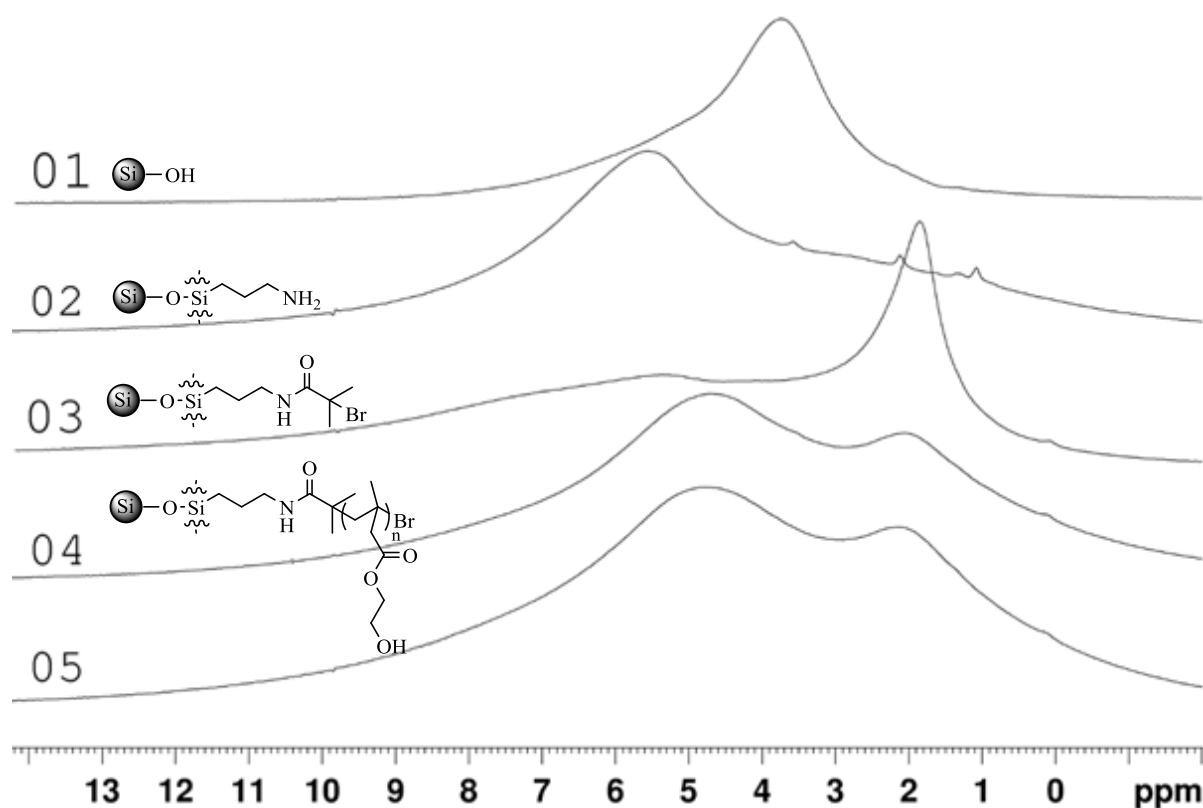


Figure 34 –  $^1\text{H}$  SSNMR of the functionalised ZEOprep silica materials. ‘01’ shows the spectra obtained for the silica starting material, ‘02’ shows the spectra obtained for attached APTES, ‘03’ shows the spectra obtained for attached BIBB, ‘04’ shows the spectra after the grafting of polymer and ‘05’ shows the spectra obtained after grafting of polymer but also after many washings to ensure the material is attached.

The starting material, ZEOprep silica shows one broad peak at 3.8 ppm but also a shoulder at 4.6 ppm. These correspond to the hydroxyl groups that exist on the silica surface and also likely to be related to residual water within the material. When the TGA results are taken into consideration (TGA analysis of ZEOprep silica, page 99), it shows that water is likely to make up ca. 4% of the mass. After this, the sample loses further mass up to temperatures of

1000 °C. As this slope does not level out, it suggests further mass still was due to be lost at these high temperatures. This loss in mass must be due to hydroxyl groups at the surface of the silica material as nothing other than Si-O bonds exists. Therefore it is reasonable to suggest that the peak at 3.8 ppm is highly likely to be related to the Si-OH that is attached to the surface of the silica whilst the smaller shoulder is consistent with a slightly smaller quantity of residual water.

The next step is the addition of APTES. The SSNMR illustrates a peak 5.6 ppm which is likely to be the generation of a new peak for the three sets of CH<sub>2</sub> that exists in the APTES and/or the inclusion of the NH peak. Three small peaks are shown at 3.6 ppm, 2.2 ppm and 1.1 ppm and Kim *et al.*<sup>149</sup> report three peaks at similar shifts relating to free APTES. This leaves the four environments of protons attached to the surface to be responsible for the broad peak observed at 5.6 ppm.

The third material was that following the deposition of BIBB. Two small shoulders at 5.6 ppm and 7.8 ppm show the NH<sub>2</sub> and CH<sub>2</sub> groups still exist but now less mobile hence shallow and broad in appearance. A new sharper peak exists at 1.8 ppm which can only correspond to the two new CH<sub>3</sub> groups as this is the only proton environment that has been added. The two groups are in the same environment and therefore would only show one peak. They are also more mobile being CH<sub>3</sub> at the end of a chain, and therefore produce sharper peaks.<sup>150</sup>

The final proton spectra (04 and 05) are that with grafted PHEMA. Spectrum 05 shows a sample washed multiple times illustrating little difference, suggesting that many washes are not required. Two very broad peaks now exist at 4.7 ppm and 2 ppm. With a large amount of similar environments and overlapping of peaks, exact details are impossible to interpret. The side chains of the polymer are expected to hold the most 'mobile' environments such as the hydroxyl group on the end of the side chain and CH<sub>3</sub>, so it is most likely these protons that promote the spectra observed.

### 5.2.1.2 $^{13}\text{C}$ SSNMR of ZEOprep silica materials

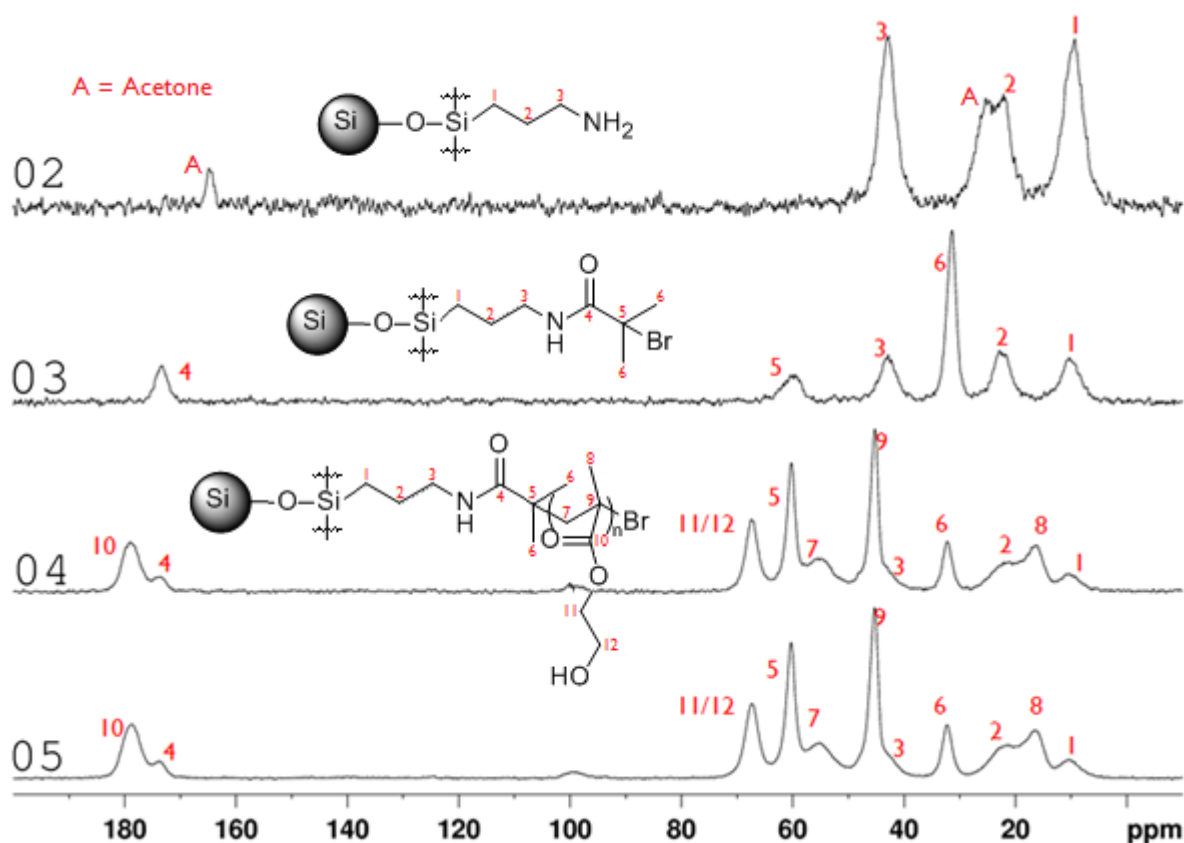


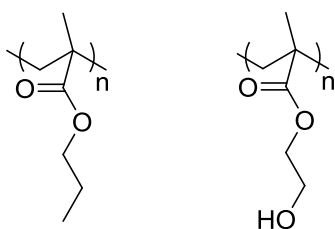
Figure 35 –  $^{13}\text{C}$  SSNMR of the functionalised ZEOprep silica materials ‘02’ shows the spectra obtained for attached APTES, ‘03’ shows the spectra obtained for attached BIBB, ‘04’ shows the spectra after the grafting of PHEMA and ‘05’ shows the spectra obtained after grafting of PHEMA but after many washings to ensure the material is attached.

The deposition of APTES sees the addition of carbon atoms. This enables  $^{13}\text{C}$  spectra to be used for more detail regarding these samples. Three peaks are expected for the three individual environments of the carbon atoms. However, on the spectra five are observed. During the synthesis, acetone was used which explains the peak observed at 163 ppm. The peak at 28 ppm is the most likely to correspond to the two  $\text{CH}_3$  groups that relate to the acetone, whilst the three peaks at 10 ppm (1), 23 ppm (2) and 42 ppm (3) would be the three carbon atoms in the APTES group (numbers correlate to Figure 35) as have been reported by other groups.<sup>151,152</sup>

Following deposition of BIBB a shifted carbon peak would be expected for the carbonyl, this is observed at 173 ppm (4), with the acetone peak at 163 ppm now absent. A shifted peak for C-Br is observed at 60 ppm (5) whilst a new sharp peak, most likely for the two  $\text{CH}_3$  groups (based on the sharpness of its appearance and its location within the structure) is observed at 32 ppm (6). The three  $\text{CH}_2$  groups that are part of the APTES group see a decrease in relative

peak height due to this CH<sub>3</sub> peak. Castelvetro *et al.*<sup>139</sup> have reported the use SSNMR to help characterise their cotton fibers encapsulated with copolymers which also uses BIBB as an initiator. A similar but unassigned spectrum is reported for the structure containing BIBB and the carbonyl peak is certainly at a similar shift to where it is observed in Figure 35. As mentioned in the proton discussion, this process was carried out in THF, therefore no acetone peaks are observed.

The addition of PHEMA produces spectra much more complicated than previously observed. The addition of more carbon atoms in similar positions results in the overlap of peaks and shoulders of peaks need to be considered. The simplest carbon to determine is the carbonyl within the polymeric repeat unit (10). This is observed at 179 ppm whilst the shoulder of the carbonyl within the amide still remains at 173 ppm (4) but at a height of ca. ¼ to the new 179 ppm peak. The relative peak height could suggest that there were ca. four repeat units attached, but this technique cannot be relied upon for quantitative analysis and would only be an average across all the repeat units attached – hence TGA and elemental analysis have been used alongside SSNMR to help quantify the results. A closer inspection at the lower shift end of the spectra suggests that the two CH<sub>2</sub> (C11 and C12) groups fall into the broad peak observed at 68 ppm. Mirau<sup>153</sup> has reported poly(butyl methacrylate) which has almost identical carbon environments (see Figure 36) and this was used to help determine the peak assignment of 04 and 05 in Figure 35.



**Figure 36 – Poly(butyl methacrylate) (left) and PHEMA (right).**

Mirau<sup>153</sup> reports the quaternary carbon (9) exactly where a new peak is observed with this spectra, at 45 ppm. Also, a CH<sub>2</sub> (7) is interpreted near to where a third new peak is observed at 60 ppm. Finally, the remaining new peak is seen at 17 ppm, likely to be the CH<sub>3</sub> (8). Due to the CH<sub>2</sub> (2) already positioned at 23 ppm, only a shoulder is now observed, forming a broad peak as it overlaps with the CH<sub>3</sub> (8). Again, the sample washed several times (bottom spectrum of Figure 35, spectrum 05) shows little difference to the sample washed only once (second from bottom of Figure 35, spectrum 04).

### 5.2.1.3 NQS Experiment of ZEOprep silica material

Non-quaternary suppression (NQS) is used to help confirm which peaks are related to the quaternary carbons. A similar spectrum is obtained to that of a DEPT in solution state, but in this case, the reverse is observed where the quaternary carbons are displayed. Due to the nature of the CH<sub>3</sub> groups and their mobility, these are also displayed on the spectra. Taking this into account, the NQS spectrum has peaks at 179 ppm (10), 173 ppm (4), 60 ppm (5), 45 ppm (9), 32 ppm (6) and 17 ppm (8).

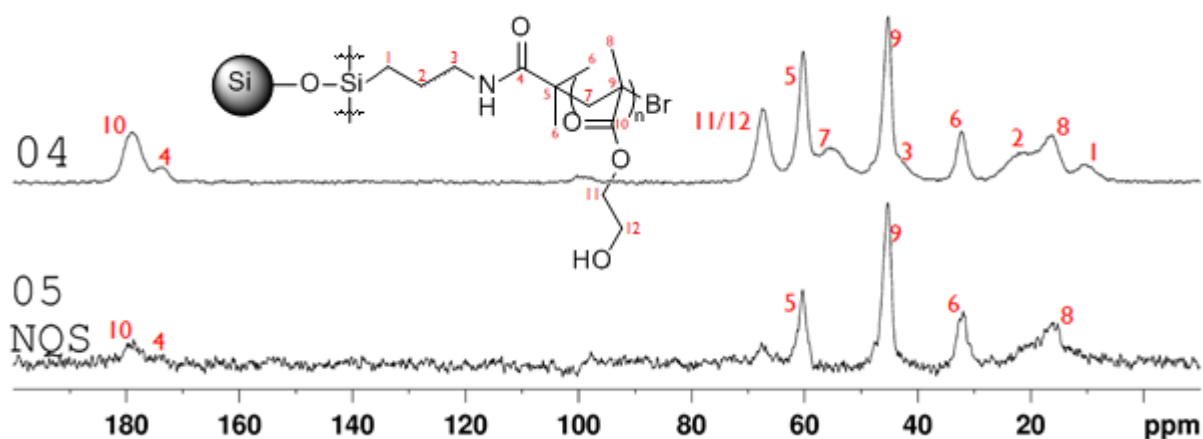


Figure 37 – NQS experiment to show which peaks are related to quaternary carbons but also to CH<sub>3</sub> groups due to their mobility.

### 5.2.1.4 <sup>29</sup>Si SSNMR of ZEOprep silica material

Finally, <sup>29</sup>Si experiments were run to help further understand the makeup of the silica used in this work. This enables one to distinguish silicon atoms involved in siloxane bridges (Q<sup>4</sup>), single silanol (Q<sup>3</sup>) and geminal silanol groups (Q<sup>2</sup>) on the surface of silica.<sup>154</sup>

The Direct Polarisation (DP) Technique (which is quantitative) shows that unsurprisingly, siloxane bridges (Q<sup>4</sup>) make up the majority of the material (this spectrum is observed at the bottom of Figure 40, DP 05). As illustrated in Figure 38, these silica atoms are bonded to four oxygen atoms, which are then attached to another silicon atom, making them unavailable for this modification work.

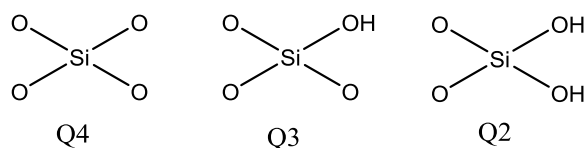
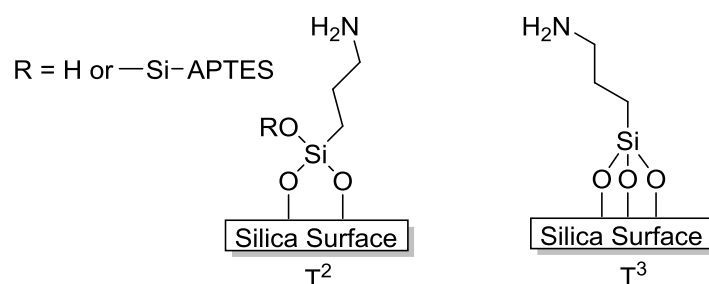


Figure 38 – Illustration to show siloxane bridges Q4, single silanol Q3 and geminal silanol groups Q2.

Figure 40 shows the  $^{29}\text{Si}$  spectra recorded for the functionalised materials. In each of the CP experiments, the spectra shows the new silicon atoms (from the APTES silane) to be attached. This is the case for each step following this surface modification and helps support the idea that the surface attached material is in fact attached.

It is important to remember that CP is a very filtered and biased experiment to show what is attached.  $^{29}\text{Si}$  spin polarisation is derived from the proton-spin reservoir which discriminates against silicon nuclei in the interior of a silica particle and in favour of surface silicon atoms which are nearer the available (hydroxyl) protons.<sup>155</sup> These experiments suggest the modifications have been successful by the appearance of  $\text{T}^2$  and  $\text{T}^3$  peaks<sup>156</sup> (see Figure 39), but in reality, the final spectrum (DP (05)) in Figure 40 show that the majority of the silica remains as the bulk  $\text{Q}^3$  and  $\text{Q}^4$ . This is not dissimilar to what would be expected, considering the chemistry being carried out is only on the surface.



**Figure 39 – Structures of the  $\text{T}^2$  and  $\text{T}^3$  species that are present on APTES-functionalised silica surfaces.**

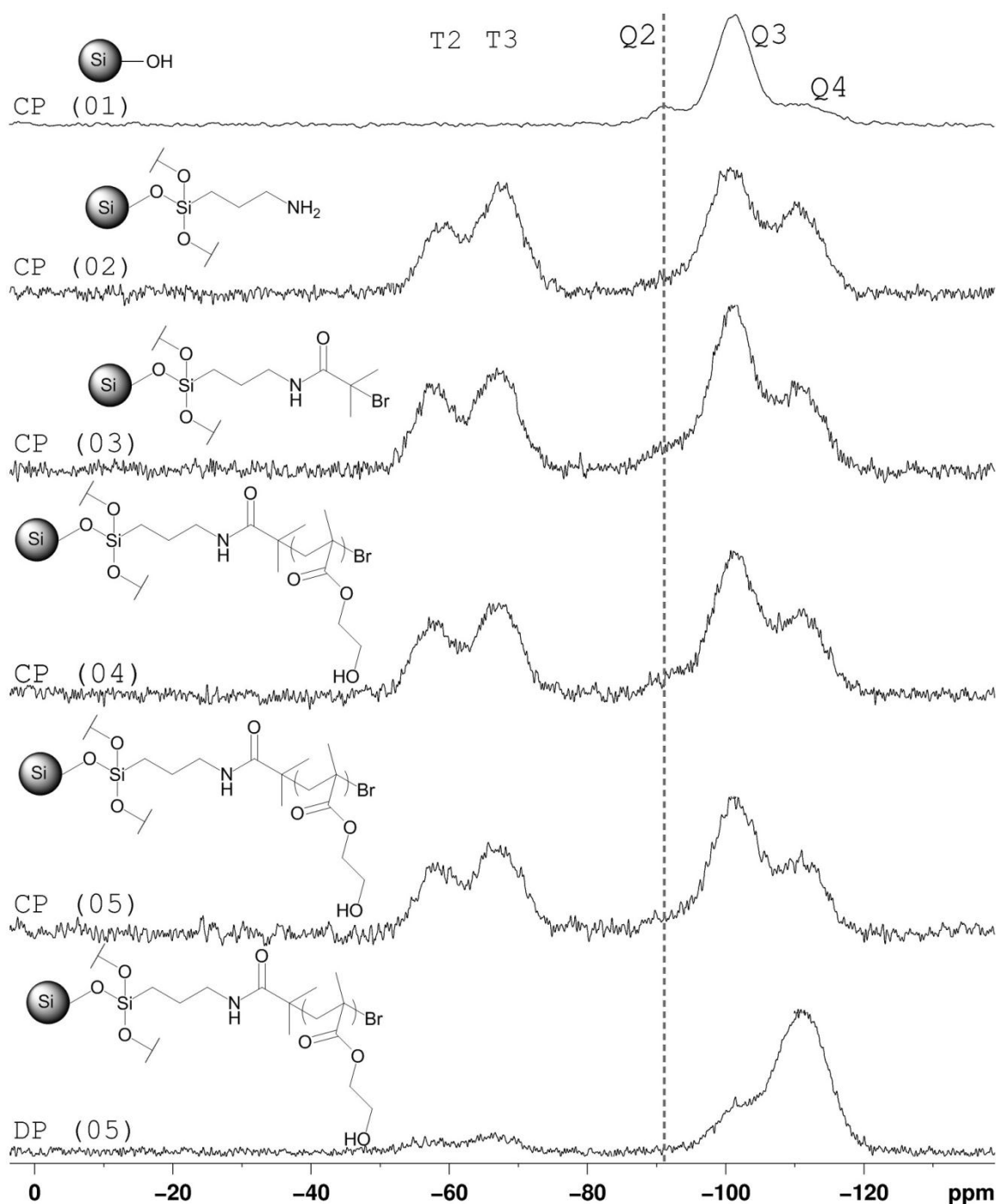


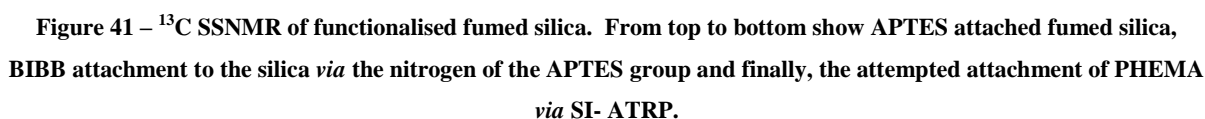
Figure 40 –  $^{29}\text{Si}$  SSNMR spectra of ZEOprep silica and all its functionalised materials. (05) is the same material as (04) but has undergone many washings as seen in the previous spectra. The final spectra (DP (05)), illustrates quantifiably the silica environments in the material.

### 5.2.1.5 $^{13}\text{C}$ SSNMR of fumed silica materials

Similar experiments have been carried out for the fumed silica samples on which the same modifications have been attempted. Figure 41 shows the spectra recorded for these experiments for the three stages of the modification process.



The peaks observed have very similar shifts to those seen on the ZEOprep silica surface, strongly supporting the original peak assignment. Five peaks are observed in the first spectrum, once more two have been assigned to residual acetone present from the APTES reaction. Peaks at 10 ppm (1), 23 ppm (2) and 42 ppm (3) have been assigned to the three carbons in the APTES molecule based on work reported by other groups as before.<sup>151,152</sup>



Following deposition of BIBB, a spectrum is observed that is consistent with the ZEOprep material.

The third and final spectrum shows a very different spectrum to the two previously discussed. Added to this, only the outermost carbons are observed and only appear to be those associated with the polymer. Unlike previously in Figure 35 where all carbons could be assigned to a peak at this stage of the modification, here there are a limited number of peaks to be assigned. There are two reasons that could explain this.

The first could be that so much PHEMA has attached to the surface of the silica that these have swamped the spectrum, making the carbons closer to the bulk silica invisible

The second reason, and perhaps more plausible is that very little of the polymer had attached to the silica. Instead, the spectrum has been swamped by free PHEMA. Many free radicals are created during this reaction and although some will have attached to the silica, free polymer could have been initiated during this process and may have simply wrapped itself around the silica material.

When looking forward to the TGA plots (Figure 42 for ZEOprep and Figure 43 for fumed silica), there does appear to be a marginal difference in the way mass is lost for the PHEMA functionalised silica. PHEMA functionalised ZEOprep silica shows a staggered decrease in mass whilst in the case of the fumed silica, the decrease in mass matches closer to the free PHEMA before levelling off around 20 % – leaving the original fumed silica. This could suggest why only the PHEMA is observed in the SSNMR spectrum –but not a great deal more than speculation can be made about this.

### 5.2.2 TGA analysis of ZEOprep silica

ZEOprep silica, with an average particle size of ca. 70 µm was investigated to determine how much of the weight is due to water molecules and any impurities. A triplicate analysis was carried out for accuracy. Equation 10 explains how this is calculated.

$$\frac{\text{Starting Mass}}{\text{RMM Starting Material}} = \frac{\text{Final Mass}}{\text{RMM Product}}$$

Equation 10 – Equation to calculate the RMM of a starting material using TGA.<sup>146</sup>

One must assume the final RMM of the product is that of SiO<sub>2</sub> and that all hydroxyl groups (residual water or bound to the silica surface) have been removed so that there is confidence

in the starting material RMM. The original ZEOprep silica sample size used was 15.0650 mg and following heating, had reduced by 8.53 % to 13.7851 mg.

$$\frac{15.0132 \times 10^{-3}}{RMM (SiO_2 \cdot xH_2O)} = \frac{13.7333 \times 10^{-3}}{60.084}$$

$$\frac{15.0132 \times 10^{-3}}{RMM (SiO_2 \cdot xH_2O)} = 2.2856 \times 10^{-4}$$

$$\frac{15.0132 \times 10^{-3}}{2.2856 \times 10^{-4}} = 65.6860$$

RMM of SiO<sub>2</sub> = 60.0840, leaving 5.6020 unaccounted for. Equation 11 demonstrates the number of water molecules that are therefore calculated.

$$\frac{5.6020}{18} = 0.31$$

**Equation 11 – Calculation to indicate the number of water molecules present in the silica sample.**

Hence the formula of the ZEOprep silica is calculated to be SiO<sub>2</sub>.0.31H<sub>2</sub>O.

### 5.2.2.1 ZEOprep Si-APTES

A total loss of 13.37 % of weight was observed from a sample weighing 35.0065 mg. By assuming that 8.53 % of that mass is related to the water molecules previously accounted for, it can be expected that the 4.84 % of the lost mass is that of the APTES group that has been synthesised to the silica surface (residual acetone reported in SSNMR was removed by leaving the sample in an oven at 80 °C overnight). Further calculations establish that a total of 4.5564 mg, 5.286 x 10<sup>-5</sup> moles (1.51 x 10<sup>-3</sup> mol g<sup>-1</sup>) of APTES was attached to the silica.

### 5.2.2.2 ZEOprep Si-BIBB

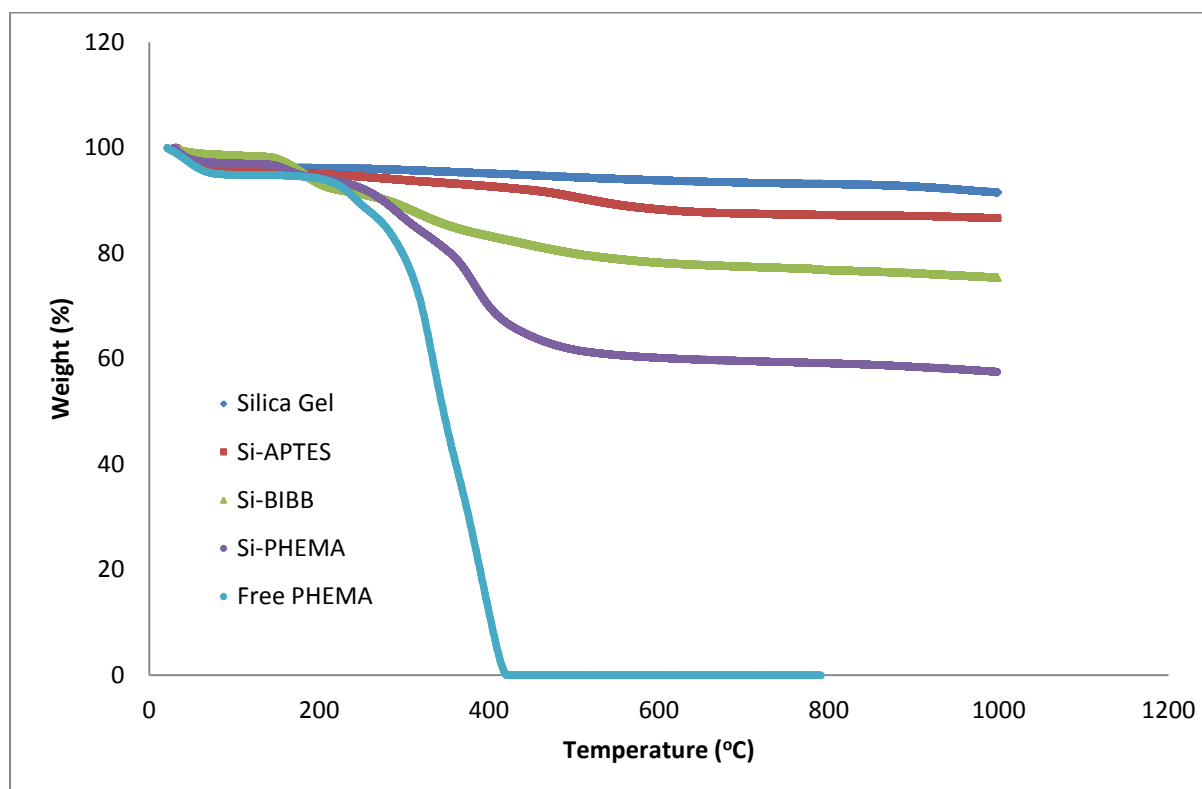
To calculate the amount of bromine groups attached to the silica surface, the amount of APTES had to be subtracted as well as the water molecules. The total loss of weight was 24.63 % of a sample originally weighing 12.6103 mg. Calculations show that 2.6907 mg belonged to the BIBB group, equating to 1.782 x 10<sup>-5</sup> moles (1.41 x 10<sup>-3</sup> mol g<sup>-1</sup>), essentially giving a ratio of 1:1. A yield of 93 % is also calculated.

### 5.2.2.3 ZEOprep Si-PHEMA

A total mass loss of 42.49 % was observed for this sample, immediately suggesting that a significant amount of polymer had attached itself to the surface. The sample being analysed

initially weighed 14.5991 mg. A total mass of 6.3277 mg of PHEMA was found to be attached to the silica surface, equating to  $4.862 \times 10^{-5}$  moles ( $3.33 \times 10^{-3} \text{ mol g}^{-1}$ ). The ratio therefore of the BIBB-functionalised silica to PHEMA in moles is  $1.41 \times 10^{-3} \text{ mol g}^{-1} : 3.33 \times 10^{-3} \text{ mol g}^{-1}$ . In simpler terms, a ratio of 1 : 2.36.

The mass loss data for the ZEOprep materials is shown graphically in Figure 42.



**Figure 42 – Comparison of the mass lost on each ZEOprep silica sample *via* TGA analysis. Free PHEMA is included to compare the surface attached results to but this graphical interpretation clearly demonstrates more organic material is removed after each modification step, as would be expected.**

Table 5 displays the original masses used in grams for the ZEOprep silica TGA studies and shows the findings of calculated values of attached APTES, BIBB and PHEMA. The molecular weight of APTES was revised from 221.37 to 82.16 due to SSNMR indicating no ethyl groups to be present, whilst the molecular weight of BIBB was also revised from 229.90 to 151.00 as the acid bromide is removed in the reaction to form the new amide bond.

	Sample Mass (g)	Mass of end group (g)	Moles of end group	Moles of end group per gram of material
ZEOPrep Si-APTES	0.0350065	0.0045564	$5.286 \times 10^{-5}$	$1.51 \times 10^{-3}$
ZEOPrep Si-BIBB	0.012613	0.0026907	$1.782 \times 10^{-5}$	$1.41 \times 10^{-3}$
ZEOPrep Si-PHEMA	0.0145991	0.0063277	$4.862 \times 10^{-5}$	$3.33 \times 10^{-3}$

**Table 5 – Masses of each functionalised ZEOPrep silica sample used on TGA with calculated mass of end group attached. The moles of the end group are then calculated, followed by a final calculated value of moles of end group per gram of material.**

Table 5 clearly shows the relationship between Si-BIBB and Si-PHEMA (using HEMA monomer RMM as no atoms are lost in ATRP) and suggests that the degree of polymerisation (DP) is ca. 2. Although this is very low, it supports the SSNMR data where it was predicted to be ca. 4 by estimating the peak area.

### 5.2.3 TGA analysis of fumed silica

Following the ZEOPrep silica results, the fumed silica was investigated *via* the same method. By using this silica, it was expected that more organic material would attach to the silica than had been observed with the ZEOPrep silica due to its much larger surface area. Taking the same assumption into account that the final RMM of the product is that of SiO<sub>2</sub>, quantifiable attachment can be analysed. The sample size used for this investigation was a lot less than the same investigation with the ZEOPrep silica at 3.3379 mg due to the characteristics of the fumed silica being so fine and electrostatic that it was virtually impossible to get any more into the TGA pan.

Following heating, a total of only 2.065 % had been lost in mass to leave 3.269 mg. Using the equation shown in Equation 10, the RMM of the starting material is found to be 61.3506, leaving the number of water molecules to be lower at 0.0704.

#### 5.2.3.1 Fumed Si-APTES

The silica attached APTES, (with a starting mass of 12.1116 mg) had a total mass loss higher than the ZEOPrep silica at 14.38 %. Taking into consideration the loss of water molecules from the fumed silica, further calculations found that a total of 1.7051 mg,  $1.978 \times 10^{-5}$  moles of the APTES was attached to the silica ( $1.63 \times 10^{-3}$  mol g<sup>-1</sup>).

### 5.2.3.2 Fumed Si-BIBB

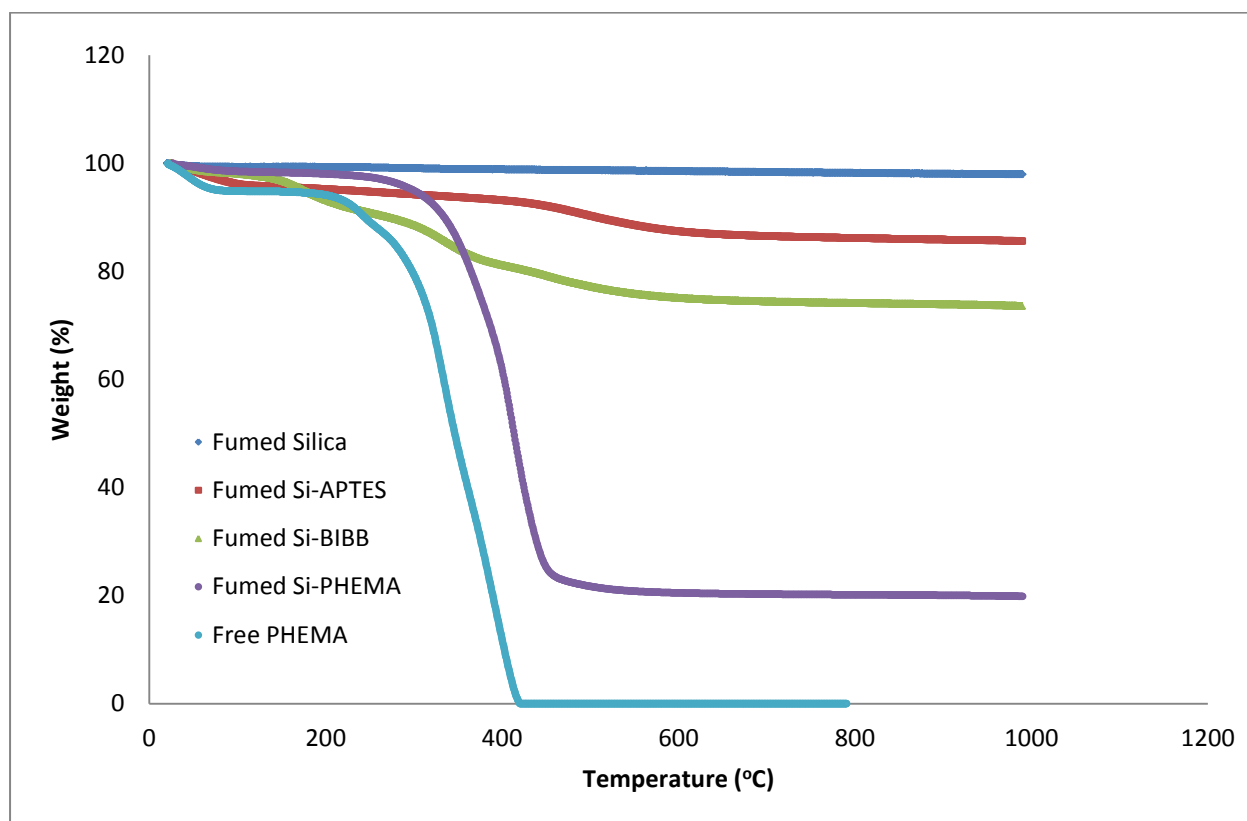
The initial weight loss of the silica attached bromine (with a starting mass of 14.0076 mg) was again higher than the same sample of ZEOprep material at 26.40 %. Calculations show that 3.1667 mg was owed to the BIBB group, equating to  $2.097 \times 10^{-5}$  moles ( $1.50 \times 10^{-3}$  mol  $\text{g}^{-1}$ ) - a yield of 92 %.

### 5.2.3.3 Fumed Si-PHEMA

Finally, the silica attached PHEMA (with a starting mass of 16.7156 mg) produced a total weight loss of 80.12 % – almost double the figure seen with the ZEOprep material.

A total mass of 9.8570 mg of PHEMA was found to be attached to the silica surface, equating to  $7.5741 \times 10^{-5}$  moles ( $4.53 \times 10^{-3}$  mol  $\text{g}^{-1}$ ). The ratio therefore of the BIBB-functionalised silica to PHEMA in moles is  $1.50 \times 10^{-3} : 4.53 \times 10^{-3}$ . In simpler terms, a ratio of 1 : 3.02.

The mass loss data for the fumed silica materials is shown graphically in Figure 43.



**Figure 43 – Comparison of the mass lost on each fumed silica material sample *via* TGA analysis. Free PHEMA is included to compare the surface attached results to but this graphical interpretation clearly demonstrates more organic material is removed after each modification step, as would be expected.**

Table 6 displays the original masses used in grams for the fumed silica TGA studies and show the findings of calculated values of attached APTES, BIBB and PHEMA. Again, the molecular weights have been revised.

	Sample Mass (g)	Mass of end group (g)	Moles of end group	Moles of end group per gram of material
Fumed Si- APTES	0.0121116	0.0017051	$1.978 \times 10^{-5}$	$1.63 \times 10^{-3}$
Fumed Si- BIBB	0.0140076	0.0031667	$2.10 \times 10^{-5}$	$1.50 \times 10^{-3}$
Fumed Si- PHEMA	0.0167156	0.009857	$7.57 \times 10^{-5}$	$4.53 \times 10^{-3}$

**Table 6– Masses of each functionalised fumed silica sample used on TGA with calculated mass of end group attached. The moles of the end group are then calculated, followed by a final calculated value of moles of end group per gram of material.**

Table 6 clearly shows the relationship between Si-BIBB and Si-PHEMA and suggests that the degree of polymerisation (DP) is ca. 3. Again, this is very low but it is expected to be a higher value than the ZEOprep based on the TGA analysis showing more materials lost in mass. It does however remain unclear whether or not this PHEMA is bonded to the silica particles or whether it is silica particles physisorbed with free PHEMA.

#### **5.2.4 TGA analysis of porous silica microparticles**

Following the results with the silica materials investigated thus far, silica microparticles designed and made by Holdich *et al.*<sup>121</sup> were explored *via* TGA also. As explained earlier in chapter 4, a sample with an average pore size of 2.6 nm was obtained and by utilising the surface of the pores along with the outer surface, it was thought that this material may produce better results than the two already examined.

However, after attaching only a small amount of APTES, the BIBB synthesis proved impossible *via* the same route used with the ZEOprep silica and fumed silica. No amide shifts on the IR spectrum could be seen: only the amine shift from the small amount of APTES. Only after the addition of premade BIBAPTES did one see the amide shifts on the FTIR spectrum. TGA was used to help understand why this was the case.

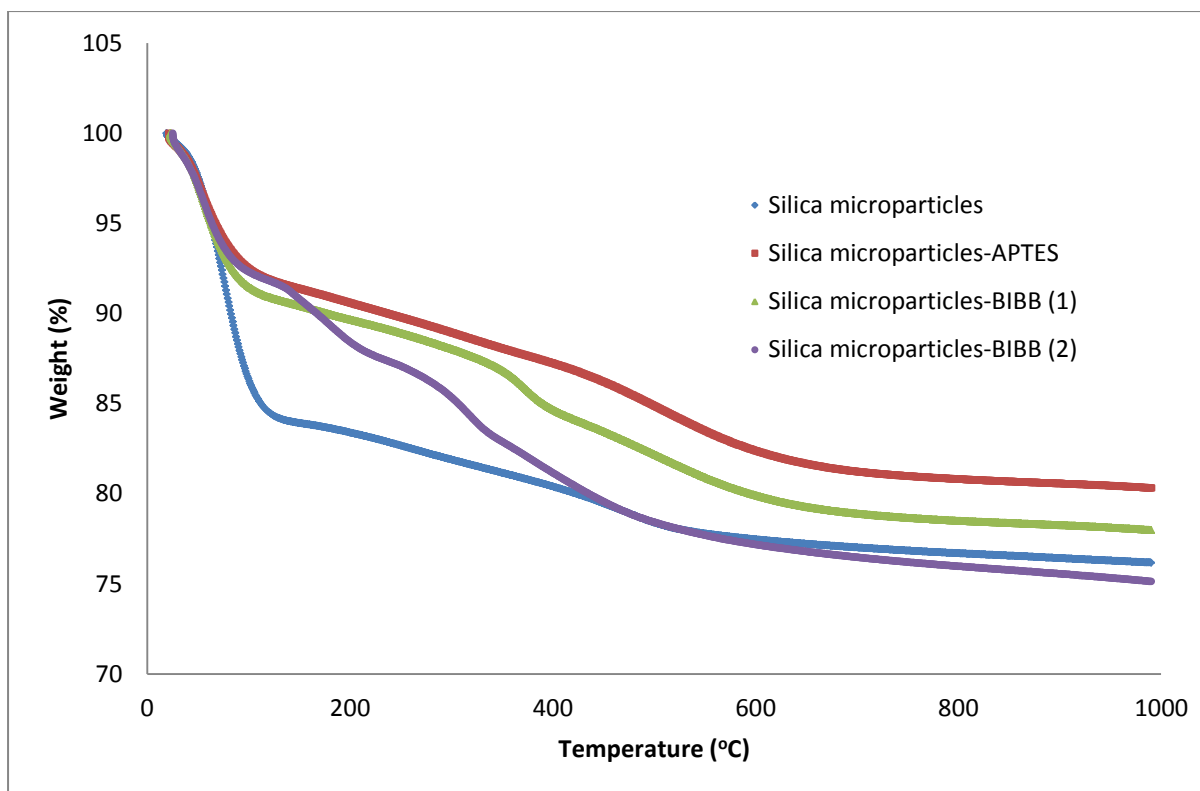


Figure 44 – Comparison of the mass lost on each silica microparticle material *via* TGA analysis.

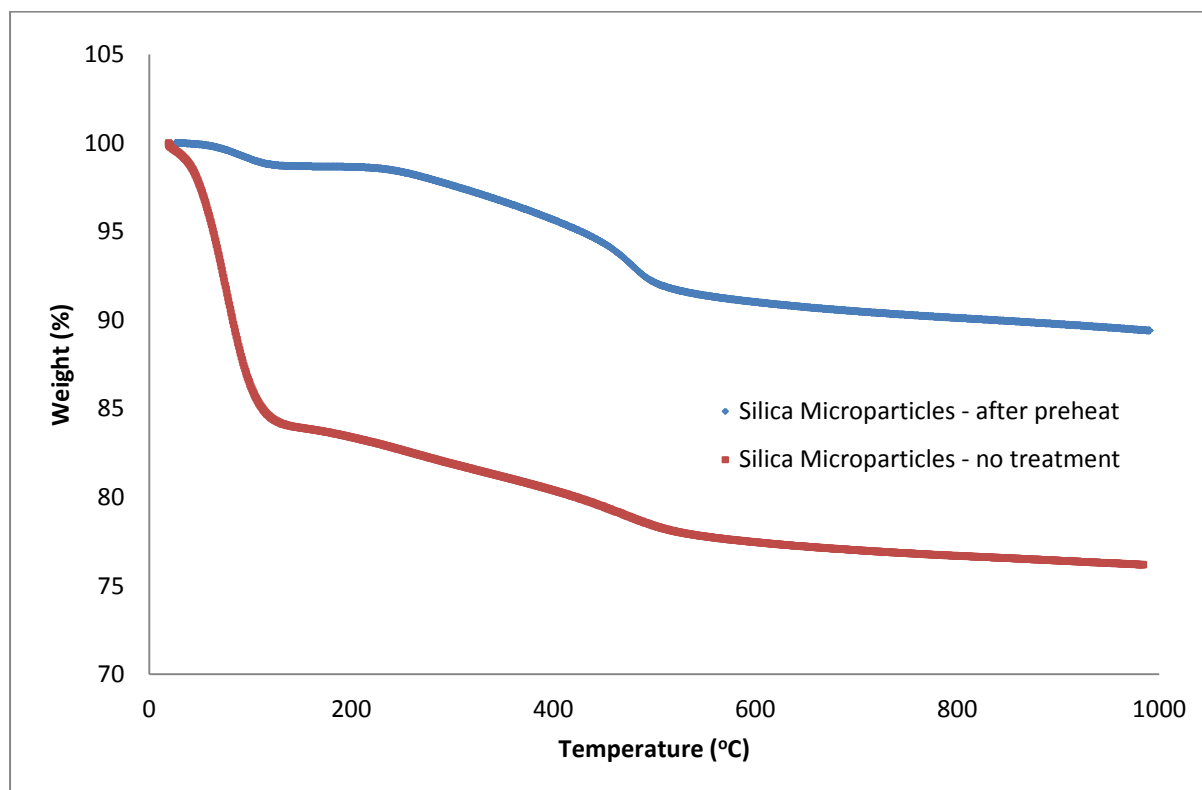
Figure 44 shows the mass loss when heating the materials to 1000 °C at the same rate. The first major observation is that all the mass losses are very close to each other, unlike the results observed with the other silica materials previously discussed. Secondly, the mass loss of the silica microparticles without any modification is considerably higher at 23.8 % compared to the 8.5 % observed for the ZEOprep silica and 2.1 % observed for the fumed silica. There could be more than one reason for this.

Firstly, the product that remains when heated to 1000 °C is black coloured: suggesting carbon is present. Sodium silicate solution is used in the process of producing these microparticles in kerosene which could mean that the pores are being held at their specific size by carbon frameworks. If this is the case, the pores would not be available to utilise for ligand attachment or polymer growth and thus, radically reducing the surface area originally thought to be available for synthetic modification.

Secondly, the process used to create these pore sizes and pore spacing requires a solvent system containing kerosene which could mean the microparticles have absorbed this and not undergone a stringent wash to remove it.



However, with over 15 % of the mass appearing to be removed at around 100 °C, it seems more likely that the silica microparticles are hygroscopic and require drying before use. A sample was placed in the vacuum oven at 150 °C and left overnight before being analysed *via* TGA.



**Figure 45 – Comparison of weight loss for the silica microparticles *via* TGA when heated to 150 °C beforehand and when not pre-treated at all.**

Although some of the mass loss can now be accounted for, the remaining mass loss of 10.6 % was still unexplained and the material after analysis again remained black coloured.

Elemental analysis showed that 2.28 % of the mass was carbon and 1.04 % was hydrogen. These values are remarkably high when compared to 0.04 % and 0.32 % to the ZEOprep and fumed silica respectively for carbon and 0.34 % and 0.20 % for hydrogen, signifying that some form of carbon framework exists within the material.

Further elemental analysis investigations from other work by Dann *et al.*<sup>157</sup> showed that when an organic template did exist, the carbon content was just over 2 %, and when it was removed, the content level was as low as 0.01 %. This is consistent with a carbon framework being present in the pores of this material which would explain why it has not been possible to attach as much organic material as expected.

### 5.2.5 TGA analysis of silica coated iron oxide microparticles

TGA was not carried out on silica coated iron oxide microparticles due to too small a sample and investigations with the material were focussed on sequestration of metal as a proof of concept.

### 5.2.6 CHN Elemental analysis on functionalised silicas

CHN Elemental analysis results are tabulated below and clearly show the addition of organic carbon after each step, the most obvious step being the polymerisation – as expected. Nitrogen content rises after the addition of APTES but then starts to lower as more carbon, hydrogen and oxygen atoms are attached without any further nitrogen. Silicon and oxygen cannot be analysed *via* this method but the CHN content gives good assurances that the modifications have been successful. Silicon and oxygen fall into the ‘R’ percentage.

Sample	Sample mass (µg)	% Carbon	% Hydrogen	% Nitrogen	% R
ZEOPrep silica	1722.3	0.04	0.34	0.04	99.59
ZEOPrep Si-APTES	1102.4	5.16	1.02	1.64	92.18
ZEOPrep Si-BIBB	2393.6	9.39	1.58	1.48	87.55
ZEOPrep Si-PHEMA	1894.6	30.17	4.26	0.81	64.76

Table 7 – CHN Elemental analysis of ZEOPrep silica and its functionalised derivatives.

Sample	Sample mass (µg)	% Carbon	% Hydrogen	% Nitrogen	% R
Fumed silica	706.3	0.32	0.20	0.07	99.40
Fumed Si-APTES	1753.2	6.88	1.44	2.31	89.37
Fumed Si-BIBB	1017.2	10.88	1.60	1.69	85.84
Fumed Si-PHEMA	2271.7	43.91	6.29	0.51	49.29

Table 8 – CHN Elemental analysis of fumed silica and its functionalised derivatives.

The nitrogen percentage in the case of the silica attached APTES can be used to calculate the number of moles of APTES attached. Only one nitrogen atom exists in each molecule of APTES, leaving a direct relationship to be made between the two.

Mass of N in ZEOprep Si-APTES sample	$1.76 \times 10^{-5} \text{ g}$
Moles of N in ZEOprep Si-APTES sample	$1.26 \times 10^{-6} \text{ mol}$
Moles of N per 1 g ZEOprep Si-APTES	$1.14 \times 10^{-3} \text{ mol g}^{-1}$
Moles of APTES per 1 g ZEOprep Si-APTES	$1.14 \times 10^{-3} \text{ mol g}^{-1}$

**Table 9 – Values for the content of nitrogen found in a mass of 1102.4 µg of ZEOprep Si-APTES and hence calculated to show the number of moles of APTES per gram of material.**

Mass of N in fumed Si-APTES sample	$3.93 \times 10^{-5} \text{ g}$
Moles of N in fumed Si-APTES sample	$2.80 \times 10^{-6} \text{ mol}$
Moles of N per 1 g fumed Si-APTES	$1.59 \times 10^{-3} \text{ mol g}^{-1}$
Moles of APTES per 1 g fumed Si-APTES	$1.59 \times 10^{-3} \text{ mol g}^{-1}$

**Table 10 – Values for the content of nitrogen found in a mass of 1753.2 µg of fumed Si-APTES and hence calculated to show the number of moles of APTES per gram of material.**

Although it is already known more APTES was successfully attached to the fumed silica than ZEOprep from the CHN percentages and TGA, moles per gram values allow more to be learnt about the uptake of metal in later stages of the work. As (unexpectedly) the results are very similar, a considerable difference between the two materials would not be expected. A hypothesis is given in the conclusion as to why a similar  $\text{mol g}^{-1}$  is observed.

Using the CHN percentages and revised RMM of APTES, BIBB and PHEMA, a percentage yield and DP calculation has been made to compare this method with TGA. TGA is a much more accurate way of measuring these values but the CHN results can be used to support and strengthen the credibility of these findings. The results are shown in Table 11 and Table 12.

Sample	$\text{mol g}^{-1}$ of material		TGA comparison	
ZEOprep Si-APTES	$9.07 \times 10^{-4}$		$1.51 \times 10^{-3} \text{ mol g}^{-1}$	
ZEOprep Si-BIBB	$8.25 \times 10^{-4}$	91 % yield	$1.41 \times 10^{-3} \text{ mol g}^{-1}$	93 % yield
ZEOprep Si-PHEMA	$2.71 \times 10^{-3}$	DP = 3.28	$3.33 \times 10^{-3} \text{ mol g}^{-1}$	DP = 2.36

**Table 11 – Values calculated *via* CHN for moles of functional group per gram of material and compared to TGA values.**

Sample	mol g <sup>-1</sup> of material		TGA comparison	
Fumed Si-APTES	1.23 x 10 <sup>-3</sup>		1.63 x 10 <sup>-3</sup> mol g <sup>-1</sup>	
Fumed Si-BIBB	9.38 x 10 <sup>-4</sup>	76 % yield	1.50 x 10 <sup>-3</sup> mol g <sup>-1</sup>	92 % yield
Fumed Si-PHEMA	3.90 x 10 <sup>-3</sup>	DP = 4.16	4.53 x 10 <sup>-3</sup> mol g <sup>-1</sup>	DP = 3.02

**Table 12 – Values calculated *via* CHN for moles of functional group per gram of material and compared to TGA values.**

A difference in values between the TGA and CHN techniques would be expected but for the majority, the results are very similar. These findings are supported by work reported by Bartholome *et al.*<sup>141</sup> who used TGA and CHN to calculate and compare grafting density and yields of their materials and also reported similar results from the two methods. The difference between the values calculated for percentage yield of BIBB-functionalised fumed silica is the most significant difference but a yield of 70 % or greater would still be regarded as a good yield in synthetic organic chemistry.<sup>158</sup>

### 5.3 Conclusion

The three techniques described in this chapter have proved to be invaluable for the characterisation of the materials synthesised in this work. To the author's knowledge, the silica materials studied in detail (ZEOprep and fumed) have not been used for this type of work in the past. The detailed analysis of the materials appears to be a relatively novel approach although Bartholome *et al.*<sup>141</sup> have used a similar procedure to obtain qualitative and quantitative data for nitroxide-mediated polymerisations from silica nanoparticles. However, a different approach was used to graft the polymer which did not involve APTES or BIBB and focussed on styrene rather than HEMA. SSNMR and TGA analysis was also used by Castelvetro *et al.*<sup>139</sup> to strengthen the structural understanding for ATRP grafted polymers from cotton fibres but did not use elemental analysis.

SSNMR has helped to improve the understanding of the material make-up whilst TGA and elemental analysis has enabled supporting calculations to be made to accurately compare the differences between the functionalised materials. The information from SSNMR allowed RMM calculations to be made on the organic molecules attached based on the structure of the materials formed.

SSNMR spectra obtained for the PHEMA attached to fumed silica has shown that the polymer may not be attached. The clarity of the peaks suggest high mobility of the end groups<sup>159</sup> but the fact that carbons known to be attached to the silica support cannot be seen

prevents a full analysis of the structure from being carried out. The alternative hypothesis of so much PHEMA being grafted from the surface that the side chains have swamped the spectrum seems highly unlikely based on the DP of 3 that was calculated *via* TGA.

Table 13 shows how the two techniques have been used to give reliable results to quantify the APTES bound to its surface and offers a clear comparison of the two.

Material	TGA	CHN
ZEOPrep Si-APTES	$1.51 \times 10^{-3} \text{ mol g}^{-1}$	$1.14 \times 10^{-3} \text{ mol g}^{-1}$
Fumed Si-APTES	$1.63 \times 10^{-3} \text{ mol g}^{-1}$	$1.59 \times 10^{-3} \text{ mol g}^{-1}$

**Table 13 – Comparison of values for silica attached APTES *via* TGA and CHN calculations.**

Both TGA and CHN analysis show fumed Si-APTES to contain more APTES per gram of material than the ZEOPrep equivalent. This would be expected given the properties of the two silicas where a much larger surface area and smaller particle size exists for the fumed silica. However the difference between the two is not that great and therefore similar results between the two might be expected when sequestering metal with these materials.

Exactly why this is the case is not completely clear, but a hypothesis is given here. It is reported that fumed silica has an individual particle size of 0.007  $\mu\text{m}$  and ZEOPrep silica particles are 40-63  $\mu\text{m}$  but it is clear that the methodology used is unable to exploit this surface area. Scanning Transmission Electron Microscope (STEM) imaging carried out in the following chapter (for europium(III) mapping) has given an insight into the morphology of the fumed silica (Figure 71). As a monolayer is added (such as APTES), it is proposed that these individual particles are partially agglomerated and rather than functionalising each particle, instead multiple particles are lost inside a ‘ball’ of fumed silica. The result of this leaves a limited amount of surface area to be functionalised.

TGA and CHN analysis have also shown to provide strong supporting information based on the percentage yield of deposition of BIBB on the ZEOPrep and fumed silica whilst DP calculations were within ca. 1 repeat unit of each other.

The functionalised ZEOPrep and fumed silica materials were next prepared on a scale large enough to produce enough material to carry out batch investigations on metal sequestration. These results are presented and discussed in the following chapter.

## **5.4 Future Work**

Although a great deal of information has been found from the three characterisation techniques reported for the ZEOprep and fumed silica materials, a lack of material for the PSM and SMP prevented these from being characterised in as much detail.

If the PSMs potential was met, one believes that it could match the ZEOprep and fumed silica's ability for APTES attachment which could be used immediately for metal sequestration. Currently this is not the case and work moved away from this area when other materials were seen to be more worthwhile.

A similar problem existed with the SMPs whereby a limited stock prevented further and larger scale tests. A proof of concept has been attempted in chapter 6 but with a larger sample. A reliable estimation of APTES attached to the surface of the silica could be calculated and compared with other materials such as the ZEOprep and fumed silica.

## 6 Sequestration of metals, kinetics and $R_d$

### 6.1 Introduction

The materials designed and discussed in this work have all been made to assess their potential to sequester metals from aqueous solutions. In several cases, radioisotopes of metals investigated were used to spike solutions, enabling analytical methods such as Liquid Scintillation Counting (LSC) and gamma counting to be used as well as Inductively Coupled Plasma (ICP) techniques. This also demonstrated that the materials could deal with these low radioactive levels without the material degrading.

The metal ions investigated in synthetic solutions included Co(II), Ni(II), Cu(II),  $Zn^{2+}$ ,  $Cd^{2+}$ , Eu(III) and  $[UO_2]^{2+}$ . Radioisotopes included  $^{57}Co$ ,  $^{63}Ni$ ,  $^{109}Cd$ ,  $^{152}Eu$  and  $^{238}U$ . The reasons for choosing these metals are discussed further in this chapter when the silica materials are tested for their ability to remove them from solution and ease of removal from a single metal solution with functionalised silica materials.

#### 6.1.1 Radioisotopes used in this work

$^{57}Co$  disintegrates by 100 % electron capture to the excited levels of 706.42 keV (0.18 %) and 136.47 keV (99.92 %) of  $^{57}Fe$ . Table 14 shows the main emissions of  $^{57}Co$  (in keV) which has a specific activity of  $3.12 \times 10^{14}$  Bq/g and a half-life of 371.8 days.<sup>160</sup>

	Gamma or X		Beta ( $E_{max}$ )		Electrons		Alpha	
	E	Yield	E	Yield	E	Yield	E	Yield
E1	14	9			6	106		
E2	122	86			7	70		
E3	137	11						

Table 14 –  $^{57}Co$  radioisotope data.<sup>160</sup>

$^{63}Ni$  decays by  $\beta^-$  emission to the ground state of  $^{63}Cu$ . Table 15 shows the main emissions of  $^{63}Ni$  (in keV) which has a specific activity of  $2.10 \times 10^{12}$  Bq/g and a half-life of 100 years.<sup>160</sup>

	Gamma or X		Beta ( $E_{max}$ )		Electrons		Alpha	
	E	Yield	E	Yield	E	Yield	E	Yield
E1			66	100				

Table 15 –  $^{63}Ni$  radioisotope data.<sup>160</sup>

$^{109}\text{Cd}$  decays by electron capture to the isomeric state (88 keV) of  $^{109}\text{Ag}$ . Table 16 shows the main emissions of  $^{109}\text{Cd}$  (in keV) which has a specific activity of  $9.58 \times 10^{13}$  Bq/g and a half-life of 462.6 days.<sup>160</sup>

	Gamma or X		Beta ( $E_{\text{max}}$ )		Electrons		Alpha	
	E	Yield	E	Yield	E	Yield	E	Yield
E1	22	83			63	41		
E2	25	15			84	45		
E3	88	4			87	10		

Table 16 –  $^{109}\text{Cd}$  radioisotope data.<sup>160</sup>

$^{152}\text{Eu}$  decays 72.1 % by electron capture and about 0.027 % by positron emission to  $^{152}\text{Sm}$ , and by  $\beta^-$  emission (27.9 %) to  $^{152}\text{Gd}$ . Table 17 shows the main emissions of  $^{152}\text{Eu}$  (in keV) which has a specific activity of  $6.45 \times 10^{12}$  Bq/g and a half-life of 13.5 years.<sup>160</sup>

	Gamma or X		Beta ( $E_{\text{max}}$ )		Electrons		Alpha	
	E	Yield	E	Yield	E	Yield	E	Yield
E1	344	27	388	2	75	19		
E2	1112	14	699	14	114	11		
E3	1408	21	1478	8				

Table 17 –  $^{152}\text{Eu}$  radioisotope data.<sup>160</sup>

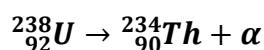
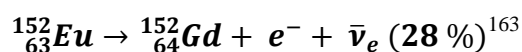
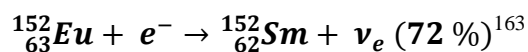
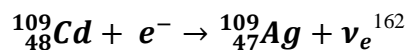
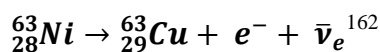
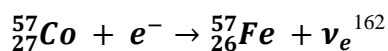
$^{238}\text{U}$  disintegrates by alpha emission to two excited levels and  $^{234}\text{Th}$ . Branching decay by spontaneous fission is at a level of  $5.45 \times 10^{-5}$  %.<sup>161</sup> Table 18 shows the main emissions of  $^{238}\text{U}$  (in keV) which has a specific activity of  $1.24 \times 10^4$  Bq/g and a half-life of  $4.47 \times 10^9$  years.<sup>160</sup>

	Gamma or X		Beta ( $E_{\text{max}}$ )		Electrons		Alpha	
	E	Yield	E	Yield	E	Yield	E	Yield
E1	15	9					4039	<1
E2	50	<1					4147	23
E3							4196	77

Table 18 –  $^{238}\text{U}$  radioisotope data.<sup>160</sup>



### 6.1.1.1 Decay equations for the isotopes used in this work



### 6.1.2 Analytical techniques

#### 6.1.2.1 Inductively Coupled Plasma (ICP)

ICP techniques can be very powerful tools for detecting and analysing trace elements. Plasma is an ionised gas that is macroscopically neutral. Argon is commonly used to produce the plasma because like any noble gas, it is monoatomic with a high ionisation energy (15.76 eV) and is chemically inert. It also has the capability to excite and ionise most of the elements of the periodic table and no stable compounds are formed between argon and the analytes. Furthermore, argon is the cheapest noble gas owing to its 1 % concentration in air.<sup>164</sup>

The ICP source is used for both optical emission spectroscopy (ICP-OES) and mass spectrometry (ICP-MS). The basic components that are used to generate the source are a plasma torch, a radio frequency (RF) coil and an RF power supply. The plasma torch consists of three concentric tubes (made usually from quartz). The gas used to form the plasma is passed between the outer and middle tubes at a flow rate of ca. 12-17 L min<sup>-1</sup>. A second gas flow, the auxiliary gas, passes between the middle tube and the sample injector at ca. 1 L min<sup>-1</sup> and is used to change the position of the base of the plasma relative to the tube and the injector. Finally a third gas flow, the nebuliser gas, also flowing at ca. 1 L min<sup>-1</sup> carries the sample in the form of a fine-droplet aerosol from the sample introduction system. This is sufficient, in the small diameter injector tube, to produce a high velocity jet of gas which punches a cooler hole through the centre of the plasma, termed the central or axial channel. The plasma torch is positioned centrally in the RF coil, approximately 10-20 mm from the interface.<sup>165,166,167</sup>

The formation of an ICP discharge is carried out *via* the following method. A tangential flow of argon gas is focussed between the outer and middle tube of the torch. A load coil, commonly made of copper, surrounds the top end of the torch and is connected to an RF generator. When the RF power (typically 750-1500 W) is applied to the load coil, an alternating current oscillates with the coil at a rate corresponding to the frequency of the generator, commonly either 27 or 40 MHz. RF oscillation of the current in the coil causes an intense electromagnetic field to be created in the area at the top of the torch. When argon gas is flowing through the torch, a high-voltage spark is applied to the gas which causes some electrons to be stripped from their argon atoms. Within the magnetic field these electrons are accelerated and collide with other argon atoms, removing additional electrons. This collision induced ionisation of the argon continues in a chain reaction, breaking down the gas into argon atoms, ions and electrons to form what is known as inductively coupled plasma discharge. This discharge is sustained with the torch and load coil as RF energy is continually transferred to it through the inductive coupling process. Following this, the sample aerosol is then introduced into the plasma through a third tube called the sample injector.<sup>165</sup>

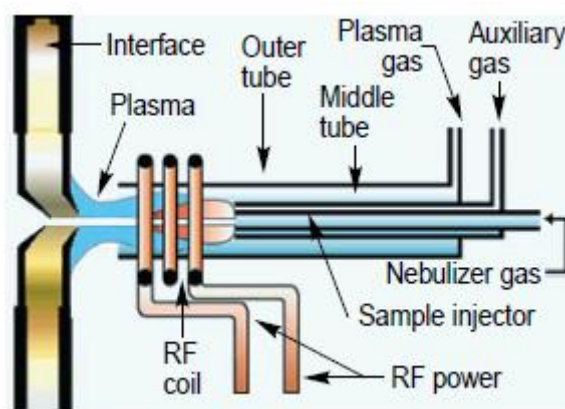


Figure 46 – Detailed view of a plasma torch and RF coil.<sup>165</sup>

#### 6.1.2.1.1 ICP-Optical Emission Spectroscopy

When the analyte enters the central channel of the ICP a number of processes occur. The sample desolvates, the matrix decomposes and the resulting analyte undergoes excitation to produce molecular, atomic and ionic species in various energy states. Some of this energy is released in the form of electromagnetic radiation of a wavelength that is characteristic of the emitting species. It is this property of the plasma that is utilised for analytical purposes in the ICP-OES.<sup>164</sup>

A monochromator is used to resolve specific wavelengths of interest and a detector can be used to measure the intensity of the emitted light. The concentration of the element or elements in question can then be calculated from their intensity.<sup>168</sup>

#### 6.1.2.1.2 ICP-Mass Spectrometry

Using an ion lens system, analyte isotopes are separated according to their mass/charge ratio by use of a quadrupole. Ions with specific  $m/z$  ratios are transmitted sequentially to the ion detection system. Ions that have a lower or higher mass  $m/z$  ratio have different trajectories and are therefore filtered out of the system. The most common form of detector used in ICP-MS is an electron multiplier where the signal intensity is measured simultaneously at two different points. In the upper stage of the detector (responsible for measuring high intensity signals), the signal is measured as a current which is later converted to a counts per second (cps) equivalent. The lower pulse stage measures low intensity signals in cps. The detectors life span is prolonged and damage minimised by preventing signals of exceedingly high intensities from entering it.<sup>165,169</sup>

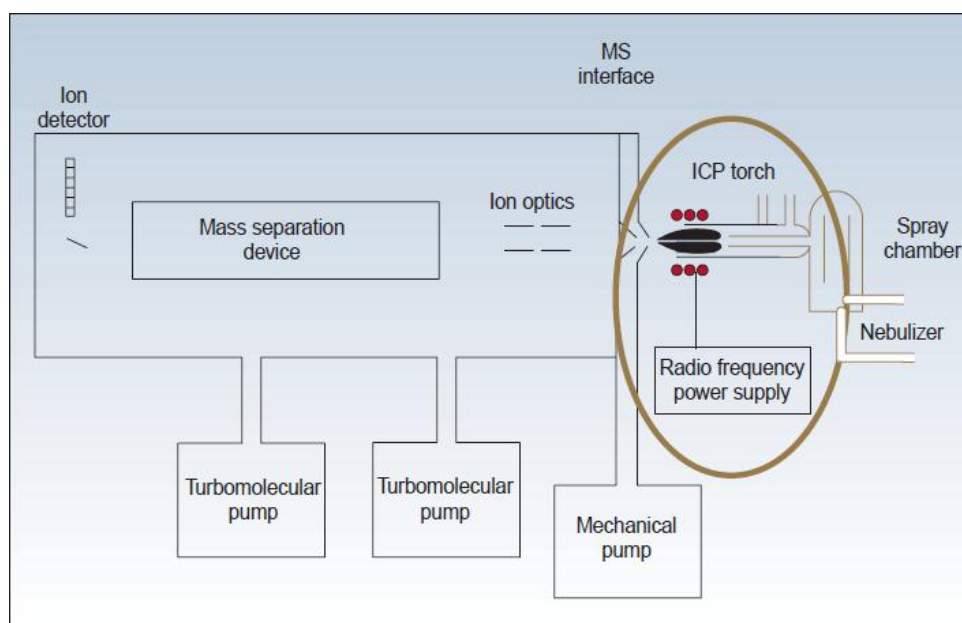


Figure 47 – Schematic of an ICP-MS system showing the location of the plasma torch and radio frequency (RF) power supply.<sup>165</sup>

#### 6.1.2.1.3 Benefits of using both ICP-OES and MS

ICP-OES is very useful for measuring concentrations above 3-5 ppm (depending on metal, see section 2.1.6 for metals observed in this work). When lower levels of metal were present, either due to starting with a lower concentration because little material was available or as a

result of material reducing an initial concentration beyond the sensitivity of the ICP-OES, ICP-MS provides lower detection limits (ppb-ppt) for these scenarios.

For the majority of this work, ICP-OES was used and ICP-MS was only used when concentration levels were below the limit of detection and quantification as reported in Table 2 in section 2.1.6 (e.g. reversibility studies illustrated in Appendix 2 – Reversibility and dissolution of metal ions following sequestration).

### **6.1.2.2 Liquid Scintillation Counting**

Liquid Scintillation Counting (LSC) is a technique for measuring ionising radiation mainly from beta-emitting nuclides. The process works by incorporating the radioactive isotope with a liquid chemical medium that is capable of transferring the kinetic energy of the nuclear emissions into light energy, the amount of light can then be detected by the counter. The liquid scintillation cocktail carries this out by absorbing the energy, before re-emitting it as flashes of light. The cocktail contains two basic components, solvent and phosphors. The majority of energy absorption is carried out by the solvent, before the phosphors (dissolved in the solvent) convert this into light (photons). With the use of a photomultiplier tube (PMT), the photons can be counted.<sup>170,171</sup>

A ‘coincidence unit’ is used in conjunction with two PMTs so to reduce background noise and therefore improve the signal/noise ratio. When a flash of light is emitted from the solution isotropically, both PMTs will count this and the coincidence unit will record this by sending a single signal to the multichannel analyser. This improves the accuracy of the instrument and reduces background levels because the probability of both PMTs recording a stray photon is significantly low.<sup>172,173</sup> Figure 48 is used to illustrate how the liquid scintillation counter works.

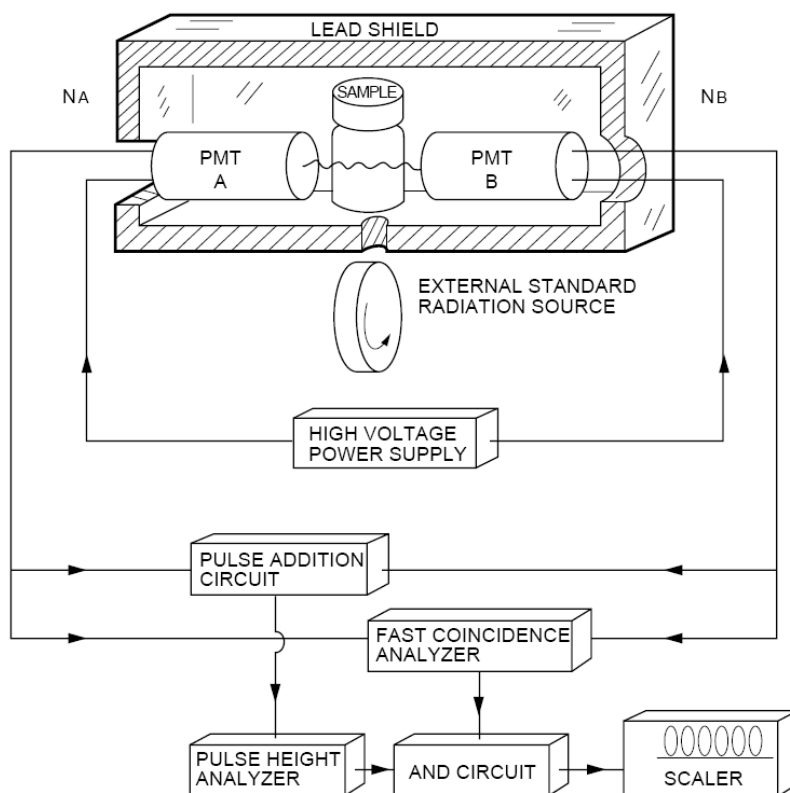


Figure 48 – Basic construction of a liquid scintillation counting instrument.<sup>173</sup>

### 6.1.2.3 Gamma spectrometry

In principle, a gamma counter is much like a liquid scintillation counter where light is produced and detected. Unlike liquid scintillation counting, a detector (often a NaI crystal which is thallium activated) surrounds the sample which absorbs the gamma rays to produce this light. The number of flashes per unit time is proportional to the number of photons per unit time as in LSC. Figure 49 illustrates a block diagram of the processes that take place for gamma spectrometry.

The gamma photons produce charged electrons by three different processes, these are the photoelectric effect, the Compton Effect (also known as Compton scattering) and pair production. It is these fast electrons that produce the scintillations and the observed spectral distribution will depend on the detailed interaction process of the gamma rays in the crystal.<sup>174</sup>

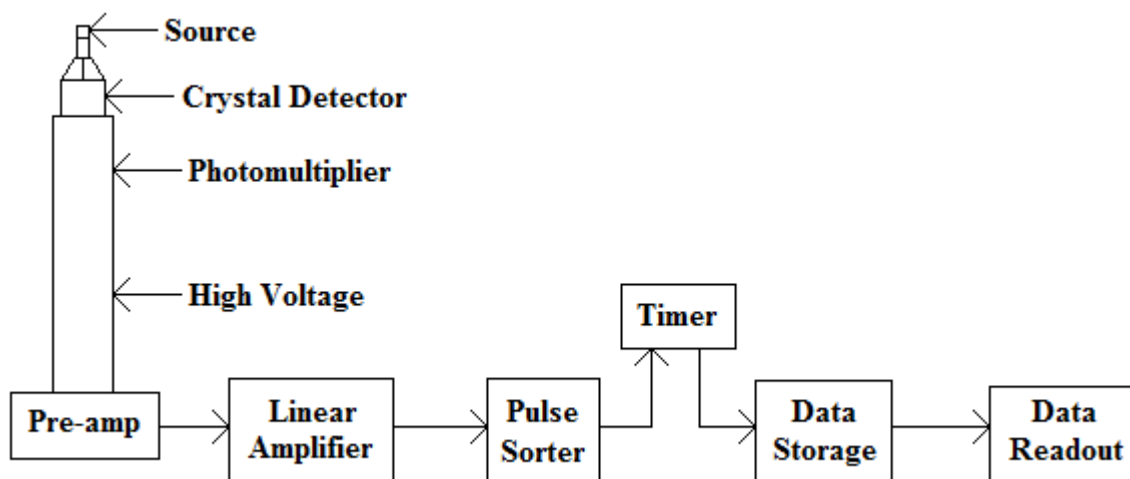


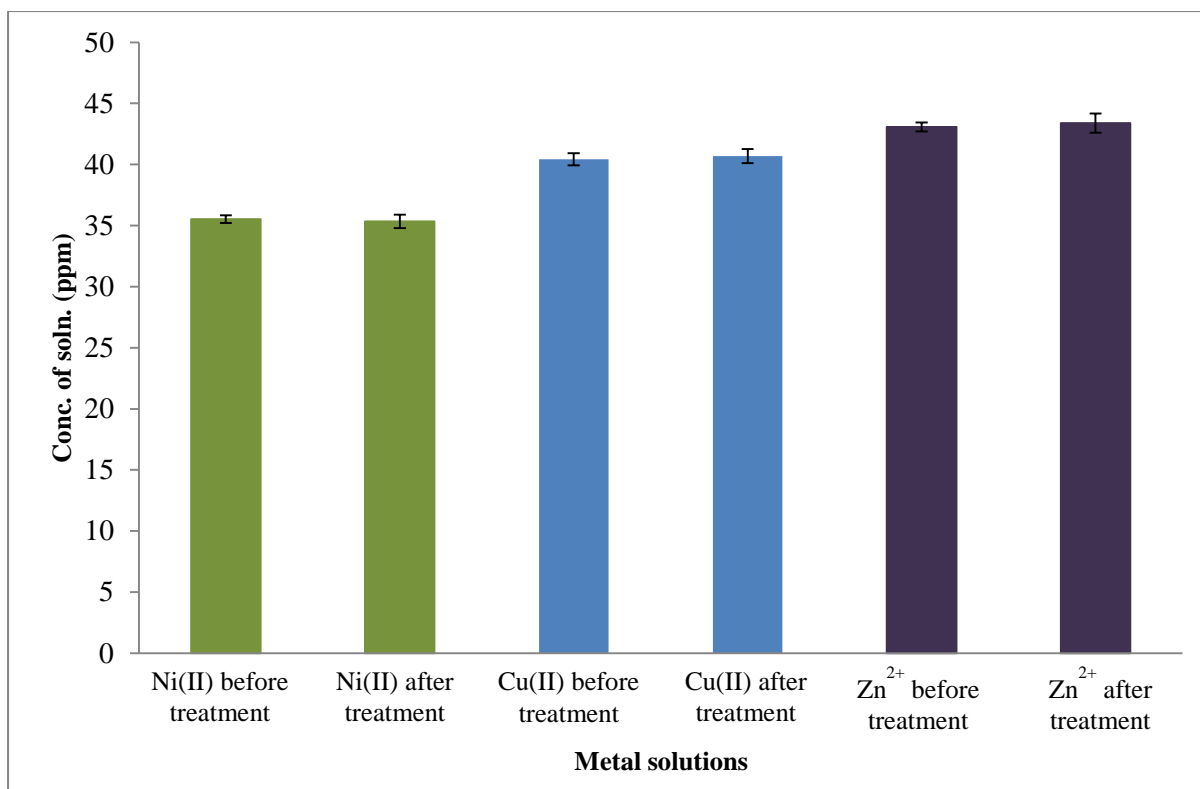
Figure 49 – Gamma counter block diagram.<sup>175</sup>

## 6.2 Results and Discussion

### 6.2.1 Metal ion sequestration with free PHEMA and PHEMA-Malonate

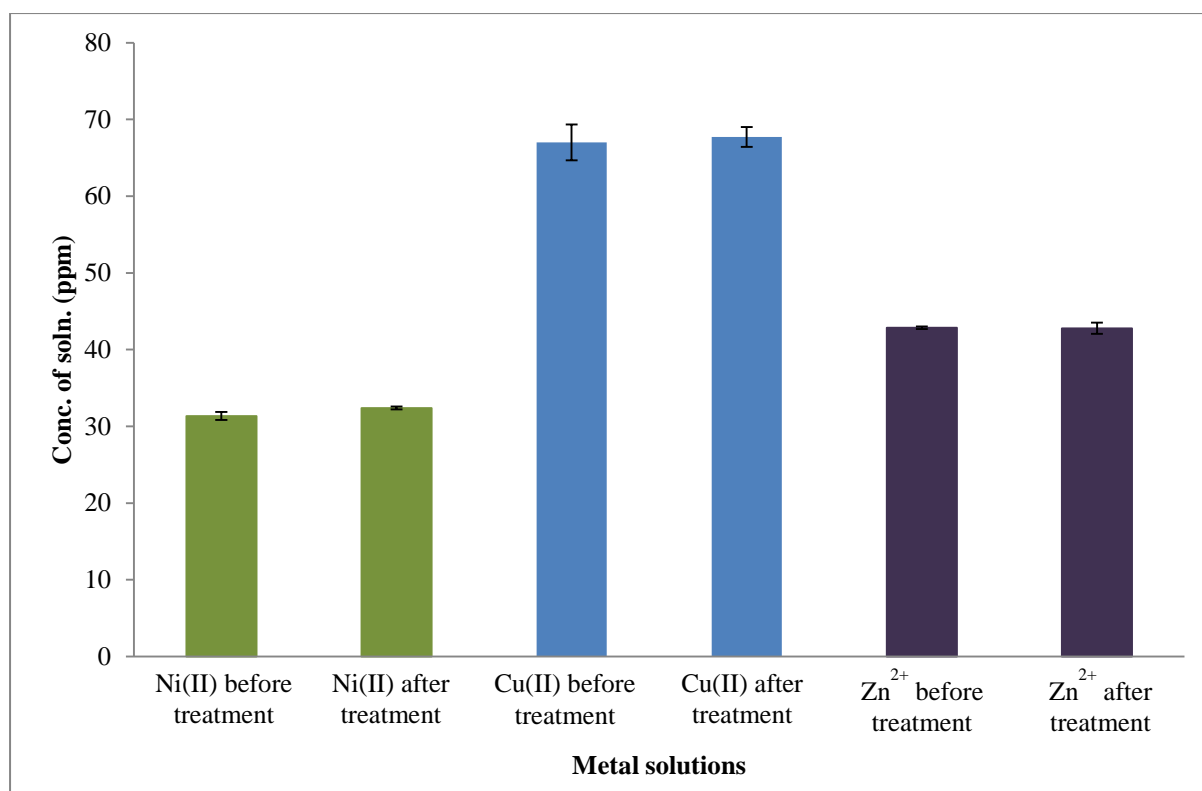
The first material to be produced and tested for sequestration of metal ions was PHEMA. Cu(II) is known to contaminate the PHEMA<sup>38</sup> product when synthesised *via* ATRP and hence a rigorous wash of the product is required. This is one of the reasons it was originally used to test PHEMA as a potential material for its sequestration from solutions. This was shown when initial investigations of adding the PHEMA to a Cu(II) solution raised the initial concentration of Cu(II). Rigorous washings of PHEMA were carried out from this point to ensure this did not re-occur as described in the experimental chapter 2.2. To avoid any anomalous findings, Ni(II) and Zn<sup>2+</sup> solutions were also tested. Being found either side of copper on the period table, the two metal ions have their similarities i.e. coordination number although obviously have their differences in size.

The hydroxyl end groups in PHEMA were thought to be a good reference point where one would expect to see sequestration of metal ions but that could be improved on with modifications and more effective or specific ligands. Figure 50 shows the results observed with these transition metals over a 24 hour period whilst the method can be found in section 2.27.



**Figure 50 – Aqueous concentrations of Ni(II), Cu(II) and Zn<sup>2+</sup> before and after addition of free PHEMA for 24 hours. No change in concentration was observed for any of the metals with this polymer. Initial pH readings were ca. 6.04, 5.37 and 6.22 for nickel, copper and zinc respectively.**

A colour change was observed for the swelled PHEMA when it had been present in the solutions, especially in the case of the Cu(II) solution. However, it appeared this was due to the copper being present in the water which was swelling the polymer, rather than the copper being bound to the polymer. Once dry, there was no colouring to suggest that the polymer was any different to before it had been in the solution. Solutions of much stronger concentration (ca. 700 ppm) were also tested but again, no change in concentration was observed.



**Figure 51 – Aqueous concentrations of Ni(II), Cu(II) and Zn<sup>2+</sup> solutions before and after addition of free PHEMA-malonate for 24 hours. No change in concentration was observed for any of the metals with this polymer. Initial pH readings were ca. 6.12, 5.30 and 6.20 for Ni(II), Cu(II) and Zn<sup>2+</sup> respectively.**

The product recovered after the attempted reaction of PHEMA with malonate was also tested for its metal sequestration ability but again, as Figure 51 shows, no change in concentration was observed for any of the metals trialled, also over 24 hours. A substantial drop in pH was noted however, suggesting that the acid chloride used in the malonate attachment may be causing this effect and hence supporting the theory that the synthetic modification had not been successful. No colour change was seen in any case for these investigations, especially as the product was already brown coloured, unlike the white PHEMA.

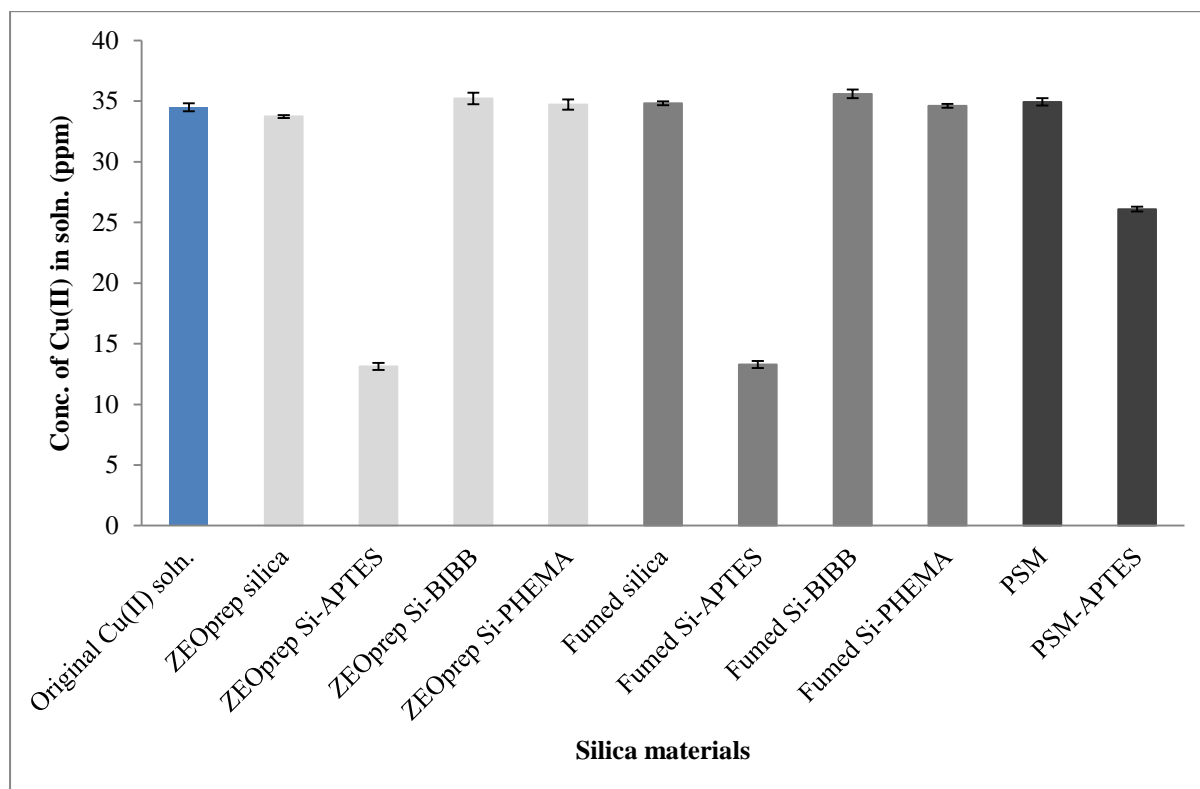
As an alternative method of measuring the concentration change, liquid scintillation counting was used for testing PHEMA on <sup>63</sup>Ni. The results of this still showed PHEMA to be ineffective. The method for this is given in section 2.28.

### **6.2.2 Initial metal ion sequestration with functionalised silica materials**

Figure 52 shows the results of the initial tests carried out *via* ICP-OES on the silica attached materials. Each stage of the modification process described in chapter 4 was tested on a Cu(II) solution of ca. 35ppm. The general method can be found in section 2.29. This method



was used for all tests carried out in the remaining results of this section unless otherwise stated.



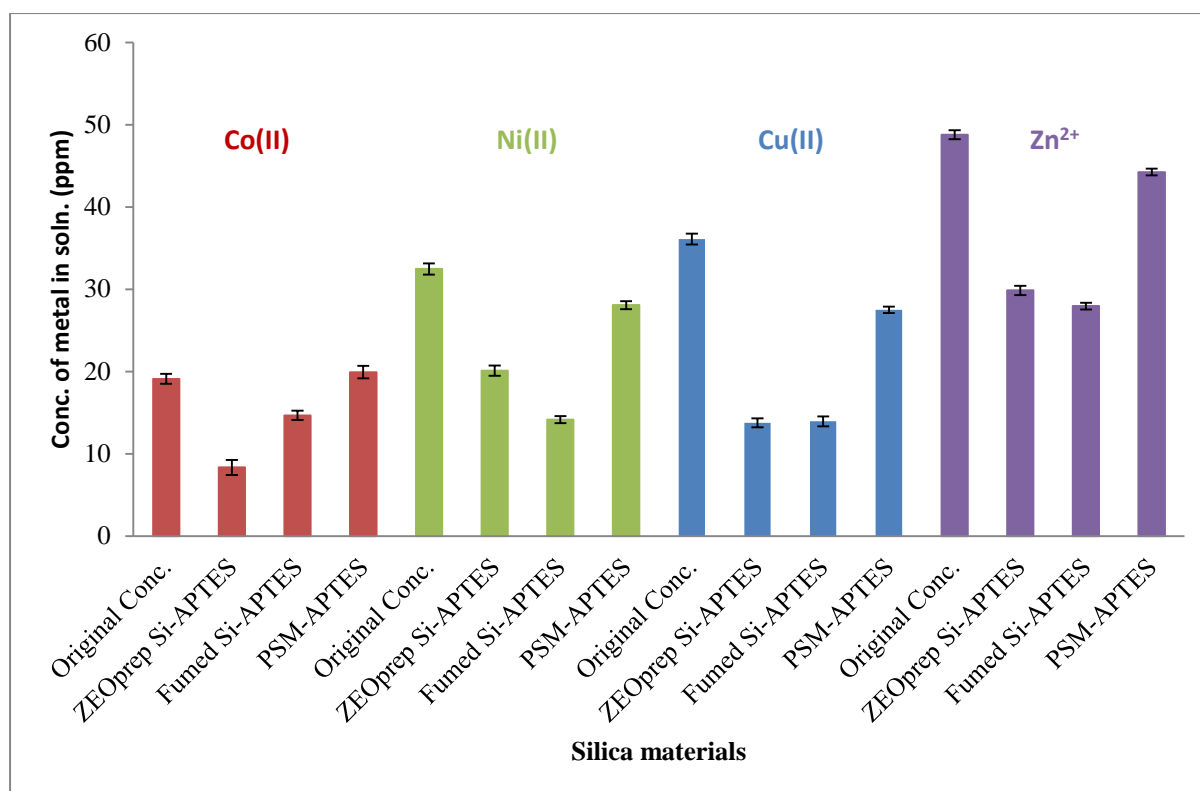
**Figure 52 – Aqueous concentrations of Cu(II) after being treated for 24 h with functionalised silica materials. A clear indication was given as to where work should progress from after the results of silica attached APTES were observed.**

The significant result observed in Figure 52 shows the APTES ligand to have made a significant difference to the concentration of Cu(II) remaining in solution. APTES-functionalised ZEOprep and fumed silica produced similar results whereas the porous silica microparticles (PSM) did not appear to be as effective. This result was to be expected based on the findings from the characterisation discussed in chapter 5, where it is apparent the pores are not available for APTES attachment and therefore less APTES per gram of material exists.

### 6.2.3 Sequestration of metal ions with silica attached APTES

The same tests were carried out on Ni(II) and  $\text{Zn}^{2+}$  solutions and similar results were observed. A cobalt solution was also prepared where only the APTES materials were tested.

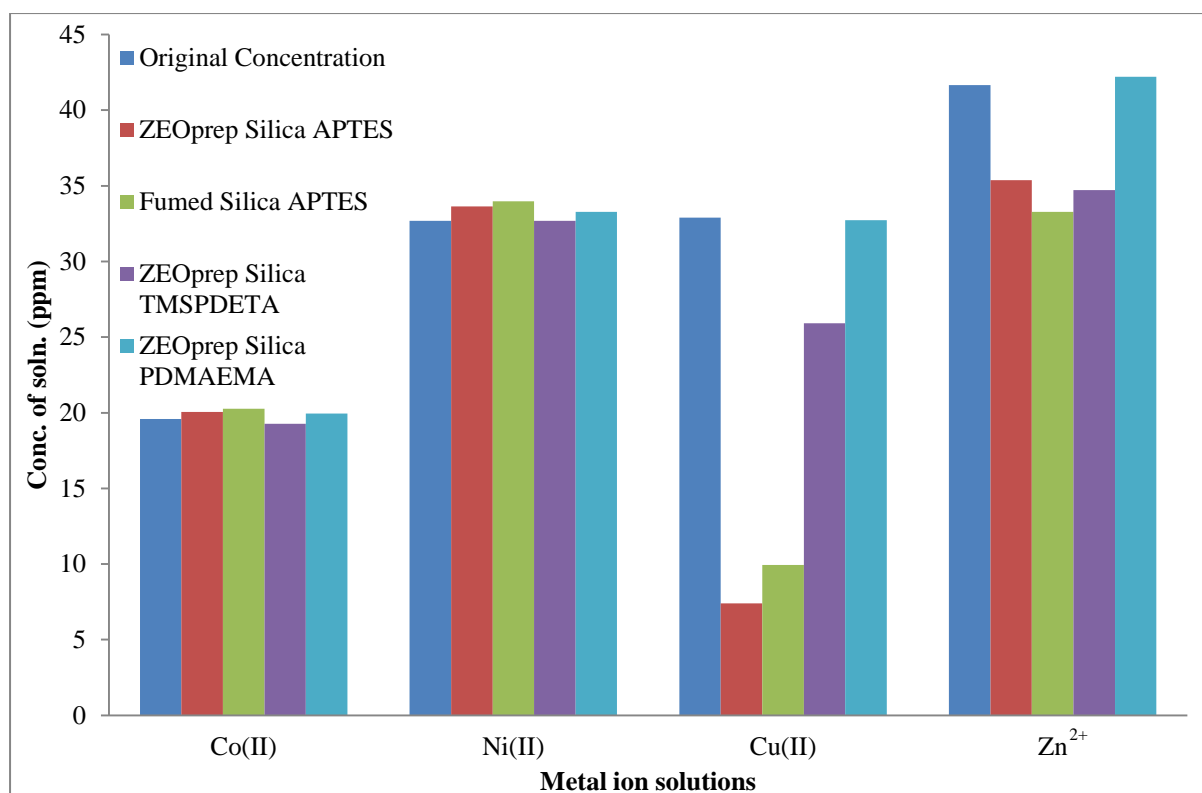
Figure 53 displays the results of the four metals in four separate aqueous solutions and the effect of the APTES attached material on each of these solutions.



**Figure 53 – Aqueous concentrations of cobalt, nickel, copper and zinc solutions before and after addition of various silica attached APTES for 24 h. Overall, the porous silica microparticles with APTES performed the worst at removing metal but the ZEOprep and fumed silica generally performed to a similar level.**

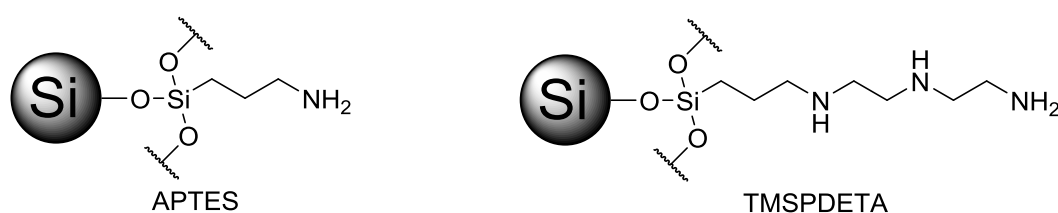
Each of the materials shows a clear reduction in metal concentration across the four solutions investigated but also clearly depicts the ability of the porous silica microparticles is not as efficient as the ZEOprep and fumed materials. Although the ZEOprep and fumed silica have very different particle sizes and hence surface area, the APTES-functionalised materials show very little difference in their abilities to sequester more or less than the other.

Figure 54 illustrates the APTES-functionalised ZEOprep silica to be marginally superior to the equivalent fumed silica sample in a 24 hour investigation. The method for this was similar to that given in section 2.29, but the four metals were in the same solution. Due to this being an initial investigation, no repeats were carried out hence, no error bars are given. However, the graph clearly shows the selectivity for Cu(II) over the other metal cations, with only the Zn<sup>2+</sup> solution also being slightly reduced. Both Co(II) and Ni(II) concentrations remained essentially unchanged.



**Figure 54 – Initial selectivity study carried out with functionalised silica materials on transition metals for 24 h. No repeats were carried out: hence no error bars can be applied. APTES shows a large preference for copper, with a small amount of zinc removed whilst cobalt and nickel are left unchanged. Although TMSPDETA has three nitrogen groups to APTES' one, APTES clearly has a larger impact.**

Other than APTES, the additional ligand showing a sizable reduction in concentration was TMSPDETA. Surprisingly, this ligand appeared less effective than APTES despite the fact it holds three times more nitrogen atoms.



**Figure 55 – Structures of the APTES and TMSPDETA ligands attached to the silica surface.**

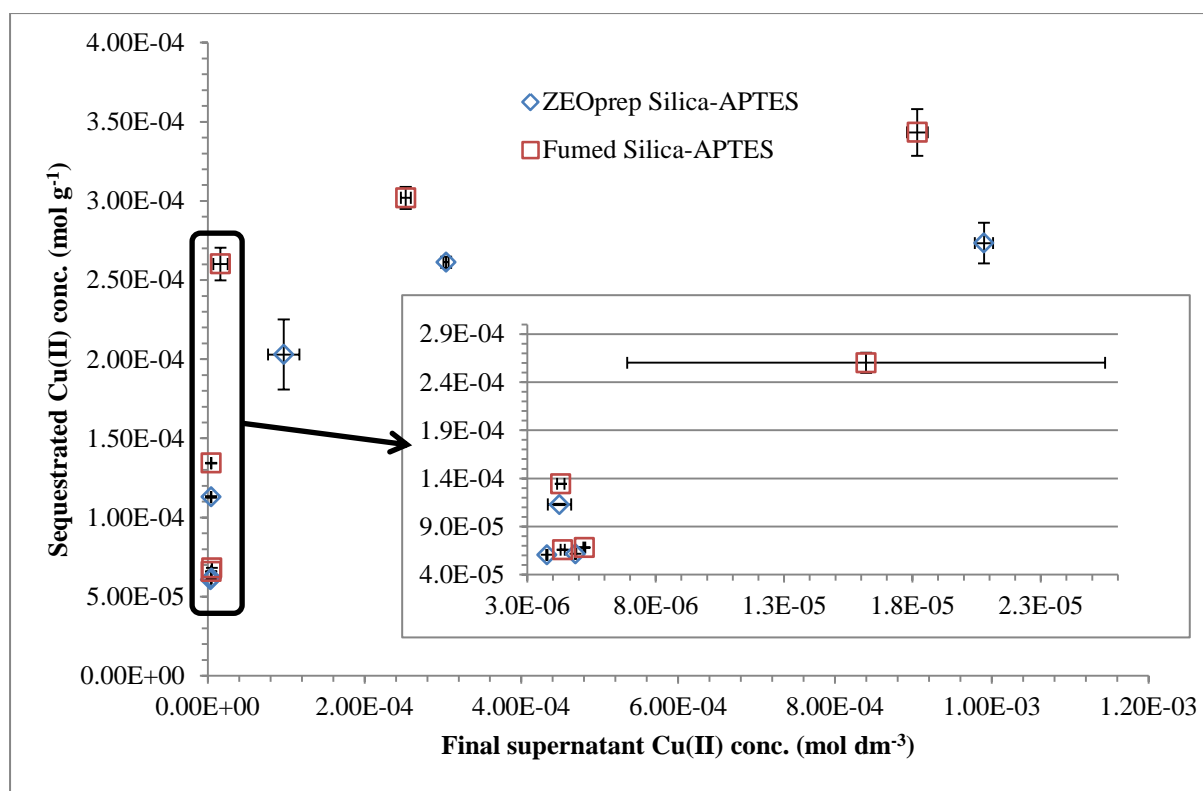
This suggests the primary nitrogen at the end of the ligand is the most effective as this is where it is located on APTES. TMSPDETA is a much bigger/longer molecule than APTES and therefore the density at which the TMSPDETA is grafted from the surface will be less (i.e. less molecules per square nm) simply because it is bigger and fewer primary amines will exist. Figure 55 shows the structure but it is unlikely all the molecules would be stretched out as shown. Instead, some may lie along the surface, taking up space and causing this effect.

This sequestration result does agree with McEleney *et al.*<sup>8</sup> who reported better results with the APTES ligand than TMSPDETA when removing Grubbs catalyst (ruthenium) from aqueous solutions at various concentrations. However it does seem not quite to the extent observed with these results, although comparison is difficult due to the way the results have been reported.

#### **6.2.3.1 Cu(II) studies with silica attached APTES**

Copper is a very common substance that is used widely by humans. With copper production still rising, rivers are depositing sludge on their banks that is contaminated with copper due to the disposal of copper-containing wastewater. In the environment, copper does not break down and because of this, it can accumulate in plants and animals when found in soils. These copper-rich soils allow only a limited number of plants a chance of survival and hence, little plant diversity is observed at copper-disposing factories.<sup>176</sup>

To fully assess the sequestration ability of the APTES-functionalised silica with copper, 50 mg of material were added to a range of concentrations were made in deionised water including 80 ppm, 40 ppm, 20 ppm, 10 ppm, 5 ppm and 2.5 ppm over a 24 hour period. From the results observed using ICP-OES, an isotherm was plotted and is shown in Figure 56.  $\text{CuCl}_2 \cdot 2\text{H}_2\text{O}$  was the salt used to produce the solutions where Cu(II) is the major species in water up to pH 6<sup>177</sup> – which is the pH range investigated in this work.



**Figure 56 – Isotherm for Cu(II) removal from deionised water with APTES-functionalised ZEOprep and fumed silica materials.**

This graph shows the two silica materials to be quite similar in sequestration capability. However, the APTES-functionalised fumed silica does show a slightly larger capacity at similar concentrations of copper as the ZEOprep material. With remarkably small errors incorporated and two sets of results that follow a very clear trend, these results prompted one to pilot this material with the active nickel source of <sup>63</sup>Ni that is relatively easy to handle and simple to analyse – providing an ideal isotope to begin radioactive tests.

To help interpret the results, sorption models are applied which can be used compare the existence of metal between two phases as a ratio. This was first introduced in the chapter 1 but has been discussed here also where it becomes relevant to the results obtained in this thesis. The parameter known as the partition (or distribution) coefficient,  $K_d$ , is one of the most important parameters used in estimating the migration potential of contaminants present in aqueous solutions in contact with surface, subsurface and suspended solids.<sup>178</sup> It is a thermodynamic measure of sorption of contaminants or ions to geomeia and is defined as ‘the ratio of the quantity of the adsorbate adsorbed per unit mass of solid to the amount of the adsorbate remaining in solution at equilibrium’.<sup>178,179</sup>

$$K_d = \frac{C_0 - C_f}{C_f} \cdot \frac{V}{M}$$

**Equation 12 – Equation to show how  $K_d$  is calculated.**

Where  $C_0$  and  $C_f$  are the initial and final concentrations in the solution of the target species, often determined by ICP-OES or ICP-MS.  $V$  is the solution volume in mL and  $M$  is the mass in grams of the adsorbent.

$K_d$  is typically given in unit of  $\text{mL g}^{-1}$ .<sup>23,178</sup> For the majority of cases, the concentration of the compound retained on the solid is calculated by the difference between the initial solute concentration and the final solute concentration.<sup>180</sup>

Values for  $K_d$  can vary greatly between contaminants, but also as a function of aqueous and solid phase chemistry. The result of a collection of experiments evaluating the effect of contaminant concentration on adsorption whilst other parameters are held constant is called an ‘adsorption isotherm’.<sup>179</sup> The word ‘isotherm’ was specifically chosen because of the influence of the temperature on sorption reactions: temperature must be kept constant and specified.<sup>180</sup>

The transfer of substances from a mobile phase (liquid or gaseous) to a solid phase is a universal phenomenon. This is the reason why the isotherm (a curve describing the retention of a substance on a solid at various concentrations) is a major tool to help describe and predict the mobility of a substance in the environment. These retention/release phenomena are sometimes strongly kinetically controlled, so that time-dependence or the sorption isotherm must be specified.<sup>180</sup>

The higher the  $K_d$  the better the sorbent material will be for collection and  $K_d > 10^4$  represent relatively high affinity sorbents.<sup>45,181</sup>

An alternative approach (and perhaps a more applicable to practical measurements) to the concept of  $K_d$  (a thermodynamically determined value) is  $R_d$  (distribution ratio). This is the ratio of the solute between the solid and the liquid phases at the stated experimental conditions and is not thermodynamically determined.<sup>179</sup> It is the  $R_d$  value that is reported in this thesis to compare the metal binding capacities attached to the APTES-functionalised ZEOprep and fumed silica and uses the same formula as  $K_d$ .

ZEOprep Si-APTES			Fumed Si-APTES		
Initial Concentration of Cu		$R_d$	Initial Concentration of Cu		$R_d$
ppm	$\text{mol dm}^{-3}$	$\text{mL g}^{-1}$	ppm	$\text{mol dm}^{-3}$	$\text{mL g}^{-1}$
80.27	$1.26 \times 10^{-3}$	$2.24 \times 10^5$	81.74	$1.29 \times 10^{-3}$	$3.42 \times 10^5$
35.92	$5.65 \times 10^{-4}$	$6.96 \times 10^5$	37.36	$5.88 \times 10^{-4}$	$1.08 \times 10^6$
19.05	$3.00 \times 10^{-4}$	$1.80 \times 10^6$	19.40	$3.05 \times 10^{-4}$	$1.83 \times 10^7$
8.24	$1.30 \times 10^{-4}$	$2.42 \times 10^7$	9.76	$1.54 \times 10^{-4}$	$2.81 \times 10^7$
4.51	$7.10 \times 10^{-5}$	$1.45 \times 10^7$	4.93	$7.75 \times 10^{-5}$	$1.35 \times 10^7$
4.66	$7.34 \times 10^{-5}$	$1.14 \times 10^7$	5.14	$8.09 \times 10^{-5}$	$1.18 \times 10^7$

**Table 19 - Variation of  $R_d$  at different initial concentrations of Cu(II) from deionised water. An increase of ca. two orders of magnitude was observed as the initial concentration decreased. Initial pH's were recorded to range from 5.81 and 5.21 and decreased as the concentration increased.**

Table 19 shows the  $R_d$  for the Cu(II) sorption to the APTES-functionalised ZEOprep and fumed silica materials at room temperature at a pH of 6.5-7. Saturation of sorption sites is evident from the decrease in  $R_d$  which is nearly two orders of magnitude less at around 80 ppm when compared to around 10ppm. The difference in  $R_d$  across the range of radionuclides tested is reported and a table is used to summarise the findings following the results.

#### **6.2.3.1.1 Kinetic studies of Cu(II) sequestration with Si-APTES**

When testing the APTES-functionalised ZEOprep and fumed silica materials, it was assumed 24 h would be an appropriate time to leave the sequestration experiments due to work previously reported<sup>182</sup> and this was the case for all the individual metal cases discussed in this chapter. However, following the results found in Figure 57 (where it was found equilibrium was reached after 3-4 weeks), the selectivity studies carried out in chapter 7 were modified so that a 24 hour and a 4 week sample were taken. The kinetics testing was carried out by preparing a stock solution of Cu(II) using  $\text{CuCl}_2$  at ca. 40 ppm. 50 mg of the APTES functionalised ZEOprep and fumed silica material was added to 45 mL of the stock solution in each separate test and a sample was taken at the stated time by syringe filter and prepared for ICP-OES. The samples were then all run together after the testing period was complete.

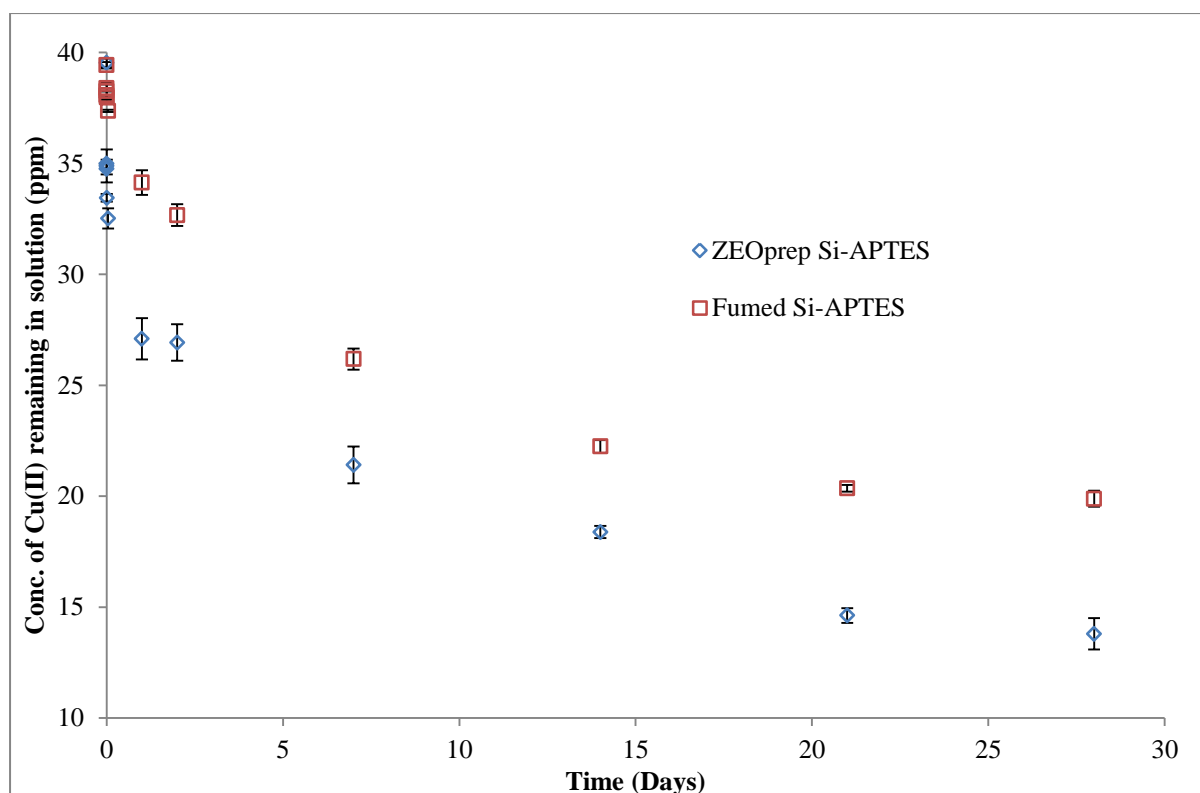


Figure 57 – Sequestration of Cu(II) over a four week period. Initial pH was 5.47 and was found to have changed to 5.92 for the ZEOprep Si-APTES sample and 5.96 for the fumed Si-APTES sample.

ZEOprep silica-APTES		Fumed silica-APTES	
Time sample taken	Concentration (ppm)	Time sample taken	Concentration (ppm)
Initial Conc.	39.54	Initial Conc.	39.43
15 seconds	34.89	15 seconds	38.40
30 seconds	34.99	30 seconds	38.26
1 minute	34.76	1 minute	38.08
3 minutes	33.45	3 minutes	37.97
1 hour	32.52	1 hour	37.37
1 day	27.10	1 day	34.14
2 days	26.92	2 days	32.67
1 week	21.42	1 week	26.18
2 weeks	18.38	2 weeks	22.24
3 weeks	14.63	3 weeks	20.36
4 weeks	13.79	4 weeks	19.88

Table 20 – Values measured for the concentration change over time when silica-APTES samples were added to a Cu(II) solution. These values are used to plot Figure 57.



Similar work has been carried out by Aguado *et al.*<sup>182</sup> using the ligand ethylenediaminopropyl ( $-\text{CH}_2\text{CH}_2\text{CH}_2\text{NHCH}_2\text{CH}_2\text{NH}_2$ ) to functionalise the silica surface of SBA-15 using a synthesis reported by Zhao *et al.*<sup>183</sup>

There is a notable difference observed between the material reported by Aguado *et al.*<sup>182</sup> and that reported within this thesis. They report an immediate change in concentration at 5 min but no change is observed after this. Three initial concentrations were used including 263, 113 and 5 ppm before also using 50 mg of functionalised silica in 45 mL solutions. The concentrations appear to be reduced to ca. 240, 90 and 0 ppm respectively, reducing the two higher concentrations by 23 ppm. When compared to the results shown in Figure 57 and Table 20 for this work, the initial copper concentration of 39.5 ppm was reduced to just 32.5 and 37.4 ppm for the ZEOprep and the fumed material respectively in 1 hour. The major difference between this work and that reported appears to be the kinetics and the fact that the ZEOprep and fumed silica keep decreasing the concentration for 3-4 weeks. After this time, the ZEOprep material sequestered 25.75 ppm whilst the fumed material sequestered 19.55 ppm.

It is difficult to make direct comparisons between these two results when the ligand they discuss is not exactly the same as it contains two nitrogen atoms, the initial concentrations are different no pHs are reported and the solid support is different. However, it does appear that the material reported by Aguado *et al.*<sup>182</sup> would work better over a shorter timescale whilst the APTES-functionalised ZEOprep silica has a greater capacity. Nevertheless it must be said that the synthetic procedure for the SBA-15 material is much longer at ca. 3 days, whilst the APTES attachment takes only 2 hours.

Panahi *et al.*<sup>29</sup> reported equilibrium of sorption being achieved in 10 minutes (see Figure 59) which was much faster than the results found with the APTES-functionalised silica materials. A reminder of the structure (originally introduced in chapter 1) is shown below in Figure 58.

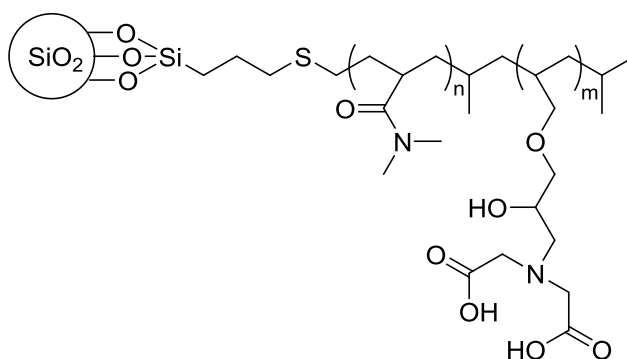


Figure 58 – Chemical structure of poly(AGE/IDA-co-DMAA)-grafted silica gel produced by Panahi *et al.*<sup>29</sup>

The obvious reasoning for this much faster equilibrium time is the many more binding sites available whilst the polymer also provides a much larger surface area. This really illustrates the benefit of using a polymer over a simple ligand in these environments with limited contact time required to saturate the sorbent.

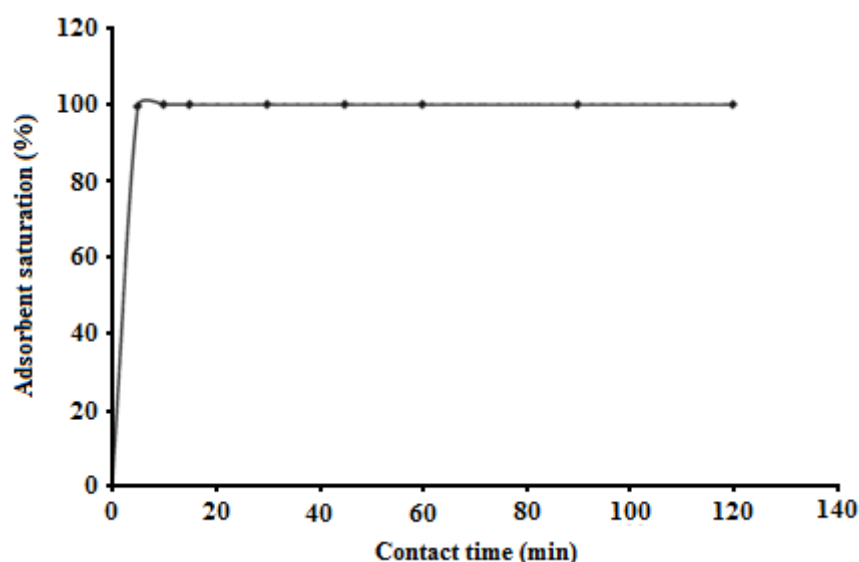
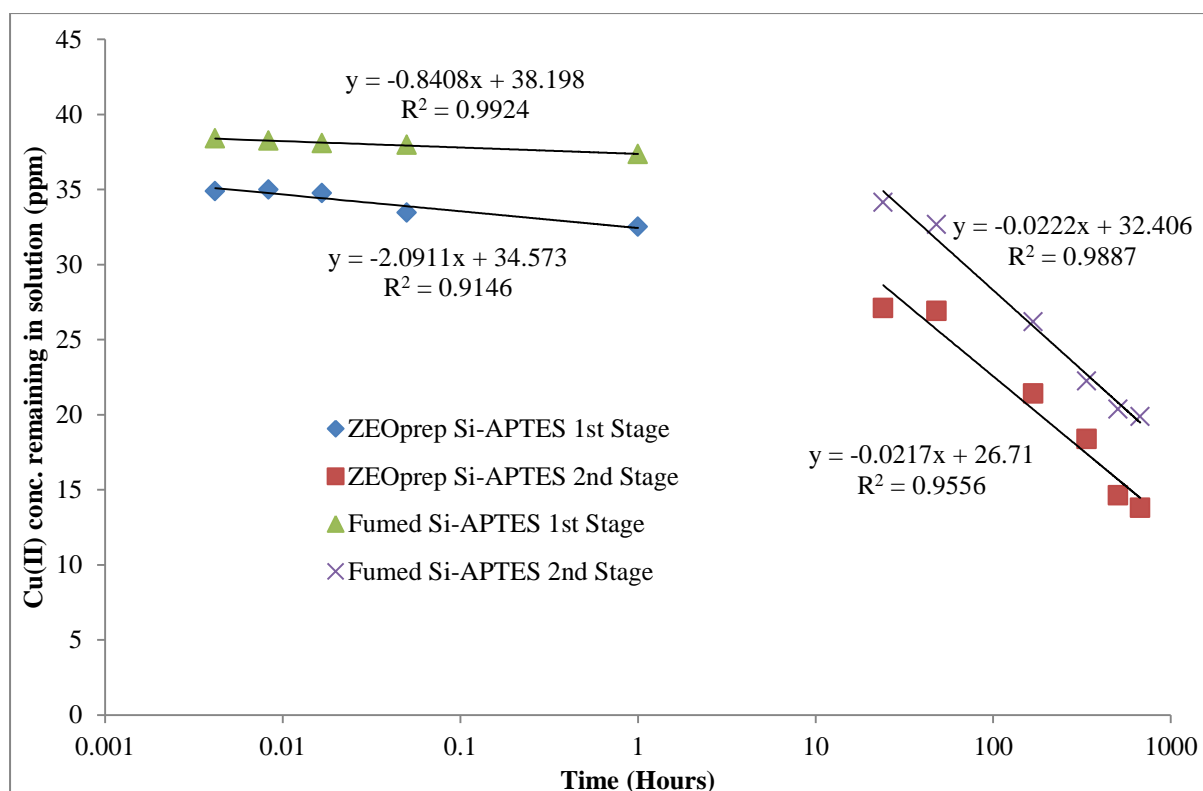


Figure 59 – Kinetics of Cu(II) on poly(AGE/IDA-co-DMAA)-grafted silica gel.<sup>29</sup>

Figure 60 shows the same data as that used to plot Figure 57 but the time is plotted on a log scale. This enables straight line plots to be made, enabling simpler comparisons and rate constants to be calculated easily. The two sets of data have been broken into two series as it was noticed that a much slower rate occurs once the materials have been in solution for over one day.



**Figure 60 – Sequestration of Cu(II) over a four week period. By breaking both studies into two series, two separate trend lines are fitted to clearly show how the rate changes from the data collected for solutions investigated under one day, and those taken after one day. The x-axis is on a logarithmic scale to produce the straight lines and hence a rate constant can be easily measured.**

The first observation to note in Figure 60 is the negative gradient value produced. This is because this graph is based on the decrease in concentration of metal ions in solution rather than the increase in concentration on the surface of the silica material. For the purposes of this, the gradient can be assumed to be positive when discussing the rate constant.

So, for the first stage of the two silica materials (over a time period of 1 hour), the gradient is found to be -2.0911 and -0.8408 for APTES-functionalised ZEOprep and fumed silica respectively corresponding to rate constants of 2.1 and 0.8 ppm hr<sup>-1</sup>. The second stage of the two silica materials (over a time period from 1 up to 28 days) shows a significant decrease in rate constants, both of which are found to be 0.02 ppm hr<sup>-1</sup>. In terms of concentration removed per day, this can be calculated to be 50 and 20 ppm day<sup>-1</sup> for the APTES-functionalised ZEOprep and fumed silica respectively before dropping to 0.5 ppm day<sup>-1</sup> in both circumstances.

The most obvious explanation for the first stage and hence faster rate constant is that the nitrogen atoms at the end of the APTES ligand is working effectively by providing a strong

ligand for the copper ions to bind to and forming a monolayer of metal ions at the surface. However, the ZEOprep material is found to work at over double the rate of the fumed silica material which suggests that there is an optimum particle size and moles of ligand attached per particle but further work would need to be done to prove this to be the case.

The second stage shows a much slower rate constant whereby the concentration is calculated at a rate of  $0.02 \text{ ppm hr}^{-1}$  for both materials, signifying the same process takes place in both these scenarios. Exactly what is happening here is unclear and evidence of unexpected results were also found when XPS was carried out on the material. A local pH change<sup>184</sup> could be the reason for this slow decrease in concentration and is explained in more detail when discussing the XPS results (section 6.2.3.1.2). Alternatively a secondary ligand binding process to the oxygen atoms present in the APTES molecule could provide the reason to why this second stage is observed, again this is discussed following the XPS results.

Literature comparison studies have proven to be challenging due to the different approaches by research groups and the vast amount of testing available with choice of metal ions and sorbent materials. Prasad *et al.*<sup>185</sup> have reported Pb(II), Cu(II) and  $\text{Zn}^{2+}$  in multi-component sorption studies with low-cost, low-grade ( $<12\% \text{ P}_2\text{O}_5$ ) phosphate rock but simply state that ‘rate constants...are found nearly constant for all the divalent metal ions under consideration.’ Although rate constants have not been regularly reported, similar graphs to that observed in Figure 57 are common and often illustrate a fast decrease in concentration before reaching equilibrium.<sup>14,126,182</sup>

#### **6.2.3.1.2 XPS studies on ZEOprep Si-APTES after Cu(II) sequestration**

X-ray photoelectron spectroscopy, XPS or ESCA (Electron Spectroscopy for Chemical Analysis) is probably one of the most widely used surface analytical tools for the study of material surfaces due to its qualitative and quantitative determination capabilities of surface composition. Typically, it probes a depth of around 5-10 nm depending on the nature of the material and can be used to identify all elements excluding hydrogen. X-rays are used to probe the sample and electrons from the core levels that leave the surface are analysed using an electron analyser. It can be carried out on virtually all flat samples with a maximum resolution of a few micrometres and is particularly well suited for metallic and inorganic materials but can also be used for the analysis of polymers.<sup>186</sup>

Photoelectron spectroscopy is based upon a single photon-in/electron-out process. The energy of the photon is given by the Einstein relation in Equation 13:

$$E = h \nu$$

**Equation 13 – Einstein relation.**

Where  $h$  is the Planck constant ( $6.62 \times 10^{-34}$  J s) and  $\nu$  is the frequency of the radiation in Hz. The photon is absorbed by an atom in a molecule or solid, leading to ionisation of the atoms and the emission of a core (inner shell) electron. Given that energy can neither be created nor destroyed, the energy going in must equal the energy going out.<sup>186</sup> Thus:

$$h \nu = E_B + E_K$$

**Equation 14 – Determination of the energy of a photon.**

or the kinetic energy

$$E_K = h \nu - E_B$$

**Equation 15 – Determination of the kinetic energy of the ejected electrons.**

Each element has a characteristic binding energy ( $E_B$ ) associated with each core atomic orbital, such that each element will give rise to a characteristic set of peaks in the photoelectron spectrum at kinetic energies ( $E_K$ ) determined by the photon energy and the respective binding energies.<sup>186</sup>

XPS uses either monochromatic aluminium  $K\alpha$  ( $AlK\alpha$  (1486.6 eV), used in this work) or non-monochromatic magnesium  $K\alpha$  ( $MgK\alpha$  (1253.6 eV)) X-rays to eject a photoelectron from an atom at the sample's surface. An electron from a higher energy level then falls to fill the hole left behind and its emitted radiation energy is used to eject an Auger electron. Thus, XPS emits both photoelectrons and Auger electrons which can be seen in the spectrum (often wide peaks). The electron kinetic energies from those ejected are analysed by the XPS detector which provides the information required to determine the elements present in the sample.<sup>187,188</sup>

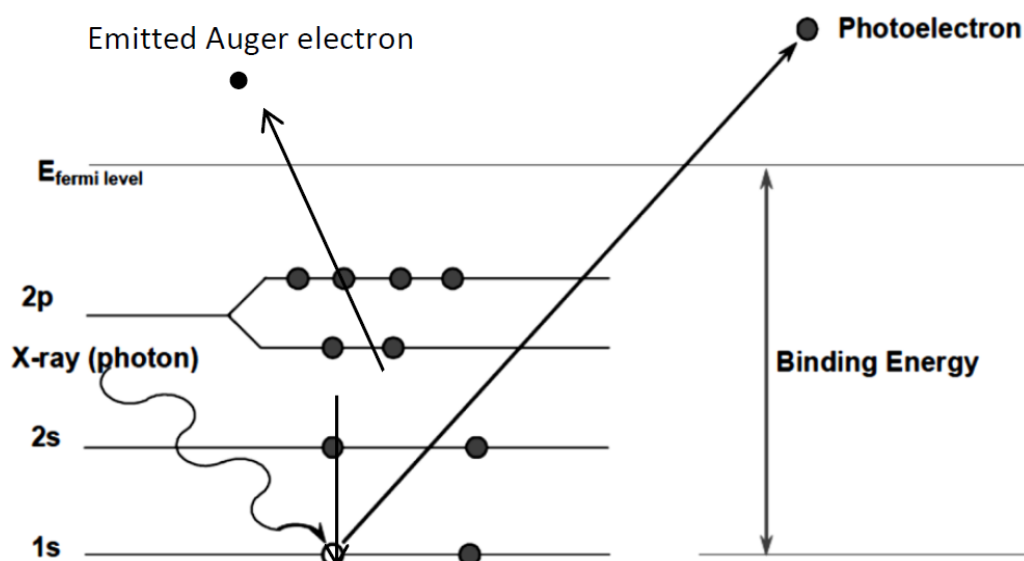
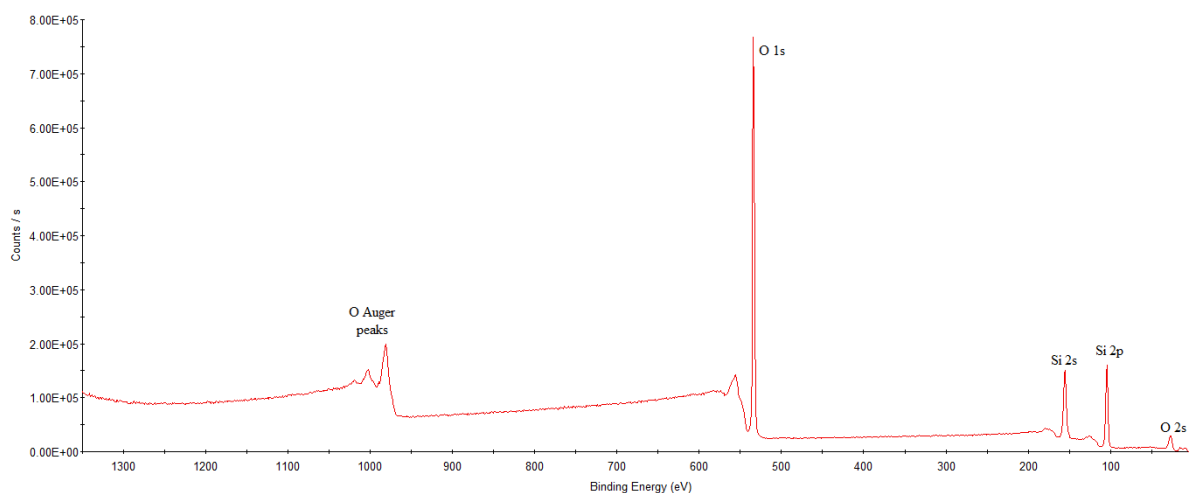


Figure 61 – Schematic representation of the X-ray photoelectron process.<sup>188</sup>

It was anticipated that XPS would deliver as an ideal instrument for aiding to show that the metal in solution (in this case copper) was present with the recovered functionalised silica. ICP-OES had already shown the copper had been removed from solution but this technique would be able to show where the metal had ended up. The fact that an obvious change in colour to the silica material was seen (see Figure 62) and there was no observed precipitation certainly provided good reason to believe this was the case, but reliable spectra to demonstrate this would be extremely valuable. Although this would not directly explain how the metal was bonded, it would help to explain the location of the metal using ratios of atoms measured.



Figure 62 – APTES-functionalised silica (left) and APTES-functionalised silica after being in a Cu(II) solution (right).

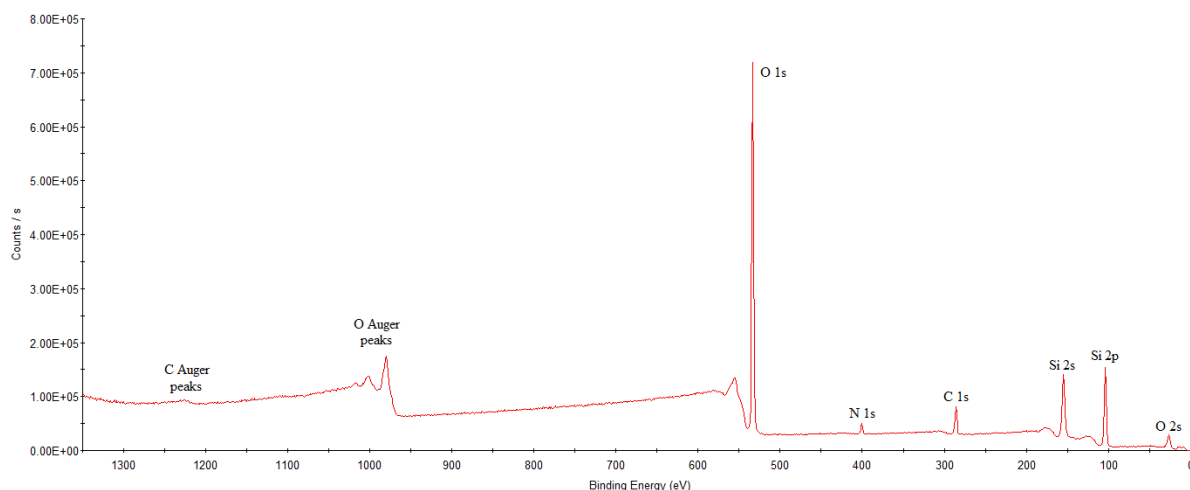


**Figure 63 – XPS spectrum of ZEOprep silica.**

Name	Peak BE	Atomic %
O1s	533.90	62.86
Si2p	104.40	37.14

**Table 21 – Peak  $E_B$  values and atomic percentages for selected peaks in ZEOprep silica (Figure 63).**

Figure 63 and Table 21 show the data obtained for the ZEOprep silica before any modification has taken place. The peaks in Figure 63 show the expected atoms to be present and suggest this technique to be appropriate for this work. Table 21 shows the atomic percentage of silicon and oxygen in the silica, the ratio is approximately 2:1. When the water content was measured *via* TGA, it was found that the formula of the silica was actually  $\text{SiO}_2 \cdot 0.31\text{H}_2\text{O}$ . Once water is accounted for (remembering that XPS does not measure hydrogen), a 2:1 ratio between oxygen and silicon is calculated with water present at 10.25 %. This equates to a formula of  $\text{SiO}_2 \cdot 0.38\text{H}_2\text{O}$ , strongly agreeing with the data found *via* TGA. Silicon Auger peaks appear at 1394 eV with the  $\text{AlK}\alpha$  X-rays and hence are not seen on these spectra.



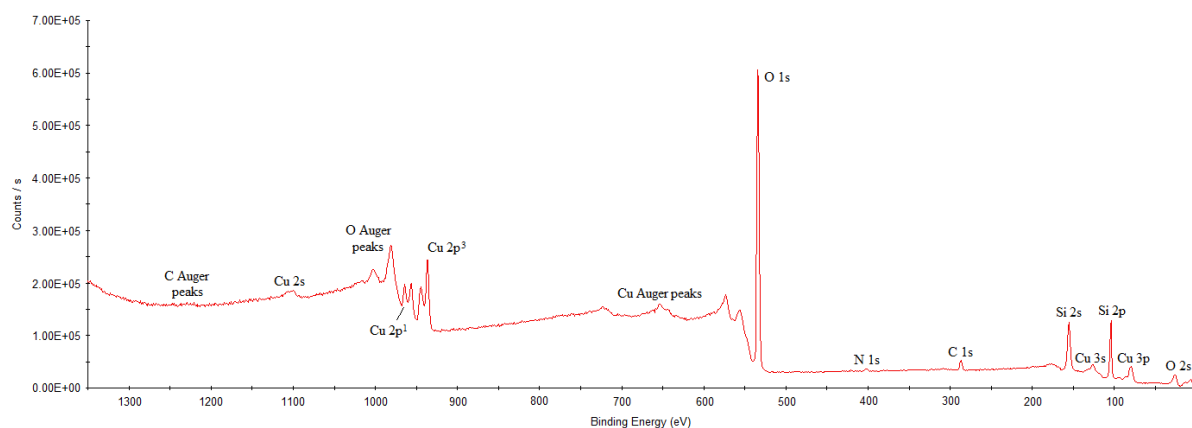
**Figure 64 – XPS spectrum of ZEOprep silica following APTES deposition. Carbon and nitrogen peaks are now visible due to the APTES group.**

Name	Peak BE	Atomic %
Si2p	103.98	33.23
O1s	533.15	52.94
C1s	286.02	11.23
N1s	400.28	2.60

**Table 22 – Peak  $E_B$  values and atomic percentages for selected peaks in ZEOprep silica following APTES deposition (Figure 64).**

The APTES-functionalised silica sees the appearance of the carbon and nitrogen peaks on the spectrum in Figure 64, much like the SSNMR discussed earlier. The atomic percentages shown in Table 22 appear to be sensible values considering the structure and the ratio between oxygen and silicon atoms is effectively the same as the non-functionalised silica results. However, the carbon percentage is significantly higher at 11.23 % compared to only 5.16 % when calculated *via* elemental analysis. Nitrogen was recorded to make up 1.64 % *via* elemental analysis but XPS shows an atomic percentage of 2.60. This is likely to be due to XPS being a ‘surface sensitive’ technique leading to more biased results. XPS is known to probe a depth of ca. 5-10 nm and as the surface becomes more functionalised with organics and metals, less of the silica may be ‘seen’ but there is no evidence to suggest this has occurred in this instance. The ratio of carbon to nitrogen would be expected to be ca. 3:1 and although the results show this to be a little higher, the results are very close to this.





**Figure 65 – XPS spectrum after APTES-functionalised silica had been in a 160 ppm Cu(II) solution for 1 week. The spectrum shows all expected peaks, suggesting the copper is bound to the functionalised silica surface.**

Name	Peak BE	Atomic %
Si2p	104.35	29.82
O1s	533.74	57.38
C1s	286.32	5.50
N1s	401.91	1.01
Cu2p <sup>3</sup>	936.45	6.29

**Table 23 – Peak E<sub>B</sub> values and atomic percentages for selected peaks after APTES-functionalised ZEOprep silica had been in a 160 ppm Cu(II) solution for 1 week (Figure 65).**

Finally, the third spectrum (Figure 65) shows the peaks previously observed and the strong indication of copper being present in the sample. Nitrogen Auger peaks are seen at 1100 eV with the AlK $\alpha$  and hence are likely to be hidden by the Cu2s peak. Table 23 shows the atomic percentage of those atoms present in Table 22 to decrease apart from oxygen which increases from 52.94 % to 57.38 %. Although carbon decreases, it falls from 11.23 % to 5.50 % which would appear quite anomalous when compared with the values of the other atoms and similarly the nitrogen value halves. The fact that the copper value is so high at 6.29 % and thus 6:1 ratio with nitrogen is a very surprising result which raises questions as to how exactly this is bonded to the surface.

There is an argument that if the copper is at the surface, XPS could be more sensitive and produce a ratio that is not strictly true. However, the results certainly show a higher amount of copper than nitrogen and it is certainly true that copper is not bound 1:1 with the nitrogen atoms of the APTES molecule.

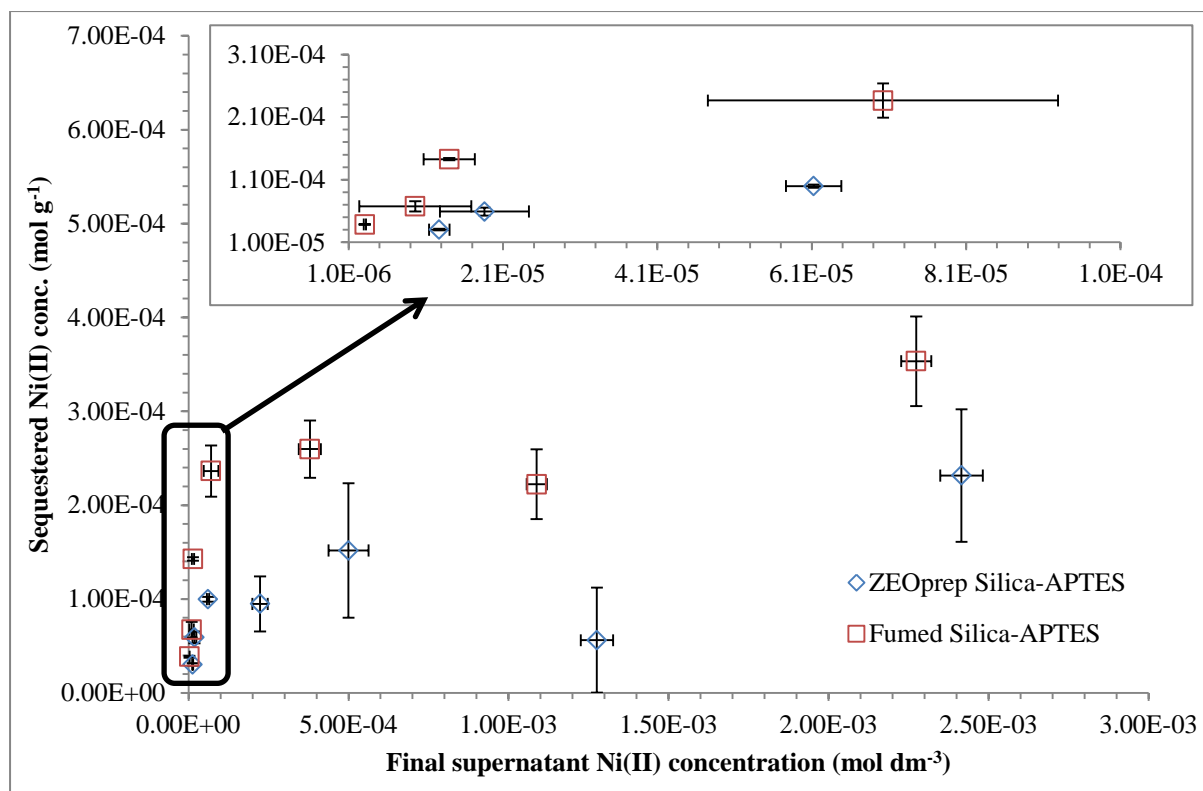
The addition of the APTES-functionalised silica to a solution of Cu(II) <20 ppm is found to increase the pH of the solution by ca. 3 to just above pH 9, however this is not the case for higher concentrations (>20 ppm). It is suggested that within the vicinity of the silica-APTES where a large presence of amine groups exists, precipitation of Cu<sub>2</sub>O or Cu(OH)<sub>2</sub> occurs<sup>189</sup> due to the local pH change<sup>184</sup> and therefore only occurs at the surface of the APTES. It would probably still be expected that the available nitrogen atoms would still be bound to Cu(II) ions with both processes taking place. To support this, the oxygen percentage would be expected to fall due to a new layer of copper atoms, however an increase in oxygen is observed and this supports the theory of Cu<sub>2</sub>O/Cu(OH)<sub>2</sub> precipitate being produced.

The one problem with this theory is the absence of increase in copper when the APTES-functionalised silica was added to a solution of deionised water to test for reversibility. The value was so low it fell below the LOD calculated for the ICP-MS in chapter 2. An explanation involving the binding with oxygen atoms within the silane molecule cannot be ruled out until further and more detailed investigations take place.

#### **6.2.3.2 Ni(II) studies with silica attached APTES**

The major use for nickel is in the preparation of alloys but is also used for batteries, catalysis, plating, coinage and other chemicals. Nickel is released into the air *via* power plants and incinerators and into surface waters as part of wastewater streams. Obviously it also occurs naturally in substances such as slate, sandstone, clay minerals and basalt.<sup>176</sup> The most important nickel sulphide mineral is pentlandite (Fe,Ni)<sub>9</sub>S<sub>8</sub> in economic deposits where it occurs with pyrrhotite, chalcopyrite and pyrite in mafic and ultramafic (iron- and magnesium-rich) igneous rocks.<sup>190</sup> Nickel is also recognised to be a dietary requirement for a number of organisms and the human body is known to contain ca. 10 mg.

Although nickel was not removed when in a solution with three other metals (cobalt, copper and zinc), initial tests when nickel was the only major ion in the system showed these materials are capable of removing it. The studies carried out in this section use <sup>63</sup>Ni as a tracer, enabling the change in concentration to be monitored by LSC as well as ICP-OES and to discover whether these materials can still function with this albeit small amount of radiation. The salt used to make these solutions was NiCl<sub>2</sub> and nickel is normally only stable in aqueous solution in the +2 oxidation state.<sup>191,192</sup>



**Figure 66 – Isotherm for Ni(II) removal from deionised water with APTES-functionalised ZEOprep and fumed silica materials over 24 h. Initial concentrations ranged from  $4.69 \times 10^{-5} - 2.67 \times 10^{-3} \text{ mol dm}^{-3}$  (2.75 – 157 ppm) whilst initial pHs ranged from 6.18 – 6.70.**

Figure 66 shows fumed silica to be a slightly more effective material. A dip in the trend appears at around  $1 \times 10^{-3} \text{ mol dm}^{-3}$  but if the error bars are taken into account, a line could be drawn to suggest the sequestered concentration is levelling out. The saturation point is clearly being reached as the final supernatant concentration increases and the sequestered concentration remains at a similar level. A range of concentrations were again used and these are made clear in Table 25 and Table 26.

Statistical measurements were carried out to investigate if outliers were to blame for the results observed. If proven to be outliers, the data points would not necessarily be removed, but used to suggest that the data maybe is not as accurate as one would hope. It could be explained by a bad batch of material being used that had not been functionalised as well as other batches. To do this Dixon's Q test was implemented which is generally accepted as the primary method for testing for the rejection of outlying values.<sup>193,194</sup>

The test is applied as follows. A range of data is ordered in ascending order:

$$X_1 < X_2 < X_3 < \dots < X_n$$

The statistical value is calculated as a ratio and defined as the difference between the suspect value and its nearest one divided by the range of the values. Thus for testing  $X_1$  or  $X_n$  in the above example of data, we use the following equations:

$$Q = \frac{X_2 - X_1}{X_n - X_1} \quad \text{or} \quad Q = \frac{X_n - X_{n-1}}{X_n - X_1}$$

**Equation 16 – Equations to show how Q is calculated from a range of data.**

The obtained value is compared to a critical Q-value found in Table 24. This value is then compared with the values that represent the number of repeats used to gain the data. If  $Q > Q_{\text{crit}}$  then the suspect value can be characterised as an outlier and hence rejected. If  $Q < Q_{\text{crit}}$  then the value must be retained. No data in this thesis was found to be an outlier.

No. of repeats	3	4	5	6	7	8	9	10
$Q_{90\%}$	0.941	0.765	0.642	0.560	0.507	0.468	0.437	0.412
$Q_{95\%}$	0.970	0.829	0.710	0.625	0.568	0.526	0.493	0.466
$Q_{99\%}$	0.994	0.926	0.821	0.740	0.680	0.634	0.598	0.568

**Table 24 – Critical values of Dixon's Q parameters at various levels confidence levels.<sup>193</sup> These are the standard parameters derived by R. B. Dean and W. J. Dixon.<sup>194</sup>**

Initial Conc.		ZEOprep silica-APTES			
		Final supernatant conc.		Sequestered conc.	
ppm	$\text{mol dm}^{-3}$	$\text{mol dm}^{-3}$		$\text{mol g}^{-1}$	
		mean	Std Dev	mean	Std Dev
157	$2.67 \times 10^{-3}$	$2.42 \times 10^{-3}$	$7.06 \times 10^{-5}$	$2.32 \times 10^{-4}$	$6.61 \times 10^{-5}$
79	$1.34 \times 10^{-3}$	$1.28 \times 10^{-3}$	$5.6 \times 10^{-5}$	$5.62 \times 10^{-5}$	$5.07 \times 10^{-5}$
39	$6.71 \times 10^{-4}$	$5 \times 10^{-4}$	$7.15 \times 10^{-5}$	$1.52 \times 10^{-4}$	$6.24 \times 10^{-5}$
20	$3.34 \times 10^{-4}$	$2.24 \times 10^{-4}$	$2.93 \times 10^{-5}$	$9.48 \times 10^{-5}$	$2.43 \times 10^{-5}$
10	$1.75 \times 10^{-4}$	$6.13 \times 10^{-5}$	$2.59 \times 10^{-6}$	$9.99 \times 10^{-5}$	$3.58 \times 10^{-6}$
5	$8.47 \times 10^{-5}$	$1.86 \times 10^{-5}$	$6.36 \times 10^{-6}$	$5.92 \times 10^{-5}$	$5.77 \times 10^{-6}$
2.75	$4.69 \times 10^{-5}$	$1.27 \times 10^{-5}$	$1.38 \times 10^{-6}$	$3.02 \times 10^{-5}$	$1.31 \times 10^{-6}$

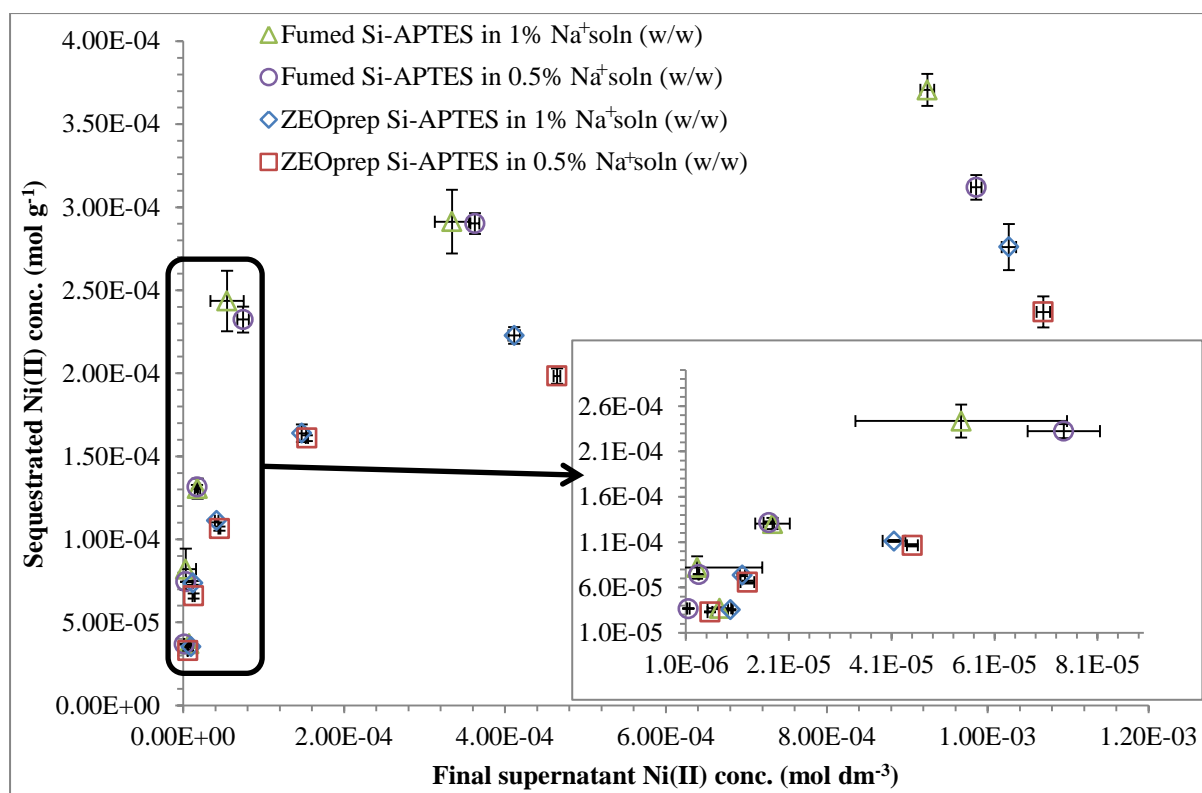
**Table 25 – Data values for Ni(II) removal from deionised water calculated for APTES-functionalised ZEOprep silica and used to plot isotherm in Figure 66. Initial concentrations ranged from  $4.69 \times 10^{-5}$  –  $2.67 \times 10^{-3} \text{ mol dm}^{-3}$  (2.75 – 157 ppm) whilst initial pHs ranged from 6.18 (20 ppm) – 7.55 (157 ppm) carried out at room temperature and silica material was present for 24 h.**

Initial Conc.		Fumed silica-APTES			
		Final supernatant conc.		Sequestered conc.	
ppm	mol dm <sup>-3</sup>	mol dm <sup>-3</sup>		mol g <sup>-1</sup>	
		mean	Std Dev	mean	Std Dev
157	2.67 x 10 <sup>-3</sup>	2.27 x 10 <sup>-3</sup>	4.77 x 10 <sup>-5</sup>	3.53 x 10 <sup>-4</sup>	4.7 x 10 <sup>-5</sup>
79	1.34 x 10 <sup>-3</sup>	1.09 x 10 <sup>-3</sup>	3.73 x 10 <sup>-5</sup>	2.22 x 10 <sup>-4</sup>	3.13 x 10 <sup>-5</sup>
39	6.71 x 10 <sup>-4</sup>	3.79 x 10 <sup>-4</sup>	3.06 x 10 <sup>-5</sup>	2.60 x 10 <sup>-4</sup>	3.44 x 10 <sup>-5</sup>
20	3.34 x 10 <sup>-4</sup>	7.02 x 10 <sup>-5</sup>	2.73 x 10 <sup>-5</sup>	2.36 x 10 <sup>-4</sup>	2.27 x 10 <sup>-5</sup>
10	1.75 x 10 <sup>-4</sup>	1.4 x 10 <sup>-5</sup>	1.84 x 10 <sup>-6</sup>	1.43 x 10 <sup>-4</sup>	3.32 x 10 <sup>-6</sup>
5	8.47 x 10 <sup>-5</sup>	9.62 x 10 <sup>-6</sup>	8.32 x 10 <sup>-6</sup>	6.75 x 10 <sup>-5</sup>	7.25 x 10 <sup>-6</sup>
2.75	4.69 x 10 <sup>-5</sup>	3.09 x 10 <sup>-6</sup>	8.79 x 10 <sup>-7</sup>	3.85 x 10 <sup>-5</sup>	1.46 x 10 <sup>-7</sup>

**Table 26 – Data values for Ni(II) removal from deionised water calculated for APTES-functionalised fumed silica and used to plot isotherm in Figure 66. Initial concentrations ranged from 4.69 x 10<sup>-5</sup> – 2.67 x 10<sup>-3</sup> mol dm<sup>-3</sup> (2.75 – 157 ppm) and initial pHs ranged from 6.18 (20 ppm) – 7.55 (157 ppm) carried out at room temperature and silica material was present for 24 h.**

In a ‘real world’ example where metal sequestration may be required, it would be highly unlikely to find a sample as clean and pure as that tested in Figure 66. A common natural source of water is seawater. The vast majority of seawater has a salinity of 3.1–3.8 %. Seawater is thought to contain 1.08 % sodium (10800 ppm) at 3.5 % salinity<sup>195</sup> and hence a synthetic solution was made of 0.5 and 1 % sodium to find the effect this had on the silica materials.

Figure 67 illustrates the findings when nickel solutions were made in the saline solutions as opposed to the deionised water solutions, thus testing the effect this ionic strength had on the materials.

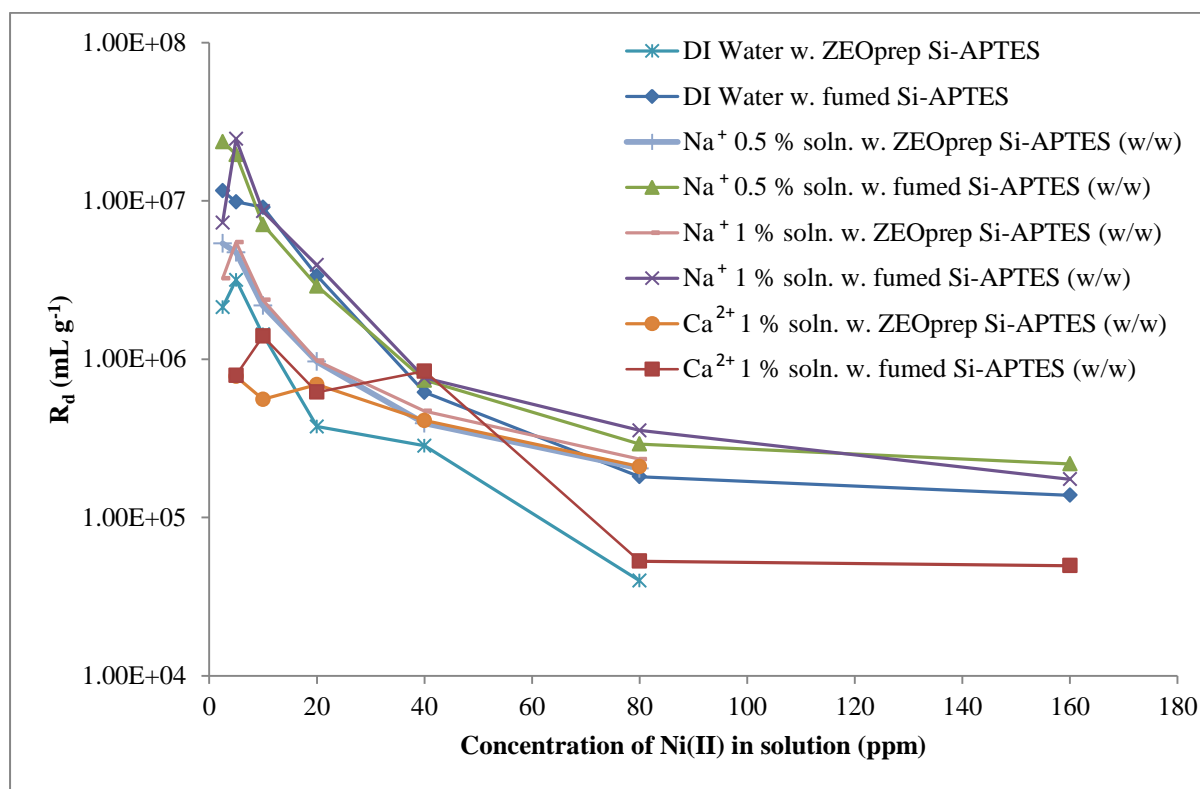


**Figure 67 – Ionic strength effect on the sequestration of Ni(II) with APTES-functionalised silicas with 0.5 % and 1 % sodium (w/w). Initial and final pH readings were slightly higher at ca. pH 6.5-7 where pH 7 was found for the lowest nickel concentration.**

This ionic strength effect does not appear to have significantly hindered the two materials ability at removing the nickel when compared to the results observed in deionised water in Figure 66. The 160 ppm solution was not carried out in this investigation, hence the graph is one point shorter but the trend is very clear. Only at higher starting concentrations can a difference between the 0.5 and 1 % solutions be seen between the silicas and the fumed silica was again found to perform marginally better. In both cases the silicas appear to achieve higher sequestered quantities in the 1 % sodium solution over the 0.5 % at the higher initial concentrations, although not by a great amount. The pH was found to be ca. 0.3 units higher on average.

$R_d$  values for these experiments and including a calcium solution that was also tested are given in Figure 68. All the investigations follow a similar pattern where the lower concentrations provide the  $R_d$  values followed by an eventual dip by 80 ppm before effectively levelling out. The calcium rich solutions appear to have the largest effect on nickel sequestration because the  $R_d$  values at the lower concentrations are the lowest observed between the four solutions. The fact that calcium exists as a dication unlike sodium

which is monocationic would seem to give the best explanation for this. With nickel also being divalent it is expected that calcium would offer a much more testing environment if the APTES ligand already has a preference for divalent ions. The size of the ionic radii would also be a factor with Ni(II) at 83 pm whilst Na<sup>+</sup> and Ca<sup>2+</sup> are reported to be 116 and 99 pm respectively.<sup>196</sup>



**Figure 68 – Effect of initial concentration of Ni(II), ionic strength and competing ions on  $R_d$  with APTES-functionalised ZEOprep and fumed silica. Overall, the Ca<sup>2+</sup> solution appears to have the largest impact on  $R_d$  at the lower concentrations whilst all values dip and level out at the higher concentrations leaving values in the range of  $1 \times 10^5$  and  $1 \times 10^6$  at 80–160 ppm.**

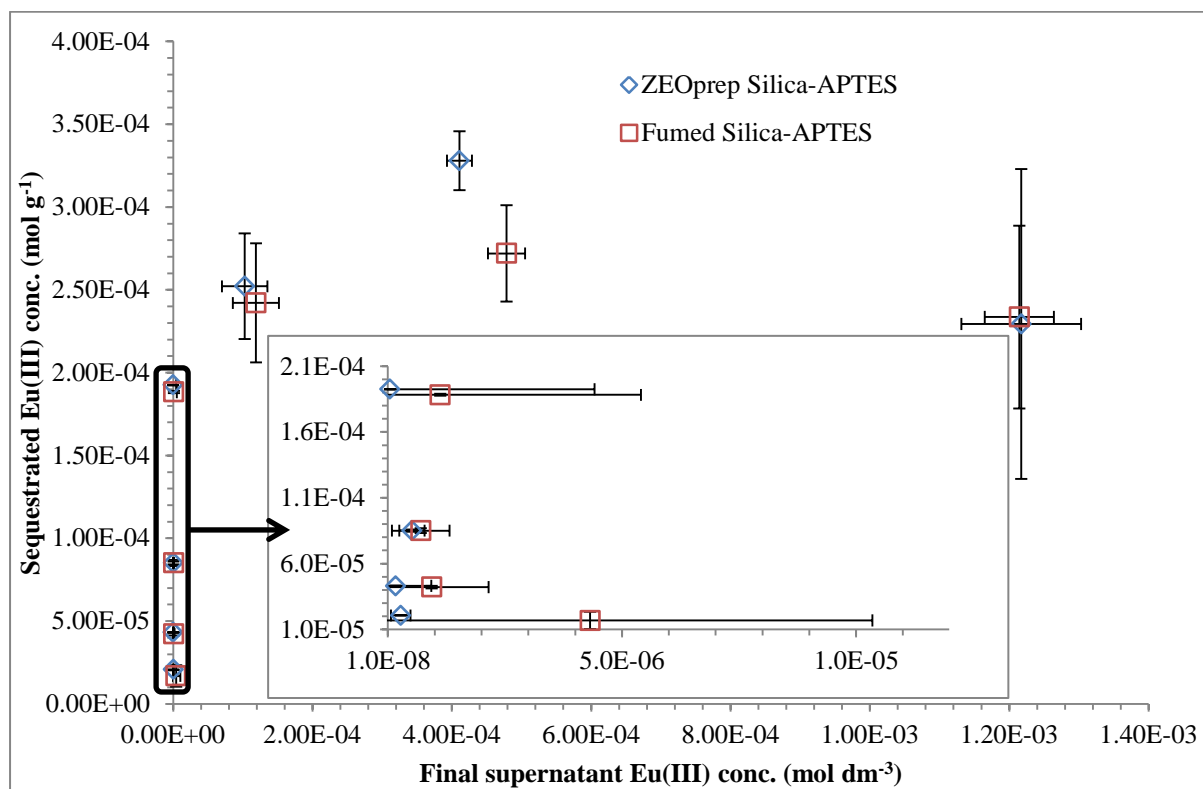
The trend across all solutions is evident that the  $R_d$  increases with decreasing concentration. The effect of sodium and calcium ions in general produces no significant effect on  $R_d$  compared to deionised water. At most there is a difference of approximately one order of magnitude which is clearer at 80 and 160 ppm.

### 6.2.3.3 Eu(III) studies with silica attached APTES

Europium is a member of the lanthanide series and usually assumes the oxidation state +3: providing one of the main reasons for investigating this metal.<sup>192</sup> It is renowned for being a particularly difficult isotope to clean up, especially from glassware if in solution. It is one of the less abundant rare-earth metals and is never found in nature as a free element.<sup>176</sup>

However it is a neutron absorber and so it is used in nuclear reactor control rods.<sup>197</sup> It has no known biological role but its salts are thought to be toxic although this has not been fully investigated.

The investigations were carried out using the isotope <sup>152</sup>Eu as a tracer, enabling gamma counting to be used to monitor the investigations whilst the europium salt used was EuCl<sub>3</sub>·6H<sub>2</sub>O.



**Figure 69 - Isotherm for Eu(III) removal from deionised water with APTES-functionalised ZEOprep and fumed silica over 24 h. Initial concentrations ranged from  $2.32 \times 10^{-5}$  –  $1.47 \times 10^{-3}$  mol dm<sup>-3</sup> (3.52 – 224.06 ppm) whilst initial pHs ranged from 5.33 – 6.43.**

Figure 69 shows a very comparable set of data and sequestering the Eu(III) to a similar level observed with Ni(II) and Cu(II), certainly in the same order of magnitude for a set concentration of metal.

This shows the APTES ligand to be quite adaptable to these metals and is unaffected by the low level radioactivity from the tracer isotope used. pH tests again showed that all the concentrations started at ca. pH 6.5 before the addition of the functionalised silica and showed no change for the higher initial concentration of 58, 119 and 224 ppm. The initial concentration of 33 ppm solution showed an increase to pH 8-9 once the silica had been



present for 24 h. Once the initial concentration was dropped below this, the pH was found to rise to ca. 9.3. With a lower concentration of metal ions being available in the solution for the nitrogen atoms to coordinate to and gamma counts reduced to background levels suggests the silica-APTES material had removed a very high percentage, if not all the Eu(III). This being the case, lone pairs on the nitrogen atoms would still be available for coordination. The protons dissociated in the solution become bound to the nitrogen instead, increasing the concentration of  $\text{OH}^-$  and therefore increasing the pH at these lower concentrations.

Initial concentration of europium		ZEOprep Si-APTES	Fumed Si-APTES
ppm	$\text{mol dm}^{-3}$	$R_d (\text{mL g}^{-1})$	$R_d (\text{mL g}^{-1})$
224.06	$1.47 \times 10^{-3}$	$1.72 \times 10^5$	$1.74 \times 10^5$
118.84	$7.82 \times 10^{-4}$	$7.08 \times 10^5$	$5.13 \times 10^5$
58.45	$3.85 \times 10^{-4}$	$2.44 \times 10^6$	$2.01 \times 10^6$
32.56	$2.14 \times 10^{-4}$		$1.91 \times 10^8$
14.69	$9.66 \times 10^{-5}$		$3.40 \times 10^7$
7.43	$4.89 \times 10^{-5}$		$8.62 \times 10^7$
3.52	$2.32 \times 10^{-5}$	$9.63 \times 10^7$	$2.21 \times 10^7$

**Table 27 – Variation of  $R_d$  at different initial concentrations of Eu(III) from deionised water. A rise of ca. two orders of magnitude was observed as initial concentration decreased. Initial pHs were recorded to range from 5.33 (58.45 ppm) – 6.43 (224.06 ppm). Blank entries in the table show where no repeatable or reliable values could be recorded.**

Initial concentration of europium		ZEOprep Si-APTES	Fumed Si-APTES
ppm	$\text{mol dm}^{-3}$	$R_d (\text{mL g}^{-1})$	$R_d (\text{mL g}^{-1})$
218.73	$1.44 \times 10^{-3}$	$3.46 \times 10^5$	$1.73 \times 10^5$
122.28	$8.05 \times 10^{-4}$	$8.96 \times 10^5$	$5.13 \times 10^5$
56.75	$3.73 \times 10^{-4}$	$2.73 \times 10^6$	$1.53 \times 10^6$
25.06	$1.65 \times 10^{-4}$		
12.20	$8.03 \times 10^{-5}$		$4.98 \times 10^7$
7.75	$5.10 \times 10^{-5}$		
3.79	$2.49 \times 10^{-5}$		$6.39 \times 10^7$

**Table 28 – Variation of  $R_d$  at different initial concentrations of Eu(III) from a 1 %  $\text{Na}^+$  solution. A rise of ca. two orders of magnitude was observed for APTES-functionalised fumed silica as initial concentration decreased but reliable values could not be recorded for the APTES-functionalised ZEOprep silica from 25 ppm and below. Initial pHs were recorded to range from 5.86 (7.75 ppm) – 7.44 (218.73 ppm). Blank entries in the table show where no repeatable or reliable values could be recorded.**

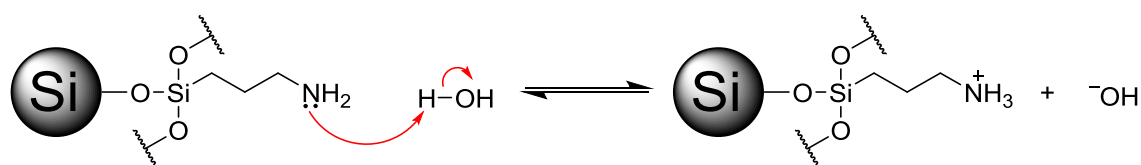
Initial concentration of europium		ZEOprep Si-APTES	Fumed Si-APTES
ppm	mol dm <sup>-3</sup>	R <sub>d</sub> (mL g <sup>-1</sup> )	R <sub>d</sub> (mL g <sup>-1</sup> )
214.77	1.41 x 10 <sup>-3</sup>	4.78 x 10 <sup>5</sup>	2.41 x 10 <sup>5</sup>
93.57	6.16 x 10 <sup>-4</sup>	8.33 x 10 <sup>5</sup>	3.17 x 10 <sup>5</sup>
51.23	3.37 x 10 <sup>-4</sup>	3.09 x 10 <sup>6</sup>	1.34 x 10 <sup>6</sup>
23.16	1.52 x 10 <sup>-4</sup>		2.06 x 10 <sup>7</sup>
11.45	7.53 x 10 <sup>-5</sup>	2.17 x 10 <sup>9</sup>	1.32 x 10 <sup>7</sup>
5.32	3.50 x 10 <sup>-5</sup>		9.93 x 10 <sup>7</sup>
2.91	1.91 x 10 <sup>-5</sup>	1.08 x 10 <sup>7</sup>	

**Table 29 – Variation of R<sub>d</sub> at different initial concentrations of Eu(III) from a 1 % Ca<sup>2+</sup> solution. A rise of ca. two orders of magnitude was observed for APTES-functionalised fumed silica as initial concentration decreased. Reliable results again proved difficult for the APTES-functionalised ZEOprep silica but the value for 2.91 ppm and 214.77 ppm suggests a similar trend to that seen by APTES-functionalised fumed silica. Initial pHs were recorded to range from 6.08 (2.91 ppm) – 7.06 (214.77 ppm). Blank entries in the table show where no repeatable or reliable values could be recorded.**

Similar R<sub>d</sub> values have been recorded for the removal of Eu(III) across the three solutions suggesting sodium and calcium ions have little effect in reducing the ability of the APTES ligand to selectively bind to the europium. The difference between effective ionic radii of Eu(III) (131 pm)<sup>196</sup> and Na<sup>+</sup> or Ca<sup>2+</sup> ions would again be expected to be a key factor for this, but also the valency of these ions may also contribute towards these findings.

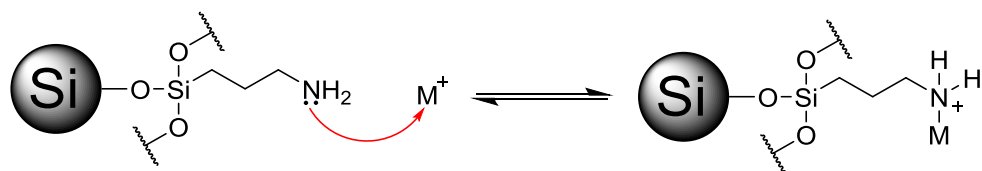
#### 6.2.3.3.1 pH studies of Eu(III) ion attachment to both silica-APTES materials

The solutions naturally started at a pH of 6.5-7. After the silica material had been in the solution, the pH was found to be around pH 8-9 for the lower concentrated solutions (2.5 ppm – 20 ppm) whilst it remained around pH 6.5-7 for the higher concentrations (40 ppm – 160 ppm). Very similar results were observed when the sodium and calcium solutions were investigated. This is best explained using the schemes below.



**Scheme 51 – Mechanism to show how the pH increases at low concentration of metal ions.**

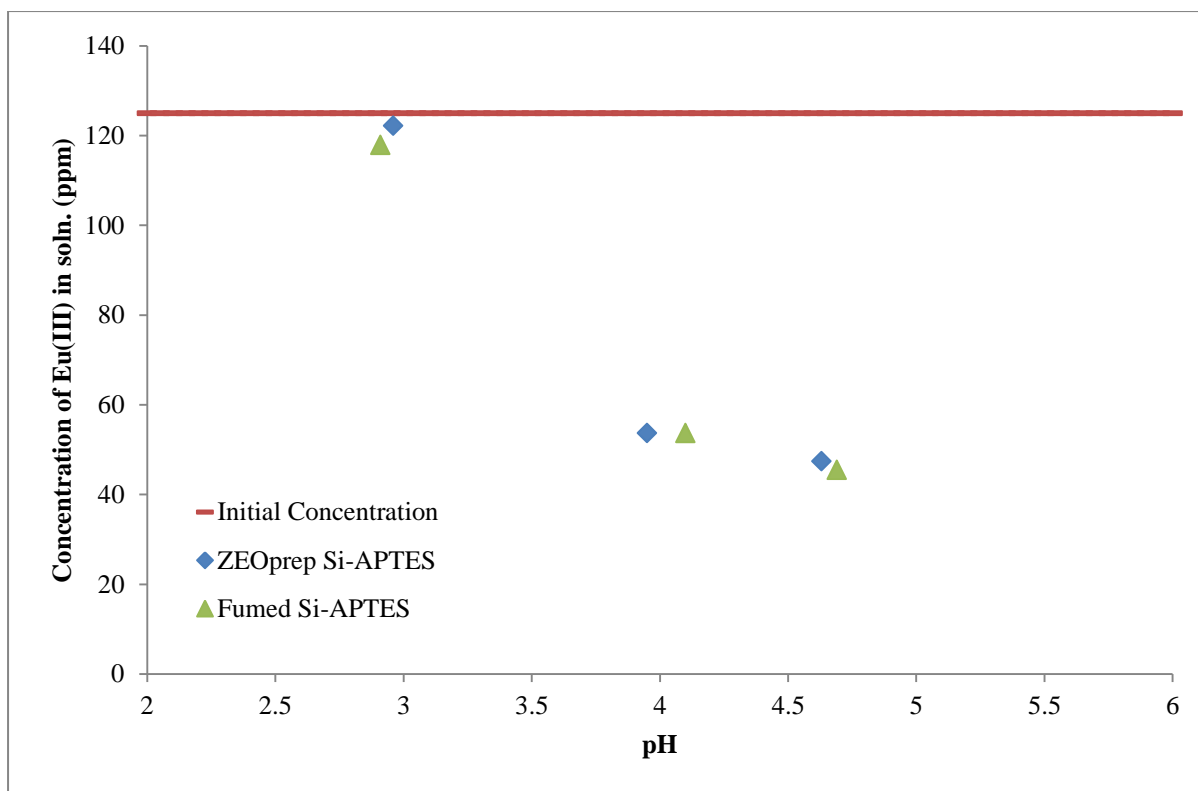
Scheme 51 illustrates that when the concentration of metal is low, the amine group is more likely to protonate and hence a higher ratio of free hydroxide is formed – leading to an increase in pH.



**Scheme 52 – Mechanism to show how the pH remains similar at high concentration of metal ions.**

Scheme 52 illustrates that a higher concentration of metal reduces the probability of amine protonation and thus, a less significant change in pH is observed.

Figure 70 shows the behaviour change and the ability of the APTES-functionalised silica to sequester the Eu(III) ions from the solution as the pH is acidified. pH 4-4.5 was found to be the optimum for largest removal of Eu(III) in terms of concentration change although alkaline pHs were not tested. Below pH 4, the metal concentration appears to rise again, suggesting the concentration of  $H^+$  has a significant effect on the ability of APTES to bind to the metal. Repeats of this experiment were carried out on different initial concentrations and all showed similar results.



**Figure 70 – Effect of pH on aqueous concentration of Eu(III) with both ZEOprep and fumed Si-APTES.**

The  $pK_a$  of APTES has been reported to be as high as 6.6<sup>198</sup> but also as low as 3.9<sup>199</sup>. If the  $pK_a$  value is taken to be 3.9, this fits the data observed in Figure 70 because in stronger acid, the amine would be protonated as  $NH_3^+$  and is unlikely to act as a ligand as no free electrons would be available to donate. At higher pHs though, the amine takes the form of  $NH_2$  so it can act as a ligand and this would explain the sudden ‘jump’ observed in Figure 70. The results shown here also agree with the nitrogen containing polymers that were introduced on page 14 and the results illustrated in Figure 10 where the optimum conditions were found to be pH 4. Whilst it is possible (with sufficient affinity) for metal ions to bind to protonated amines at low pH, the scenario reported in Figure 70 illustrates no sequestration was observed below pH 2.5. Thus, this effect does not appear to happen to a measurable effect.

#### **6.2.3.3.2 TEM studies of Eu(III) ion attachment to fumed silica-APTES**

Transmission Electron Microscopy (TEM) is a unique material characterisation technique that enables essentially simultaneous examination of microstructural features through high-resolution imaging and the acquisition of chemical and crystallographic information from submicrometer regions of the sample. It has become a well-established research instrument for the microstructural analysis of metallic, ceramic, and organic materials. Electrons (the source of illumination) are transmitted through the sample (thin enough to be considered

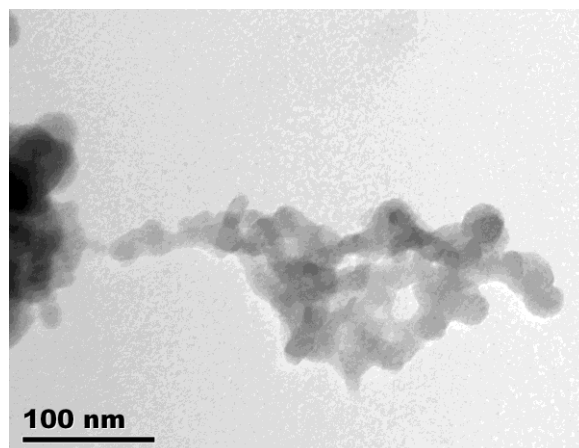
‘electron transparent’) to generate some form of contrast that enables observation of the internal structure of the sample. Very high resolution images display the samples structural detail in the order of fractions of nanometer, allowing examination of the structure on a microscopic scale.<sup>187</sup>

To attain an understanding of how and where the europium is located across the material’s surface, Energy Dispersive X-ray Spectroscopy (EDS) was used - an analytical technique used for the elemental analysis of a sample.<sup>200</sup> This would help to identify if the surface area was being used effectively and could assist in explaining whether precipitation was occurring or Eu(III) was bonded to the surface. Using a Scanning Transmission Electron Microscope (STEM), a hybrid of SEM and TEM (developed by Albert Crewe<sup>201</sup> at the University of Chicago in 1968), this has been achieved.

By scanning a focussed electron beam that passes through a thin sample with little spreading, the STEM has excellent local chemical analysis capabilities and good spatial resolution to produce images of atoms.<sup>202</sup> Coupled with STEM, a High Angle Annular Dark Field (HAADF) detector (also known as Z-contrast imaging<sup>203</sup>) was used, providing image contrast that is sensitive to the local chemical composition and hence europium was chosen as the metal to analyse. The atomic mass of europium is so much more than any of the elements present that one can be confident this element has not been mistaken with another during this mapping process.

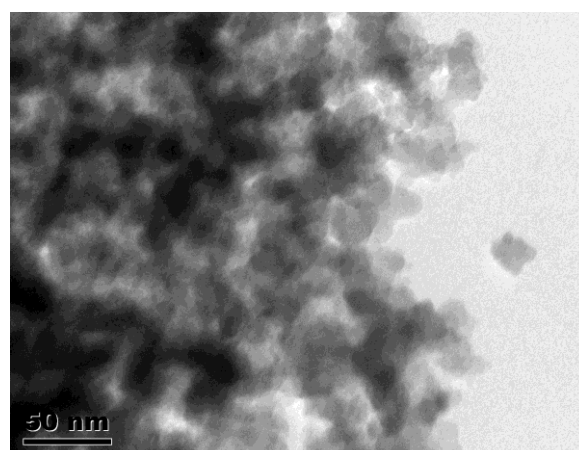
TEM images were collected using a JEOL 2000FX whilst the mapping shown in Figure 74 was carried out on a Phillips/FEI Tecnai F20.

Figure 71 is an image of the fumed silica material. The material was found to be largely agglomerated and this is thought to reduce the surface area that would be available for APTES attachment and hence, reducing the potential capacity for metal-ligand binding. This would also explain why techniques used in chapter 5 found a similar quantity of APTES bound to the ZEOprep and fumed silica.



**Figure 71 – TEM image of fumed silica. The images collected for fumed silica showed a clear indication that the material was largely agglomerated. This could significantly reduce the surface area expected to be available for APTES attachment.**

Figure 72 is an image of what was observed of the fumed silica following APTES deposition. The darker areas show a greater agglomeration of the APTES-functionalised silica compared to Figure 71.

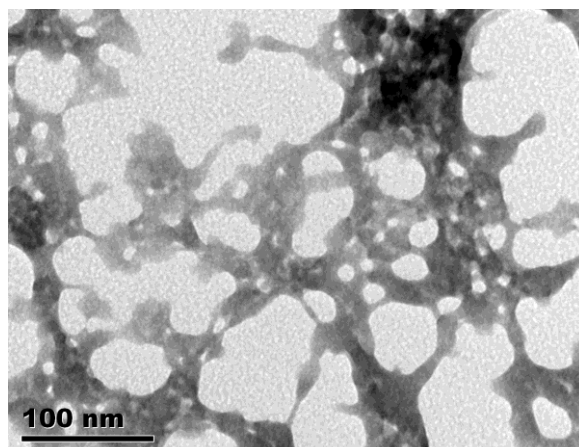


**Figure 72 – TEM image of APTES-functionalised fumed silica. Agglomeration of the particles is once again present and darker images were more common, suggesting dense layers of material.**

Each APTES has 3 binding sites which could act as ‘glue’, bringing together 3 individual particles. APTES deposition also considerably changes the surface charge. Silica in water is quite stable because all particles are negatively charged so all particles are forced apart but when functionalised with APTES, some of the particles will become neutralised which in turn would increase agglomeration.

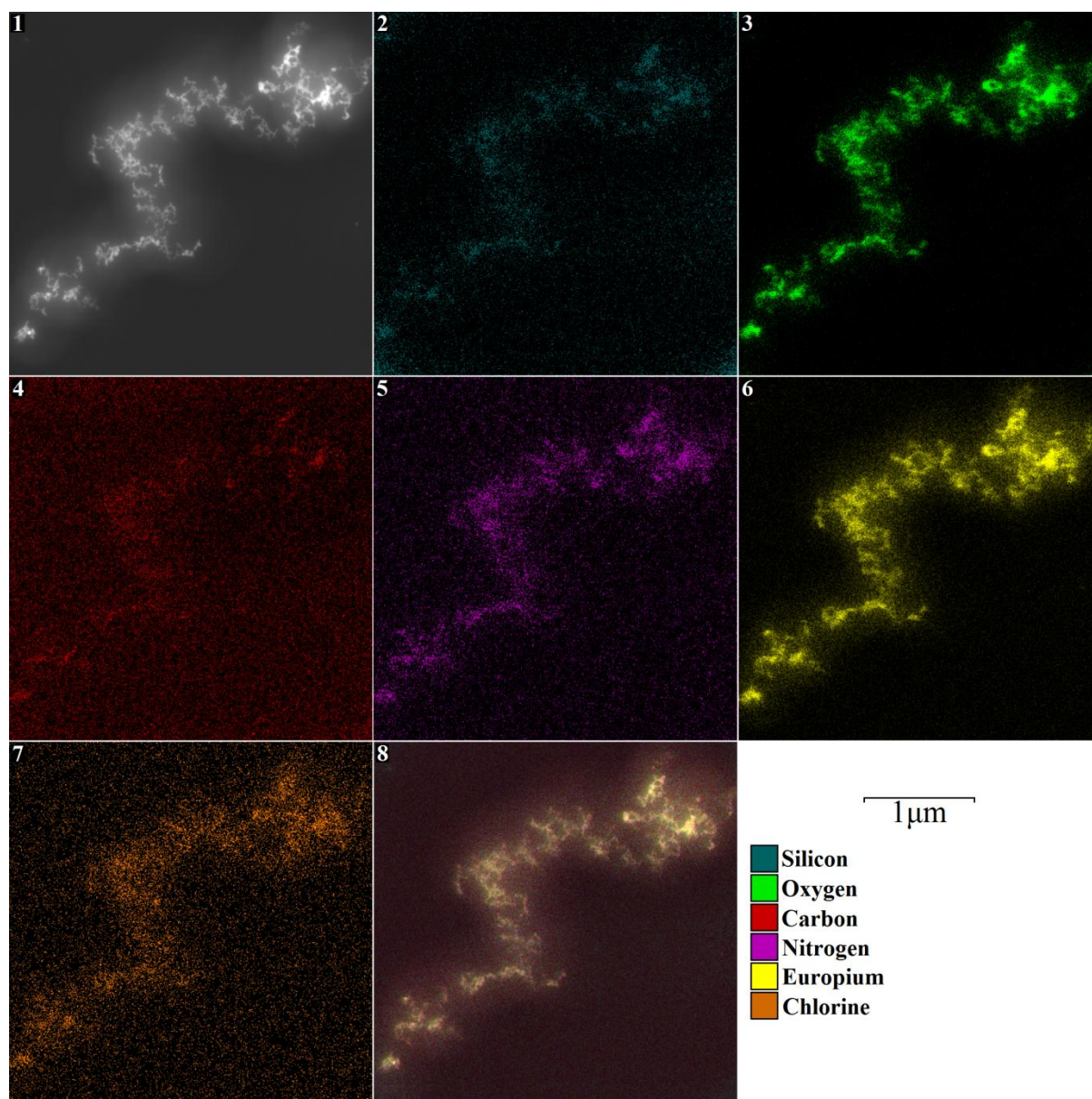
Figure 73 demonstrates a very different morphology of the material to what was observed in the previous images. This image displays the APTES-functionalised fumed silica following a

week in a solution of Eu(III) chloride hexahydrate at 160 ppm. Being in the solution appears to have considerably changed the appearance of the material to produce a more ‘stringy’ structure.



**Figure 73 – TEM image of APTES-functionalised fumed silica after being in a solution of Eu(III) for one week. The morphology of the material has completely changed to that seen in Figure 71 and Figure 72.**

A full explanation of this change has not yet been agreed but if the metal is precipitating, this is much heavier than Si and because of the way TEM works, primarily it would detect Eu(III) (due to the heavier mass). In Figure 73 it seems that silica particles are no longer observed if based on appearance alone which could suggest precipitation has occurred. Alternatively Eu(III) ions could be bound to the nitrogen atoms and the physical appearance changes due to the fact Eu(III) ions are much denser relative to the other elements present in the material. Thus producing an image that has hidden the main structure and only Eu(III) is observed.



**Figure 74 – TEM imaging and EDS mapping of fumed Si-APTES after being in a solution of Eu(III) for one week. 1)**

**TEM image of silica, 2) EDS mapping illustrating where silicon atoms are present, 3) EDS mapping illustrating where oxygen atoms are present, 4) EDS mapping illustrating where carbon atoms are present, 5) EDS mapping illustrating where nitrogen atoms are present, 6) EDS mapping illustrating where europium atoms are present, 7) EDS mapping illustrating where chlorine atoms are present and 8) EDS mapping overlay of all the atoms present.**

Figure 74 shows a compilation of images taken of APTES-functionalised fumed silica after being added to a 160 ppm solution of europium (prepared from europium(III) chloride hexahydrate) using EDS. The salt used for this solution is of importance as this explains the findings of the chlorine atoms in this mapping experiment. Europium was used because this is one of the heaviest metals in the periodic table that is straightforward to handle in its non-active form. Being so much heavier than the other atoms being studied enables a very clear image to be created of where the metal is present. The atomic weight from carbon to chlorine



ranges from just 12.01-35.45 u whereas europium is over four times heavier than chlorine at 151.97 u.

TEM imaging has been used by number of groups including Yantasse *et al.*<sup>126</sup> and White *et al.*<sup>204</sup> but these have been to study the particle size and evidence of large aggregate formation following modification of their solid supports with the ligands and polymers used. Elemental mapping like that shown in Figure 74 has not been reported previously to show successful sequestration of metal although amine bonding to europium is known.<sup>205,206,207</sup>

This imaging has shown that the surface area of the material is well utilised in terms of both modification and metal sequestration. The fact that the whole surface appears to be covered in europium is extremely positive and shows the material is being used to good effect.

It is predicted that  $\text{Eu}(\text{OH})_3$  will precipitate at ca. pH 10<sup>189</sup> whilst Pitois *et al.*<sup>208</sup> demonstrated precipitation to occur at ca. pH 10.5. This is slightly higher than pHs observed at lower concentrations of Eu(III) solutions (the highest observed was pH 9.46) in this thesis, leading to the hypothesis that perhaps most metal was bound to the materials rather than precipitation at the surface due to the local pH effect.

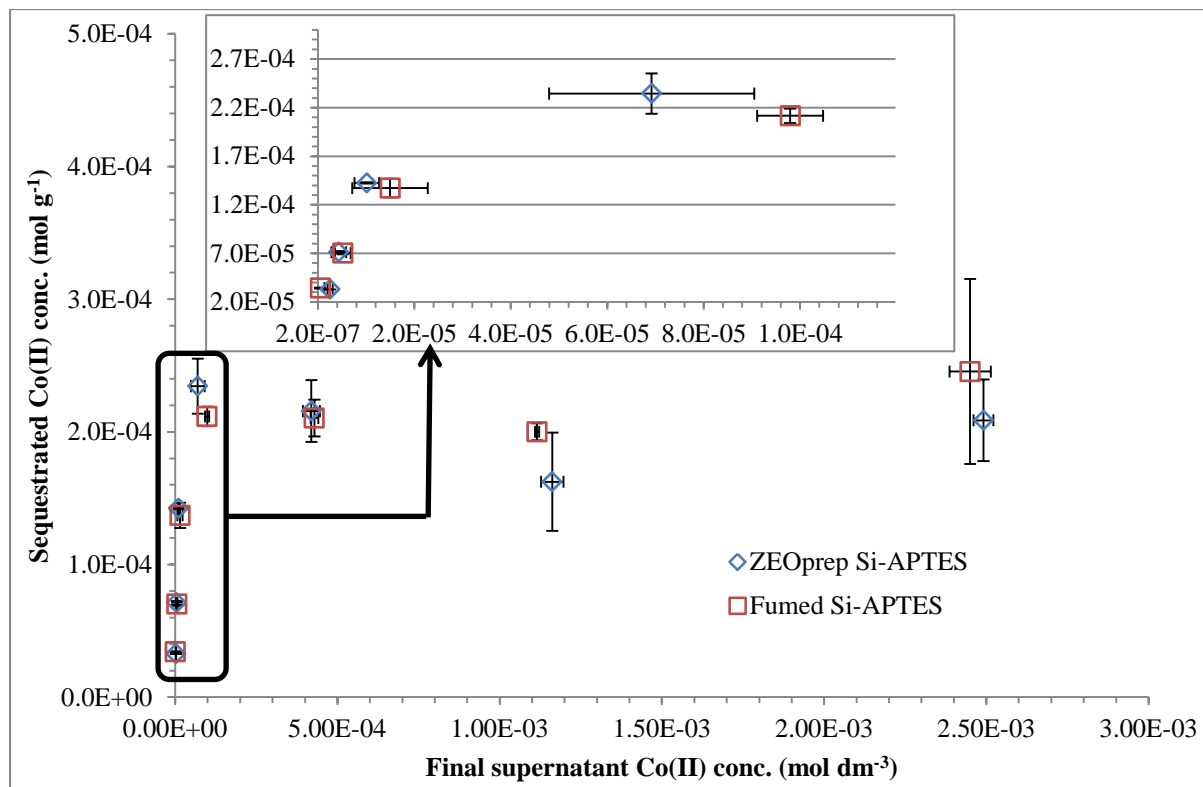
#### **6.2.3.4 Co(II) studies with silica attached APTES**

Cobalt is an essential element for humans since it is part of vitamin B12. It has been used for centuries to produce brilliant blue colours in porcelain, glass, potter and enamels and the radioisotope <sup>60</sup>Co is also used in the treatment of cancer.<sup>197</sup> However, again, exposure to larger quantities of cobalt can cause health problems including dermatitis, weight loss and respiratory hypersensitivity. The International Agency for Research on Cancer (IARC) lists cobalt and cobalt compounds among those that are possibly carcinogenic to humans.<sup>176</sup>

Humans add cobalt to the environment *via* coal combustion, mining and the production and use of cobalt chemicals. Radioisotopes do not naturally occur but are released through nuclear power plant operations.<sup>176</sup>

After the initial tests carried out with silica attached APTES, it is known that this ligand is capable of sequestering cobalt from solution (Figure 53). The following investigations were carried out using the isotope <sup>57</sup>Co as a tracer, enabling gamma counting to be used to monitor the investigations and again, the effect of sequestration when high levels of sodium and calcium are present were carried out. Co(II) and Co(III) are both very common oxidation states of cobalt<sup>192</sup>, however the pink coloured solution that was observed when solutions were

prepared with  $\text{CoCl}_2 \cdot 6\text{H}_2\text{O}$  suggests the most common oxidation state of cobalt present was that of  $\text{Co(II)}$ .



**Figure 75 – Isotherm for  $\text{Co(II)}$  removal from deionised water with APTES-functionalised ZEOprep and fumed silica materials over 24 h. Initial concentrations ranged from  $3.95 \times 10^{-5}$  –  $2.73 \times 10^{-3} \text{ mol dm}^{-3}$  (2.33 – 160.60 ppm) whilst initial pHs ranged from 5.50 – 5.21.**

Initial concentration of cobalt		ZEOprep Si-APTES	Fumed Si-APTES
ppm	$\text{mol dm}^{-3}$	$R_d (\text{mL g}^{-1})$	$R_d (\text{mL g}^{-1})$
160.60	$2.73 \times 10^{-3}$	$7.49 \times 10^4$	$8.99 \times 10^4$
79.07	$1.34 \times 10^{-3}$	$1.27 \times 10^5$	$1.58 \times 10^5$
38.97	$6.61 \times 10^{-4}$	$4.62 \times 10^5$	$4.46 \times 10^5$
19.66	$3.34 \times 10^{-4}$	$3.22 \times 10^6$	$1.95 \times 10^6$
10.08	$1.71 \times 10^{-4}$	$1.22 \times 10^7$	$1.02 \times 10^7$
4.93	$8.36 \times 10^{-5}$	$1.49 \times 10^7$	$1.21 \times 10^7$
2.33	$3.95 \times 10^{-5}$	$1.07 \times 10^7$	$8.10 \times 10^7$

**Table 30 – Variation of  $R_d$  at different initial concentrations of  $\text{Co(II)}$  from deionised water. A rise of ca. three orders of magnitude was observed as initial concentrations decreased. Initial pHs were recorded to range from 5.50 (2.33 ppm) and 5.21 (160.60 ppm).**

Initial concentration of cobalt		ZEOprep Si-APTES	Fumed Si-APTES
ppm	mol dm <sup>-3</sup>	R <sub>d</sub> (mL g <sup>-1</sup> )	R <sub>d</sub> (mL g <sup>-1</sup> )
164.24	2.79 x 10 <sup>-3</sup>	1.64 x 10 <sup>5</sup>	1.19 x 10 <sup>5</sup>
80.49	1.37 x 10 <sup>-3</sup>	2.89 x 10 <sup>5</sup>	2.42 x 10 <sup>5</sup>
37.97	6.44 x 10 <sup>-4</sup>	4.74 x 10 <sup>5</sup>	3.77 x 10 <sup>5</sup>
20.03	3.40 x 10 <sup>-4</sup>	1.31 x 10 <sup>6</sup>	9.97 x 10 <sup>5</sup>
10.41	1.77 x 10 <sup>-4</sup>	2.26 x 10 <sup>6</sup>	1.50 x 10 <sup>6</sup>
5.17	8.77 x 10 <sup>-5</sup>	2.27 x 10 <sup>6</sup>	1.29 x 10 <sup>6</sup>
2.48	4.20 x 10 <sup>-5</sup>	1.37 x 10 <sup>6</sup>	5.09 x 10 <sup>5</sup>

**Table 31 – Variation of R<sub>d</sub> at different initial concentrations of Co(II) from a 1 % Na<sup>+</sup> solution. A rise of ca. one order of magnitude was observed as initial concentrations decreased. Initial pHs were recorded to range from 5.51 (2.48 ppm) and 6.35 (164.23 ppm).**

Initial concentration of cobalt		ZEOprep Si-APTES	Fumed Si-APTES
ppm	mol dm <sup>-3</sup>	R <sub>d</sub> (mL g <sup>-1</sup> )	R <sub>d</sub> (mL g <sup>-1</sup> )
162.41	2.76 x 10 <sup>-3</sup>	1.21 x 10 <sup>5</sup>	2.33 x 10 <sup>5</sup>
78.11	1.33 x 10 <sup>-3</sup>	2.28 x 10 <sup>5</sup>	4.15 x 10 <sup>5</sup>
40.09	6.80 x 10 <sup>-4</sup>	3.83 x 10 <sup>5</sup>	1.09 x 10 <sup>6</sup>
20.39	3.46 x 10 <sup>-4</sup>	4.51 x 10 <sup>5</sup>	2.03 x 10 <sup>6</sup>
10.78	1.83 x 10 <sup>-4</sup>	5.30 x 10 <sup>5</sup>	3.44 x 10 <sup>6</sup>
4.88	8.27 x 10 <sup>-5</sup>	4.13 x 10 <sup>5</sup>	1.12 x 10 <sup>6</sup>
2.54	4.32 x 10 <sup>-5</sup>	4.76 x 10 <sup>5</sup>	1.11 x 10 <sup>6</sup>

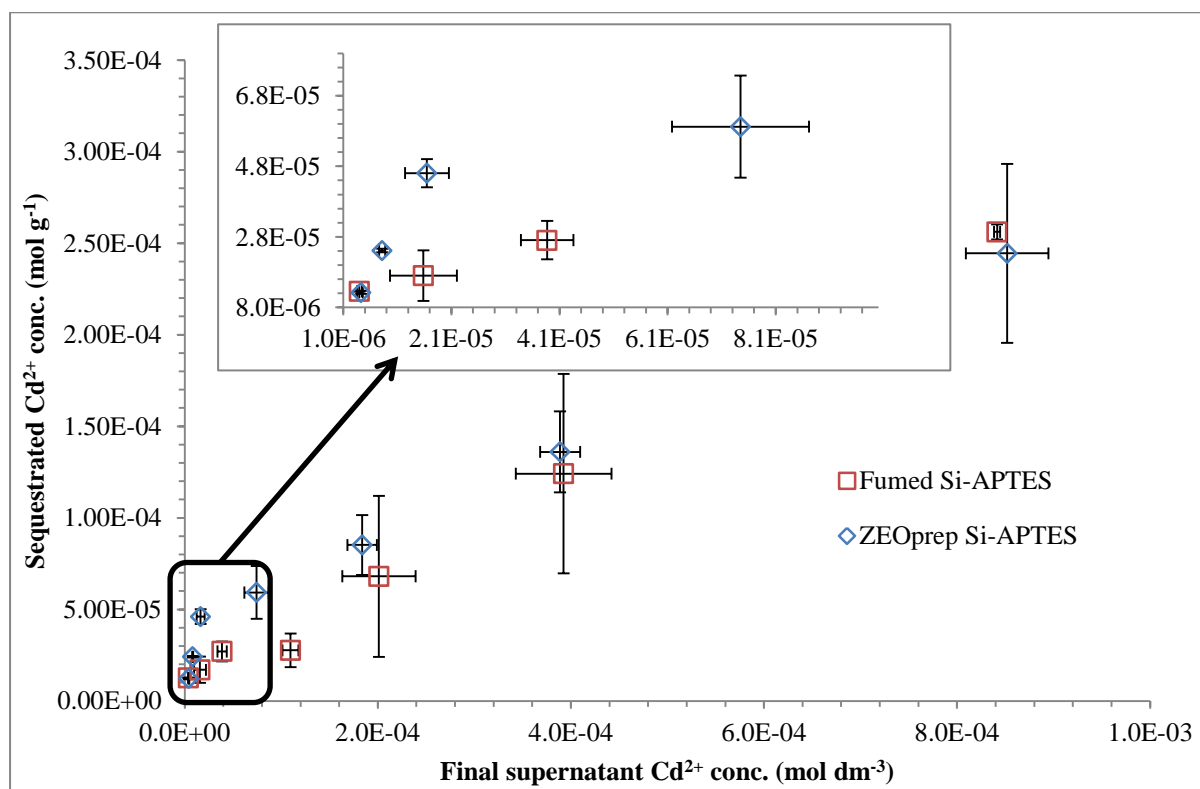
**Table 32 – Variation of R<sub>d</sub> at different initial concentrations of Co(II) from a 1 % Ca<sup>2+</sup> solution. A rise of ca. one order of magnitude was observed as initial concentrations decreased for APTES-functionalised fumed silica but little change was observed for APTES-functionalised ZEOprep silica. Initial pHs were recorded to range from 5.53 (2.54 ppm) and 6.27 (162.41 ppm).**

The consequence of the sodium and calcium ions has had a measurable effect on the removal of Co(II), reducing the rise of R<sub>d</sub> from three to only one order of magnitude as the concentration of metal decreases. At the higher concentrations, the values are similar, suggesting that there is a preference for the cobalt in these conditions. However, when the concentration of cobalt is much lower, it appears the competition of these ions is too much for the APTES to remove cobalt at the levels observed in deionised water where R<sub>d</sub> values are ca. two orders of magnitude lower for 2.48 ppm.

### 6.2.3.5 $\text{Cd}^{2+}$ studies with silica attached APTES

The removal of heavy metals such as cadmium from natural waters has attracted considerable attention because of its adverse effects on the environment and human health.<sup>126</sup> Cadmium is not generally believed to have a biological function although research by Lane *et al.*<sup>209</sup> suggest it may have a purpose in marine diatoms where low levels of zinc exist. However, excessive accumulation of cadmium can be toxic to most plants<sup>210</sup> and humans.<sup>126</sup>

The following investigations were carried out using the isotope  $^{109}\text{Cd}$  as a tracer, enabling gamma counting to be used to monitor the investigations and again, the effect of sequestration when high levels of sodium and calcium are present were carried out. Almost all cadmium compounds have the oxidation state  $+2$ <sup>211</sup> but as well as being divalent, its properties are slightly different to the other transition metals discussed so far because its electron configuration is  $[\text{Kr}] 4d^{10}$  leaving no incomplete d shell. This property results in zinc, cadmium and mercury often excluded from transition metal comparisons – all of which are located within group 12 of the periodic table.  $\text{Cd}(\text{NO}_3)_2 \cdot 4\text{H}_2\text{O}$  was used to make up the cadmium solutions to the desired concentrations.



**Figure 76 – Isotherm for  $\text{Cd}^{2+}$  removal from deionised water with APTES-functionalised ZEOprep and fumed silica materials over 24 h. Initial concentrations ranged from  $2.45 \times 10^{-5}$  –  $1.52 \times 10^{-3} \text{ mol dm}^{-3}$  (2.75 – 171.35 ppm) whilst initial pHs ranged from 5.60 (2.75 ppm) – 6.02 (171.35 ppm).**

Unlike the other ions and isotopes tested so far, cadmium has not reached saturation as the trend of the graph is still straight. However,  $2.5 \times 10^{-4} \text{ mol g}^{-1}$  appears to be around the capacity for these materials and could be that capacity has just been reached. Distribution ratios are tabulated below whilst a discussion of the observations follow.

Initial concentration of cadmium		ZEOprep Si-APTES	Fumed Si-APTES
ppm	$\text{mol dm}^{-3}$	$R_d (\text{mL g}^{-1})$	$R_d (\text{mL g}^{-1})$
171.35	$1.52 \times 10^{-3}$	$2.57 \times 10^5$	$2.73 \times 10^5$
82.27	$7.32 \times 10^{-4}$	$3.14 \times 10^5$	$2.99 \times 10^5$
42.25	$3.76 \times 10^{-4}$	$4.26 \times 10^5$	$3.36 \times 10^5$
21.48	$1.91 \times 10^{-4}$	$7.39 \times 10^5$	$2.25 \times 10^5$
10.48	$9.33 \times 10^{-5}$	$2.58 \times 10^6$	$6.43 \times 10^5$
5.31	$4.72 \times 10^{-5}$	$2.67 \times 10^6$	$1.19 \times 10^6$
2.75	$2.45 \times 10^{-5}$	$2.58 \times 10^6$	$2.82 \times 10^6$

**Table 33 – Variation of  $R_d$  at different initial concentrations of  $\text{Cd}^{2+}$  from deionised water. A rise of ca. one order of magnitude was observed as initial concentrations decreased. Initial pHs were recorded to range from 5.60 (2.75 ppm) and 6.02 (171.35 ppm).**

Initial concentration of cadmium		ZEOprep Si-APTES	Fumed Si-APTES
ppm	$\text{mol dm}^{-3}$	$R_d (\text{mL g}^{-1})$	$R_d (\text{mL g}^{-1})$
165.40	$1.47 \times 10^{-3}$	$1.15 \times 10^5$	$1.00 \times 10^5$
82.83	$7.37 \times 10^{-4}$	$1.86 \times 10^5$	$1.15 \times 10^5$
39.86	$3.55 \times 10^{-4}$	$1.99 \times 10^5$	$9.50 \times 10^4$
20.08	$1.79 \times 10^{-4}$	$1.77 \times 10^5$	$1.63 \times 10^5$
9.80	$8.72 \times 10^{-5}$	$2.12 \times 10^5$	$1.48 \times 10^5$
4.98	$4.43 \times 10^{-5}$	$2.58 \times 10^5$	$1.85 \times 10^5$
2.54	$2.26 \times 10^{-5}$	$3.37 \times 10^5$	$2.26 \times 10^5$

**Table 34 – Variation of  $R_d$  at different initial concentrations of  $\text{Cd}^{2+}$  from a 1 %  $\text{Na}^+$  solution. Values were found to stay relatively constant as initial concentration decreased. Initial pHs were recorded to range from 5.23 (4.98 ppm) and 7.21 (165.40 ppm).**

Initial concentration of cadmium		ZEOprep Si-APTES	Fumed Si-APTES
ppm	mol dm <sup>-3</sup>	R <sub>d</sub> (mL g <sup>-1</sup> )	R <sub>d</sub> (mL g <sup>-1</sup> )
152.23	1.35 x 10 <sup>-3</sup>	3.97 x 10 <sup>4</sup>	1.89 x 10 <sup>4</sup>
78.39	6.97 x 10 <sup>-4</sup>	7.82 x 10 <sup>4</sup>	7.77 x 10 <sup>4</sup>
38.81	3.45 x 10 <sup>-4</sup>	9.43 x 10 <sup>4</sup>	7.18 x 10 <sup>4</sup>
19.27	1.72 x 10 <sup>-4</sup>	1.08 x 10 <sup>5</sup>	5.31 x 10 <sup>4</sup>
9.48	8.44 x 10 <sup>-5</sup>	1.35 x 10 <sup>5</sup>	6.40 x 10 <sup>4</sup>
4.86	4.33 x 10 <sup>-5</sup>	1.30 x 10 <sup>5</sup>	9.55 x 10 <sup>4</sup>
2.50	2.23 x 10 <sup>-5</sup>	1.89 x 10 <sup>5</sup>	1.19 x 10 <sup>5</sup>

**Table 35 – Variation of R<sub>d</sub> at different initial concentrations of Cd<sup>2+</sup> from a 1 % Ca<sup>2+</sup> solution. A rise of ca. one order of magnitude was observed as initial concentrations decreased. Initial pHs were recorded to range from 5.59 (2.50 ppm) and 6.68 (152.23 ppm).**

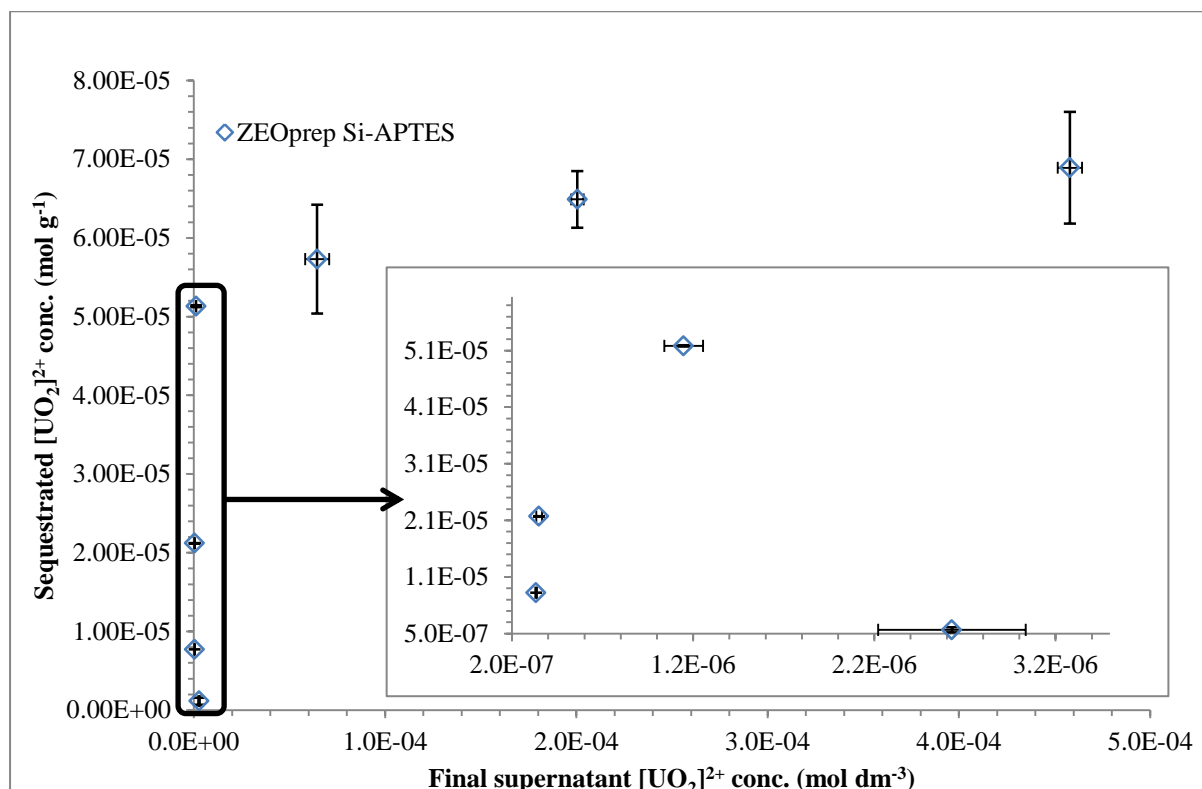
Although a 1 % Na<sup>+</sup> solution appeared to have little effect on the R<sub>d</sub> values obtained apart from the lower initial concentrations, an immediate drop by an order of magnitude is observed when Ca<sup>2+</sup> is present. After researching into why this might be the case, literature showed that a team of researchers from the DOE Office of Science's Argonne National Laboratory has demonstrated that cadmium releases calcium from bone within hours of exposure, even at low concentrations. It is thought that the size and characteristics of the two species are so similar that the body accepts cadmium, believing it to be calcium and hence bone diseases such as osteoporosis can be a result of cadmium poisoning.<sup>212</sup> This could explain the effect observed in this case where it is clear the presence of calcium has impacted the amount of cadmium ions that the APTES ligands has successfully bound with.

#### **6.2.3.6 [UO<sub>2</sub>]<sup>2+</sup> studies with silica attached APTES**

Uranium is very common in the environment, with low levels present in rocks, soil, air and water. Depleted uranium is used in bullets and missiles but also as shielding for tanks whilst the common isotope <sup>238</sup>U (99 %) is enriched with <sup>235</sup>U to ca. 3 % and used to fuel commercial nuclear power plants.<sup>176,197</sup>

Uranium has no known biological role and is toxic due to heavy metal poisoning and its radioactive state. Uranium in air exists as a dust that will fall into surface water and soils which does not pose much of a problem. However, in large amounts, it can cause health issues such as kidney disease and cancer. Enriched uranium can end up in the environment from accidents at nuclear power plants.<sup>176</sup>

Uranyl nitrate,  $\text{UO}_2(\text{NO}_3)_2$  was used for the following investigations and selectivity tests in chapter 7. The uranyl ion is an oxyanion of uranium and exists in the oxidation state +6 with the chemical formula  $[\text{UO}_2]^{2+}$ . Uranyl nitrate (obtained as yellow crystalline hydrates) is regarded as the most important uranyl compound due to its high solubility in a very wide range of organic solvents (alcohols, ketone and ethers) as well as in water<sup>213</sup> – making this an ideal source of uranium to use for this work. No tracer was required as  $^{238}\text{U}$  is already active, but as an alpha emitter hence ICP-OES was used to interpret the results.



**Figure 77 – Isotherm for  $[\text{UO}_2]^{2+}$  removal from deionised water with APTES-functionalised ZEOprep silica materials over 24 h. Initial concentrations ranged from  $1.81 \times 10^{-5} - 1.13 \times 10^{-3} \text{ mol dm}^{-3}$  (2.75 – 171.35 ppm) whilst initial pHs ranged from 5.60 (2.75 ppm) – 6.02 (171.35 ppm).**

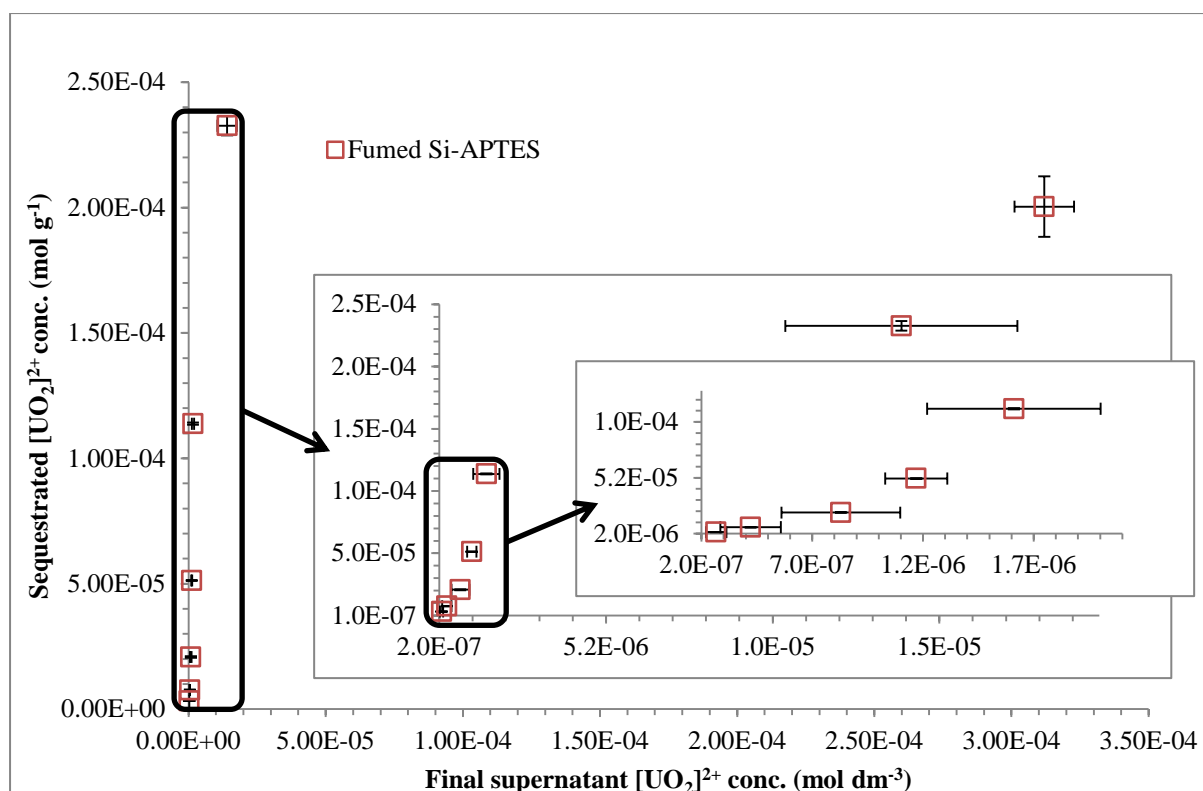


Figure 78 – Isotherm for  $[\text{UO}_2]^{2+}$  removal from deionised water with APTES-functionalised fumed silica over 24 h. Initial concentrations ranged from  $1.81 \times 10^{-5}$  –  $1.13 \times 10^{-3}$  mol dm<sup>-3</sup> (2.75 – 171.35 ppm) whilst initial pHs ranged from 5.60 (2.75 ppm) – 6.02 (171.35 ppm).

Initial concentration of uranium		ZEOprep Si-APTES	Fumed Si-APTES
ppm	mol dm <sup>-3</sup>	$R_d$ (mL g <sup>-1</sup> )	$R_d$ (mL g <sup>-1</sup> )
127.26	$5.35 \times 10^{-4}$	$1.36 \times 10^5$	$5.80 \times 10^5$
64.88	$2.73 \times 10^{-4}$	$2.92 \times 10^5$	$1.59 \times 10^7$
30.49	$1.28 \times 10^{-4}$	$8.14 \times 10^5$	$6.75 \times 10^7$
13.85	$5.82 \times 10^{-5}$	$4.06 \times 10^7$	$3.99 \times 10^7$
5.69	$2.39 \times 10^{-5}$	$5.48 \times 10^7$	$2.52 \times 10^7$
2.12	$8.91 \times 10^{-6}$	$2.09 \times 10^7$	$1.78 \times 10^7$
0.59	$2.47 \times 10^{-6}$	$4.19 \times 10^5$	$1.14 \times 10^7$

Table 36 – Variation of  $R_d$  at different initial concentrations of  $[\text{UO}_2]^{2+}$  from deionised water. Values increase overall by ca. two orders of magnitude but there appears to be no smooth trend that has been observed for other metal investigations. Initial pHs were recorded to range from 5.68 (0.59 ppm) and 9.95 (127.26 ppm).

Some of the most consistently high  $R_d$  values were achieved with the uranyl nitrate solutions when investigating the removal of  $[\text{UO}_2]^{2+}$ . These values suggest the material has a strong affinity for the uranyl ion and hence it was anticipated that when a multi-metal solution was produced (reported in chapter 7), selective removal of the uranyl ion could be achieved. The

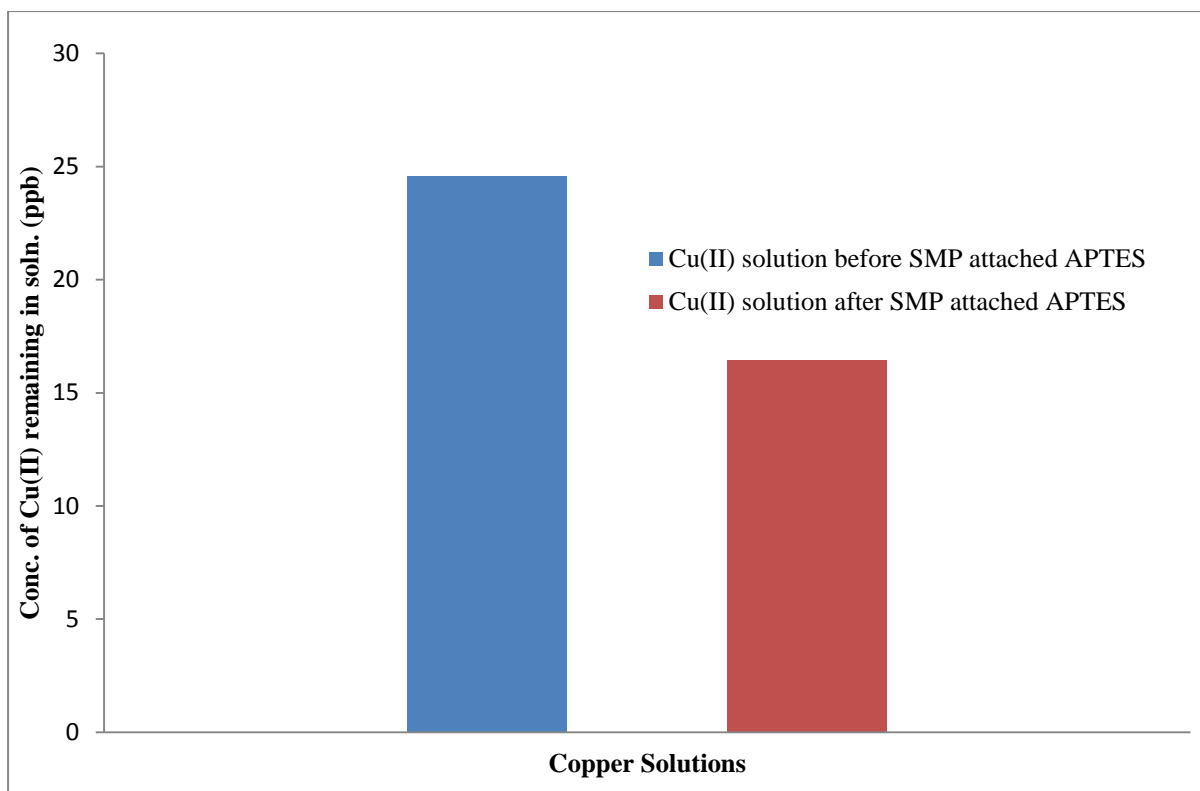


values reported in the introduction on page 8 suggest that both the APTES-functionalised ZEOprep and fumed silica behaved at extremely competitive levels as the highest  $K_d$  value reported was  $1.6 \times 10^5$  for U(VI) removal compared to  $10^7$  in Table 36.

### **6.3 Cu(II) removal with SMP attached APTES**

As briefly discussed in chapter 4, SMPs were used towards the end of the project to ascertain whether they could provide an alternative option as a solid support for ligands and polymers for metal sequestration. The limited sample size available to the group prevented an in depth review of the material but nonetheless, a trial was carried out to investigate this method.

Characterisation of the material had been limited so that a maximum quantity of the material could be used for testing so it was assumed that a thorough coating of APTES across the sample had been achieved. With only 2.5 mg of sample available, the concentration of the initial solution (which was again produced with  $\text{CuCl}_2 \cdot 2\text{H}_2\text{O}$ ) was prepared at a ppb level rather than a ppm with trace metal analysis being run *via* ICP-MS. The lack of sample prevented repeats of the investigation being carried out and the author accepts that this makes the data reported most unreliable. However, as this initial investigation was purely to show the concept could be achievable, Figure 79 illustrates the decrease of initial Cu(II) concentration from 24.6 ppb to 16.4 ppb proposing that this material may benefit from being investigated on a larger scale.



**Figure 79 – Sequestration of Cu(II) ions with silica coated ferrous oxide. No error bars are included as no repeats were carried out due to limited sample, hence a much lower initial concentration was used. However, a decrease in concentration was observed from 24.6 ppb to 16.4 ppb with just 2.5 mg of material.**

## 6.4 Langmuir isotherm model

The fitting of adsorption isotherm equations to experimental data is often an important aspect of data analysis.<sup>214</sup> The Langmuir isotherm model assumes the solid has a limited sorption capacity as well as the following assumptions:

- Adsorption occurs up to the extent of one monolayer
- All adsorption sites are identical
- Occupation of a site is independent of the occupation of neighbouring sites
- The temperature is constant
- The surface is uniform and homogenous
- The process is reversible
- Each site retains one molecule of the given compound

- All sites are energetically and sterically independent of the adsorbed quantity<sup>179,215</sup>

This model has been used in describing results that have shown deviations away from a linear distribution. Empirical models such as this (and also include the  $K_d$  model) are mathematical descriptions of the experimental data without any particular theoretical basis.<sup>216</sup> In this case, the model is used to determine the amount of contaminant that can be removed from water using the APTES-functionalised silica materials.

The Langmuir model equation takes the form as shown in Equation 17.

$$\frac{Y}{M} = \frac{kbC}{1 + kC}$$

**Equation 17 – The Langmuir isotherm equation.**<sup>217</sup>

The linearised form of the equation is represented in Equation 18.

$$\frac{1}{Y/M} = \frac{1}{kb} \times \frac{1}{C} + \frac{1}{b}$$

**Equation 18 – The manipulated linear Langmuir isotherm equation.**<sup>217</sup>

Where:

Y = concentration of metal ions adsorbed, mg L<sup>-1</sup>

M = silica concentration, mg L<sup>-1</sup>

C = equilibrium concentration of metal ions, mg L<sup>-1</sup>

b = constant (determined graphically)

k = constant (determined graphically)

The constant b is the maximum adsorption capacity of the substrate (mol g<sup>-1</sup>) whilst the constant k represents the strength with which the solute is bound to the substrate. Values of k and b can be determined by plotting the linearised equation. “1/(Y/M)” (or simply “M/Y”) is the y-axis and “1/C” is the x-axis when graphed. The value for “1/kb” is the slope and the value for “1/b” is the y-intercept and hence by rearrangement and by calculating ‘b’ first, both k and b values can be established.<sup>217</sup>

The results for these constants are shown in Table 37 and Table 38 following the linear Langmuir plots shown in Appendix 1. Although some plots do not fit that well, others such as Co(II) and Cd<sup>2+</sup> do.

Silica material	Metal ion solution	Constant k	Constant b (mol g <sup>-1</sup> )
APTES-functionalised ZEOprep silica	Co(II)	0.98	0.016
	Ni(II)	0.53	0.0072
	Cu(II)	1.79	0.014
	Cd <sup>2+</sup>	0.15	0.022
	Eu(III)	7.57	0.025
	[UO <sub>2</sub> ] <sup>2+</sup>	1.88	0.021

**Table 37 – Data collected from the linear Langmuir isotherm model to show the relative binding strength (k) and maximum adsorption capacity (b, mol g<sup>-1</sup>) of the APTES-functionalised ZEOprep silica when in a solution of the corresponding metal ion.**

Silica material	Metal ion solution	Constant k	Constant b (mol g <sup>-1</sup> )
APTES-functionalised fumed silica	Co(II)	1.42	0.014
	Ni(II)	0.93	0.016
	Cu(II)	1.02	0.023
	Cd <sup>2+</sup>	0.10	0.013
	Eu(III)	3.32	0.037
	[UO <sub>2</sub> ] <sup>2+</sup>	0.98	0.068

**Table 38 – Data collected from the linear Langmuir isotherm model to show the relative binding strength (k) and maximum adsorption capacity (b, mol g<sup>-1</sup>) of the APTES-functionalised fumed silica when in a solution of the corresponding metal ion.**

Table 38 shows that the silica materials have a very reproducible capacity across the metals tested that ranges from 0.0072-0.068 mol g<sup>-1</sup>. The highest capacities are observed for the fumed silica for uranium and europium containing solutions. This is not surprising given the much larger surface area and the strong affinity that has been observed between these ions and the APTES ligand. The capacity for these two metal ions on the ZEOprep material are also of the highest witnessed, along with cadmium. Generally however, the values are very similar ranging from 0.01-0.03 mol g<sup>-1</sup> if the highest values are discounted.

The relative binding strength does identify Eu(III) to be bound significantly stronger than the other ions tested. Europium ions are known to commonly exist in the oxidation state +3<sup>192,218</sup> and previous experimentation with europium salts and isotopes by Loughborough

Radiochemistry's researchers has shown it to have a high affinity for glass, resulting in cleaning being a much more arduous task than following the use of other metal salts. Bearing this in mind, a +3 ion would be expected to have extra affinity for an electron rich surface over a +2 or lower anyway (although ionic radii does need to be considered). In this case however, a higher value is observed for the +3 over the +2. This data is not necessarily suggesting that it would bind seven (Table 37) or three (Table 38) times stronger than other ions investigated, but that it is highly likely that it is simply bound more strongly than the other metals tested.

## 6.5 Conclusion

This chapter has demonstrated the effectiveness of the two silica attached APTES materials along with very high  $R_d$  values. The data found and used to plot the concentrations of metal ions bound to the surface of the materials has been collected and tabulated below (Table 39) to show the capacity of each metal on both surfaces.

Metal ion	ZEOprep Si-APTES capacity (mol g <sup>-1</sup> )	Fumed Si-APTES capacity (mol g <sup>-1</sup> )
Co(II)	$2.34 \times 10^{-4} \pm 2.13 \times 10^{-5}$	$2.45 \times 10^{-4} \pm 6.38 \times 10^{-5}$
Ni(II)	$2.32 \times 10^{-4} \pm 6.61 \times 10^{-5}$	$3.53 \times 10^{-4} \pm 4.70 \times 10^{-5}$
Cu(II)	$2.73 \times 10^{-4} \pm 1.15 \times 10^{-5}$	$3.43 \times 10^{-4} \pm 1.33 \times 10^{-5}$
Cd <sup>2+</sup>	Not less than $2.44 \times 10^{-4} \pm 4.28 \times 10^{-5}$	Not less than $2.56 \times 10^{-4} \pm 3.13 \times 10^{-6}$
Eu(III)	$3.28 \times 10^{-4} \pm 8.57 \times 10^{-5}$	$2.72 \times 10^{-4} \pm 2.66 \times 10^{-5}$
[UO <sub>2</sub> ] <sup>2+</sup>	$6.89 \times 10^{-5} \pm 6.37 \times 10^{-6}$	$2.00 \times 10^{-4} \pm 1.08 \times 10^{-5}$

**Table 39 – Summary of maximum capacity of each metal on the two materials from the data used to produce the graphs. All data is taken from the deionised water solutions, thus making results comparable.**

Table 39 shows very little difference between the two silica materials in terms of metal binding capacity. Eu(III) and [UO<sub>2</sub>]<sup>2+</sup> ions have been removed to very similar amounts as the smaller ions suggesting that the ionic radii have little effect on the capacity of the surface. The difference between the two silicas is perhaps the more surprising result, signifying that the optimum size for maximum surface coverage is no lower than that of ZEOprep silica. It appears that the APTES molecules effectively 'glue' the fumed silica particles to form a size similar to that of the ZEOprep silica and thus remove the benefit of using the smaller particle size material.

Across the metals targeted in this chapter, when the solution was made up with a 1 % Na<sup>+</sup> or Ca<sup>2+</sup> a significant drop in target metal removed was not seen. In general, if  $R_d$  values were

observed to drop for a given concentration when conditions were altered, this was only by one order of magnitude.

Additional studies with XPS and STEM has enabled one to provide further evidence that the metal ions are chemically bound to the surface of these functionalised silica materials. The spectra provided from XPS investigations clearly illustrates the generation of new peaks due to the additional atoms and bonding observed after each modification step. The final spectra then show copper being present after removing this from an aqueous solution. The difference in colour of the APTES-functionalised silica material before and after being subjected to this solution of Cu(II) ions strongly suggests it had successfully removed copper before any tests were carried out. The data collected from XPS has raised questions regarding the exact binding of copper ions to the material as the percentage of each atom are probably not what would be expected.

Name	Peak BE	Atomic %
Si2p	104.35	29.82
O1s	533.74	57.38
C1s	286.32	5.50
N1s	401.91	1.01
Cu2p <sup>3</sup>	936.45	6.29

**Table 40 – Peak E<sub>B</sub> values and atomic percentages for selected peaks after ZEOprep Si-APTES had been in a 160 ppm copper solution for 1 week (Figure 65).**

The data collected suggests a 6:1 copper-nitrogen binding which is impossible. It has been suggested that within the vicinity of the APTES-functionalised silica where a large presence of amine groups exist, precipitation of Cu<sub>2</sub>O or Cu(OH)<sub>2</sub> occurs<sup>189</sup> due to the local pH change<sup>184</sup> and therefore only occurs at the surface of the APTES. Reversibility and dissolution studies in chapter 7 have shown that the metal ions seem to be well attached to the material as a rise in concentration of only 0.1 ppm (although lower than the LOD of the ICP-MS) is observed when the solids are filtered off and recovered before added to a fresh deionised water solution. The second explanation for this is that copper could be binding with the lone pairs of the oxygen atoms where attachment from the silica surface to the silane of the APTES takes place, however this does not explain the rise in percentage of oxygen once the copper is attached.

STEM has illustrated that the surface of the silica attached APTES is very effectively coated, showing that most, if not all the surface area is being utilised.

Using the linear Langmuir isotherm equation, it has been shown that europium ions bind significantly stronger than the APTES ligand than the other ions investigated. The prominent reasoning for this would appear to be the oxidation state.

Following the results in this chapter, the next stage was to test the materials for selectivity when all in the same solution. The results of these and many other ligand functionalised silicas can be found in the following chapter.

## 6.6 Future Work

Studies on the exact nature of the process occurring after the APTES-functionalised ZEOprep and fumed silica material has sequestered metal ions (especially from a solution specifically containing copper ions) needs to be investigated. The fact that the rate constant drops from 2.1 and 0.8 ppm hr<sup>-1</sup> for the two materials respectively to 0.02 ppm hr<sup>-1</sup> (Figure 60) shows that sequestration does not stop but that a second process appears to take place – especially as the material was left for 4 weeks to show that the concentration did not stop decreasing until between 3 and 4 weeks (Figure 57).

The second key finding from this chapter has been the information gathered from XPS studies showing that the copper to nitrogen ratio is essentially 6:1 for that found on the surface of the ZEOprep silica surface. With this ratio being impossible (especially when the nitrogen already makes up the APTES molecule) a closer look into how such an excess of copper is being removed also needs to be investigated. This could be carried out by taking the free APTES ligand up into an aqueous solution with a similar concentration of copper ions to that tested in this work before preparing a crystal to analyse *via* X-ray crystallography (although initial tests were attempted and proved difficult due to APTES reacting with itself).

XPS and TEM have proven to be valuable techniques when assessing how the metal ions are attached and how well the surface area of the material in question is being utilised. Further details of this process could be collected by using these techniques after a given time in the solutions such as at each time interval when the copper kinetic studies were carried out. This could help to establish the process by which such a large copper to nitrogen ratio exists following its sequestration with ZEOprep Si-APTES.

Finally, the brief investigation that was carried out with SMP attached APTES showed that this material may benefit from further investigations. If it was found to deliver results as good as those observed from the ZEOprep and fumed Si-APTES then this would offer the further practicality of being able to be removed *via* magnetism once sequestration had taken place.



## **7 Selective removal of metal ions and use of materials produced by PhosphonicS Ltd**

### **7.1 Introduction**

Following the results reported in chapter 6 with APTES-functionalised silica, the aim became to test this and as many other ligands as possible for their selective removal of metal ions. For the synthetic solutions, a seven metal solution was prepared that was described in chapter 2 and silica attached ligands that were donated to the group by PhosphonicS Ltd. were tested along with the APTES-functionalised ZEOprep and fumed silica. This chapter will bring together and round up the ‘story’ that has been created by designing and synthesising these materials as a technique to selectively remove metal ions from solution.





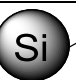




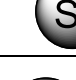

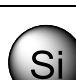
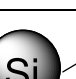
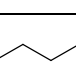
A ‘real-life’ water sample was also acquired from a nickel mine in Finland owned by Talvivaara Mining Company plc. This sample would only be used for testing the ZEOprep and fumed silica attached APTES as samples from PhosphonicS Ltd were limited.

#### **7.1.1 PhosphonicS Ltd**

PhosphonicS are a specialty chemicals company ‘supplying advanced functionalised materials to provide cost and performance benefits to a wide range of industrial, chemical and refining processes.’<sup>219</sup> Their technology was developed by Professor Alice Sullivan at Queen Mary, University of London where a general and economically viable method for silica functionalisation was discovered using vinyltrimethoxysilane (VTMS) as a coupling agent. PhosphonicS acquired the technology in 2001 to select and commercialise areas of application and in 2006 relocated from London to the Milton Science Park, Oxfordshire, UK. A full list of their patents and publications are available on their website.<sup>219</sup>

Three key areas are targeted by PhosphonicS and these include precious metal recovery (allowing recovery and recycling of precious metals from processes<sup>220</sup> and waste streams), small molecule purification (offering simple by-product and impurity removal from product streams<sup>221</sup>) and immobilised catalysts (enabling a range of reactions from acid-catalysed processes to C–C coupling to be run in clean and economical fashion<sup>222</sup>). However, with such a large combination of mixed metal possibilities, they have not tested their materials for selective removal of metals in all scenarios nor had the ability to test on radioisotopes.

In total, fourteen samples were donated for the research and the structures of these ligands, names and codes are given in Table 41. When discussing these samples and results, the code name will be used for simplicity.

Surface attached ligands	Name	Code
	2-Aminoethyl sulfide ethyl silica	SEA
	Triamine ethyl sulfide amide silica	STA3
	Pentaamine ethyl sulfide amide silica	SPA5
	Polyamine ethyl sulfide amide silica	SPAf
	3-Mercaptopropyl ethyl sulfide silica	SPM32
	Methyl thiourea ethyl sulfide ethyl silica	MTCf
	Disodium ethyl/butyl phosphonate silica	PO1
	Disodium succinate ethyl sulfide silica	STMS
	Ethyl/butyl phosphonic acid silica	POH1
	Succinic acid ethyl sulfide silica	STMA
	2-Hydroxyethyldiamine ethyl sulfide amide silica	SDEA
	N-Methyl-D-glucamine ethyl sulfide amide silica	SMG
	Polyol 2 alkyl silica	P2AS
	Bromide, tributylammonium propyl silica	BAP7

**Table 41 – A list of all materials donated to us by PhosphonicS Ltd. which were tested in a seven metal system and results shown in this chapter. For simplicity, the code name is used when referring to the materials.**

### 7.1.2 Talvivaara mine water sample

Talvivaara Mining Company Plc is an internationally significant base metals producer with its primary focus on nickel and zinc.<sup>223</sup> It is the latest commercial application of bioleaching, and the first in Europe, located in North-Eastern Finland.<sup>224</sup> Bioleaching is the process by which bacterial microorganisms are used to extract metals from its ore<sup>225,226</sup> and it provides an efficient and environmentally considerate method (often when there are lower concentrations of metal in the ore) by which bacteria feeds on nutrients in minerals, thereby separating the metal from the ore.<sup>227,228</sup>

A sample was obtained from a Pregnant Leaching Solution (PLS) pond by Hanna Tuovinen who is primarily based in Finland and studies the Talvivaara site but has also worked in the Loughborough radiochemistry department as part of her studies. The PLS pond holds the acidic, metal-rich water, readying for the metals recovery process which is carried out *via* precipitation using gaseous hydrogen sulphide and pH adjustment.<sup>224</sup> The harsh environment of this solution provided an unusual and challenging test for the silica attached APTES materials due to the strongly acid conditions (ca. pH 2.5) and the many different components present.

Analysis of the sample before and after the functionalised silica material was added was carried out using ICP-OES and these results are discussed following the synthetic seven metal solutions tested with the APTES-functionalised silicas and the PhosphonicS materials.

## 7.2 Results and Discussion

### 7.2.1 Selective metal sequestration

A 5 L solution of seven metals including Co(II), Ni(II), Cu(II),  $\text{Zn}^{2+}$ ,  $\text{Cd}^{2+}$ , Eu(III) and  $[\text{UO}_2]^{2+}$  was prepared as described in the chapter 2.30. These metal salt solutions were prepared to a concentration of ca. 20 ppm each and batches of 45 mL were prepared. 50 mg of functionalised silica was added to the solutions and allowed to equilibrate for 24 hours and 4 weeks. Each investigation was repeated five times and the standard deviation of the findings was used as the error bars for the graphs, see from Figure 80 to Figure 95.

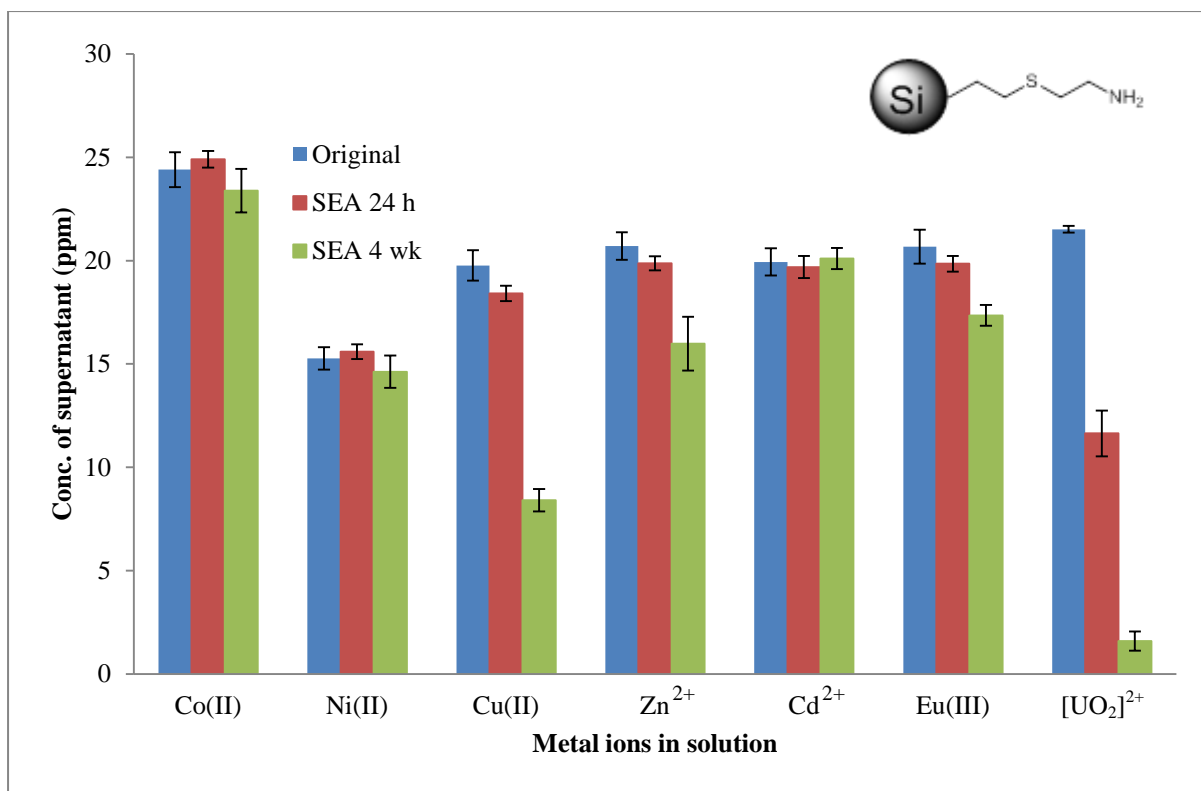


Figure 80 – Selective removal of metal by SEA from a mixed solution over 24 h and 4 w. After 24 h, [UO<sub>2</sub>]<sup>2+</sup> levels had reduced by much more than the other metals but after 4 w, Cu(II) had also reduced by a significant amount.

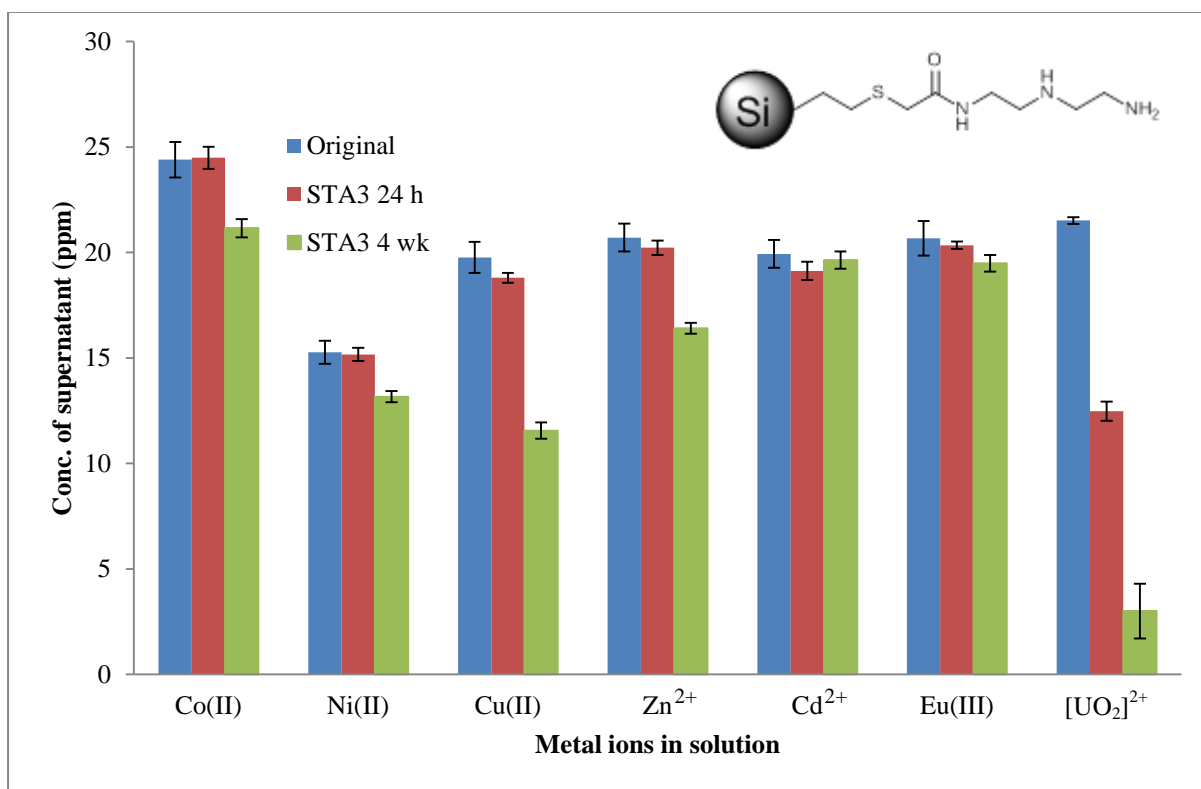


Figure 81 – Selective removal of metal by STA3 from a mixed solution over 24 h and 4 w. After 24 h, [UO<sub>2</sub>]<sup>2+</sup> levels had reduced by much more than the other metals but after 4 w, Cu(II) had also reduced by a significant amount.

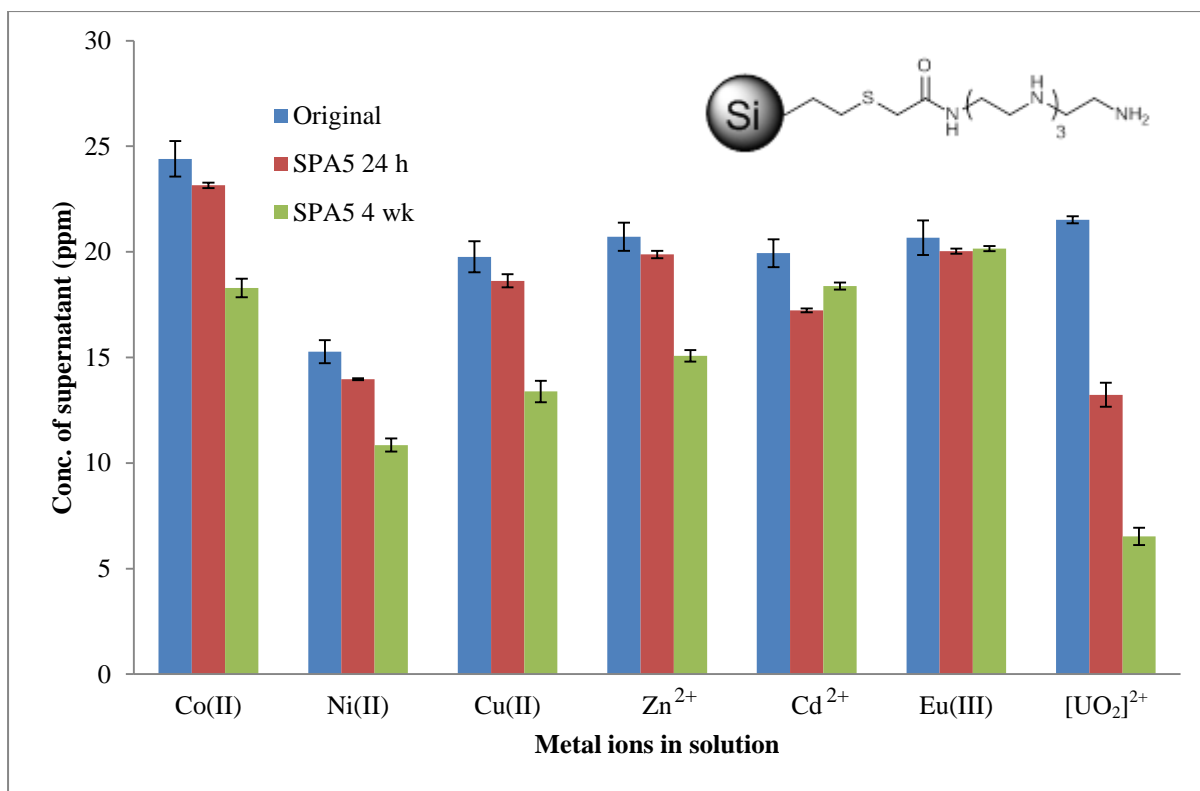


Figure 82 – Selective removal of metal by SPA5 from a mixed solution over 24 h and 4 w. After 24 h, [UO<sub>2</sub>]<sup>2+</sup> levels had reduced by much more than the other metals but after 4 w, drops in all but Eu(III) levels were observed.

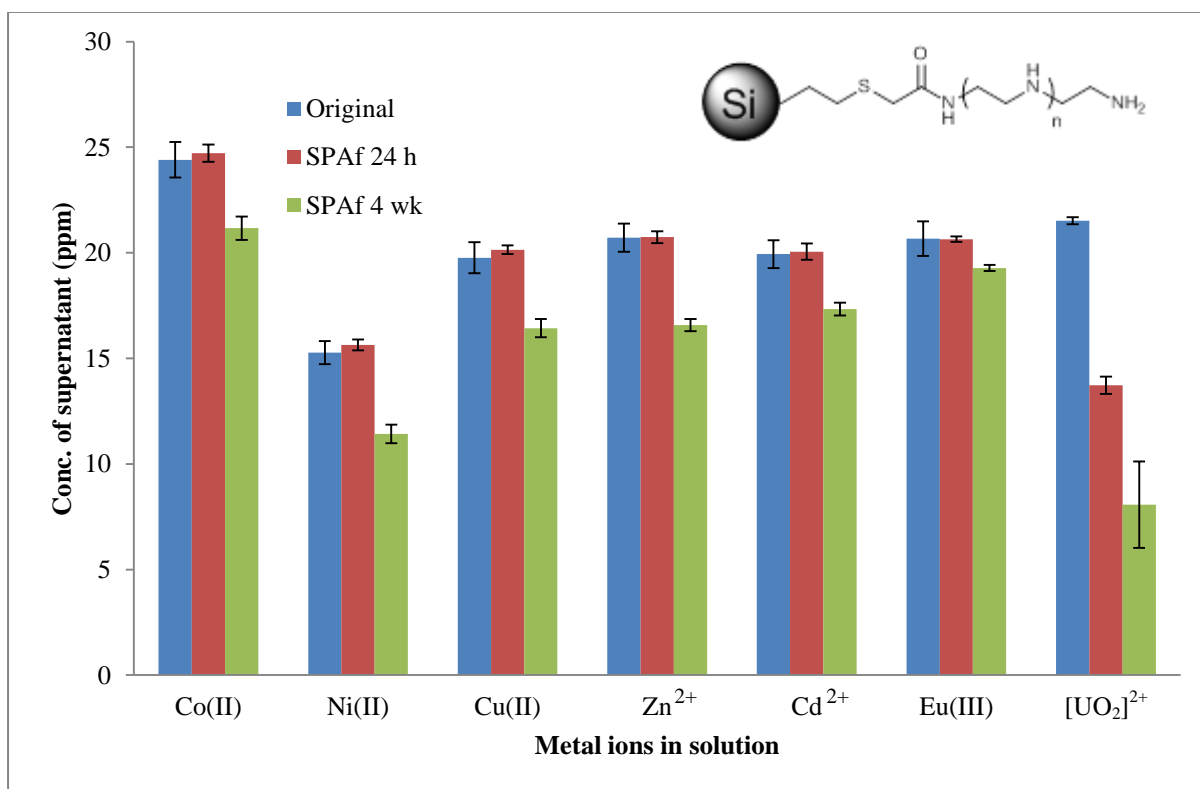
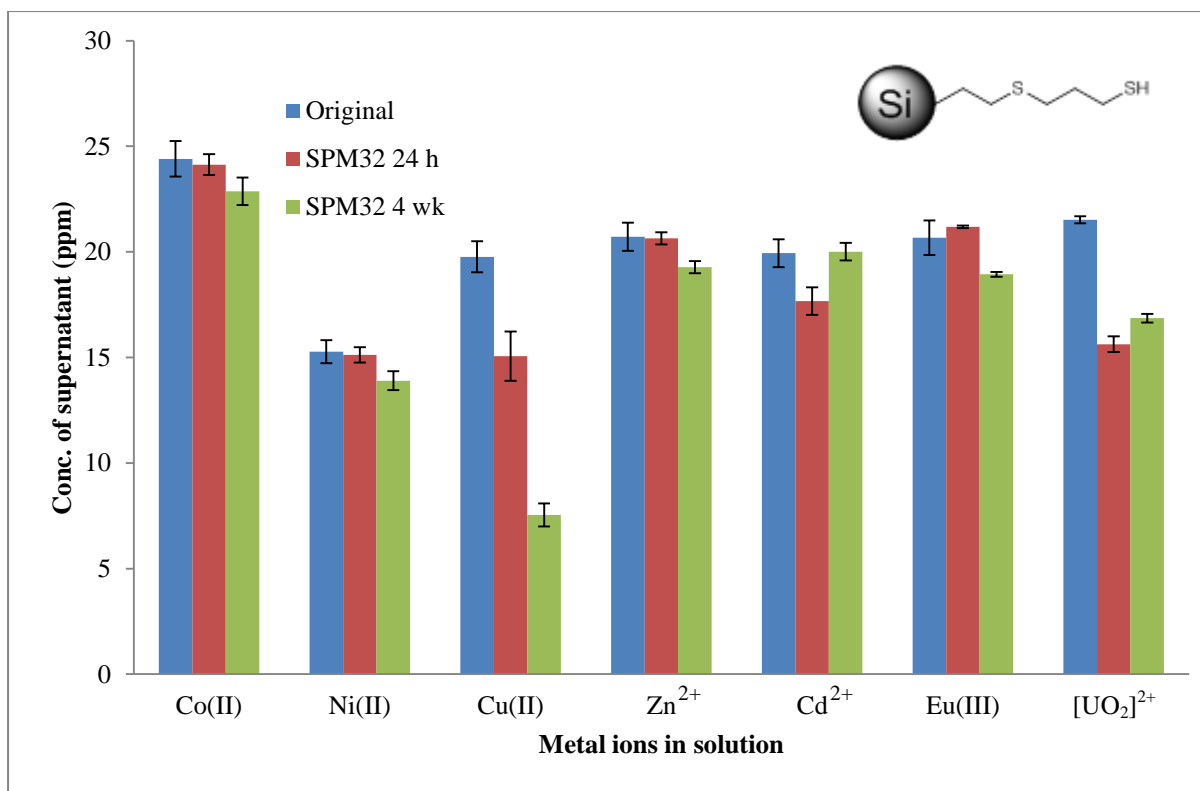
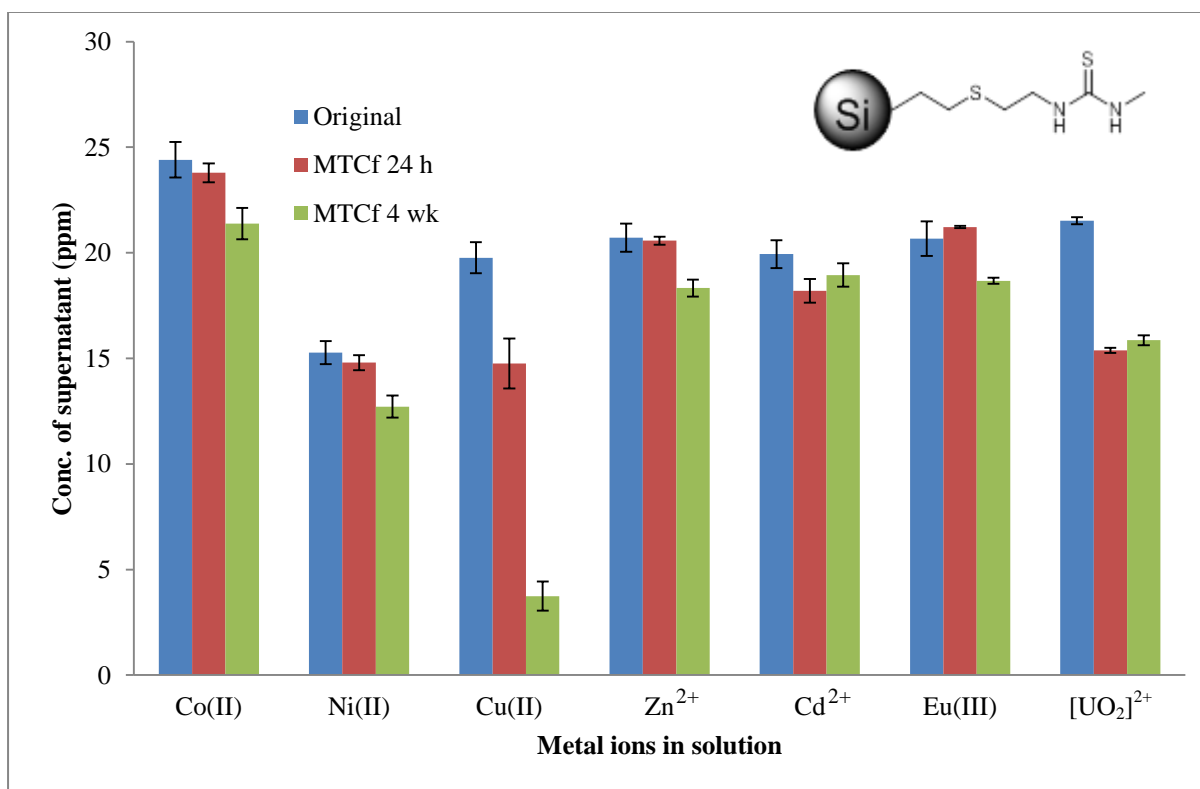


Figure 83 – Selective removal of metal by SPAf from a mixed solution over 24 h and 4 w. After 24 h, [UO<sub>2</sub>]<sup>2+</sup> levels had reduced by much more than the other metals but after 4 w, concentration levels of all metals had reduced.



**Figure 84** – Selective removal of metal by SPM32 from a mixed solution over 24 h and 4 w. Cu(II) and [UO<sub>2</sub>]<sup>2+</sup> were reduced to similar levels after 24 h, but copper was found to drop significantly further after 4 w.



**Figure 85** – Selective removal of metal by MTCf from a mixed solution over 24 h and 4 w. Cu(II) and [UO<sub>2</sub>]<sup>2+</sup> were reduced to similar levels after 24 h but Cu(II) was reduced significantly further after 4 w.

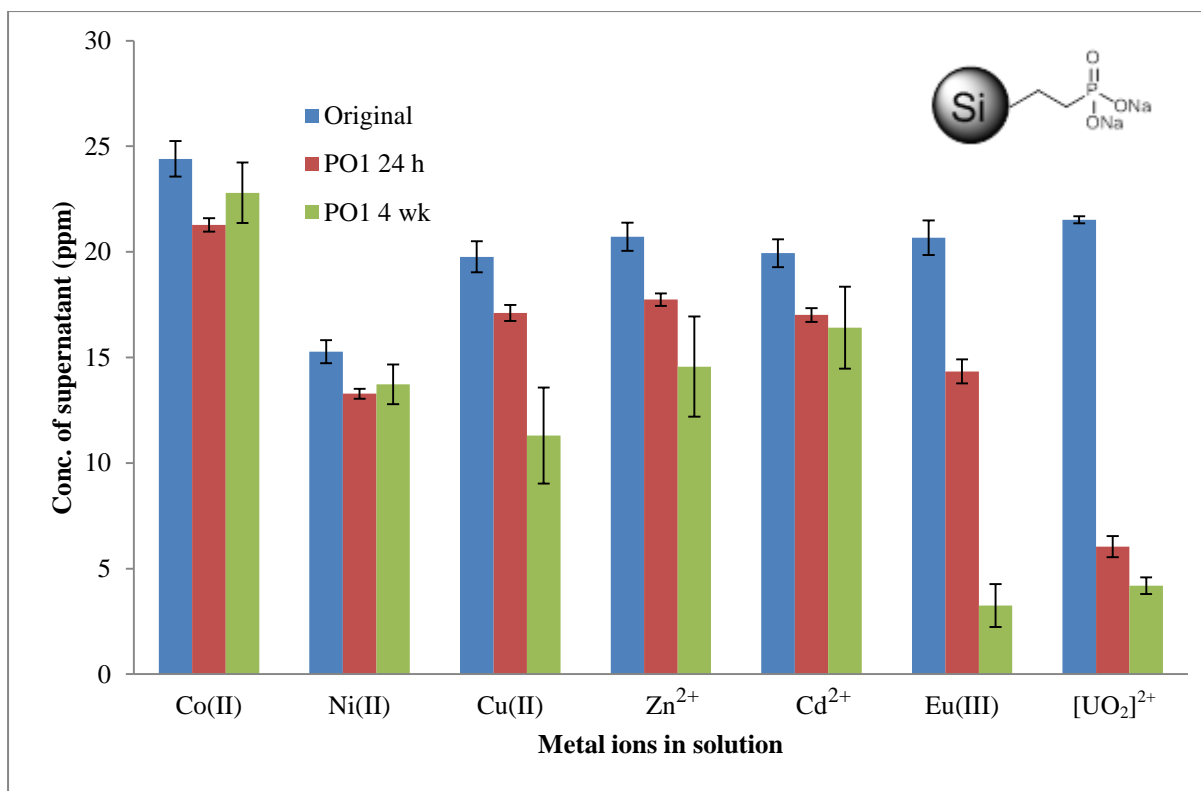


Figure 86 – Selective removal of metal by PO1 from a mixed solution over 24 h and 4 w. [UO<sub>2</sub>]<sup>2+</sup> levels saw the largest drop in concentration over 24 h but Eu(III) was observed to reduce considerably more over 4 w.

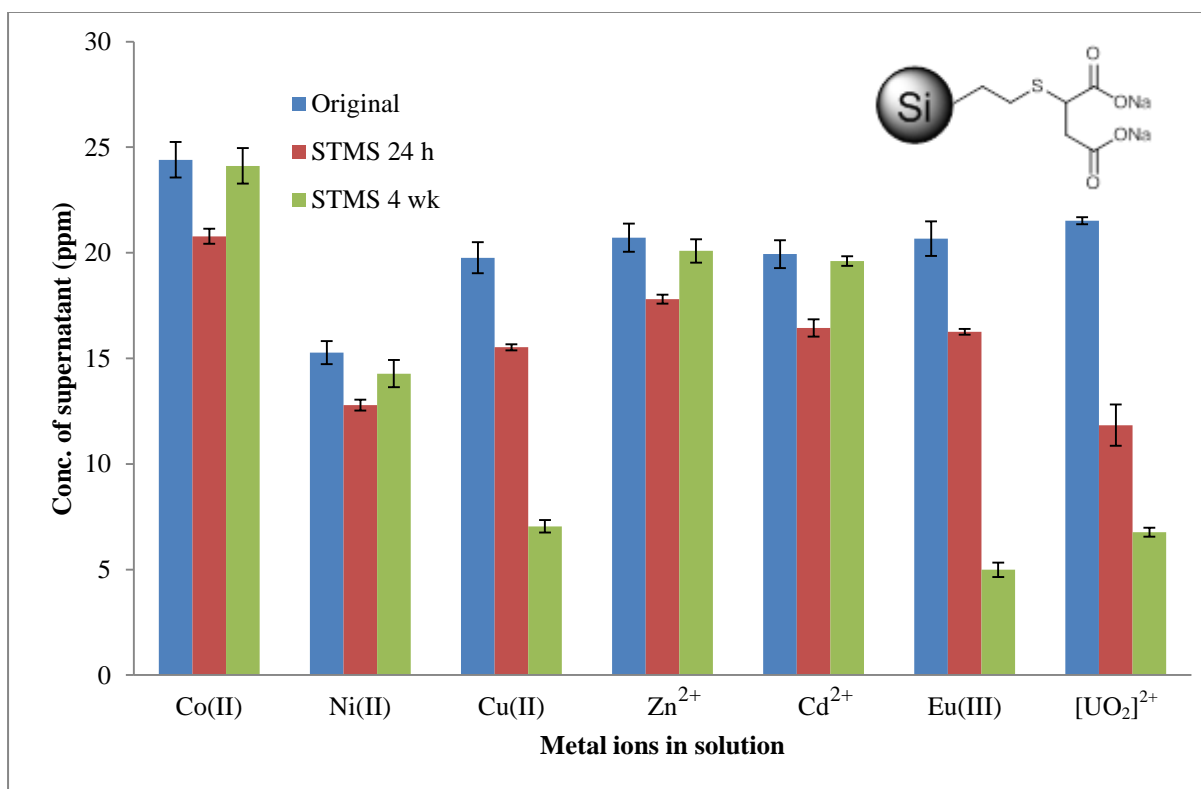
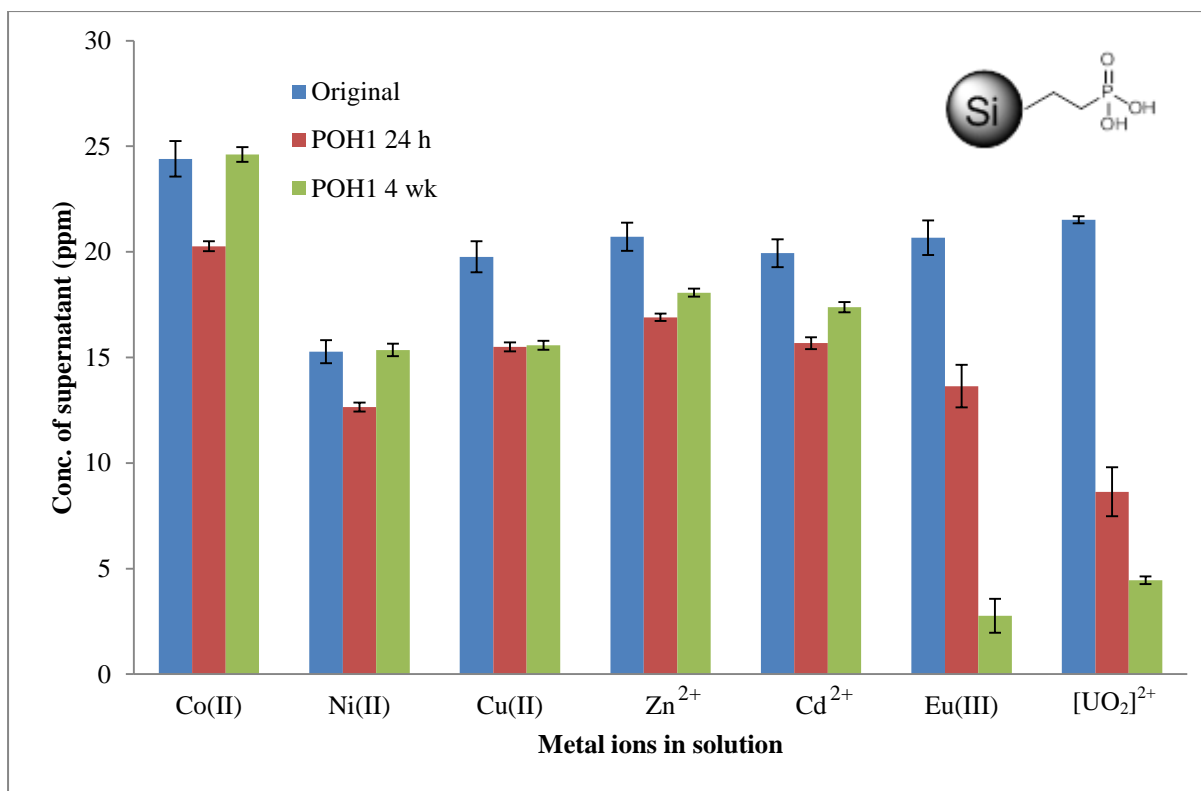
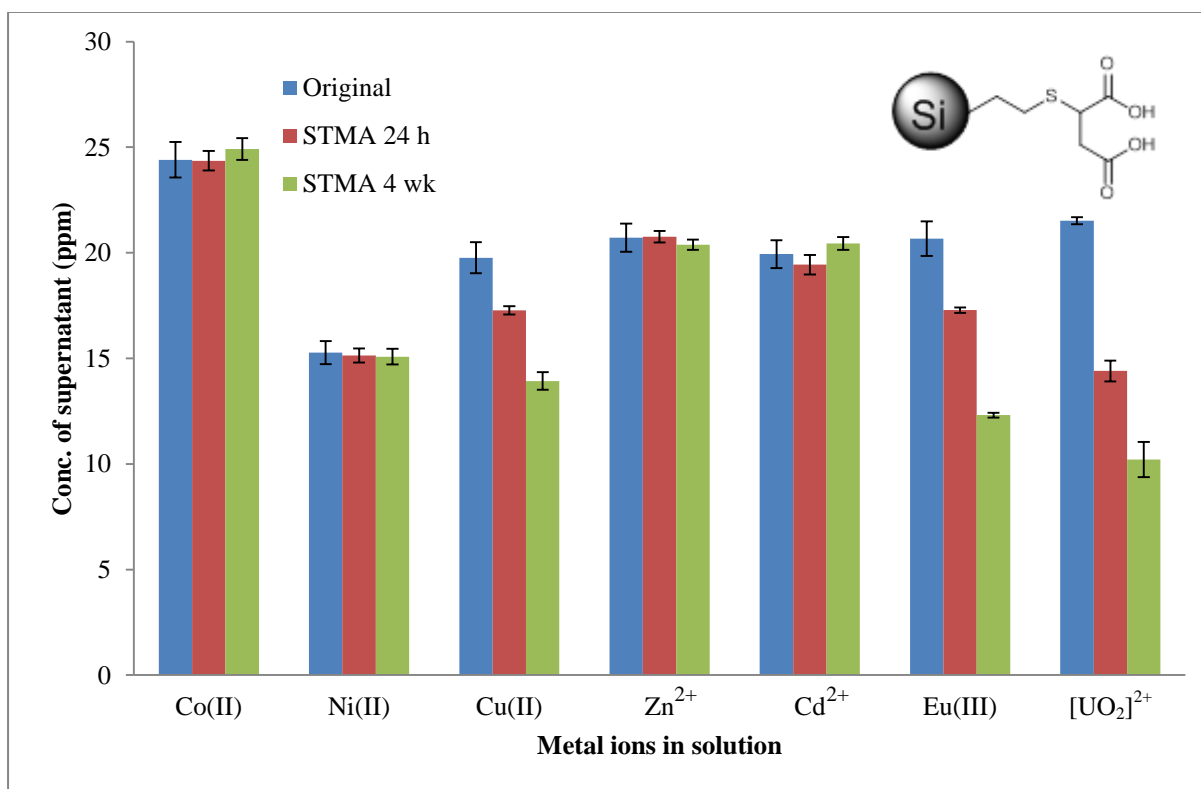


Figure 87 – Selective removal of metal by STMS from a mixed solution over 24 h and 4 w. After 24 h, no selectivity was observed but after 4 w. Cu(II), Eu(III) and [UO<sub>2</sub>]<sup>2+</sup> levels were found to have significantly dropped.



**Figure 88** – Selective removal of metal by POH1 from a mixed solution over 24 h and 4 w. All concentrations of metal see a drop after 24 h but more importantly, Eu(III) and [UO<sub>2</sub>]<sup>2+</sup> are selectively reduced after 4 w.



**Figure 89** – Selective removal of metal by STMA from a mixed solution over 24 h and 4 w. Strong selectivity for Cu(II), Eu(III) and [UO<sub>2</sub>]<sup>2+</sup> are shown as they are the only metals to be removed over 24 h and 4w in this study.



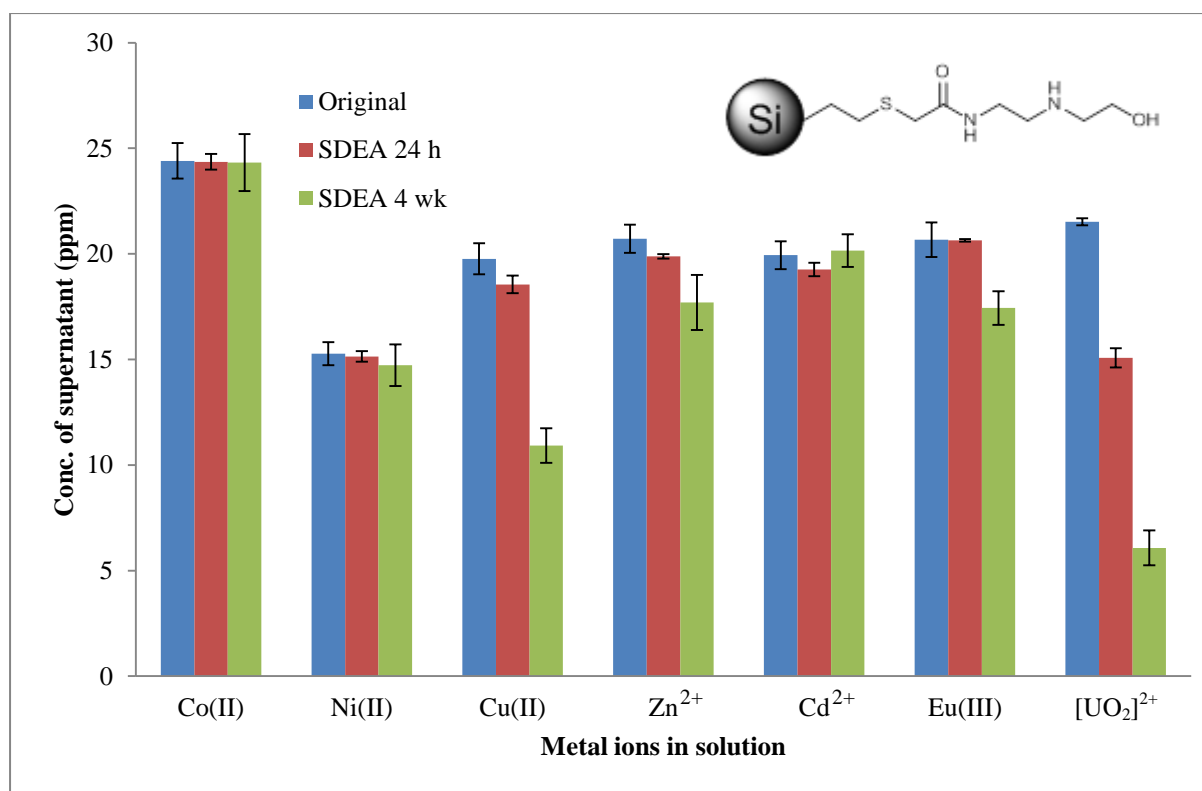


Figure 90 – Selective removal of metal by SDEA from a mixed solution over 24 h and 4 w. [UO<sub>2</sub>]<sup>2+</sup> was the highest removed metal after 24 h but Cu(II) was also significantly removed with [UO<sub>2</sub>]<sup>2+</sup> after 4 w.

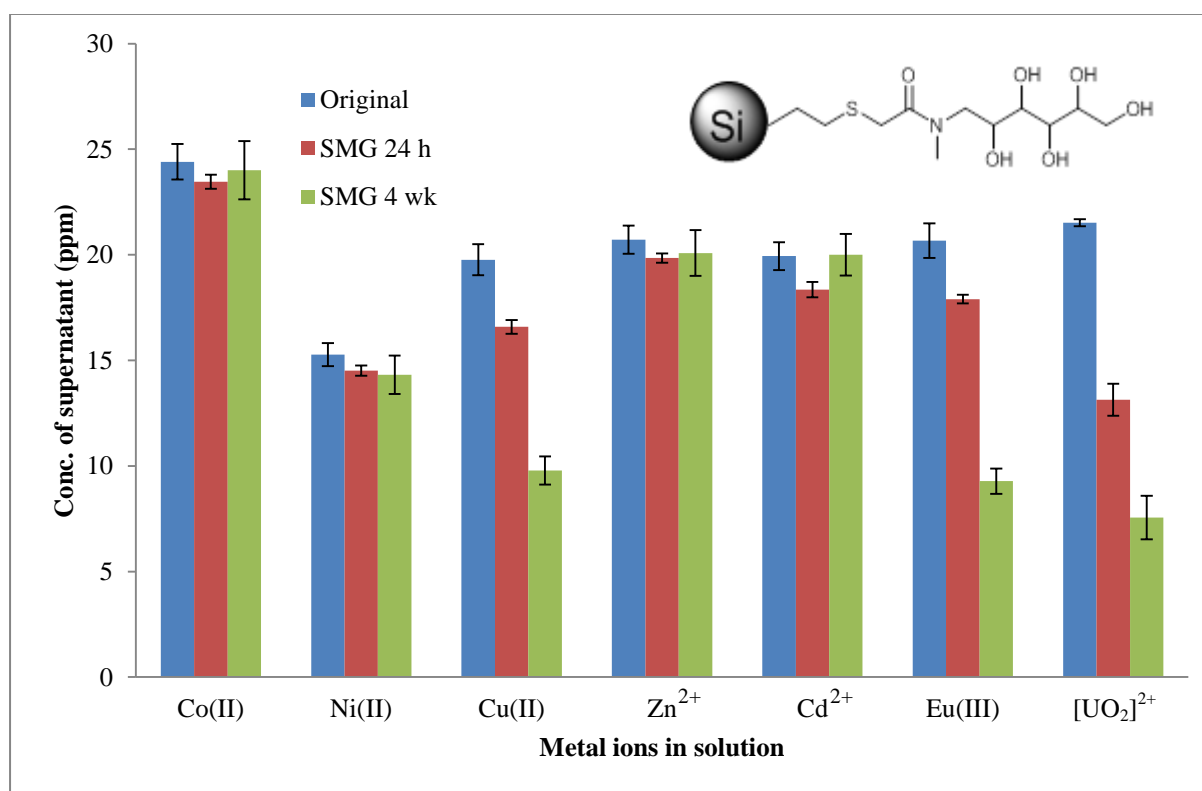


Figure 91 – Selective removal of metal by SMG from a mixed solution over 24 h and 4 w. Cu(II), Eu(III) and [UO<sub>2</sub>]<sup>2+</sup> were all reduced in concentration after 24 h and significant amounts were removed after 4 w.

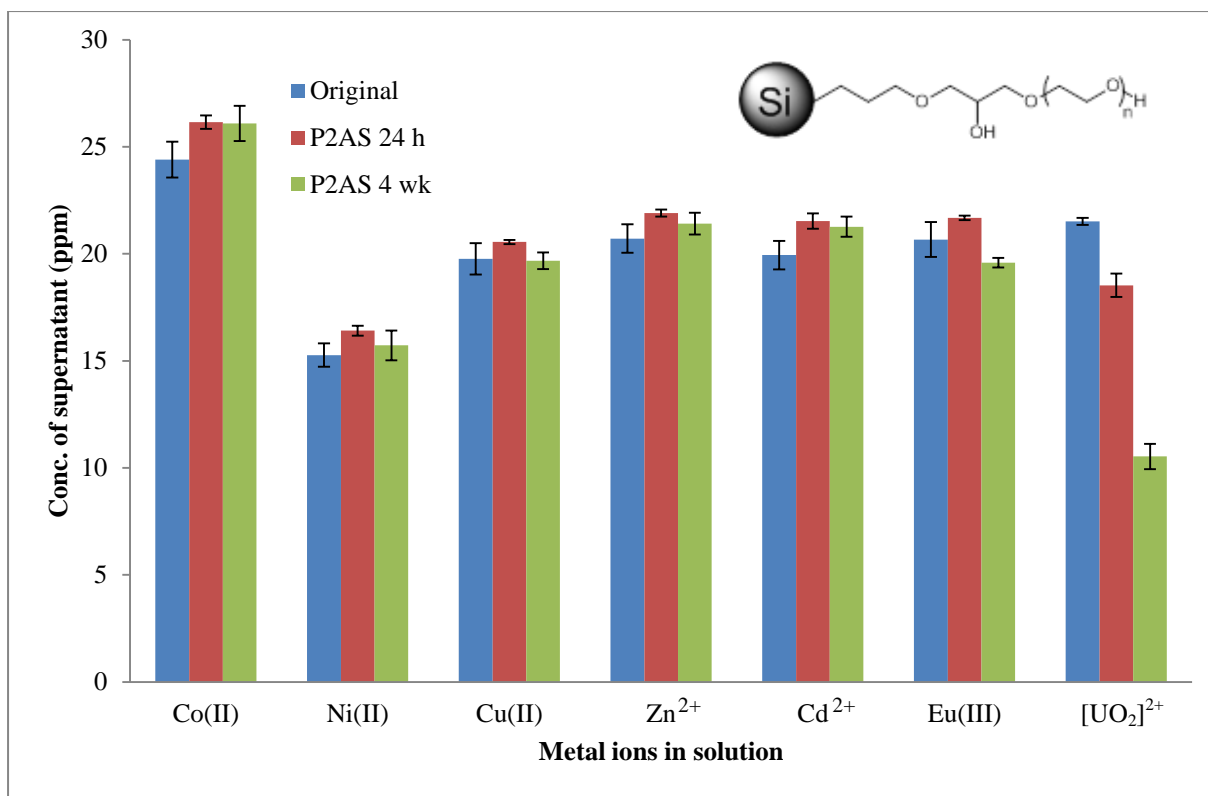


Figure 92 – Selective removal of metal by P2AS from a mixed solution over 24 h and 4 w. No significant change to concentrations other than [UO<sub>2</sub>]<sup>2+</sup> is observed, especially after 4 w where selective removal of [UO<sub>2</sub>]<sup>2+</sup> is apparent.

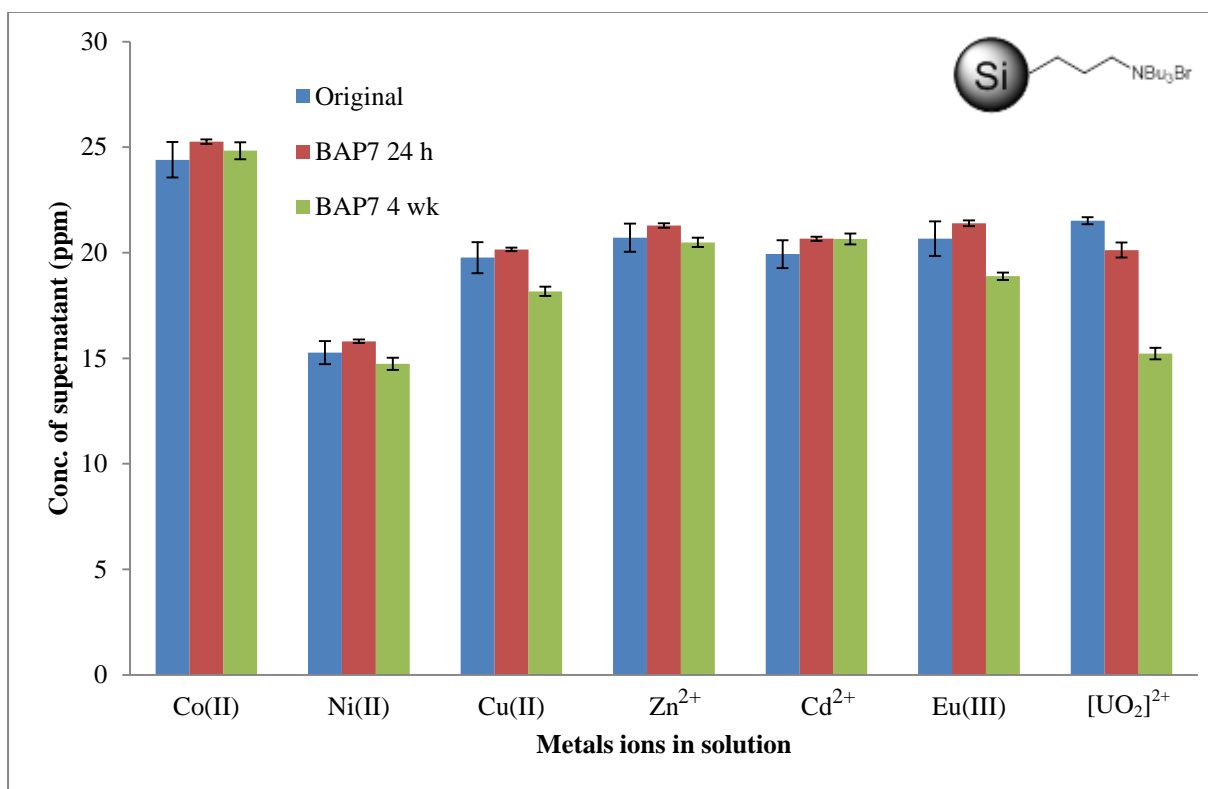
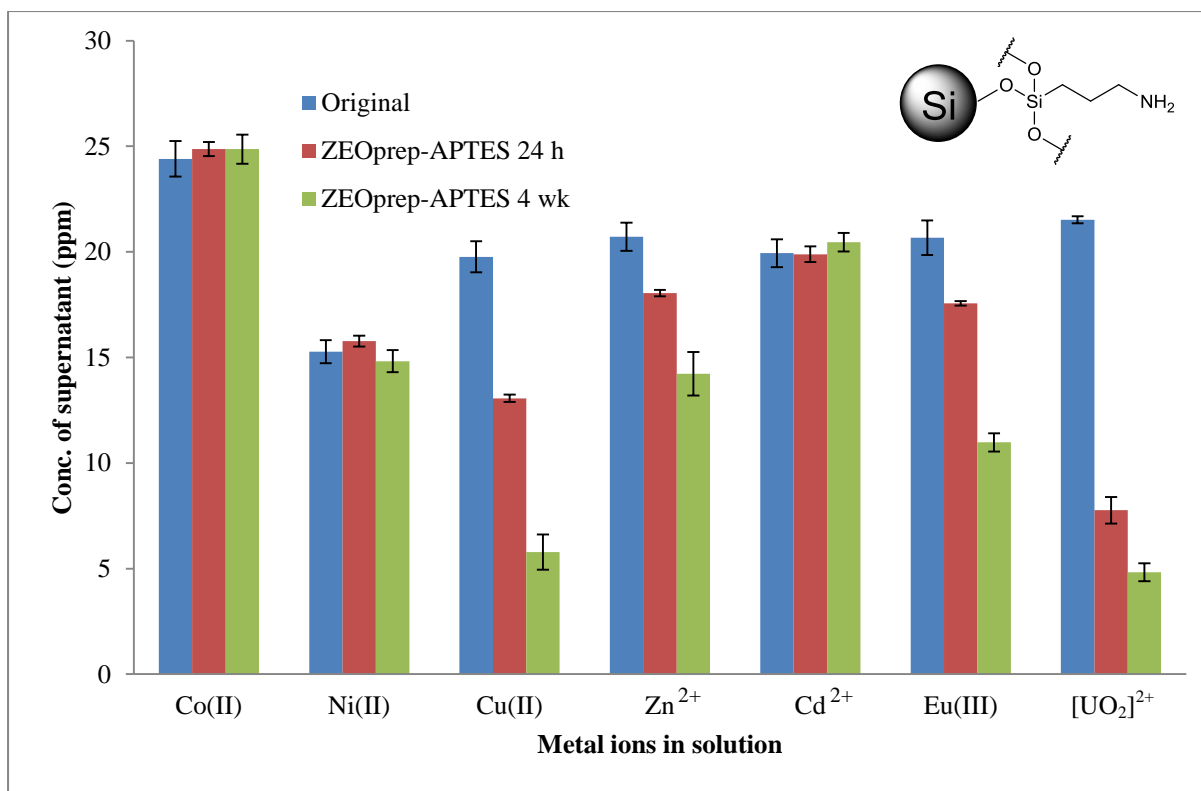
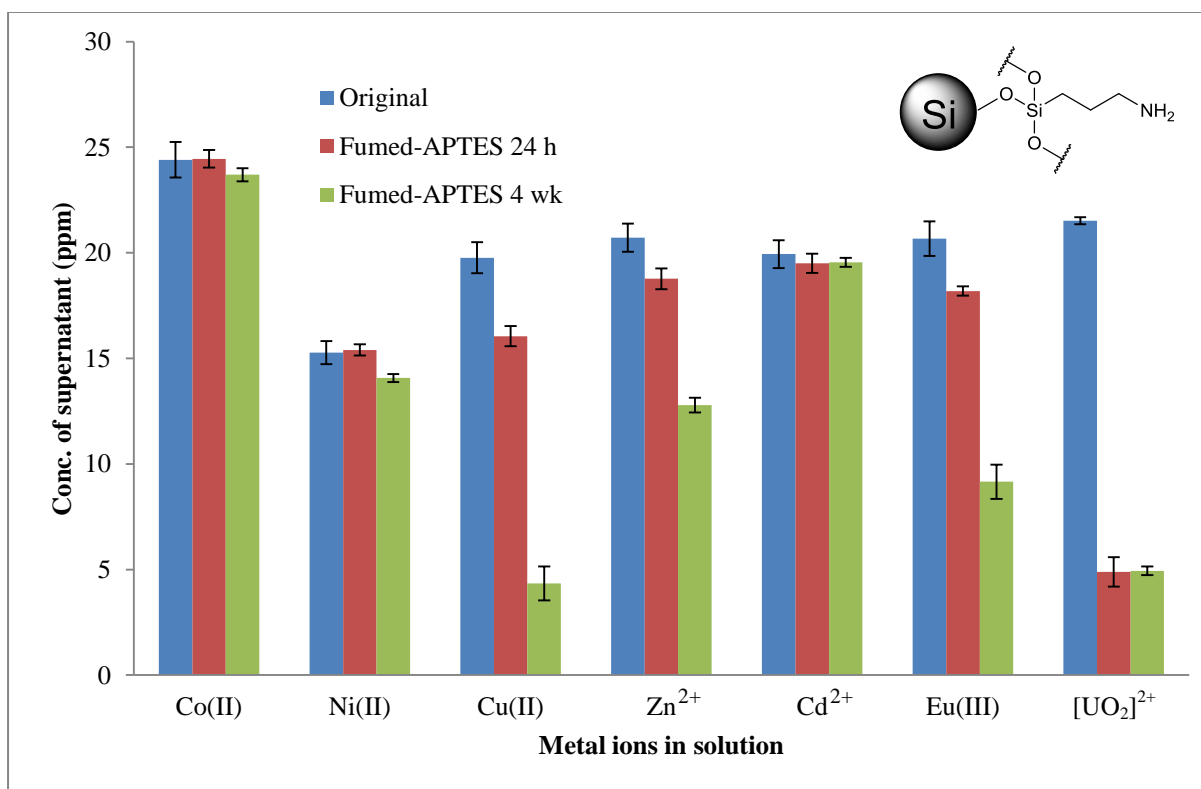


Figure 93 – Selective removal of metal by BAP7 from a mixed solution over 24 h and 4 w. No significant change in concentration was observed after 24 h but after 4 w, a reduction in [UO<sub>2</sub>]<sup>2+</sup> concentration was observed.



**Figure 94 – Selective removal of metal by ZEOprep Si-APTES from a mixed solution over 24 h and 4 w. After 24 h, it was clear that Cu(II), Zn<sup>2+</sup>, Eu(III) and [UO<sub>2</sub>]<sup>2+</sup> were favoured by APTES and this remained the case after 4 w.**



**Figure 95 – Selective removal of metal by fumed Si-APTES from a mixed solution over 24 h and 4 w. Selective removal of Cu(II), Zn<sup>2+</sup>, Eu(III) and [UO<sub>2</sub>]<sup>2+</sup> was observed but lower concentrations were reached than Figure 94.**

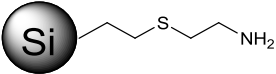
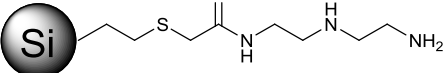
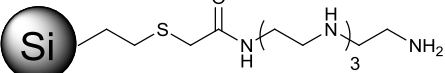
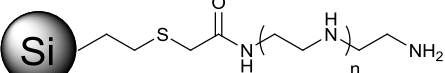
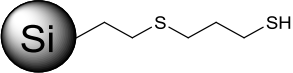
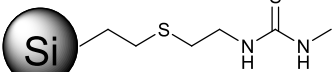
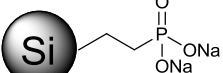
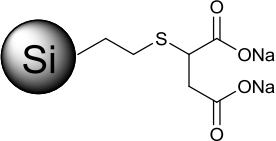
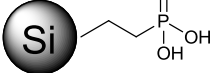
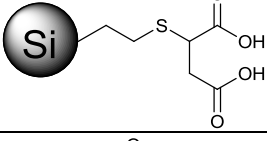
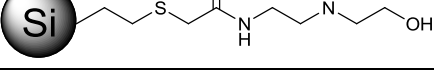
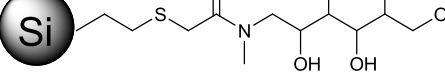
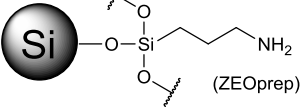
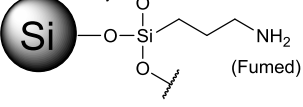
Across the range of ligands used, Co(II), Ni(II) and Cd<sup>2+</sup> proved to be the least favourable to remove. In examples where these three metals have been removed, all the divalent metal ions have shown a reduction in concentration leaving little to no selectivity.

The remaining four cations that were tested have been tabulated to assess the selectivity as a percentage of the total amount of metal removed. The total concentration removed (in ppm) is also included to help make comparisons. P2AS and BAP7 have not been included because the data is very misleading. Although selectivity for the uranyl ion was observed in the conditions tested, total concentration removed was less than 10 ppm (as opposed to the 23 – 56 ppm observed by the other materials).

PO1 and APTES-functionalised fumed silica removed the largest amount of metal ions at over 56 and 53 ppm respectively (from a total of 142 ppm) with 50 mg of material added to a 45 mL solution (as was the case in all scenarios). The most selective for the uranyl ion was SPAf (the fourth material discussed in Table 42) with a selectivity ratio of 3.3 : 1 [UO<sub>2</sub>]<sup>2+</sup> : Zn<sup>2+</sup>. Nitrogen containing ligands demonstrated a strong affinity for the uranyl ion. Interestingly however, increasing the number of nitrogen atoms did not increase the quantity of [UO<sub>2</sub>]<sup>2+</sup> removed or its selectivity over other metal ions.

Conversely, nitrogen containing ligands were found to be poor for the sequestration of Eu(III) and sulfur also appeared to have little effect. When oxygen atoms were present however, Eu(III) removal made up over 40 % of the ions removed (see POH1). Limited selectivity of Eu(III) could be achieved however as [UO<sub>2</sub>]<sup>2+</sup> was also removed well by oxygen containing ligands, illustrating that selectively removing one over the other would be extremely challenging.

The highest amount of Cu(II) removal was achieved with the use of SPM32 when over 53 % of the ions removed were Cu(II) however only 22.88 ppm was removed in total. In terms of metal binding ability, only sulfur atoms are present in this material suggesting that this would be the most ideal ligand to use when attempting to separate Cu(II) ions from the species discussed. A discussion on the details of these findings follows Table 42.

Surface attached ligands	% Cu(II) removed	% Zn <sup>2+</sup> removed	% Eu(III) removed	% [UO <sub>2</sub> ] <sup>2+</sup> removed	Total conc. removed
	27 ± 1	12 ± 3	8 ± 1	49 ± 1	40.83 ppm
	22 ± 1	11.3 ± 0.7	3 ± 1	49 ± 3	37.85 ppm
	16 ± 1	14.2 ± 0.7	1.3 ± 0.3	38 ± 1	39.60 ppm
	10 ± 1	12.9 ± 0.9	4 ± 0.5	42 ± 6	32.00 ppm
	53 ± 2	6 ± 1	7.6 ± 0.5	20.4 ± 0.9	22.88 ppm
	49 ± 2	7 ± 1	6 ± 0.4	17.4 ± 0.7	32.62 ppm
	15 ± 4	11 ± 4	32 ± 2	30.9 ± 0.7	56.02 ppm
	28 ± 0.7	1 ± 1	34.5 ± 0.8	35.5 ± 0.5	45.40 ppm
	9.5 ± 0.5	6 ± 0.4	41 ± 2	38.7 ± 0.4	44.06 ppm
	23 ± 2	1 ± 1	33.4 ± 0.5	45 ± 3	25.00 ppm
	29 ± 3	10 ± 4	10 ± 3	50 ± 3	30.95 ppm
	27 ± 2	2 ± 3	31 ± 2	37 ± 3	37.24 ppm
	30 ± 2	14 ± 2	20.9 ± 0.9	36 ± 0.9	43.30 ppm
	29 ± 2	14.8 ± 0.7	21 ± 2	30.8 ± 0.4	53.74 ppm

**Table 42 – The difference in metal ion uptake observed from each ligand based on the total concentration of metal ions removed. Total concentration removed is also stated for comparisons. Results were obtained after 4 weeks.**

To help explain the selectivity findings, hard soft acid base (HSAB) theory was used in order to improve the understanding and explanation of these results.

The HSAB theory is a concept widely used in chemistry for explaining the stability of compounds, reaction mechanisms and pathways. Ralph Pearson introduced the concept in the early 1960's in an attempt to explain and unite inorganic and organic reaction chemistry. The terms 'hard' and 'soft', 'acid' and 'base', refer to chemical species. Species that are small, with high charge states and are weakly polarisable refers to 'hard' species, whilst 'soft' is assigned to a species that is big, holds a low charge state and is strongly polarisable.

HSAB theory is used where qualitative descriptions in the understanding of the factors which drive chemical reactions and provide chemical properties are required over a quantitative explanation.<sup>229</sup>

Table 43 and Table 44 illustrate the hard, soft and intermediate (borderline) acids and bases according to Pearson<sup>230</sup> and Hancock *et al.*<sup>26</sup> The tables provide a reliable reference when considering the selectivity observed in this work.

Hard	Soft	Borderline
$H^+$ , $Li^+$ , $Na^+$ , $K^+$	$Cu^+$ , $Ag^+$ , $Au^+$ , $Tl^+$ , $Hg^+$ , $Cs^+$ , $I^+$ , $Br^+$	$Fe^{2+}$ , $Co^{2+}$ , $Ni^{2+}$
$Be^{2+}$ , $Mg^{2+}$ , $Ca^{2+}$ , $Sr^{2+}$ , $Sn^{2+}$	$Pd^{2+}$ , $Cd^{2+}$ , $Pt^{2+}$ , $Hg^{2+}$	$Cu^{2+}$ , $Zn^{2+}$ , $Pb^{2+}$
$Al^{3+}$ , $Sc^{3+}$ , $Ga^{3+}$ , $In^{3+}$ , $La^{3+}$ , $Cr^{3+}$ , $Co^{3+}$ , $Fe^{3+}$ , $As^{3+}$ , $Ir^{3+}$	$Tl^{3+}$	$B(CH_3)_3$ , $SO_2$ , $NO^+$
$Si^{4+}$ , $Ti^{4+}$ , $Zr^{4+}$ , $Th^{4+}$ , $Pu^{4+}$ ,	$Tl(CH_3)_3$ , $BH_3$	
$VO^{2+}$	$HO^+$ , $RO^+$ , $CH_3Hg^+$ , $RS^+$ , $RSe^+$ , $RTe^+$	
$[UO_2]^{2+}$ , $(CH_3)_2Sn^{2+}$	$O$ , $Cl$ , $Br$ , $I$ , $R_3C^+$	
$Be(CH_3)_2$ , $BF_3$ , $BCl_3$ , $B(OR)_3$ , $Al(CH_3)_3$ , $Ga(CH_3)_3$ , $In(CH_3)_3$	$I_2$ , $Br_2$ , $ICN$ , etc. Trinitrobenzene, etc.	
$RPO_2^+$ , $ROPO_2^+$ , $RSO_2^+$ , $ROSO_2^+$ , $SO_3^+$ $R_3C^+$ , $RCO^+$ , $CO_2$ , $NC^+$ $I^{5+}$ $I^{7+}$ , $Cl^{7+}$ $HX$ (H bonding molecules)	Chloranil, Quinones, etc. Tetracyanoethylene, etc. $M^0$ (Metal atoms) Bulk Metals	

Table 43 – Classification of Lewis acids according to Pearson<sup>230</sup>

Hard	Soft	Borderline
H <sub>2</sub> O, ROH, R <sub>2</sub> O, NH <sub>3</sub> , RNH <sub>2</sub> , NH <sub>2</sub> NH <sub>2</sub>	R <sub>2</sub> S, RSH, SCN, R <sub>3</sub> P, R <sub>3</sub> As, (RO) <sub>3</sub> P, RNC, CO, C <sub>2</sub> H <sub>4</sub>	C <sub>6</sub> H <sub>5</sub> NH <sub>2</sub> , C <sub>5</sub> H <sub>5</sub> N, N <sub>2</sub>
F <sup>-</sup> , Cl <sup>-</sup>	I <sup>-</sup> , H <sup>-</sup> , R <sup>-</sup>	Br <sup>-</sup>
OH <sup>-</sup> , ClO <sub>4</sub> <sup>-</sup> , NO <sub>3</sub> <sup>-</sup> , RO <sup>-</sup>	RS <sup>-</sup> , CN <sup>-</sup>	N <sub>3</sub> <sup>-</sup> , NO <sub>2</sub> <sup>-</sup>
CH <sub>3</sub> CO <sub>2</sub> <sup>-</sup>	S <sub>2</sub> O <sub>3</sub> <sup>2-</sup>	SO <sub>3</sub> <sup>2-</sup>
CO <sub>3</sub> <sup>2-</sup> , SO <sub>4</sub> <sup>2-</sup>		
PO <sub>4</sub> <sup>3-</sup>		

Table 44 – Classification of Lewis bases according to Hancock *et al.*<sup>26</sup>

From the selectivity results tabulated in Table 42, it is clear that the uranyl ion is removed most effectively when nitrogen and/or oxygen ligands are present with nitrogen being slightly more effective. Using the two tables reported by Pearson<sup>230</sup> and Hancock *et al.*<sup>26</sup> [UO<sub>2</sub>]<sup>2+</sup> is expressed as a ‘hard’ along with ROH and RNH<sub>2</sub>. These two ligands are common in the structures used to modify the silica and help to explain what is observed. Similarly, Eu(III) (which is also considered as a hard Lewis acid<sup>231</sup>) is removed to greater effect when oxygen atoms are present. Both the nitrogen and oxygen appear to have a preference for [UO<sub>2</sub>]<sup>2+</sup> and hence Eu(III) is not seen to be selectively removed rather, both are removed at a higher percentage than other metals in the system.

The results also show sulfur containing structures to have a preference for Cu(II) where over 53 % (SPM32) and 49 % (MTCf) of the total metal removed were copper ions. Sulfur is considered a ‘soft’ base and Cu(II) is reported as borderline where it has shown indications of behaving as a ‘hard’ and ‘soft’ acid although in these cases appears to follow the ‘soft’ characteristics and hence explains the high selectivity observed.

HSAB theory has helped to explain the findings of this investigation but is certainly not comprehensive. Due to the finite categories of ‘hard’ and ‘soft’ HSAB theory cannot predict which hard acid may be selected over another, especially those considered ‘borderline’.

It is important to note that sulfur atoms are present in most of the materials provided by PhosphonicS Ltd due to the synthesis process that is used. It is highly likely that the selectivity of materials where oxygen and nitrogen atoms exist within the structure could be improved by removing the ‘soft’ sulfur from structures that predominantly contain hard bases.

Silica Type	Starting pH (mean)	pH after 24 h aliquot (mean)	pH after 4 wk aliquot (mean)
SEA	4.67	5.40	5.82
STA3	4.67	4.81	5.31
SPA5	4.67	4.97	5.28
SPAf	4.67	4.90	5.54
SPM32	4.67	3.92	3.74
MTCf	4.67	4.25	3.77
PO1	4.67	4.65	4.74
STMS	4.67	4.93	4.55
POH1	4.67	3.14	3.07
STMA	4.67	3.65	3.40
SDEA	4.67	5.19	5.58
SMG	4.67	4.65	4.49
P2AS	4.67	4.56	4.51
BAP7	4.67	4.66	4.69
ZEOprep Si-APTES	4.67	6.08	6.08
Fumed Si-APTES	4.67	6.16	6.27

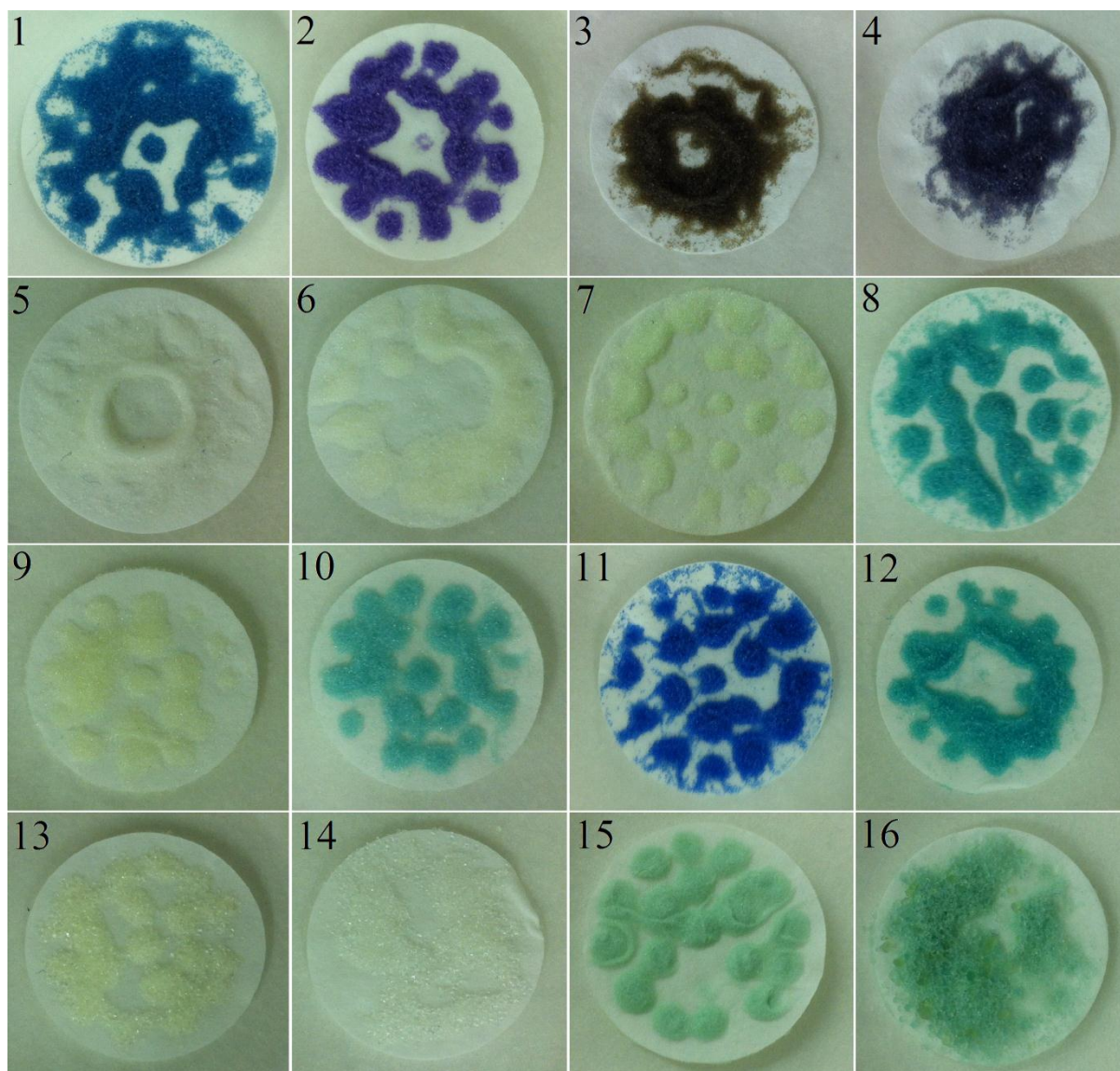
**Table 45 – pH changes to solutions upon addition of the APTES-functionalised silica after a 24 hour period and a 4 week period. Values are the mean of three different solutions tested.**

Table 45 displays the pH changes in the solutions after each silica sample had been in the solution for 24 hours and 4 weeks. The starting pH was the same for each solution as a 5 L solution was made before being separated into batches – this way the initial concentrations of each ion across the batch of experiments could be kept the same and make comparisons much simpler. Nothing unusual was found: those with more acidic groups such as POH1 and STMA had reduced the initial concentrations by over one pH unit whilst those with basic groups such as SEA and APTES had increased the pH by over one pH unit.

Figure 96 is a collection of the images of silica after a period of four weeks in the mixed metal solutions. Strong colour changes could be seen after 3-4 minutes in some of the samples and this gave a good indication to expect a change in concentration. Sample 14 (P2AS) did not significantly change colour and when the results of this material are reviewed in Figure 93, it was one of the poorer performers where only a small reduction of uranium was observed. A limited change in concentration was also observed for copper and europium



but these changes were very low in comparison to other ligands tested. The remaining metal ions in the solution effectively remained at starting concentrations.



**Figure 96 – Silica samples after being in the mixed metal solutions for 4 weeks. Colour changes could be seen in most cases after ca. 3-4 minutes. (1) SEA, (2) STA3, (3) SPA5, (4) SPAf, (5) SPM32, (6) MTCf, (7) PO1, (8) STMS, (9) POH1, (10) STMA, (11) SDEA, (12) SMG, (13) P2AS, (14) BAP7, (15) ZEOprep Si-APTES, (16) Fumed Si-APTES. Structures for the codes can be found in Table 41.**

The reversibility of the metal ion attachment to these materials was tested by taking the silica after the four week period (as seen in Figure 96) in the mixed metal solutions and put back into a 45 mL solution of deionised water for one week. This water was the same as that used to make the original mixed metal solutions and its pH was measured to be 5.77. The levels that were washed back into the water from the material were so low that ICP-OES could not detect any change to the solutions as they were below its limit of detection. Instead they were

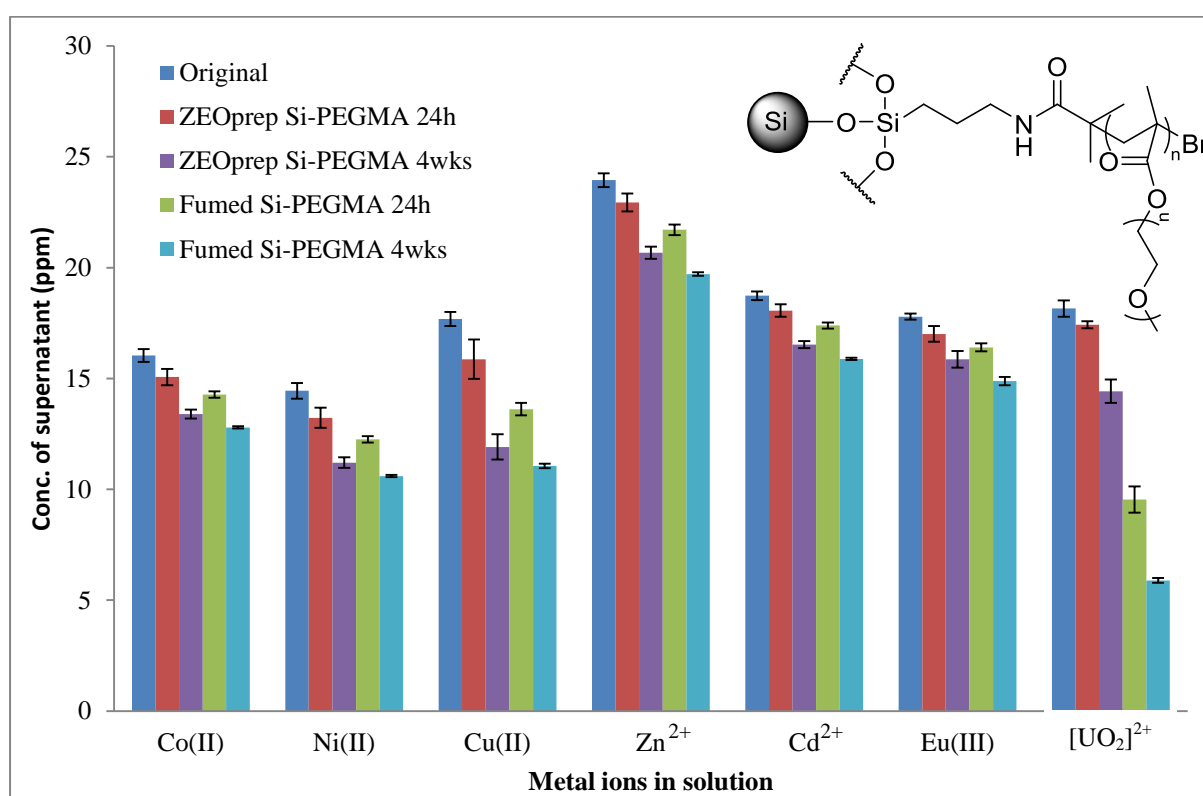
run on the ICP-MS to quantify this amount and the data for these can be found in Appendix 2 – Reversibility and dissolution of metal ions following sequestration. The largest amount to be washed off any material was 0.21 ppm Cu(II) from SEA. A range of ions were leached into the water at levels between 0.05 and 0.18 ppm but many of the waters did not reach levels greater than 0.04 ppm suggesting strong ligand attachment to the sorbent. This also essentially eradicates the suggestion that the metal ions may simply be sticking to the surface of the materials due to precipitation from the local pH change.

Silica Type	[Co] ppb	[Ni] ppb	[Cu] ppb	[Zn] ppb	[Cd] ppb	[Eu] ppb	[U] ppb
Blank	5.5 ± 0.1	7.3 ± 0.7	2 ± 2	<LOD	5.7 ± 0.6	4 ± 6	3.6 ± 0.4
SEA	19 ± 2	19 ± 2	210 ± 23	169 ± 24	25 ± 2	<LOD	3.9 ± 0.5
STA3	19 ± 0.5	28 ± 2	135 ± 4	175 ± 13	22 ± 1	15 ± 3	5.2 ± 0.4
SPA5	24 ± 1	53 ± 2	14 ± 0.8	145 ± 11	77 ± 5	15 ± 2	14 ± 3
SPAf	18.3 ± 0.4	22.2 ± 0.3	3.4 ± 0.7	95 ± 3	121 ± 3	19 ± 2	22.5 ± 0.8
SPM32	12.4 ± 0.7	13.4 ± 0.9	17 ± 2	5 ± 2	15 ± 1	2.2 ± 0.5	13.8 ± 0.6
MTCf	13 ± 0.3	12.7 ± 0.5	18 ± 4	6 ± 1	36 ± 12	4 ± 1	20 ± 2
PO1	59 ± 3	41 ± 3	43 ± 4	49 ± 3	57 ± 3	<LOD	6.7 ± 0.4
STMS	27 ± 2	23 ± 2	27 ± 4	21 ± 3	30 ± 3	<LOD	8.5 ± 0.8
POH1	14 ± 1	14 ± 0.6	3.9 ± 0.7	5 ± 1	14 ± 2	<LOD	4.4 ± 0.5
STMA	11.3 ± 0.9	10.3 ± 0.8	1.1 ± 0.2	2 ± 1	12 ± 1	<LOD	7 ± 7
SDEA	16.9 ± 0.4	14.5 ± 0.5	96 ± 12	73 ± 34	21 ± 1	<LOD	4.6 ± 0.9
SMG	22.1 ± 0.4	18.8 ± 0.7	20 ± 2	17 ± 5	24 ± 2	1 ± 2	9.3 ± 0.3
P2AS	18 ± 1	15 ± 1	8 ± 1	12 ± 3	19.4 ± 0.8	<LOD	17 ± 4
BAP7	12.9 ± 0.6	13 ± 1	10 ± 1	8 ± 2	15 ± 1	5 ± 2	54 ± 4
ZEOprep- APTES	14.6 ± 0.5	13.8 ± 0.8	68 ± 10	91 ± 11	23 ± 2	27 ± 0.9	7 ± 4
Fumed Si- APTES	18.5 ± 0.8	15 ± 2	87 ± 7	110 ± 6	31 ± 1	89 ± 13	5 ± 1

**Table 46 – Concentration of metal ions measured in the water samples following reversibility investigations. Blank indicates the natural deionised water levels as a reference. The error is calculated as the standard deviation of five samples recorded by ICP-MS.**

For many examples in Table 46, the concentration of Eu(III) ions are below the limit of detection which shows that however much of this species is attached, unquestionably is not coming off in a solution of water.

It was also noticed (as mentioned in chapter 4) that the chemical structure of P2AS is essentially the same as PEGMA. Due to this observation and the fact that no polymer or surface attached polymer used had yet produced successful results for metal sequestration, PEGMA functionalised silica was produced on both the ZEOprep and the fumed silica materials (Figure 97). Similar results were found to the P2AS although a reduction in the copper concentration was noticeable which was not observed with the P2AS material. A likely reason for this is the larger number of repeat units and hence oxygen atoms in the PEGMA functionalised silica resulting in the removal of more ions over a given period of time.



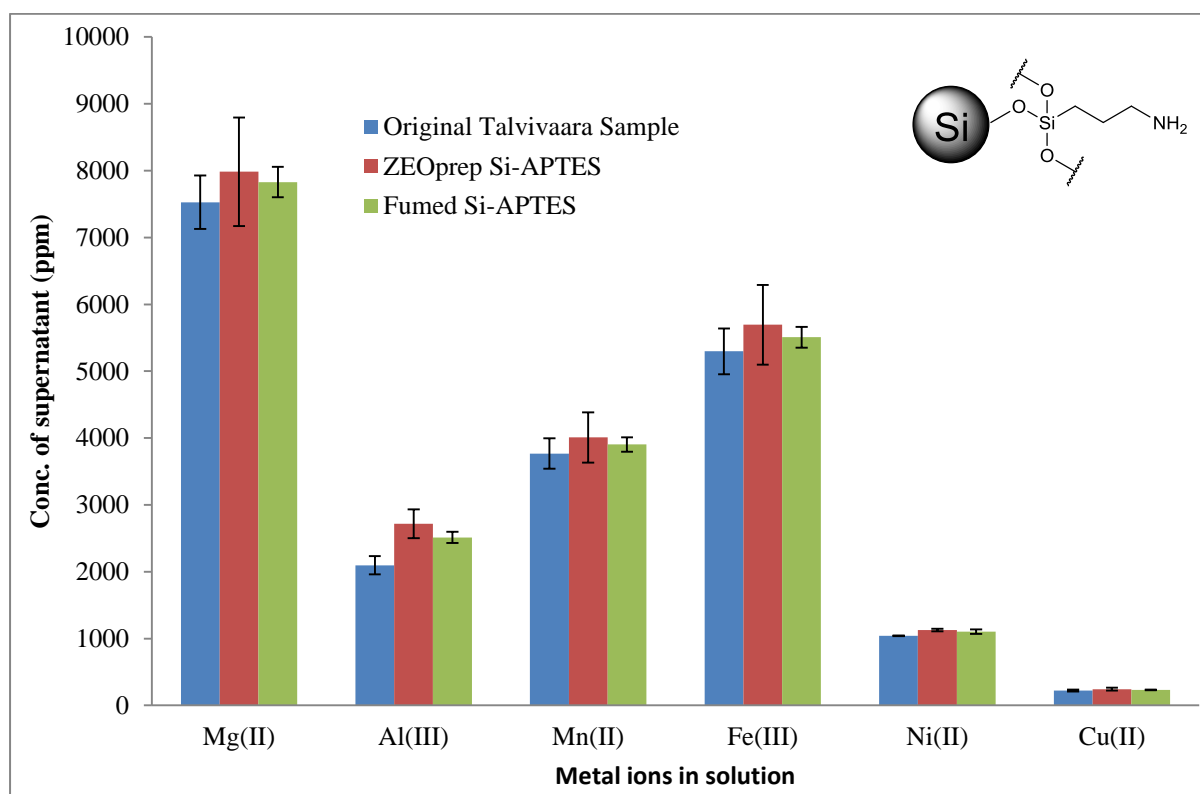
**Figure 97 - Selective removal of metal by PEGMA functionalised silica (the only surface grafted polymer tested that showed significant changes to a solution) from a mixed solution over 24 h and 4 w. Overall, [UO<sub>2</sub>]<sup>2+</sup> was again found to be reduced in concentration the most with copper being the next selected metal ion. All concentration levels of the remaining metal ions were reduced by similar amounts, ca. 2-3 ppm.**

## 7.2.2 Talvivaara mine water sample

Initially the mine water sample was diluted and analysed by ICP-OES for all possible elements. This was compared to a 50 ppm solution of a 28 element standard to give an indication of what was present and their concentrations. These early tests found the elements iron, magnesium and manganese to fall outside the limits of detection but were found to be

present in very high concentrations once further dilutions had been carried out. Uranium is also known to be present in the water at Talvivaara<sup>232</sup> but due to the dilutions required to analyse the exceptionally high concentration of transition metals, the uranium was too dilute to analyse *via* this method, hence was not investigated and left for future work.

Although Talvivaara is known primarily for its nickel production it is important to understand why such high concentrations of other metals were discovered when analysed. The mine is expected to produce about 60000 t year<sup>-1</sup> of zinc, 10000 t year<sup>-1</sup> of copper and 1200 t year<sup>-1</sup> of cobalt. The process plant processes 600 m<sup>3</sup> h<sup>-1</sup> of the PLS solution and consists of copper recovery, zinc recovery, neutralisation and aluminium removal, nickel and cobalt recovery, iron removal and then final precipitation. Manganese is also known to be present in high concentration whilst a number of mineral ores are also listed.<sup>224,227,233,234</sup>



**Figure 98 – Talvivaara metal concentrations before and after attempted removal with APTES-functionalised ZEOprep and fumed silica materials. The silica materials were added to the original solution but all analysis carried out *via* ICP-OES was done once the samples had been diluted to within range of the ICP sensitivity before being calculated back up.**

Figure 98 for all intents and purposes shows that the APTES-functionalised silica has had no effect as all concentrations of metal have remained essentially unchanged. Following the pH study conducted on europium(III) in the previous chapter, solutions below pH 3 would be

expected to show little to no change when the silica attached APTES materials are used for sequestration. This PLS solution was recorded to be pH 2.50 and hence the conditions appear too harsh for any effect to be seen. This also supports the literature of Vezenov *et al.*<sup>199</sup> that the  $pK_a$  of APTES is ca. 3.9.

### 7.3 Conclusion

The results reported in this chapter have successfully demonstrated some selective properties of the ligands in these environments, but also the limits in which they function. The solutions of multiple metals at similar concentrations in which the materials were tested for their selectivity has produced a series of substantial findings. In each case, results and observations clearly display preferences for particular metal ions over others, with the most common being the uranyl ion. Other metal ions that proved to be more readily removed *via* this method and the ligands tested were copper and europium ions. Zinc, cadmium, nickel and cobalt ions were not observed to significantly reduce in concentration following these sequestration tests.

Concerns were raised that the uranyl ion may be precipitating from the solution due to the change in local pH as it was this ion that was commonly being significantly reduced in concentration. No sign of this was observed by simply looking at the solution where it might be expected that precipitation would be evident. However, this was tested by filtering off all solid and added back to a new solution of deionised water before being run on the ICP-MS. This found that all metal ions appeared to be strongly bound to the materials as none of the metal concentrations increased beyond 0.21 ppm which was the copper ion from the 'SEA' material.

HSAB theory has been used to help understand some of the selectivity observations that have been made throughout the studies. Although it does not explain all the observations, it provides a strong argument for why the large increase in selective removal of Cu(II) ions where sulfur ligands were used was observed and why  $[UO_2]^{2+}$  was removed well with nitrogen and oxygen based ligands. To build a more complete table of selectivity, instances where two metal ions were removed well could be made up into a solution of their own to determine the true preference and selectivity factor of one over the other.

As reported in the body of the results and discussion, the initial pH of the solutions produced were relatively mild at pH 4.67. Although slightly acidic, this fell within the range that illustrated very good results for the europium cation in chapter 6. The nature of the ligand

attached to the silica determined how the pH of the solution changed and this varied from 3.07 (POH1) to 6.27 (APTES-functionalised fumed silica).

Talvivaara mine water was used as an extreme example of where these materials could be used to help selectively extract metals to assist with the mining of them. However, all attempts to use the APTES ligand failed and this was largely down to the harsh acidic pH conditions. Other factors may include the large number of competing ions in the solution but as chapter 6 showed, once the pH falls below 3, no significant reduction in concentration is observed. This shows that these conditions are out of the range of the metal sequestration capability of the APTES ligand and cannot be used for this.

## **7.4 Future Work**

The seven metal systems that were synthesised for selectivity investigations were designed to produce a solution that offered differing metals in terms of their oxidation state and natural existence but also included metal ions that offered very similar properties. This has led to stimulating findings and new knowledge on the preferences of metal ions by the ligands trialled but on most occasions more than one metal ion was significantly reduced in concentration. In order to improve the understanding of the ligands preference it is suggested that a solution be made where the most selected metal ions are the only ones used in a second solution and the materials in question are then tested for their selectivity when other competition is removed.

pH is obviously a key factor in these investigations and by altering the starting pH to a more acidic or alkali environment would be sure to reveal differing preferences for the ligands although precipitation would need to be avoided in these environments.

It is unlikely that many, if any of the PhosphonicS ligands tested in this work would be able to deal with the harsh conditions that Talvivaara's mine water offers but as these were not tested due to a finite amount of sample, these tests would complete the investigation.

As the uranium concentration fell below the limit of detection once the solution was diluted down to keep the majority of ions within the limit of detection and quantification, studying the concentration change of this ion *via* ICP-MS could provide significant results due to how successful results were when removing it from the synthetic solutions. Again, the pH of the solution may just be too harsh for any effect to be had.

Following the results of these investigations and the highly likely scenario that none of the ligands are adequate, it is proposed that more appropriate and efficient materials and methods are studied for these extreme conditions.

## 8 Summary and concluding remarks

This project has produced some exciting and novel results in which thorough analysis and characterisation of the synthesised materials have provided a detailed understanding of the materials structures. The modular approach enabled the break down of the overall aim into shorter projects which as a result, benefitted the development with a detailed method to each of the chapters discussed.

Although some topics of the project were not as successful as others such as the free polymer modification synthesis, a lot was learnt from it. An alternative approach to the post-polymerisation functionalisation has been discussed and there is good reason to believe this would be successful. From the success of the work in chapter 7 where selectivity studies were carried out, a large number of ligands have demonstrated to be worth using and if these could be attached to an unsaturated monomer, ATRP or ARGET ATRP could still demonstrate to have a use in this work. Failing this, one of many other polymerisation techniques, albeit not as controlled, could still provide a process by which a highly functionalised and large surface area, solid supported material could be produced.

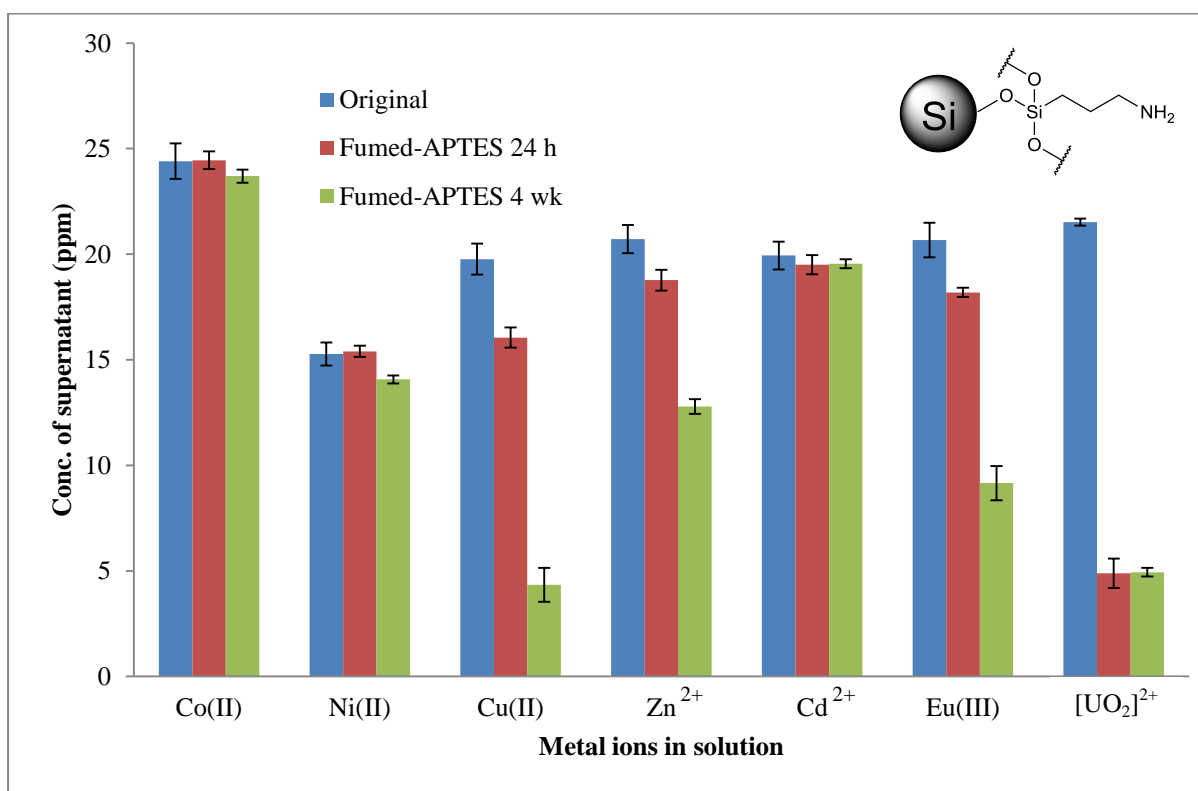
The characterisation techniques have been used in a supportive way to help reinforce the information provided by the other. Most effectively, SSNMR has shown the successful attachment of APTES, BIBB and PHEMA whilst TGA has shown a larger amount of organic material burning off following each step. Meanwhile elemental analysis showed an increase in carbon content following the attachment of APTES and BIBB before an even larger increase of carbon (9.39 % and 30.17 %) was observed before the HEMA had been polymerised from the surface. Using the nitrogen content increase also permitted the moles of APTES attached to the silica surface to be calculated and allowed a comparison of the two different silica materials discussed in detail in this thesis to be made. Table 47 is a replicate of that found in chapter 5 but demonstrates the difference in moles of APTES attached to one gram of silica. Surprisingly the difference is not that great considering the particles are so different in size, but the two techniques used to calculate these values did find quite similar and hence reliable values for this investigation.



Material	TGA	CHN
ZEOprep Si-APTES	$1.51 \times 10^{-3} \text{ mol g}^{-1}$	$1.14 \times 10^{-3} \text{ mol g}^{-1}$
Fumed Si-APTES	$1.63 \times 10^{-3} \text{ mol g}^{-1}$	$1.59 \times 10^{-3} \text{ mol g}^{-1}$

**Table 47** – Comparison of values for silica attached APTES *via* TGA and CHN calculations as reported in Table 13 in chapter 5.

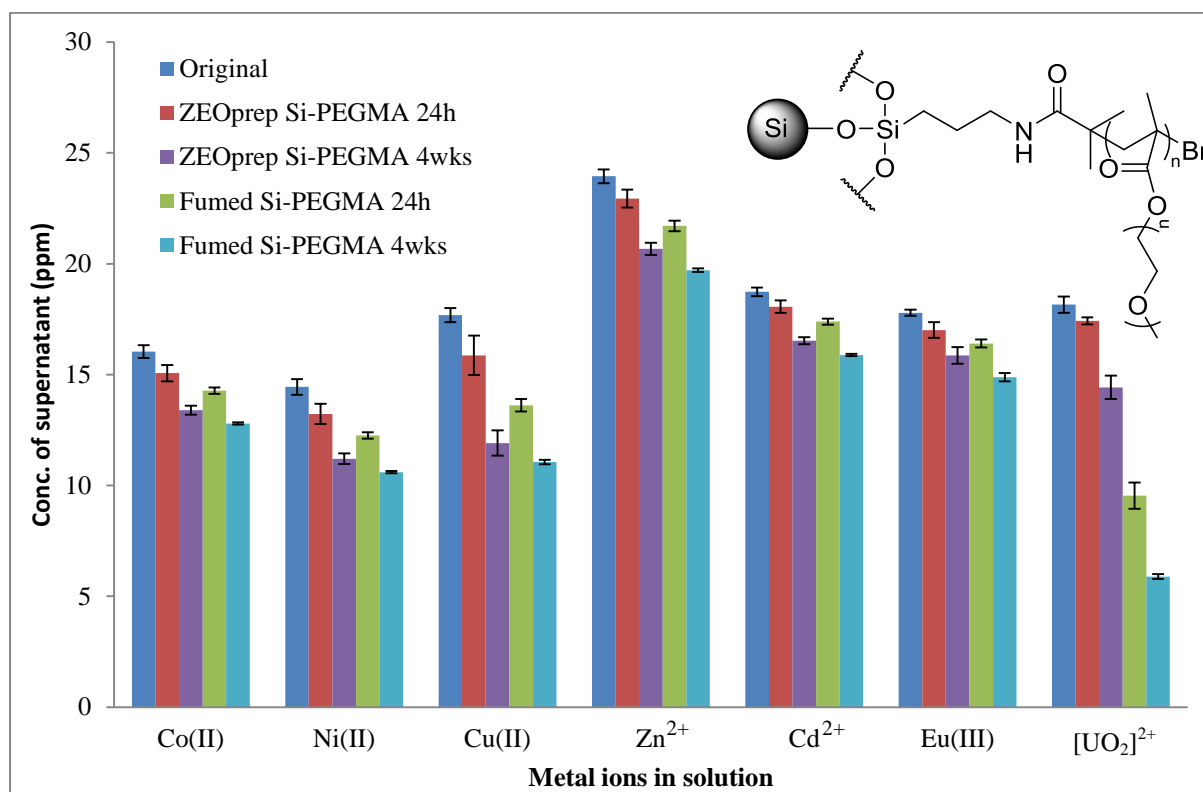
When the APTES-functionalised ZEOprep and fumed silice were tested for the ability to remove metals in a non-competitive solution, very high  $R_d$  values were recorded. When compared to work reported from groups who have measured this value, these materials prove to be extremely competitive.<sup>14,23,45,181</sup> A limited effect was had on these values when  $\text{Na}^+$  and  $\text{Ca}^{2+}$  were added to the solutions at ca. 1 % (w/w) concentration suggesting that these materials would be able to function in environments such as sea water.



**Figure 99** – Selective removal of metal APTES-functionalised fumed silica from a mixed solution over 24 h and 4 w. Originally reported in chapter 7, see Figure 95.

The selectivity work reported in chapter 7 brings together the work of the previous chapters and demonstrates an end product being applied for what it was designed to do. The results that followed then validated the reasons for this research, showing significant selectivity differences between the materials. APTES-functionalised silica demonstrated strong selectivity whilst the materials supplied by PhosphonicS significantly reduced the time spent

on synthesis allowing for more investigations to be carried out on the ligands' behaviour. It is clear that the project has benefitted considerably from this with fifteen different ligands tested in total. PEGMA functionalised silica (see Figure 100) was produced based on the results of the P2AS material, once again demonstrating the significance of collaboration with PhosphonicS.



**Figure 100 – Selective removal of metal by PEGMA functionalised silica from a mixed solution over 24 h and 4 w.**  
Originally reported in chapter 7, see Figure 97.

Aside from the future work discussed at the end of each chapter, the project as a whole would benefit from considering which methodology would work best in a 'real-world' case. It is highly unlikely that one method would ever fit all circumstances, hence materials such as the silica coated SMP were briefly investigated in this work. Discussions on specific methodology have taken place such as the use of dialysis tubing whereby the material would be packed inside the tubing and once extraction of metal ions had taken place, removal of the tubing and with it the target contaminant, can be implemented. These discussions have led to grant applications being submitted and the group is optimistic that this research will be continued.

## 9 References

- 1 M. I. Ojovan and W. E. Lee, *Met. Mater. Trans. A*, 2011, 42A, 837–851.
- 2 H. H. Anderson and L. B. Asprey, 1960, 2–5.
- 3 F. Lewis, M. Hudson, and L. Harwood, *Synlett*, 2011, 18, 2609–2632.
- 4 T. G. Carter, W. Yantasee, T. Sangvanich, G. E. Fryxell, D. W. Johnson, and R. S. Addleman, *Chem. Commun.*, 2008, 5583–5585.
- 5 B. E. Johnson, P. H. Santschi, R. S. Addleman, M. Douglas, J. Davidson, G. E. Fryxell, and J. M. Schwantes, *Anal. Chim. Acta*, 2011, 708, 52–60.
- 6 A. Saglan, S. Bektas, S. Patir, O. Genc, and A. Denizli, *React. Funct. Polym.*, 2001, 47, 185–192.
- 7 G. E. Fryxell, S. V. Mattigod, Y. Lin, H. Wu, S. Fiskum, K. Parker, F. Zheng, W. Yantasee, T. S. Zemanian, R. S. Addleman, J. Liu, K. Kemner, S. Kelly, and X. Feng, *J. Mater. Chem.*, 2007, 17, 2863–2874.
- 8 K. McEleney, D. P. Allen, A. E. Holliday, and C. M. Crudden, *Org. Lett.*, 2006, 8, 2663–2666.
- 9 P. Liu, Y. Liu, and Z. Su, *Ind. Eng. Chem. Res.*, 2006, 45, 2255–2260.
- 10 B. F. Şenkal and N. Biçak, *React. Funct. Polym.*, 2001, 49, 151–157.
- 11 A. Gopalan, H. Jacobs, N. Koshti, P. Stark, V. Huber, L. Dasaradhi, W. Caswell, P. H. Smith, and G. Jarvinen, *5th Annu. WERC Tech. Devel. Conf.*, 1995, 123–132.
- 12 W. Bisset, H. Jacobs, N. Koshti, P. Stark, and A. Gopalan, *React. Funct. Polym.*, 2003, 55, 109–119.
- 13 Y. Lin, S. K. Fiskum, W. Yantasee, H. Wu, S. V Mattigod, E. Vorpagel, G. E. Fryxell, K. N. Raymond, and J. Xu, *Environ. Sci. Technol.*, 2005, 39, 1332–1337.

- 14 G. Fryxell, Y. Lin, S. Fiskum, J. Birnbaum, H. Wu, K. Kemner, and S. Kelly, *Environ. Sci. Technol.*, 2005, 39, 1324–1331.
- 15 X. Feng, G. E. Fryxell, L.-Q. Wang, A. Y. Kim, J. Liu, and K. M. Kemner, *Science* (80-. ), 1997, 276, 923–926.
- 16 B. J. Liu, X. Feng, G. E. Fryxell, L.-Q. Wang, A. Y. Kim, and M. Gong, *Adv. Mater.*, 1998, 10, 161–165.
- 17 C. T. Kresge, M. E. Leonowicz, W. J. Roth, J. C. Vartuli, and J. S. Beck, *Nature*, 1992, 359, 710–712.
- 18 A. Sayari, *Chem. Mater.*, 1996, 8, 1840–1852.
- 19 K. D. Schierbaum, T. Weiss, E. U. T. van Velzen, J. F. J. Engbersen, D. N. Reinhoudt, and W. Gopel, *Science* (80-. ), 1994, 265, 1413–1415.
- 20 A. Ulman, *Chem. Rev.*, 1996, 96, 1533–1554.
- 21 W. C. Bigelow, D. L. Pickett, and W. A. Zisman, *J. Colloid Interf. Sci.*, 1946, 1, 513–538.
- 22 G. E. Fryxell, H. Wu, Y. Lin, W. J. Shaw, J. C. Birnbaum, J. C. Linehan, Z. Nie, K. Kemner, and S. Kelly, *J. Mater. Chem.*, 2004, 14, 3356–3363.
- 23 W. Yantasee, G. E. Fryxell, R. S. Addleman, R. J. Wiacek, V. Koonsiripaiboon, K. Pattamakomsan, V. Sukwarotwat, J. Xu, and K. N. Raymond, *J. Hazard Mater.*, 2009, 168, 1233–1238.
- 24 C. Kantipuly, S. Katragadda, A. Chow, and H. D. Gesser, *Talanta*, 1990, 37, 491–517.
- 25 K. Geckeler, G. Lange, H. Eberhardt, and E. Bayer, *Pure Appl. Chem.*, 1980, 52, 1883–1905.
- 26 R. D. Hancock and A. E. Martell, *Chem. Rev.*, 1989, 89, 1875–1914.
- 27 A. Gopalan and H. Jacobs, *ECM Press*, 1995.

- 28 H. Irving and R. J. P. Williams, *J. Chem. Soc.*, 1949, 1841–1847.
- 29 H. A. Panahi, N. Mehmandost, E. Moniri, and I. Y. Galaev, *J. Appl. Polym. Sci.*, 2012, 126, 480–489.
- 30 P. Liu and J. Guo, *Colloid. Surface. A*, 2006, 282-283, 498–503.
- 31 U. Paik, J. P. Kim, Y. S. Jung, Y. G. Jung, T. Katah, J. G. Park, and V. A. Hackley, *J. Korean Phys. Soc*, 2001, 39, 201–204.
- 32 A. E. Bennett, C. M. Rienstra, M. Auger, K. V. Lakshmi, and R. G. Griffin, *J. Chem. Phys.*, 1995, 103, 6951.
- 33 J. N. Miller and J. C. Miller, *Statistics and Chemometrics for Analytical Chemistry*, Pearson Education Limited, 6th edn., 2010.
- 34 L. A. Baillie, *Int. J. Appl. Radiat. Is.*, 1960, 8, 1–7.
- 35 <https://www.nationaldiagnostics.com/liquid-scintillation/article/counting-efficiency-and-quenching>, Accessed 20th Feb 2014.
- 36 <http://www.malvern.com/en/products/product-range/mastersizer-range/mastersizer-2000/default.aspx>, Accessed 10th Mar 2014.
- 37 SP Industries, *VirTis BenchTop 2K, 4K and 6K*, 2009.
- 38 K. L. Robinson, M. A. Khan, M. V. de Paz Báñez, X. S. Wang, and S. P. Armes, *Macromolecules*, 2001, 34, 3155–3158.
- 39 S. Niwayama, H. Cho, and C. Lin, *Tetrahedron Lett.*, 2008, 49, 4434–4436.
- 40 S. Edmondson, Selwyn College University of Cambridge, Ph.D Thesis, 2006.
- 41 A. Stolle, J. Ollivier, P. P. Piras, J. Salaiin, and A. de Meijere, *J. Am. Chem. Soc.*, 1992, 114, 4051–4061.
- 42 S. Karamdoust, B. Yu, C. V. Bonduelle, Y. Liu, G. Davidson, G. Stojcevic, J. Yang, W. M. Lau, and E. R. Gillies, *J. Mater. Chem.*, 2012, 22, 4881–4889.

- 43 J. Chen, M. Hu, W. Zhu, and Y. Li, *Appl. Surf. Sci.*, 2011, 257, 6654–6660.
- 44 J. J. O' Mahony, M. Platt, D. Kilinc, and G. U. Lee, *Langmuir*, 2013, 29, 2546–2553.
- 45 B. E. Johnson, P. H. Santschi, R. S. Addleman, M. Douglas, J. D. Davidson, G. E. Fryxell, and J. M. Schwantes, *Appl. Radiat. Isot.*, 2011, 69, 205–216.
- 46 Y. Yagci and M. A. Tasdelen, *Prog. Polym. Sci.*, 2006, 31, 1133–1170.
- 47 G. Odian, *Principles Of Polymerization*, 2004.
- 48 G. Moad, B. S. Sumerlin, and N. V. Tsarevsky, *Fundamentals of Controlled/Living Radical Polymerization*, Royal Society of Chemistry, 2012.
- 49 K. Matyjaszewski, *Macromolecules*, 2012, 45, 4015–4039.
- 50 J.-S. Wang and K. Matyjaszewski, *J. Am. Chem. Soc.*, 1995, 117, 5614–5615.
- 51 E. Duquesne, J. Habimana, P. Dege, and P. Dubois, *Macromolecules*, 2005, 38, 9999–10006.
- 52 C. Granel, P. Dubois, R. Jerome, and P. Teyssie, *Macromolecules*, 1996, 29, 8576–8582.
- 53 K. Matyjaszewski, M. Wei, J. Xia, and N. E. McDermott, *Macromolecules*, 1997, 30, 8161–8164.
- 54 T. Ando, M. Kamigaito, and M. Sawamoto, *Macromolecules*, 1997, 30, 4507–4510.
- 55 M. Kato, M. Kamigaito, M. Sawamoto, and T. Higashimuras, *Macromolecules*, 1995, 28, 1721–1723.
- 56 V. Percec, B. Barboiu, A. Neumann, J. C. Ronda, and M. Zhao, *Macromolecules*, 1996, 29, 3665–3668.
- 57 P. Lecomte, I. Drapier, P. Dubois, P. Teyssie, and R. Jerome, *Macromolecules*, 1997, 30, 7631–7633.

- 58 F. di Lena and K. Matyjaszewski, *Prog. Polym. Sci.*, 2010, 35, 959–1021.
- 59 K. Matyjaszewski and J. Xia, *Chem. Rev.*, 2001, 101, 2921–2990.
- 60 K. Matyjaszewski, H. Dong, W. Jakubowski, J. Pietrasik, and A. Kusumo, *Langmuir*, 2007, 23, 4528–4531.
- 61 R. Nicolaÿ, Y. Kwak, and K. Matyjaszewski, *Angew. Chem.*, 2010, 49, 541–544.
- 62 V. M. C. Coessens and K. Matyjaszewski, *J. Chem. Educ.*, 2012, 87, 916–919.
- 63 K. Min, H. Gao, and K. Matyjaszewski, *Macromolecules*, 2007, 40, 1789–1791.
- 64 K. Matyjaszewski, N. V Tsarevsky, W. A. Braunecker, H. Dong, J. Huang, W. Jakubowski, Y. Kwak, R. Nicolay, W. Tang, and J. A. Yoon, *Macromolecules*, 2007, 40, 7795–7806.
- 65 K. Matyjaszewski, W. Jakubowski, K. Min, W. Tang, J. Huang, W. a Braunecker, and N. V Tsarevsky, *P. Natl. Acad. Sci. USA*, 2006, 103, 15309–15314.
- 66 N. Chan, M. F. Cunningham, and R. A. Hutchinson, *Macromol. Chem. Physic.*, 2008, 209, 1797–1805.
- 67 S. Paterson, M. Baker, D. Brown, T. Chirila, I. Keen, and A. Whittaker, *ARGET ATRP of 2-hydroxyethyl methacrylate using ascorbic acid as a reducing agent*.
- 68 K. Matyjaszewski and T. P. Davis, *Handbook of Radical Polymerization*, 2002.
- 69 J. Clayden, N. Greeves, S. Warren, and P. Wothers, *Organic Chemistry*, 2001.
- 70 E. Mastan, D. Zhou, and S. Zhu, *J. Polym. Sci. Pol. Chem.*, 2014, 52, 639–651.
- 71 B. Zhu, Loughborough University, 2012.
- 72 N. Schüwer, T. Geue, J. P. Hinestrosa, and H. Klok, *Macromolecules*, 2011, 44, 6868–6874.
- 73 S. Edmondson and W. T. S. Huck, *J. Mater. Chem.*, 2004, 14, 730–734.

- 74 J. Kahovec and J. Coupek, *React. Polym.*, 1988, 8, 105–111.
- 75 C. Boyer, A. H. Soeriyadi, P. J. Roth, M. R. Whittaker, and T. P. Davis, *Chem. Commun.*, 2011, 47, 1318–1320.
- 76 A. S. Goldmann, M. Glassner, A. J. Inglis, and C. Barner-Kowollik, *Macromol. Rapid Commun.*, 2013, 34, 810–849.
- 77 M. Kempe, G. Barany, and P. S. S. E, *J. Am. Chem. Soc.*, 1996, 118, 7083–7093.
- 78 K. L. Thompson, E. S. Read, and S. P. Armes, *Polym. Degrad. Stabil.*, 2008, 93, 1460–1466.
- 79 J.-P. Montheard, M. Chatzopoulos, and D. Chappard, *J. Macromol. Sci. Pt. C Polym. Rev.*, 1992, 32, 1–34.
- 80 Z. Merican, D. W. Green, T. V Chirila, and I. Blakey, *Surface modification and topology profiling of PHEMA for biomaterial applications*, 2011.
- 81 K. L. Beers, S. Boo, S. G. Gaynor, and K. Matyjaszewski, *Macromolecules*, 1999, 32, 5772–5776.
- 82 S. M. Paterson, D. H. Brown, T. V. Chirila, I. Keen, A. K. Whittaker, and M. V. Baker, *J. Polym. Sci. Pol. Chem.*, 2010, 48, 4084–4092.
- 83 J. V. M. Weaver, I. Bannister, K. L. Robinson, X. Bories-Azeau, S. P. Armes, M. Smallridge, and P. McKenna, *Macromolecules*, 2004, 37, 2395–2403.
- 84 H. E. Gottlieb, V. Kotlyar, and A. Nudelman, *J. Org. Chem.*, 1997, 21, 7512–7515.
- 85 W. Huang, J.-B. Kim, M. L. Bruening, and G. L. Baker, *Macromolecules*, 2002, 35, 1175–1179.
- 86 X. Wang, X. Xiao, X. Wang, J. Zhou, L. Li, J. Xu, and B. Guo, *Macromol. Rapid Comm.*, 2007, 28, 828–833.
- 87 F. J. Xu, S. P. Zhong, Y. W. Tong, E. T. Kang, and K. G. Neoh, *Tissue Eng.*, 2005, 11, 1736–1748.



- 88 F. Zhang, Z. L. Shi, P. H. Chua, E. T. Kang, and K. G. Neoh, *Ind. Eng. Chem. Res.*, 2007, 46, 9077–9086.
- 89 C. Gao, C. D. Vo, Y. Z. Jin, W. Li, and S. P. Armes, *Macromolecules*, 2005, 38, 8634–8648.
- 90 E. L. Brantley, T. C. Holmes, and G. K. Jennings, *Macromolecules*, 2005, 38, 9730–9734.
- 91 N. V. Tsarevsky and W. Jakubowski, *J. Polym. Sci. Pol. Chem.*, 2011, 49, 918–925.
- 92 R. Krishnan and K. S. V. Srinivasan, *Macromolecules*, 2003, 36, 1769–1771.
- 93 A. Hayek, Y. Xu, T. Okada, S. Barlow, X. Zhu, J. H. Moon, S. R. Marder, and S. Yang, *J. Mater. Chem.*, 2008, 78, 1–5.
- 94 R. Barbey and H.-A. Klok, *Langmuir*, 2010, 26, 18219–18230.
- 95 M. Kim, S. Kiyohara, S. Konishi, S. Tsuneda, K. Saito, and T. Sugo, *J. Membr. Sci.*, 1996, 117, 33–38.
- 96 C. Liu, R. Bai, and L. Hong, *J. Colloid Interf. Sci.*, 2006, 303, 99–108.
- 97 D. Williams and I. Fleming, *Spectroscopic methods in organic chemistry; 6th Edn*, McGraw-Hill Higher Education, 6th edn., 2008.
- 98 R. Barbey, L. Lavanant, D. Paripovic, N. Schüwer, C. Sugnaux, S. Tugulu, and H.-A. Klok, *Chem. Rev.*, 2009, 109, 5437–5527.
- 99 G. W. Kabalka, M. Varma, and R. S. Varma, *J. Org. Chem.*, 1986, 51, 2386–2388.
- 100 F. Reymond, C. Vollet, Z. Plichta, and D. Horák, *Biotechnol. Progr.*, 2013, 29, 532–542.
- 101 K. Matyjaszewski, *Controlled/Living Radical Polymerization: From Synthesis to Materials*, Oxford University Press, 2006.

- 102 S. E. Shim, S. Yang, H. H. Choi, and S. Choe, *J. Polym. Sci. Pol. Chem.*, 2004, 42, 835–845.
- 103 R. Perrier-Cornet, V. Héroguez, A. Thienpont, O. Babot, and T. Toupance, *J. Chromatogr. A.*, 2008, 1179, 2–8.
- 104 F. Ge, M.-M. Li, H. Ye, and B.-X. Zhao, *J. Hazard Mater.*, 2012, 211-212, 366–372.
- 105 Y.-T. Wei, Y.-M. Zheng, and J. P. Chen, *Langmuir*, 2011, 27, 6018–6025.
- 106 M. Jonsson, D. Nyström, O. Nordin, and E. Malmström, *Eur. Polym. J.*, 2009, 45, 2374–2382.
- 107 C. Perruchot, M. A. Khan, A. Kamitsi, S. P. Armes, T. Von Werne, and T. E. Patten, *Langmuir*, 2001, 17, 4479–4481.
- 108 S. Hansson, E. Ostmark, A. Carlmark, and E. Malmström, *ACS Appl. Mater. Interfaces*, 2009, 1, 2651–2659.
- 109 H. J. Issaq, *A Century of Separation Science*, CRC Press, 1st edn., 2001.
- 110 K. Zhang, H. Li, H. Zhang, S. Zhao, D. Wang, and J. Wang, *Mater. Chem. Phys.*, 2006, 96, 477–482.
- 111 I. Haller, *J. Am. Chem. Soc.*, 1978, 100, 8050–8055.
- 112 W. K. T. Coltro, R. D. S. Neves, A. D. J. Motheo, J. A. F. da Silva, and E. Carrilho, *Sensor. Actuat. B-Chem.*, 2014, 192, 239–246.
- 113 A. R. Silva and J. Botelho, *J. Mol. Catal. A-Chem.*, 2014, 381, 171–178.
- 114 S. Z. Nergiz, N. Gandra, and S. Singamaneni, *Carbon N. Y.*, 2014, 66, 585–591.
- 115 J. Liu, N. Feng, S. Chang, and H. Kang, *Appl. Surf. Sci.*, 2012, 258, 6127–6135.
- 116 Z. Wu, H. Chen, X. Liu, Y. Zhang, D. Li, and H. Huang, *Langmuir*, 2009, 25, 2900–6.

- 117 Q. Yu, Y. Zhang, H. Chen, Z. Wu, H. Huang, and C. Cheng, *Colloid. Surface. B*, 2010, 76, 468–74.
- 118 [Http://www.wiredchemist.com/chemistry/data/bond\\_energies\\_lengths.html](http://www.wiredchemist.com/chemistry/data/bond_energies_lengths.html), Accessed 3rd May 2014.
- 119 G. Bayramoglu, E. Yavuz, B. F. Senkal, and M. Y. Arica, *Colloid. Surface. A*, 2009, 345, 127–134.
- 120 L. Zhou, W. Yuan, J. Yuan, and X. Hong, *Mater. Lett.*, 2008, 62, 1372–1375.
- 121 M. M. Dragosavac, G. T. Vladislavljević, R. G. Holdich, and M. T. Stillwell, *Langmuir*, 2012, 28, 134–143.
- 122 [Www.chromstore.com/zeoprep-60-eco-silica-gel-40-63-micron-274-p.asp](http://www.chromstore.com/zeoprep-60-eco-silica-gel-40-63-micron-274-p.asp), Accessed 12th Dec 2013.
- 123 S. T. Agnese, F. W. Spirto, and W. H. Hannon, *Clin. Biochem.*, 1983, 16, 98–100.
- 124 [Http://www.sigmaaldrich.com/catalog/product/aldrich/s5130?lang=en&region=GB](http://www.sigmaaldrich.com/catalog/product/aldrich/s5130?lang=en&region=GB), Accessed 28th Jan 2013.
- 125 Sigma Aldrich, *Fumed Silica Product Information*.
- 126 W. Yantasee, C. L. Warner, T. Sangvanich, R. S. Addleman, T. G. Carter, R. J. Wiacek, G. E. Fryxell, C. Timchalk, and M. G. Warner, *Environ. Sci. Technol.*, 2007, 41, 5114–5119.
- 127 L. C. P. M. de Smet, D. Ullien, M. Mescher, and E. J. R. Sudhölter, *Organic surface modification of silicon-nanowire-based sensor devices*, CC BY-NC-SA, 2011.
- 128 M. Yamaura, R. . Camilo, L. . Sampaio, M. . Macêdo, M. Nakamura, and H. . Toma, *J. Magn. Magn. Mater.*, 2004, 279, 210–217.
- 129 R. M. Pasternack, S. Rivillon Amy, and Y. J. Chabal, *Langmuir*, 2008, 24, 12963–12971.

- 130 B. Borak, A. Baszczuk, M. Jasiorski, and K. Matyjaszewski, *Surface functionalization of the silica spherical particles*.
- 131 L. Zhao, J. Sun, Y. Zhao, L. Xu, and M. Zhai, *Chem. Eng. J.*, 2011, 170, 162–169.
- 132 N. D. Ghatge, B. . M. Shinde, and S. M. Jagadale, *J. Polym. Sci. Pol. Chem. Edn.*, 1984, 22, 985–994.
- 133 D. A. Smith, R. H. Cunningham, and B. Coulter, *J. Polym. Sci. Pol. Chem.*, 1970, 8, 783–784.
- 134 B. Almarzoqi, A. V. George, and N. S. Isaacs, *Tetrahedron*, 1986, 42, 601–607.
- 135 [Http://www.faculty.umassd.edu/xtras/catls/resources/binarydoc/2412.pdf](http://www.faculty.umassd.edu/xtras/catls/resources/binarydoc/2412.pdf), Accessed 28th Nov 2013.
- 136 C. Perruchot, M. A. Khan, A. Kamitsi, S. P. Armes, J. F. Watts, T. von Werne, and T. E. Patten, *Eur. Polym. J.*, 2004, 40, 2129–2141.
- 137 F. Hu, K. G. Neoh, L. Cen, and E.-T. Kang, *Biomacromolecules*, 2006, 7, 809–816.
- 138 L. S. Cahill, Z. Yao, A. Adronov, J. Penner, K. R. Moonosawmy, P. Kruse, and G. R. Goward, *J. Phys. Chem. B.*, 2004, 108, 11412–11418.
- 139 V. Castelvetro, M. Geppi, S. Giaiacopi, and G. Mollica, *Biomacromolecules*, 2007, 8, 498–508.
- 140 D. Xiao and M. J. Wirth, *Macromolecules*, 2002, 35, 2919–2925.
- 141 C. Bartholome, E. Beyou, E. Bourgeat-Lami, P. Chaumont, and N. Zydowicz, *Macromolecules*, 2003, 36, 7946–7952.
- 142 J. Crisp, Loughborough University, Ph.D Thesis, 2011.
- 143 P. A. Mirau, *Rapra Rev. Reports*, 2001, 11, 23.
- 144 M. Rangus, *NMR spectroscopy in solids: A comparison to NMR spectroscopy in liquids*, 2007.

- 145 M. J. Duer, *Solid-state NMR spectroscopy principles and applications*, Blackwell Science Ltd, 2002.
- 146 S. E. Dann, *Reactions and Characterization of Solids*, Royal Society of Chemistry, 1st edn., 2000.
- 147 A. W. Coats and J. P. Redfern, *Analyst*, 1963, 88, 906–924.
- 148 Exeter Analytical Inc., *CE440 Elemental Analyser Manual, Operating Instructions*.
- 149 S.-H. Kim, O.-H. Han, J.-K. Kim, and K.-H. Lee, *B. Kor. Chem. Soc.*, 2011, 32, 3644–3649.
- 150 [Http://www.ru.nl/science/solidstatenmr/people/group-members/sander-lambregts/](http://www.ru.nl/science/solidstatenmr/people/group-members/sander-lambregts/), Accessed 23rd April 2014.
- 151 H. H. P. Yiu, P. A. Wright, and N. P. Botting, *J. Mol. Catal. B-Enzym.*, 2001, 15, 81–92.
- 152 A. S. Maria Chong and X. S. Zhao, *J. Phys. Chem. B.*, 2003, 107, 12650–12657.
- 153 P. A. Mirau, *A practical guide to understanding the NMR of Polymers*, John Wiley & Sons, Inc., Hoboken, New Jersey, 2005.
- 154 A. P. L. M. Luhmer, J. B. D’Espinose, H. Hommel, *Magn. Reson. Imaging*, 1996, 14, 911–913.
- 155 D. w. Sindorf and G. E. Maciel, *J. Am. Chem. Soc.*, 1983, 105, 1487–1493.
- 156 M. Lelli, D. Gajan, A. Lesage, M. A. Caporini, V. Vitzthum, P. Mieville, F. Heroguel, F. Rascon, A. Roussey, C. Thieuleux, M. Boualleg, L. Veyre, G. Bodenhausen, C. Coperet, and L. Emsley, *J. Am. Chem. Soc.*, 2011, 133, 2104–2107.
- 157 R. S. P. King, S. E. Dann, M. R. J. Elsegood, P. F. Kelly, and R. J. Mortimer, *J. Eur. Chem.*, 2009, 15, 5441–5443.
- 158 A. I. Vogel, A. R. Tatchell, B. S. Furnis, A. J. Hannaford, and P. W. G. Smith, *Vogel’s Textbook of Practical Organic Chemistry*, 5th edn., 1996.

- 159 <https://www.dur.ac.uk/resources/SSNMR/AP3.pdf>, Accessed 24th April 2014.
- 160 D. Delacroix, J. P. Guerre, P. Leblanc, and C. Hickman, *Radionuclide and Radiation Protection Data Handbook 2002*, Nuclear Technology Publishing, 2nd edn., 2002, vol. 98.
- 161 V. Chisté and M. M. Bé, *U-238 Comments on evaluation of decay data*, 2006.
- 162 M.-M. Bé, V. Chisté, C. Dulieu, E. Browne, V. Chechev, N. Kuzmenko, R. Helmer, A. Nichols, E. Schönfeld, and R. Dersch, *Table of Radionuclides*, 2004, vol. 1.
- 163 M.-M. Bé, V. Chisté, C. Dulieu, E. Browne, V. Chechev, N. Kuzmenko, R. Helmer, A. Nichols, E. Schönfeld, and R. Dersch, *Table of Radionuclides*, 2004, vol. 2.
- 164 S. J. Hill, *Inductively Coupled Plasma Spectrometry and its Applications*, BlackwellPublishing Ltd, 2nd edn., 2007.
- 165 <http://www.spectroscopyonline.com/spectroscopy/data/articlestandard/spectroscopy/452001/1096/article.pdf>, 16, Accessed 15th Nov 2013.
- 166 K. E. Jarvis, A. L. Gray, and R. S. Houk, *Inductively Coupled Plasma Mass Spectrometry*, Blackie Academic & Professional, 1st edn., 1995.
- 167 H. Haraguchi, T. Hasegawg, and M. Abdullaht, *Pure Appl. Chem.*, 1988, 60, 685–696.
- 168 <http://em-1.stanford.edu/Schedule/ICP/abouticp.htm>, Accessed 17th Oct 2013.
- 169 R. S. Houk, V. A. Fassel, G. D. Flesch, H. J. Svec, A. L. Gray, and C. E. Taylor, *Anal. Chem.*, 1980, 52, 2283–2289.
- 170 University of Wisconsin - Milwaukee, *Environmental health, safety and risk management radiation safety program - Liquid Scintillation Counting*.
- 171 National Diagnostics Laboratory Staff, *Principles and Applications of Liquid Scintillation Counting*, 2004.
- 172 M. F. L'Annunziata, *Handbook of Radioactivity analysis*, Academic Press Limited, 1998.

- 173 S. Kingsley, *Hamamatsu Photomultiplier Tubes handbook*, 2003.
- 174 K. Siegnahn, *Alpha, Beta and Gamma Ray Spectroscopy*, North-Holland Publishing Company, 1st edn., 1979.
- 175 [Http://www.tpub.com/content/doe/h1013v2/css/h1013v2\\_73.htm](http://www.tpub.com/content/doe/h1013v2/css/h1013v2_73.htm), Accessed on 17th Nov 2013.
- 176 [Http://www.lenntech.com](http://www.lenntech.com), Accessed 15th Oct 2013.
- 177 J. Donohue, J. K. Fawell, E. Ohanian, M. Giddings, P. Toft, Y. Magara, and P. Jackson, *Copper in Drinking-water. Background document for development of WHO Guidelines for Drinking-water Quality*, 3rd edn., 2004.
- 178 United States Environmental Protection Agency Office of Air and Radiation, *Understanding variation in partition coefficient K<sub>d</sub> values. Volume II: Review of geochemistry and available K<sub>d</sub> values for cadmium, cesium, chromium, lead, plutonium, radon, strontium, thorium, tritium and uranium*, 1999.
- 179 E. F. Sameh, Loughborough University, 2010.
- 180 G. Limousin, J.-P. Gaudet, L. Charlet, S. Szenknect, V. Barthès, and M. Krimissa, *Appl. Geochem.*, 2007, 22, 249–275.
- 181 B. E. Johnson, P. H. Santschi, C.-Y. Chuang, S. Ootosaka, R. S. Addleman, M. Douglas, R. D. Rutledge, W. Chouyyok, J. D. Davidson, G. E. Fryxell, and J. M. Schwantes, *Environ. Sci. Technol.*, 2012, 46, 11251–11258.
- 182 J. Aguado, J. M. Arsuaga, A. Arencibia, M. Lindo, and V. Gascón, *J. Hazard Mater.*, 2009, 163, 213–221.
- 183 D. Zhao, J. Feng, Q. Huo, N. Melosh, G. H. Fredrickson, B. F. Chmelka, and G. D. Stucky, *Science* (80-. ), 1998, 279, 548–552.
- 184 H. I. Silman and A. Karlin, *Biochem.*, 1967, 58, 1664–1668.
- 185 M. Prasad, H. Xu, and S. Saxena, *J. Hazard Mater.*, 2008, 154, 221–229.

- 186 R. Forch, H. Schonherr, and A. T. A. Jenkins, *Surface Design: Applications in Bioscience and Nanotechnology*, WILEY-VCH, 1st edn., 2009.
- 187 K. Mills and R. E. Whan, *ASM Handbook Volume 10 Materials Characterisation*, ASM Handbook Committee, 9th edn., 1986.
- 188 [Http://wiki.utep.edu/download/attachments/51216567/XPS+-+Ruth+M+Dasary.pdf?version=1.](http://wiki.utep.edu/download/attachments/51216567/XPS+-+Ruth+M+Dasary.pdf?version=1.), Accessed 12th Oct 2013.
- 189 Geological Survey of Japan Open File Report No. 419, *Atlas of Eh-pH diagrams; Intercomparison of thermodynamic databases*, 2005.
- 190 T. Bide, L. Hetherington, G. Gunn, and A. Minks, *Br. Geol. Surv.*, 2008, 1–24.
- 191 D. G. E. Kerfoot, “Nickel” *Ullmann’s Encyclopedia of Industrial Chemistry*, WILEY-VCH, 2012, vol. 24.
- 192 [Http://www.saylor.org/site/wp-content/uploads/2011/06/List-of-Oxidation-States-of-the-Elements.pdf](http://www.saylor.org/site/wp-content/uploads/2011/06/List-of-Oxidation-States-of-the-Elements.pdf), Accessed 20th Jan 2014.
- 193 D. B. Rorabacher, *Anal. Chem.*, 1991, 63, 139–146.
- 194 R. B. Dean and W. J. Dixon, *Anal. Chem.*, 1951, 23, 636–638.
- 195 [Http://www.seafriends.org.nz/oceano/seawater.htm#composition](http://www.seafriends.org.nz/oceano/seawater.htm#composition), Accessed 25th Sept 2013.
- 196 [www.webelements.com](http://www.webelements.com), Accessed 30th Oct 2014.
- 197 [Http://www.rsc.org](http://www.rsc.org), Accessed 16th Oct 2013.
- 198 K. van der Maaden, K. Sliedregt, A. Kros, W. Jiskoot, and J. Bouwstra, *Langmuir*, 2012, 28, 3403–3411.
- 199 D. V. Vezenov, A. Noy, L. F. Rozsnyai, and C. M. Lieber, *J. Am. Chem. Soc.*, 1997, 119, 2006–2015.



- 200 D. B. Williams and C. B. Carter, *Transmission Electron Microscopy: Part IV Spectrometry*, Plenum Press, New York, 1st edn., 1996.
- 201 A. V. Crewe, M. Isaacson, and D. Johnson, *Rev. Sci. Instrum.*, 1969, 40, 241–246.
- 202 Z. Zhou, University of Sheffield, Ph.D Thesis, 2010.
- 203 D. B. Williams and C. B. Carter, *Transmission Electron Microscopy: Part III Imaging*, Plenum Press, New York, 1st edn., 1996.
- 204 M. A. White, J. A. Johnson, J. T. Koberstein, and N. J. Turro, *J. Am. Chem. Soc.*, 2006, 128, 11356–11357.
- 205 Q.-Y. Cao, Y.-H. Chen, J.-H. Liu, and X.-C. Gao, *Inorg. Chem. Commun.*, 2009, 12, 48–51.
- 206 P.-Z. Qin, C.-G. Niu, M. Ruan, G.-M. Zeng, and X.-Y. Wang, *Analyst*, 2010, 135, 2144–2149.
- 207 A. Bremer, D. M. Whittaker, C. A. Sharrad, A. Geist, and P. J. Panak, *Dalt. Trans.*, 2014, 43, 2684–2694.
- 208 A. Pitois, P. I. Ivanov, L. G. Abrahamsen, N. D. Bryan, R. J. Taylor, and H. E. Sims, *J. Environ. Monit.*, 2008, 10, 315–324.
- 209 T. W. Lane and F. M. Morel, *P. Natl. Acad. Sci. USA*, 2000, 97, 4627–4631.
- 210 D. E. Salt, M. Blaylock, N. P. B. A. Kumar, V. Dushenkov, B. D. Ensley, I. Chet, and I. Raskin, *Nat. Biotechnol.*, 1995, 13, 468–474.
- 211 U.S. Department of Health and Human Services, *Report on Carcinogens*, 12th edn., 2011.
- 212 [Http://www.eurekalert.org/features/doe/2003-07/ddoe-cqc071403.php](http://www.eurekalert.org/features/doe/2003-07/ddoe-cqc071403.php), Accessed 20th Mar 2014.
- 213 S. Cotton, *Lanthanides and Actinides*, Macmillan Education Ltd, 1st edn., 1991.

- 214 D. G. Kinniburgh, *Environ. Sci. Technol.*, 1986, 20, 895–904.
- 215 I. Langmuir, *J. Am. Chem. Soc.*, 1918, 40, 1361–1403.
- 216 United States Environmental Protection Agency Office of Air and Radiation, *Understanding variation in partition coefficient K<sub>d</sub> values. Volume I: The K<sub>d</sub> model, methods of measurement and application of chemical reaction codes*, 1999.
- 217 [Http://water.me.vccs.edu/courses/ENV115/lesson20\\_4.htm](http://water.me.vccs.edu/courses/ENV115/lesson20_4.htm), Accessed 20th Jan 2014.
- 218 N. N. Greenwood and A. Earnshaw, *Chemistry of the Elements*, Oxford: Butterworth-Heinemann, 2nd edn., 1997.
- 219 [Http://www.phosphonics.com](http://www.phosphonics.com), Accessed 28th Sept 2013.
- 220 N. Galaffu, S. P. Man, R. D. Wilkes, and J. R. H. Wilson, *Org. Process Res. Dev.*, 2007, 11, 406–413.
- 221 G. Reginato, P. Sadler, and R. D. Wilkes, *Org. Process Res. Dev.*, 2011, 15, 1396–1405.
- 222 J. Brown, A. Chighine, M. a. Colucci, N. Galaffu, S. C. Hirst, H. M. Seymour, J. J. Shiers, R. D. Wilkes, J. G. Williams, and J. R. H. Wilson, *Tetrahedron Lett.*, 2008, 49, 4968–4971.
- 223 [Http://www.talvivaara.com](http://www.talvivaara.com), Accessed 29th Sept 2013.
- 224 M. Riekkola-Vanhanen, *Miner. Eng.*, 2013, 48, 2–9.
- 225 T. Rohwerder, T. Gehrke, K. Kinzler, and W. Sand, *Appl. Microbiol. Biot.*, 2003, 63, 239–248.
- 226 G. J. Olson, J. A. Brierley, and C. L. Brierley, *Appl. Microbiol. Biot.*, 2003, 63, 249–257.
- 227 P. Saari and M. Riekkola-Vanhanen, *J. S. Afr. I. Min. Met.*, 2012, 112, 1013–1020.
- 228 H. R. Watling, *Hydrometallurgy*, 2006, 84, 81–108.

- 229 C. E. Housecroft and A. G. Sharpe, *Inorganic Chemistry (3rd Ed.)*, Pearson Education Limited, 3rd edn., 2008.
- 230 R. G. Pearson, *J. Am. Chem. Soc.*, 1963, 85, 3533–3539.
- 231 H.-J. Im, K. K. Park, and E. C. Jung, *Nanoscale Res. Lett.*, 2012, 7, 1–5.
- 232 [Http://www.stuk.fi/sateily-ymparistossa/uraani/talvivaaran-kaivos/en\\_GB/talvivaaran-kaivosalueen-vesistojen-uraani/](http://www.stuk.fi/sateily-ymparistossa/uraani/talvivaaran-kaivos/en_GB/talvivaaran-kaivosalueen-vesistojen-uraani/), Accessed 4th Oct 2013.
- 233 <http://www.mining-technology.com/projects/talvivaara/>, Accessed 23rd Feb 2014.
- 234 M. Riekkola-Vanhanen, *Nov. Biotechnol.*, 2010, 10, 7–14.

## 10 Appendix 1 – Linear Langmuir plots

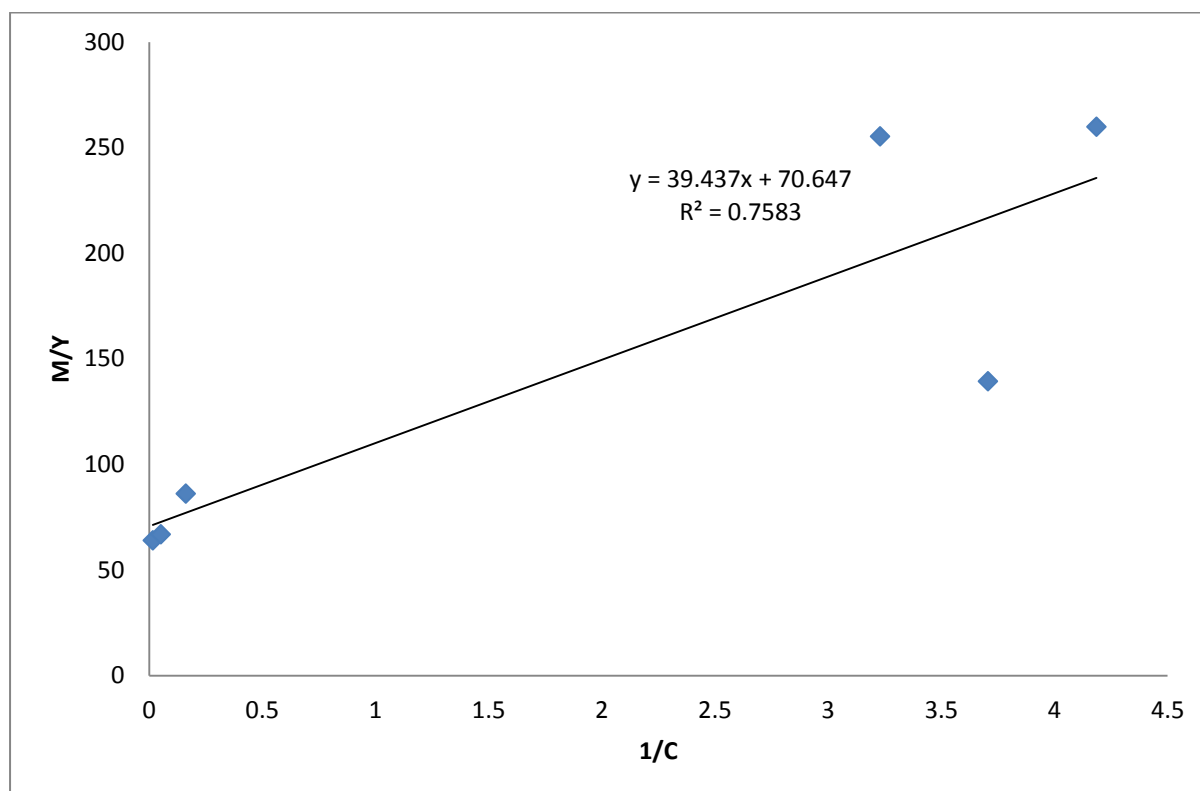


Figure 101 – Linear Langmuir plot for ZEOprep Si-APTES in Cu(II) solutions.

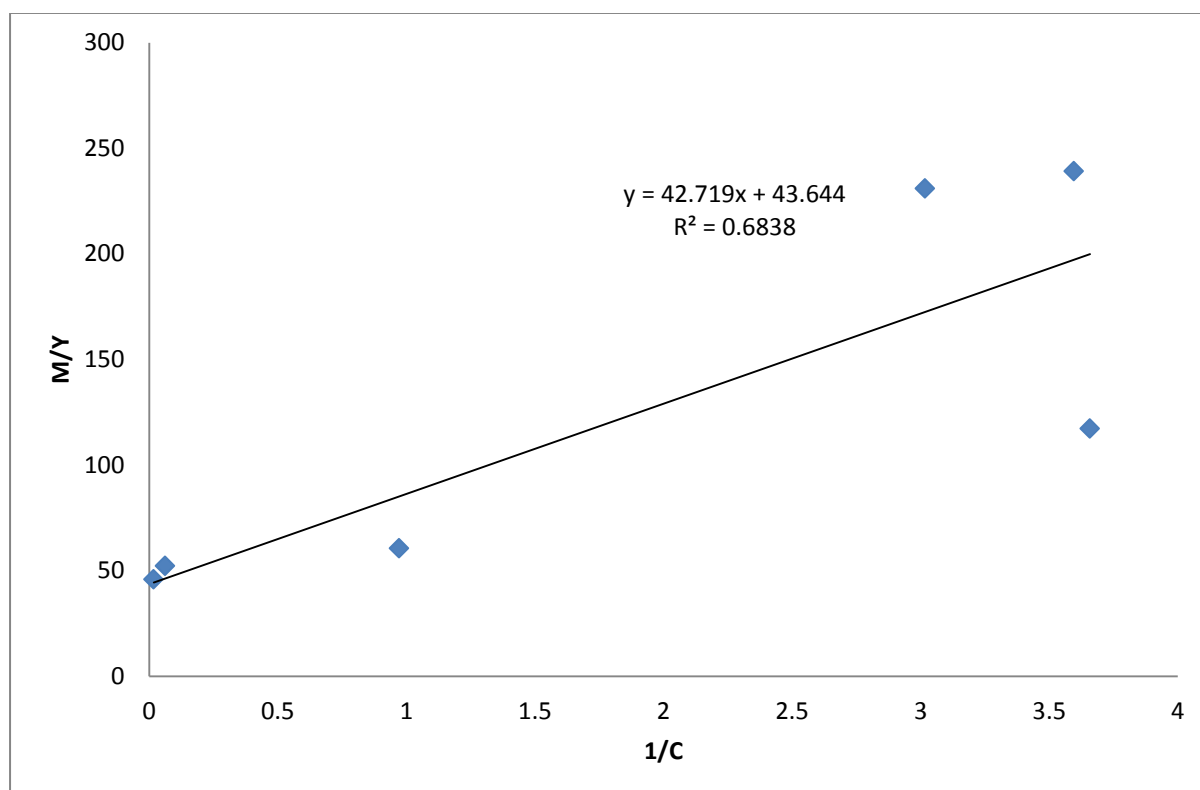


Figure 102 – Linear Langmuir plot for fumed Si-APTES in Cu(II) solutions.

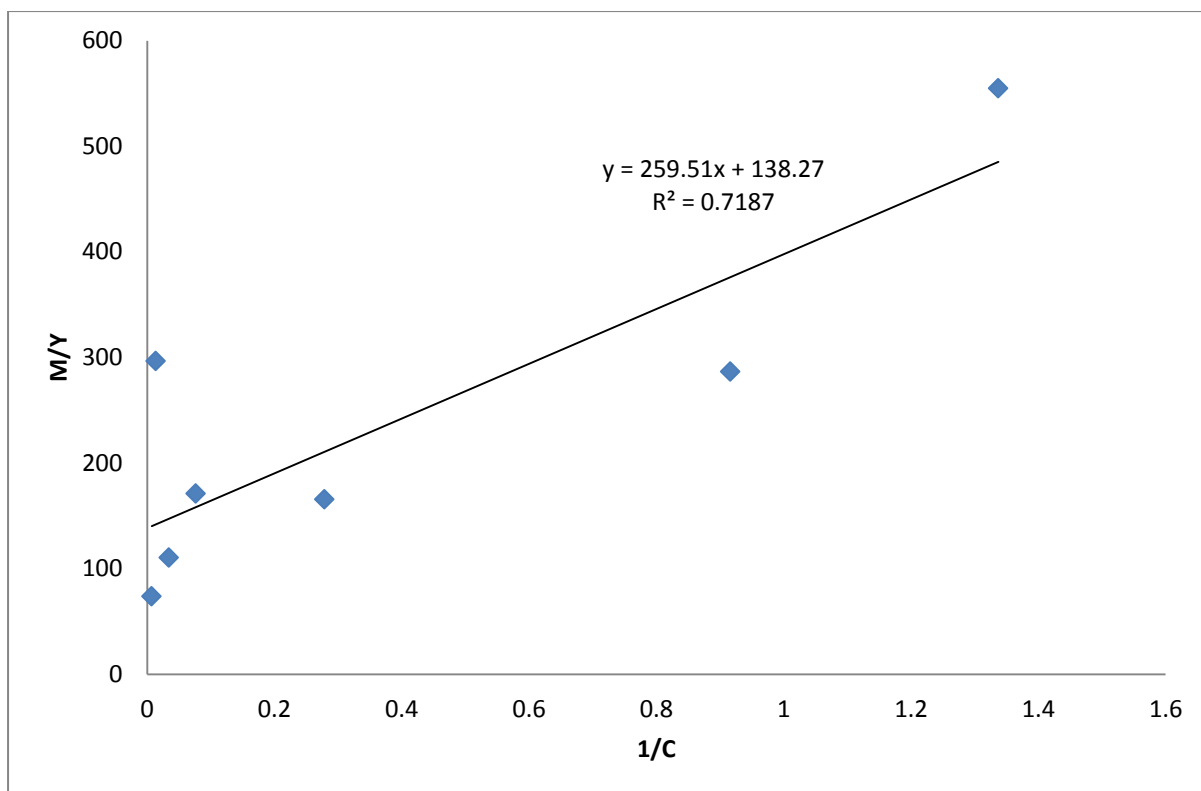


Figure 103 – Linear Langmuir plot for ZEOprep Si-APTES in Ni(II) solutions.

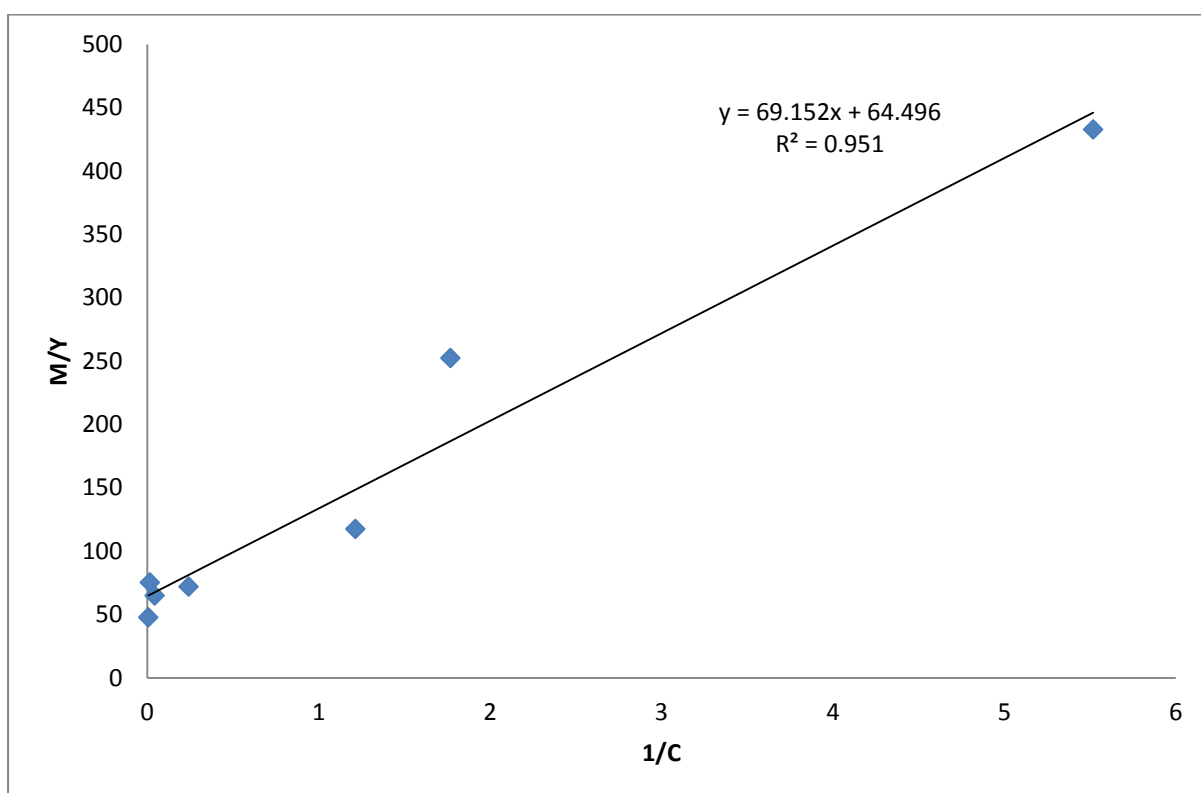


Figure 104 – Linear Langmuir plot for fumed Si-APTES in Ni(II) solutions.

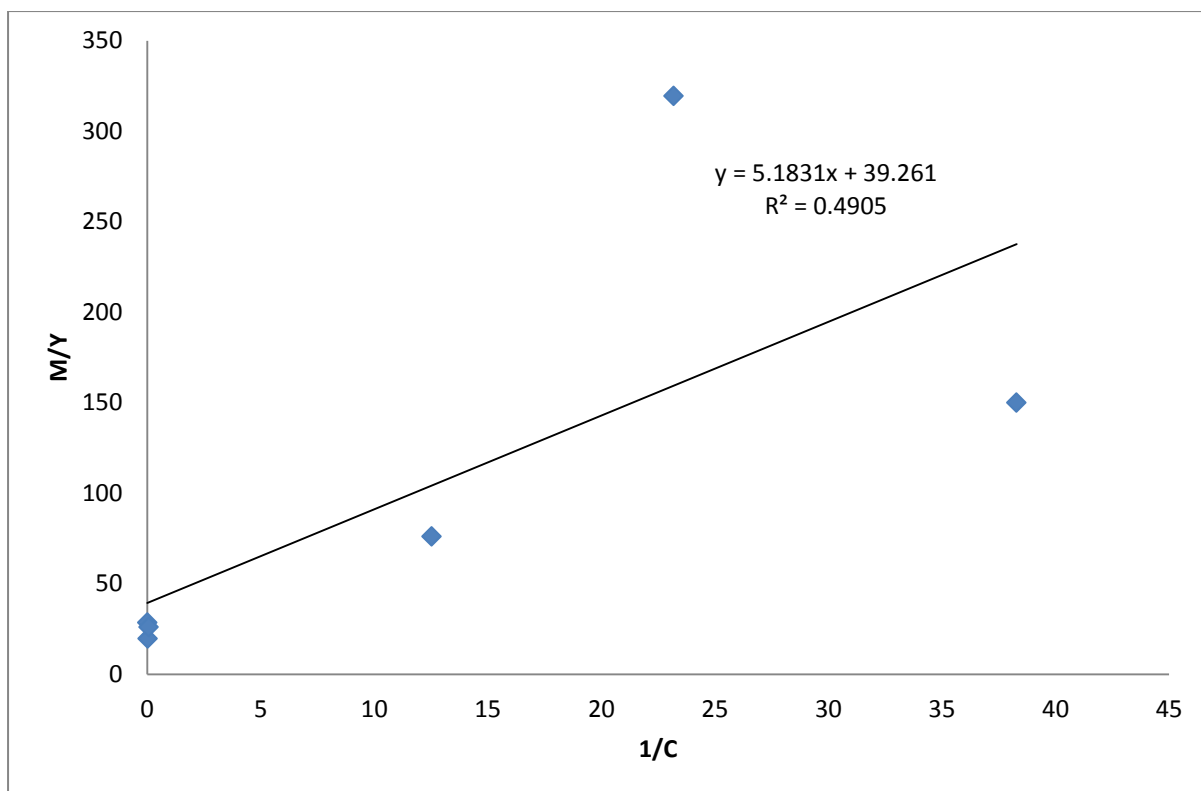


Figure 105 – Linear Langmuir plot for ZEOprep Si-APTES in Eu(III) solutions.

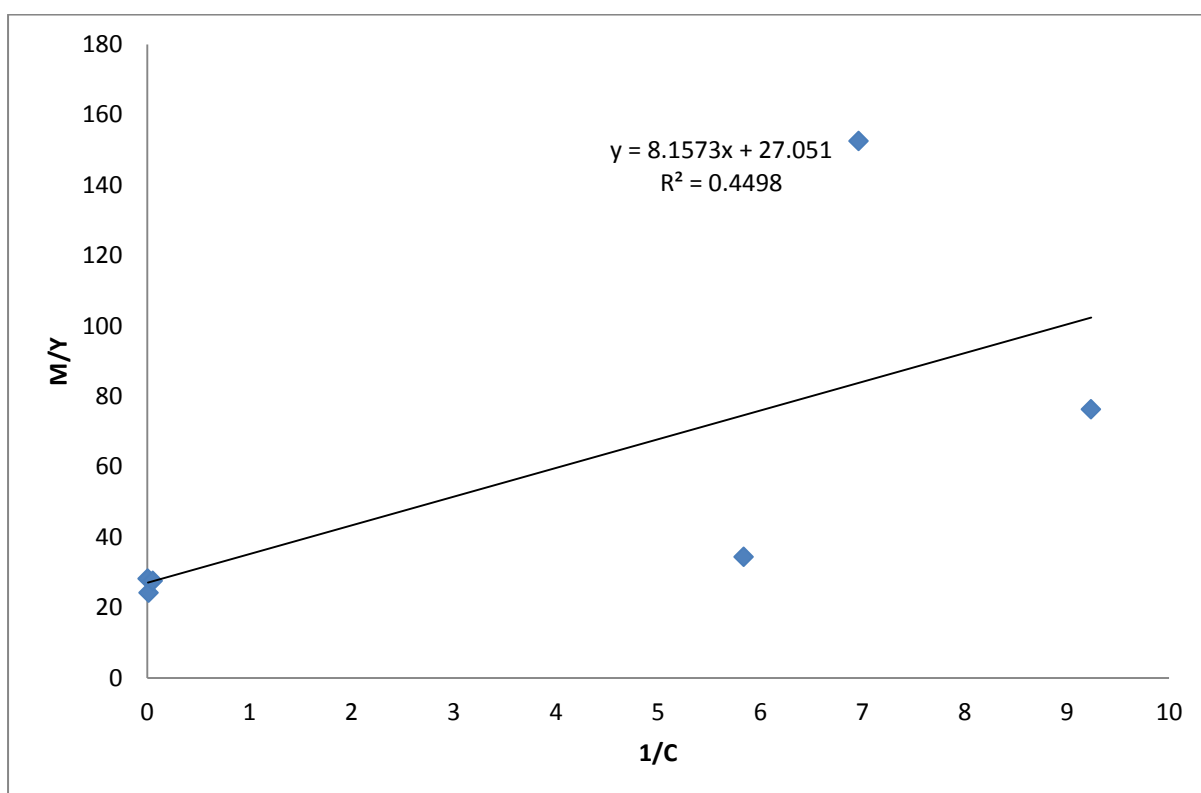


Figure 106 – Linear Langmuir plot for fumed Si-APTES in Eu(III) solutions.

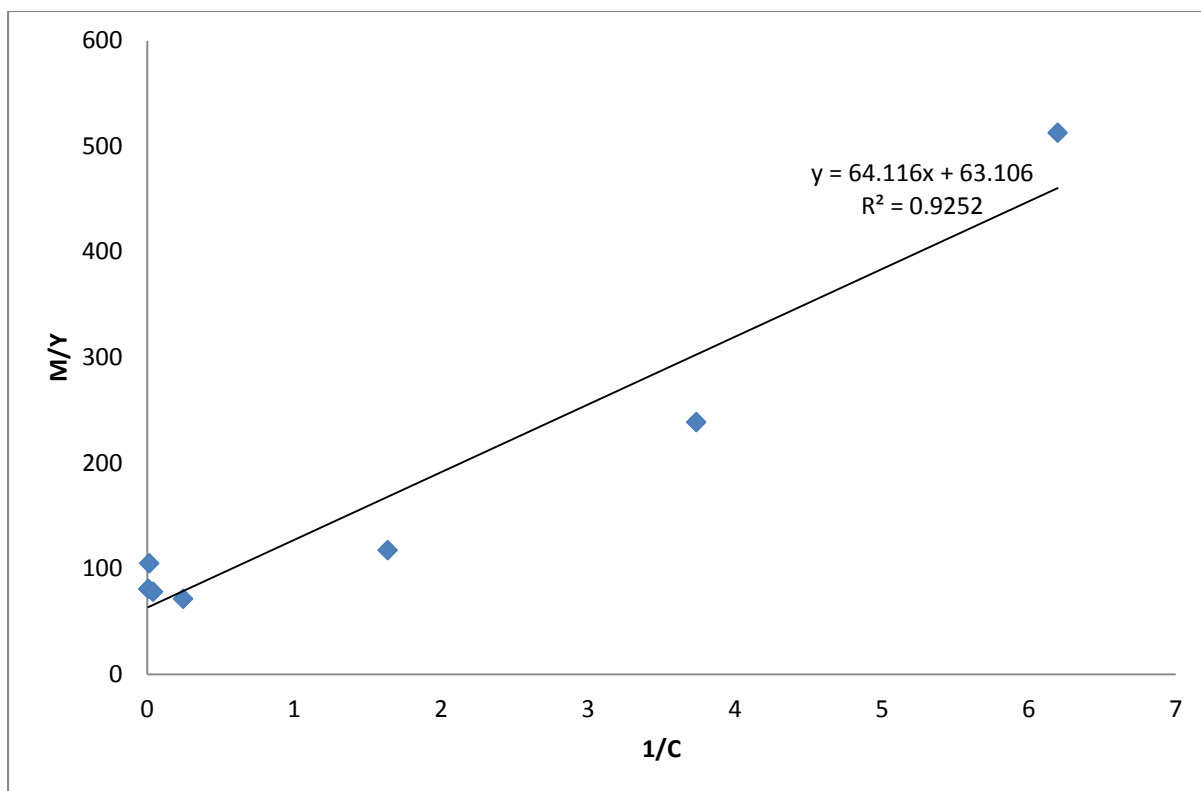


Figure 107 – Linear Langmuir plot for ZEOprep Si-APTES in Co(II) solutions.

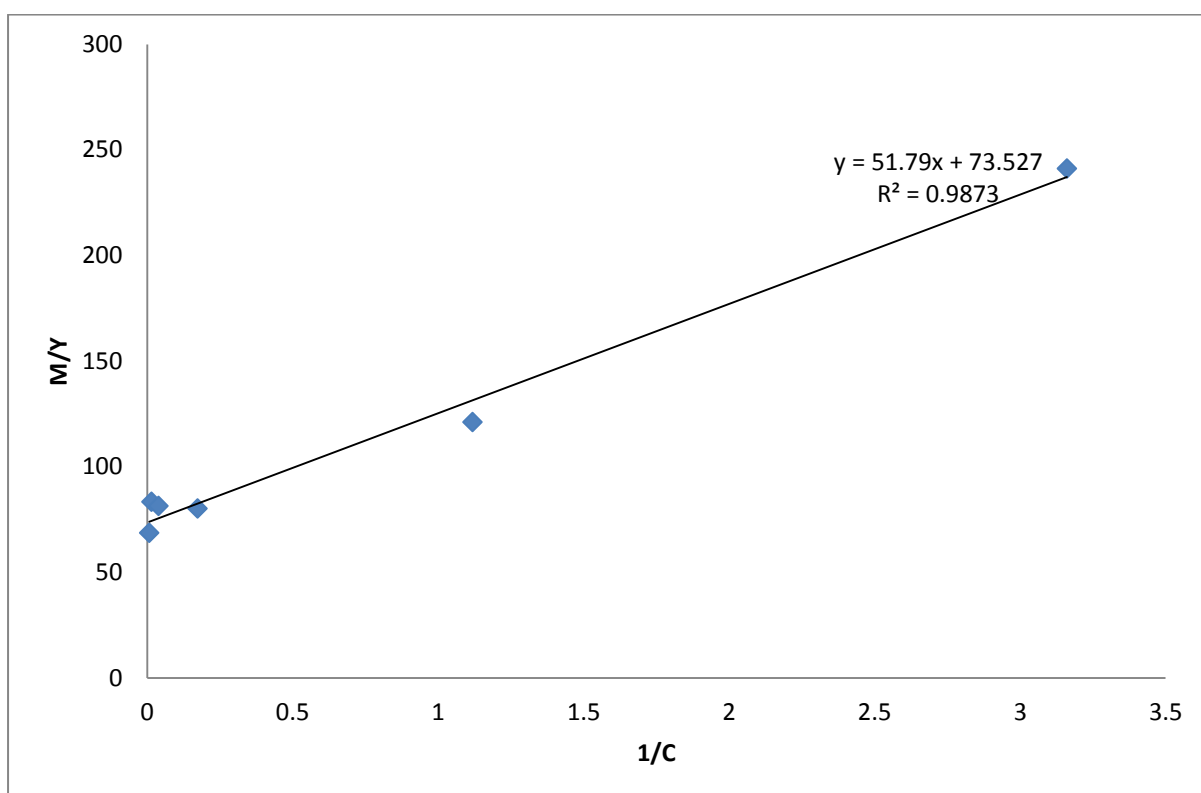


Figure 108 – Linear Langmuir plot for fumed Si-APTES in Co(II) solutions.

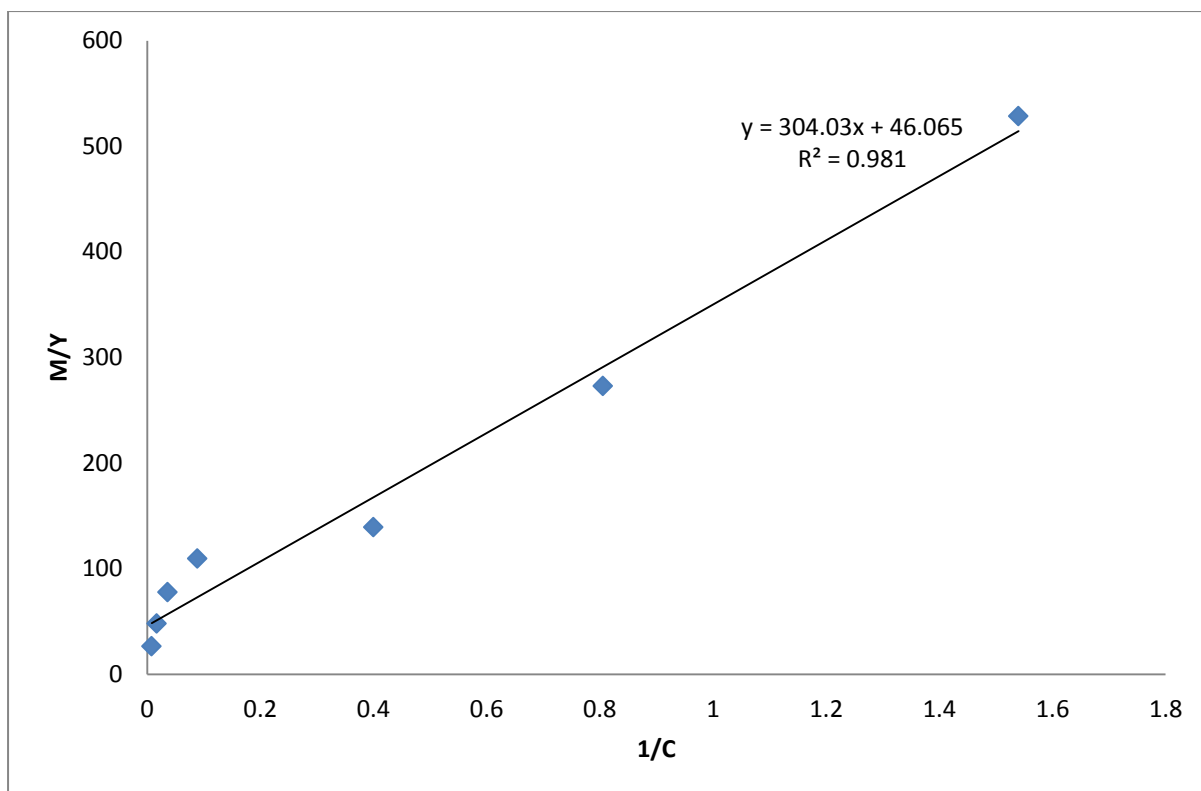


Figure 109 – Linear Langmuir plot for ZEOprep Si-APTES in  $\text{Cd}^{2+}$  solutions.

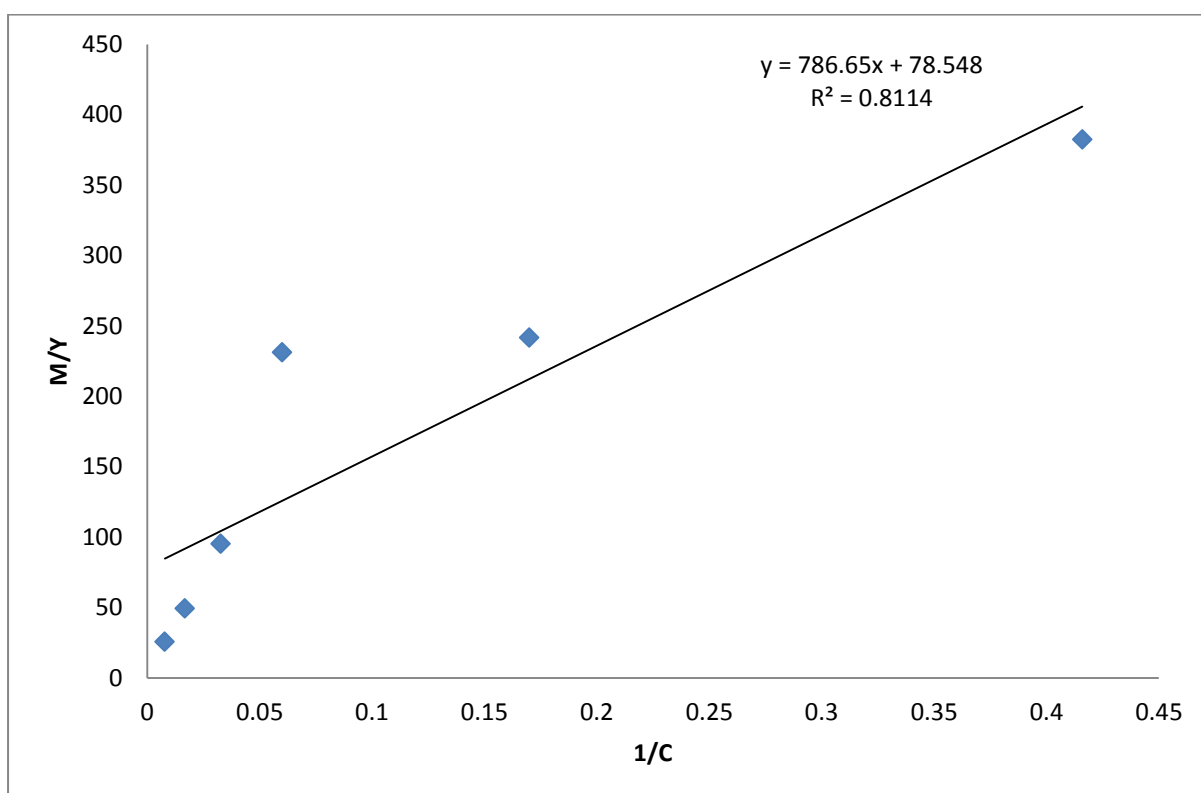


Figure 110 – Linear Langmuir plot for fumed Si-APTES in  $\text{Cd}^{2+}$  solutions.



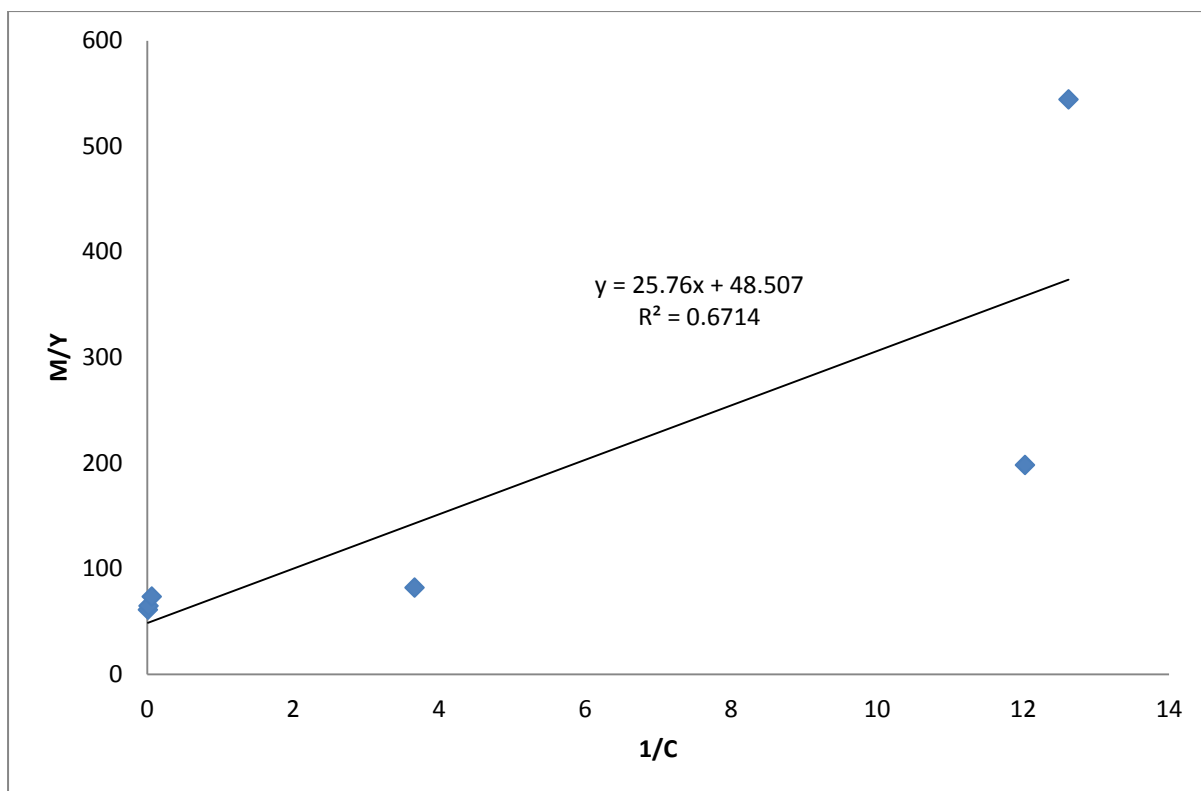


Figure 111 – Linear Langmuir plot for ZEOprep Si-APTES in  $[\text{UO}_2]^{2+}$  solutions.

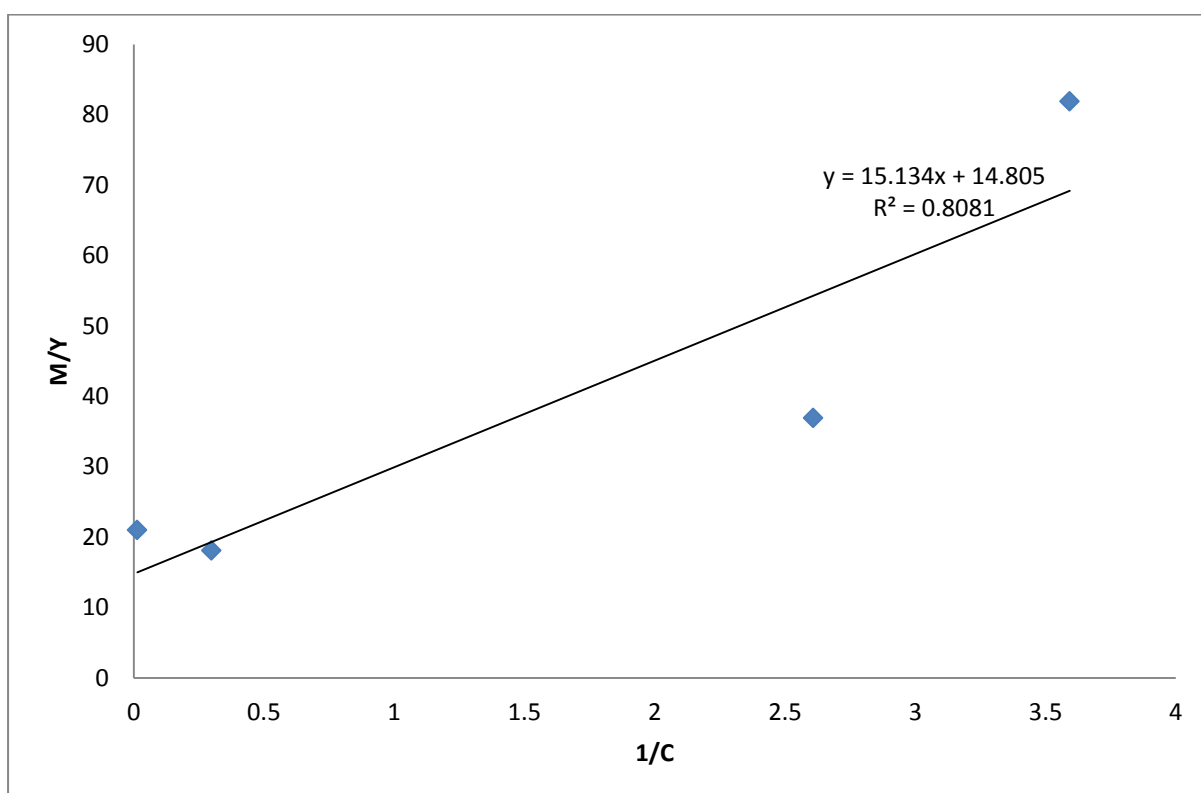


Figure 112 – Linear Langmuir plot for fumed Si-APTES in  $[\text{UO}_2]^{2+}$  solutions.

## 11 Appendix 2 – Reversibility and dissolution of metal ions following sequestration

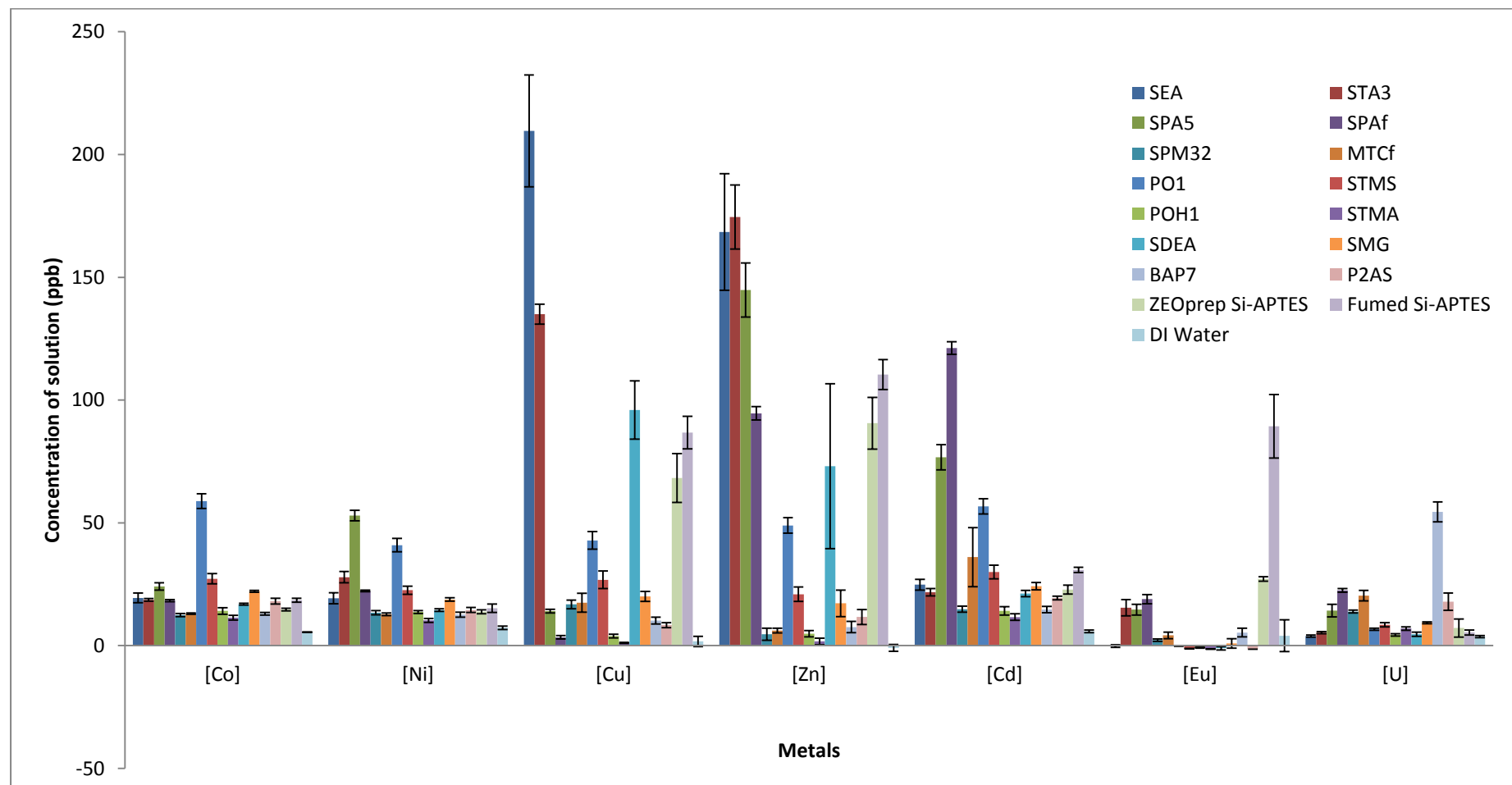


Figure 113 – Concentration of metal ions in a water solution following the addition of used silica materials, after having sequestered the corresponding metals in the graphs at the start of chapter 7 (Figure 80 to Figure 95).

## 12 Appendix 3 – Particle size of PhosphonicS Ltd samples

Silica Sample	Volume Weighted Mean ( $\mu\text{m}$ )	Specific Surface Area ( $\text{m}^2 \text{g}^{-1}$ )
SEA	144.877	0.0188
STA3	174.619	0.0153
SPA5	174.054	0.0153
SPAf	196.54	0.0137
SPM32	179.637	0.0148
MTCf	167.112	0.0161
PO1	171.06	0.0156
STMS	167.014	0.0159
POH1	155.595	0.0168
STMA	189.181	0.0139
SDEA	157.822	0.0172
SMG	164.214	0.0162
P2AS	448.88	0.00558
BAP7	321.867	0.00923

**Table 48 – Measured particle sizes of materials donated for this work by PhosphonicS Ltd. Samples were measured on a Malvern Mastersizer 2000 as described in the instrumentation section of the experimental.**